Decoding Lysine-11 Signals in Ubiquitination

Guinevere Grice

This dissertation is submitted for the degree of

Doctor of Philosophy

Department of Medicine, Cambridge Institute for Medical Research and Darwin College, University of Cambridge.

January 2018

Summary

The diverse outcomes of ubiquitination primarily relate to the flexibility of ubiquitin in forming homo- or heterotypic chains on each of its seven lysine residues which in turn stimulate distinct downstream signaling pathways. These ubiquitin signals must be selectively initiated on the substrate protein and subsequently decoded to facilitate the desired cellular function. These initiation and decoding steps often involve additional post-translational modifications and ubiquitin receptor proteins, but the enzymes and ubiquitin chains involved for many ubiquitinated substrates are not clear. Here, I have explored the initiation and decoding of ubiquitin signals, focusing on lysine-11 (K11) linked polyubiquitin chains and their role in protein degradation. I established *in vitro* assays to understand how K11-chains are decoded and whether these chains act as a signal for proteasome-mediated degradation. Pure homotypic K11-chains did not bind the proteasome or its associated ubiquitin binding proteins, but did bind to the mitophagy ubiquitin receptors, MyosinVI and TAX1BP1. Heterotypic K11/K48 linkages not only bound the proteasome but also stimulated degradation of the cell cycle substrate, cyclin B1. To further explore the functions of K11-chains I focused on the hypoxia inducible transcription factor (HIF) pathway, as K11-ubiquitination had been implicated in proteasome-independent degradation of the transcription factor. I established an *in vitro* assay to initiate HIF ubiquitination, via prolyl hydroxylation, and determine the type of ubiquitin chains involved. Recombinant HIF isoforms were rapidly hydroxylated when incubated with cell extracts. Moreover, the levels of iron and small molecule metabolites within the lysates regulated HIF hydroxylation. However, this hydroxylation was insufficient to reproducibly promote HIF ubiquitination or determine the ubiquitin chains involved. While the nature of the polyubiquitin chains formed in the HIF pathway remain elusive, my studies identify distinct roles for homotypic and heterotypic K11-polyubiquitination in proteasome-mediated degradation.

Declaration

This dissertation is my own work and includes nothing which is the outcome of work done in collaboration except as declared in the Preface and specified in the text.

It is not substantially the same as any that I have submitted, or, is being concurrently submitted for a degree or diploma or other qualification at the University of Cambridge or any other University or similar institution except as declared in the Preface and specified in the text. I further state that no substantial part of my dissertation has already been submitted, or, is being concurrently submitted for any such degree, diploma or other qualification at the University of Cambridge or any other University of similar institution except as declared in the Preface and specified in the text.

It does not exceed the prescribed word limit for the relevant Degree Committee.

Acknowledgements

In preparation of this thesis, I would like to thank all those who have donated materials. I thank Fred Goldberg (Harvard Medical School) for the pET26bHis10-UIM2-S5a (UIM of Rpn10/S5a), pDEST15-UBL-hHR23B, pGEX GST-E6AP, pGEX GST-Nedd4, pGEX4 T2 GST-RAD23B, pET15b-E1, and pET15b-His-Ubch5b constructs, Sylvie Urbe (University of Liverpool) for the pGEX-6P-1 GST-AMSH construct, Marc Kirschner (Harvard Medical School) for the pET28his-Ube2S construct, Randall King (Harvard Medical School) for the pET28a HA-WT Ncyclin B1-6His pET28a and HA-WT Ncyclin B1 K64 -6His constructs, Lauren Jackson (Vanderbilt University) for the pGEX PreScission construct, Patrick Maxwell (CIMR, Cambridge) for the pCDNA3 HIF1α-HA construct, Vangelis Christodoulou and Katrin Rittinger (Francis Crick Institute) for the pET47b Kan^R N term His tag 3C and pET49b Kan^R N term GST tag 3C constructs and David Barford (MRC Laboratory of Molecular Biology) for the reconstituted APC/C and recombinant Cdh1 proteins.

I would like to thank my supervisor, Paul Lehner, and all the members of the Nathan and Lehner laboratories who have helped and supported my work. In particular, I am grateful to James Nathan for overseeing much of my experimental work and with whom I conducted several experiments as detailed in the text. Also, I thank Stephen Burr for generating the OGDHc, LIAS and PHD2 null cell lines and lysates, Anna Miles for her helpful insights into the V-ATPase and iron regulation in cells and Peter Bailey for making the pHRSIN-pSFFV-HIF2α-Puro construct. I thank Vangelis Christodoulou and Katrin Rittinger (Francis Crick Institute), who kindly taught me the Ligation Independent Cloning technique and generously donated LIC constructs. I also thank my collaborators: Folma Buss, Jake Kendrick-Jones and Antonina Kruppa (CIMR, Cambridge). I would also like to thank Mike Weekes and Robin Antrobus (CIMR, Cambridge) for the mass spectrometry work.

On a personal note, I am very grateful to my supervisor, Paul Lehner, for his continued support and guidance throughout my studies and during the

preparation of this manuscript. Finally, I would like to thank my husband, my children – Millie, Will and Ben, and my parents – Tricia and Roger Grice, for their unsurpassed patience, kindness, resilience and humour and to all of whom I dedicate this thesis.

Publications arising from work detailed in thesis

1. **Grice G.L.,** Lobb I.T., Weekes M.P., Gygi S.P., Antrobus R, and Nathan J.A. (2015). The proteasome distinguishes between heterotypic and homotypic lysine-11 linked polyubiquitin chains. *Cell Rep.* Jul 28;12(4):545-53. PMC4533228

2. **Grice G.L.,** Nathan J.A. The recognition of ubiquitinated proteins by the proteasome. *Cell Mol Life Sci.* 2016. May 2. PMC49804124. *Review.*

3. Burr S.P., Costa A.S.H., **Grice G.L.,** Timms R.T., Lobb I.T., Freisigner P., Dodd R.B., Dougan G., Lehner P.J., Frezza C., and Nathan J.A. Mitochondrial protein lipoylation and the 2-oxoglutarate dehydrogenase complex controls HIF1α stability in aerobic conditions. *Cell Metabolism* 2016 Nov 8;24(5):740-752. PMC5106373

4. Miles, A.L.*, Burr, S.P.*, **Grice, G.L.,** and Nathan, J.A. (2017). The vacuolar-ATPase complex and assembly factors, TMEM199 and CCDC115, control HIF1alpha prolyl hydroxylation by regulating cellular iron levels. *eLife* Mar 15;6. pii: e22693. doi: 10.7554/eLife.22693. PMC5391204

5. Kruppa A.J., Kishi-Itakura C., Masters T.A., Rorbach J.E., **Grice G.L.,** Arden S.D., Kendrick-Jones J., Nathan J.A., Minczuk M., Buss F.,. Parkin-dependent ubiquitination recruits MYO6 linking actin assembly to mitochondrial quality control. *Dev Cell (in press)*.

Abbreviations

2-HG	2-hydroxyglutarate
2-OG	2-oxoglutarate, alpha-ketoglutarate
2-OG-DD	2-oxoglutarate dependent dioxygenase
5caC	5-carboxylcytosine
5fC	5-formylcytosine
5hmC	5-hydroxymethylcytosine
5mC	5-methylcytosine
A20 ZnF	A20 zinc finger
AAA ATPases	ATPases Associated with diverse cellular Activities
Acetyl CoA	Acetyl Coenzyme A
ADP	Adenosine diphosphate
AMSH	Associated Molecule with the SH3 domain of STAM
ANKRD13	Ankyrin Repeat Domain 13
APC/C	Anaphase promoting complex/ cyclosome
AQUA	Absolute Quantification
ATP	Adenosine triphosphate
Baf A	Bafilomycin A
BNIP3	BCL2 Interacting Protein 3
C. elegans	Caenorhabditis elegans
CAD	C-terminal activating domain
Cav-1	Caveolin-1
CBD	Cargo binding domain
CBP	CREB binding protein
CHIP	Carboxyl terminus of Hsc70-interacting protein
cIAP-1	Cellular inhibitor of apoptosis protein-1
CIMR	Cambridge Institute for Medical Research
CMA	Chaperone mediated autophagy
CP	Core particle
CPH	Collagen prolyl hydroxylase
CRISPR	Clustered regularly interspaced short palindromic repeats
CUE	Coupling of ubiquitin conjugation to ERAD

Cul-2	Cullin-2
Cy-B1 NTK64	Cyclin B1 N-terminus with a single lysine at site 64
D-2-HG	D enantiomer of 2-hydroxyglutarate
D-2-HGDH	D-2-hydroxyglutarate dehydrogenase
DFO	Desferrioxamine
DHFR	Dihydrofolate reductase
DLD	Dihydrolipoamide
DLST	Dihydrolipoamide S-succinyltransferase
DMOG	Dimethyloxalylglycine
DNA	Deoxyribonucleic acid
DNMT	DNA methyl transferase
DTT	Dithiothreitol
DUB	Deubiquitinating enzyme
DUIM	Double-sided UIM
DUSP	Domain present in ubiquitin-specific proteases
E. coli	Escherichia coli
E6AP	E6-associated protein
EC	Endothelial cell
EGF	Epidermal growth factor
EGFR	Epidermal growth factor receptor
EGL-9	Egg-laying-defective 9
EGLN	Egg-laying-defective nine
EPO	Erythropoietin
ERAD	ER-associated degradation
ERAP1	Endoplasmic reticulum aminopeptidase 1
ERK	Extracellular signal-regulated kinase
ES	Embryonic stem
ESCRT0	Endosomal complexes required for transport
ESI-MS	Electrospray Ionisation Mass Spectrometry
FACS	Fluorescence-activated cell sorting
FADH2	Flavin adenine dinucleotide
FANCL	Fanconi anaemia complementation group L
FD	Flavodoxin-like fold

FH	Fumarate hydratase
FIH	Factor inhibiting HIF
FPLC	Fast Protein Liquid Chromatography
FT	Flow through
GAT	GGA and TOM
GFP	Green fluorescent protein
GLUE	Gram-like ubiquitin binding in EAP45
GLUT1	Glucose transporter 1
GSH	Glutathione Sepharose
GST	Glutathione S-transferase
HA	Hemagglutinin
HC	Heavy chain
HECT	Homologous to the E6-associated protein C-terminus
HEK	Human embryonic kidney
HeLa	Henrietta Lacks
hHR23	human Rad23
HIF	Hypoxia Inducible transcription Factor
HIFα	refers to both HIF1α and HIF2α subunits
His	Histidine
HLH	Helix-loop-helix
HPH	HIF prolyl hydroxylase
HRE	HIF-responsive element
Hrs	Hepatocyte receptor substrate
Hul5	HECT ubiquitin ligase
I44	Isoleucine 44
IDH	Isocitrate dehydrogenase
IFN	Interferon
IKK	IκB kinase
IP	Immunoprecipitation
IPTG	Isopropyl β-D-1 thiogalactopyranoside
JAMMs	JAB1/MPN/MOV34 metalloenzymes
JHDM	JumonjiC domain-containing histone demethylase
JmjC	JumonjiC

K11	Lysine 11
K27	Lysine 27
K29	Lysine 29
K33	Lysine 33
K48	Lysine 48
K5	Kaposi Sarcoma associated herpes virus 5
K6	Lysine 6
K63	Lysine 63
KO	Knock out
L-2-HG	L enantiomer of 2-hydroxyglutarate
L-2-HGDH	L-2-hydroxyglutarate dehydrogenase
LC	Light chain
LC/MS	Liquid chromatography-mass spectrometry
LDH	Lactate dehydrogenase
LDHA	Lactate dehydrogenase A
LIAS	Lipoic acid synthase
LIC	Ligation independent cloning
LUBAC	Linear ubiquitin chain assembly complex
MDa	Megadalton
MDH	Malate dehydrogenase
Met-linked	Methionine-linked
MHC	Major histocompatibilty complex
MINDY	MIU-containing novel DUB family
MITA	Mediator of IRF3 activation
MIU	Motif interacting with ubiquitin
mM	millimolar
mRNA	messenger RNA
MS	Mass spectrometry
MS/MS	Tandem mass spectrometry
NAD	N-terminal activating domain
NADH	Nicotinamide adenine dinucleotide
NDRG3	N-myc downstream-regulated gene 3 protein
NF-κB	Nuclear factor-κB

NIMR	National Institute for Medical Research
NiNTA	Nickel nitrilotriacetic acid
NMR	Nuclear Magnetic Resonance
NZF	Npl4 zinc finger
ODD	Oxygen dependent degradation domain
OGDH	Oxoglutarate dehydrogenase
OGDHc	Oxoglutarate dehydrogenase complex
OTU	Ovarian tumour protease
PAS	PER-ARNT-SIM
PCR	Polymerase chain reaction
PDH	Pyruvate dehydrogenase
PDK	Pyruvate dehydrogenase kinase
PER-ARNT-SIM	Period circadian protein-aryl hydrocarbon receptor nuclear translocator protein-single minded protein
PEST	Proline, glutamic acid, serine, threonine
PFU	PLAA family ubiquitin binding domain
PHD	Prolyl Hydroxylase
PHYL	Phyllopod
PINK1	PTEN-induced putative kinase 1
PTEN	Phosphatase and tensin homolog
pVHL	protein encoded by VHL
RCC4	Renal cell carcinoma
RING	Really Interesting New Gene
RNA	Ribonucleic acid
RNAi	RNA interference
RNF	Ring finger
ROS	Reactive oxygen species
RP	Regulatory particle
SANS	Small Angle Neutron-scattering
SCF	Skp, Cullin, F-box containing
SDH	Succinate dehydrogenase
SDS-PAGE	Sodium dodecyl sulphate polyacrylamide gel electrophoresis

SEM	Standard error of the mean
Ser/Thr	Serine/threonine
sgRNA	Single guide RNA
SHARP1	Enhancer-of-split and hairy-related protein 1
SIAH	Seven in Absentia homolog
SiRNA	Small interfering RNA
STAM1	Signal-transducing adaptor molecue 1
TAX1BP1	Tax1 binding protein 1
TBB	Tris binding buffer
TBS	Tris buffered saline
TCA	Tricarboxylic acid
TCAF-1	TRPM8 Channel Associated Factor 1
TCL	Total cell lysate
TET	Ten-eleven translocation
TNF	Tumour necrosis factor
TRABID	TRAF-binding domain-containing protein
TRAF6	TNF receptor associated factor 6
TRIM	Tripartite motif containing
Trx	Thioredoxin
TUBEs	Tandem Ubiquitin Binding Entities
Ub	Ubiquitin
Ub Ald	Ubiquitin aldehyde
Ub^4	Tetraubiquitin
UBA	Ubiquitin associated
Ubc	Ubiquitin conjugating enzyme
UBD	Ubiquitin binding domain
Ubi-CREST	Ubiquitin Chain Restriction Analysis
Ub^{KO}	Ubiquitin in which all lysines have been mutated
UBL	Ubiquitin-like
UBM	Ubiquitin binding motif
Ub^{Me}	Methyl ubiquitin
UBP	Ubiquitin binding protein
UBP ZnF	Ubiquitin-specific protease processing zinc finger

Ubp6	Ubiquitin-specific protease 6
UBQLN	Ubiquilin
UBZ	Ubiquitin-binding ZnF domain
UEV	Ubc E2 variant domain
UIM	Ubiquitin interacting motif
UPS	Ubiquitin proteasome system
USP	Ubiquitin specific protease
V-ATPase	H+Vacuolar-ATPase
VCP	Valosine containing protein (P97)
VEGF	Vascular endothelial growth factor
VHL	Von Hippel Lindau
VHS	Vps27/Hrs/STAM
WT	Wildtype
βTrCP	Beta-transducin repeat-containing protein

Table of Contents

List of Figures

List of Tables

Chapter 1: Introduction

1.1 The Ubiquitin Proteasome System

The ubiquitin proteasome system (UPS) is the major pathway for regulating the breakdown of intracellular proteins, involving the conjugation of the small 76 amino acid polypeptide, ubiquitin, to a protein substrate, by a carefully controlled enzymatic cascade (Hershko and Ciechanover, 1998; Pickart, 2001). However, ubiquitination is not just a signal for protein degradation, but also acts as an essential post translational modification required for most cellular processes, including cell signaling, cell cycle regulation, DNA repair, and endosomal-lysosomal trafficking (Ikeda and Dikic, 2008). A key feature of ubiquitination that allows these diverse functions is the ability of ubiquitin to form chains on itself via one of its seven lysine residues (K6, K11, K27, K29, K33, K48 and K63) or its N-terminus (Met-linked or linear chains) (Ikeda and Dikic, 2008; Kim et al., 2009). These chains may contain one type of linkage (homotypic) or a mixture of different linkages (heterotypic) (Boname et al., 2010). Consequently, the range of outcomes allowed by the possible combinations of ubiquitin chains and their individual linkages are hugely diverse.

1.1.1 How are ubiquitin chains formed?

Ubiquitin conjugation is controlled by an enzymatic cascade involving three different classes of enzymes: (i) the E1 activating enzyme, which catalyses the activation of ubiquitin in an ATP-dependent step (Ema et al.), (ii) the E2 conjugating enzymes that form a thioester attachment to ubiquitin and catalyse the transfer of ubiquitin to an E3 ligase, and (iii) the E3 ligases, which catalyse the transfer and covalent attachment of ubiquitin to a lysine residue in the protein substrate either directly, in the case of the Really Interesting New Gene (RING) E3 ligases, or by forming a thioester intermediate, in the case of the homologous to the E6-associated protein C-terminus (HECT) E3 ligases (Hershko and Ciechanover, 1998; Pickart, 2001) (**Figure 1.1**). In addition, RING-Between-

RING E3 ligases, such as Parkin (Marin et al., 2004), share features of both HECT and RING E3 ligases, in which thioester-bound E2 enzymes are bound to the RING while ubiquitin is transferred to a catalytic cysteine of a separate domain (Spratt et al., 2014). There is one major E1 enzyme, approximately 50 E2 enzymes and around 700 E3 ligases. It has also been described that some ubiquitin ligases may act as E4 enzymes which modify substrates previously ubiquitinated by an E3 ligase (Koegl et al., 1999; Richly et al., 2005).

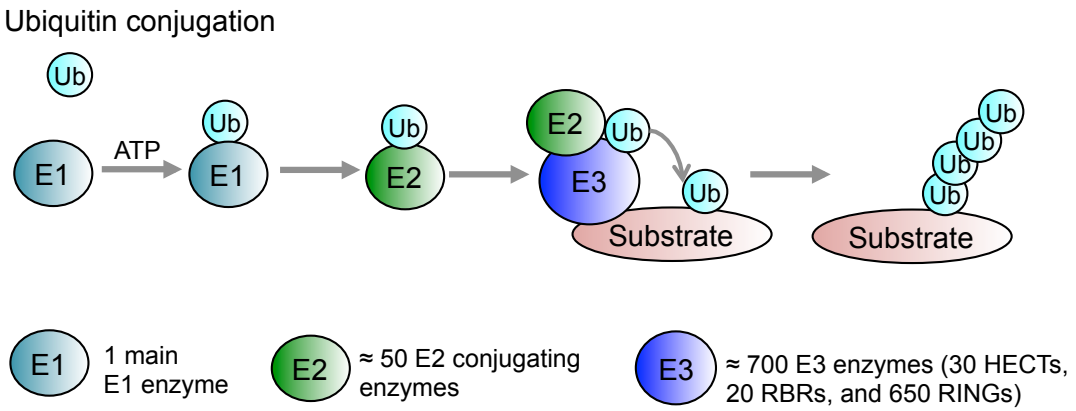

Figure 1.1: The ubiquitin conjugation cascade. Schematic of the enzymes involved in the formation of ubiquitin chains, ubiquitin conjugation. The approximate number of mammalian ubiquitin enzymes involved in ubiquitin conjugation are indicated.

E3 ligases are principally responsible for substrate specificity, as they recruit the E2 enzyme and bind to the protein substrate. However, the outcome of ubiquitination is dependent on the type of linkage formed and recognition of the ubiquitin signal by ubiquitin binding proteins (UBPs) (**see 1.1.3**). In some cases ubiquitin linkages are determined by the E2 or E3 enzyme involved. The E2, Ubc13 (UBE2N), only forms K63-linked chains (Hofmann and Pickart, 2001), whereas Ube2S predominantly forms K11-linked chains (Jin et al., 2008; Wu et al., 2010). However, the abundant UbcH5 (UBE2D) family can form all types of ubiquitin chains *in vitro* (Brzovic and Klevit, 2006). E3 ligases can also show similar linkage specificity, as observed for the HECT ligases, such as Nedd4, which forms K63-linked chains, and E6AP, which forms K48-linked chains. More recently, linear ubiquitin chain formation has been shown to be dependent on the linear ubiquitin chain assembly complex (LUBAC) E3 ligase complex

(Shimizu et al., 2015). Indeed, it is likely that most E2 and E3 interactions will determine the nature of the ubiquitin chain formed.

While the number of E3 ligases is partly responsible for diversity in the ubiquitin system, it is important to note that ubiquitin conjugation is reversible, through cleavage of the isopeptide bond by deubiquitinating enzymes (DUBs) (Reyes-Turcu and Wilkinson, 2009)(**See 1.1.4**). Therefore, DUBs increase the complexity of the ubiquitin system through their ability to remove or edit ubiquitin linkages.

1.1.2 Complexity and diversity in ubiquitination

While all linkages are known to exist in cells, the best characterised of these linkages are K48 and K63-linked polyubiquitin chains. K48-chains are the canonical signal for protein degradation by the 26S proteasome (Thrower et al., 2000), whereas K63-chains do not signal proteasomal degradation but are involved in intracellular signalling or directing proteins to the endosomal lysosomal pathway (Ikeda and Dikic, 2008). The functions of the other chain types, which all exist in cells, are less well defined (Xu et al., 2009; Yau and Rape, 2016). Linear chains have a specific role in immunity and are required for NF-κB activation (Shimizu et al., 2015). These chains are formed by the LUBAC E3 ligase complex, and have a structure very similar to K63-linked chains, which are also involved in NF-κB signaling (Shimizu et al., 2015). Of the other chain linkages, K11 are the next most abundant (Xu et al., 2009) and have been shown to be involved in cell cycle control (Jin et al., 2008), regulation of the hypoxia response (Bremm et al., 2014) and ER-associated degradation (ERAD)(Xu et al., 2009). Interestingly, K11-chains may also have non-degradative outcomes involved in cell signaling, including haematopoiesis (Dao et al., 2012) and the immune response (Qin et al., 2014). How K11-chains are recognised in cells is not known.

K6, K27, K29 and K33-chain linkages are all present in cells in low concentrations, however their abundance increases with proteasomal inhibition, indicating they may have a role in proteasomal degradation (Xu et al., 2009). Whether they form homotypic linkages or mixed chains is not clear, but the dimeric structures of these less abundant ubiquitin linkages have been resolved

and they do have distinct conformations (Castaneda et al., 2016; Kristariyanto et al., 2015; Michel et al., 2017), suggesting that they can act as specific signals within the cell. Indeed, K6 and K27 linkages have been shown to be involved in DNA replication and repair (Gatti et al., 2015; Morris and Solomon, 2004) and K29 and K33 linkages are de-ubiquitinated by TRABID, a DUB involved in Wnt signaling (Licchesi et al., 2011).

In principle, the diversity of ubiquitin chains is increased by the possibility of mixed linkages forming heterotypic chains, which may be encoded within a single lysine chain or form branched structures. Initially, it was observed that mixed ubiquitin linkages may actually protect ubiquitinated proteins from degradation (Kim et al., 2007; Kim et al., 2009), but more recently Meyer and Rape (Meyer and Rape, 2014) showed that heterotypic K48/K11-linked chains may be a superior proteasome degradation signal compared to homotypic K48-linked chains. Heterotypic chains may also have non-degradative roles, such as the identification that mixed K63 and K11-linkages are necessary for the efficient internalization of MHC Class I molecules from the cell surface (Boname et al., 2010). Therefore, it is possible that other forms of heterotypic ubiquitin linkages will have specific cellular functions, but currently these remain to be determined.

Lastly, the presence of multiple lysine residues within a substrate allows several sites of ubiquitination which maybe modified with multi-monoubiquitination, (Dimova et al., 2012; Kravtsova-Ivantsiv et al., 2009) multiple chains of the same linkage (Lu et al., 2015) or potentially of different linkages, adding further complexity to the ubiquitin signal. One of the first examples relating to complex ubiquitin modifications was observed in studying endocytosis, where multiple monoubiquitination of receptor tyrosine kinases led to internalisation and lysosomal degradation (Haglund et al., 2003). More recently, Lu et al, suggest that the number of polyubiquitin chains formed on a protein substrate can influence the rate of protein degradation (Lu et al., 2015).

1.1.3 Recognition of polyubiquitin chains by ubiquitin binding proteins

The recognition of polyubiquitin chains by UBPs allows polyubiquitin signals to be decoded and facilitates their desired outcome (Hurley et al., 2006). UBPs contain ubiquitin binding domains (UBDs), a diverse group of protein regions that can bind ubiquitin either in mono or polyubiquitinated form. Most UBDs are comprised of a single α-helix that binds to ubiquitin through a hydrophobic region within the ubiquitin moiety at isoleucine 44 (I44 patch) (**Table 1.1**). The hydrophobic interaction between monoubiquitin and UBDs is of low affinity (mM range) but the formation of polyubiquitin chains or multi-monoubiquitins considerably increases the strength of this interaction (**Table 1.1**). Aside from chain length, the lysine linkage of the chains can also alter the affinity of UBDs for ubiquitin. The second UBA (ubiquitin associated) domain of Rad23 binds K48-linkages with higher affinity than K63-chains (Elsasser et al., 2004). Furthermore, UBPs often contain several UBDs, which increase the avidity for ubiquitin and may alter the specificity for different lysine linked chains. For example, the combined VHS and UIM domains of ESCRT0 proteins, Hrs and STAM1 have a higher affinity for K63-chains compared to K48-chains (Ren and Hurley, 2010). The Nathan lab recently showed that the Rad23 proteins, hHR23A and B, which contain two UBA domains, bind with high selectivity to K48-linked chains, whereas the ESCRT0 proteins, containing VHS, DUIM and UIM domains, bind only to K63-linked chains (Nathan et al., 2013). Whether K11-linked chains are recognised by linkage-selective UBPs is unknown.

Name of UBD	Source protein	Affinity to Ub (K_d)	Structure	Binding to Ub
UBA (ubiquitin associated)	Dsk2 hHR23A	2nd UBA 8μM for $K48Ub_4$ and 28μM $K63Ub_4$	Compact 3α helical bundles with conserved hydrophobic patch on α1 and α3 helix	Ile^{44} hydrophobic patch of Ub binds α1 and α3 conserved hydrophobic patch
UIM (ubiquitin-interacting motif)	Vps27 S5a	100μM-2mM	Single α-helix around conserved alanine residue	Binds Ile^{44} hydrophobic patch of Ub
MIU (motif interacting with ubiquitin)	Rabex-5	30μM	α helical– around conserved alanine residue	Binds Ile^{44} hydrophobic patch of Ub in opposite orientation to UIM
DUIM (double-sided UIM)	Hrs		α helical– two UIM sequences are interlaid on a single helix	Both faces are capable of binding Ile^{44} hydrophobic patch of Ub
CUE (coupling of ubiquitin conjugation to endoplasmic reticulum degradation)	Vps9 Cue2		3 α helical bundles	Binds Ile^{44} hydrophobic patch of Ub via conserved hydrophobic residues in C-terminal of α helix
GAT (GGA and TOM)	GGA3 TOM1	100μM	3 α helical bundles	Binds Ile^{44} hydrophobic patch of Ub through two sites: high and low affinity
NZF (Npl4 zinc finger)	Npl4	100μM	30 residue domains around a single zinc binding site	Binds Ile^{44} hydrophobic patch of Ub through Thr-Phe pair of 1st 'zinc knuckle' and hydrophobic residue of 2nd
A20 ZnF (A20 zinc finger)	Rabex-5	12-22μM		Binds a polar patch on Ub centred on Asp^{58}.
UBP ZnF (ubiquitin-specific processing protease zinc finger)	Isopeptidase T	3μM	130 residue domain around single zinc-binding site in N-terminal half fused to an α/β fold	Free C-terminal glycine residue of Ub binds within 'tunnel' of UBP ZnF. Also interaction with Ile^{36} region of Ub
UBZ (ubiquitin-binding ZnF domain)			30 residue domain assumed to bind a single zinc ion via its conserved cysteine and histidine residues	
Ubc (ubiquitin-conjugating enzyme- related domains) Ubcs are also known as E2 enzymes.	UbcH5		150αα catalytic core with α/β fold	Conserved cysteine forms thiolester with Ub C-terminus
UEV (Ubc E2 variant domain)	Vps23 Tsg101	100μM	Lacks catalytic cysteine of Ubcs	Via Ile^{44} patch and also hydrophilic Gln^{62} site of Ub
UBM (ubiquitin-binding motif)		180μM	30 residues centred on invariant Leu-Pro pair	Around Leu^{8} of Ub, near but not overlapping with Ile^{44} region
GLUE (Gram-like ubiquitin binding in EAP45)			Ubiquitin-binding plekstrin homology domain	
JAB1/MPN		380μM	Metalloprotease motif JAMM (JAB1/MPN domain metalloenzyme)	Thought to bind Ile^{44} based on mutational studies
PFU (PLAA family ubiquitin binding domain)	Doa1		2° structure predictions suggest similar structure to UEV	

Table 1.1: Structures and binding affinities of known UBDs. *Adapted from Hurley et al, Biochemistry Journal, 2006.*

1.1.4 Deubiquitinating enzymes and selective disassembly of ubiquitin chains.

Polyubiquitin chains can be disassembled by DUBs, of which there are six classes: 1, ubiquitin C-terminal hydrolases, 2, ubiquitin specific proteases (USPs), 3, ovarian tumour proteases (OTUs), 4, Josephins, 5, MINDY (MIU-containing novel DUB family), and 6, the JAB1/MPN/MOV34 metalloenzymes (JAMMs) (**Figure 1.2**). The first 5 DUB families are cysteine proteases, while JAMMs require zinc for their catalytic activity (Komander et al., 2009). Most DUBs have the capacity to disassemble ubiquitin chains irrespective of the ubiquitin linkage

involved, as observed with the several USPs (Komander et al., 2009). USP5, which cleaves free ubiquitin chains, recognizes the C-terminal diglycine motif regardless of the ubiquitin linkage (Reyes-Turcu and Wilkinson, 2009). However, chain specific DUBs have been identified, particularly within the OTU family, including the K11-specific DUB, Cezanne (Bremm et al., 2010) and the predominantly K29-specific DUB, TRABID (Tran et al., 2008; Virdee et al., 2010), and a K63-specific metalloprotease DUB, AMSH (McCullough et al., 2004). What determines the DUBs ability to discriminate between different chain types is unclear but may be steric, as shown by the structural resolution of AMSH bound to K63 dimers (Sato et al., 2008).

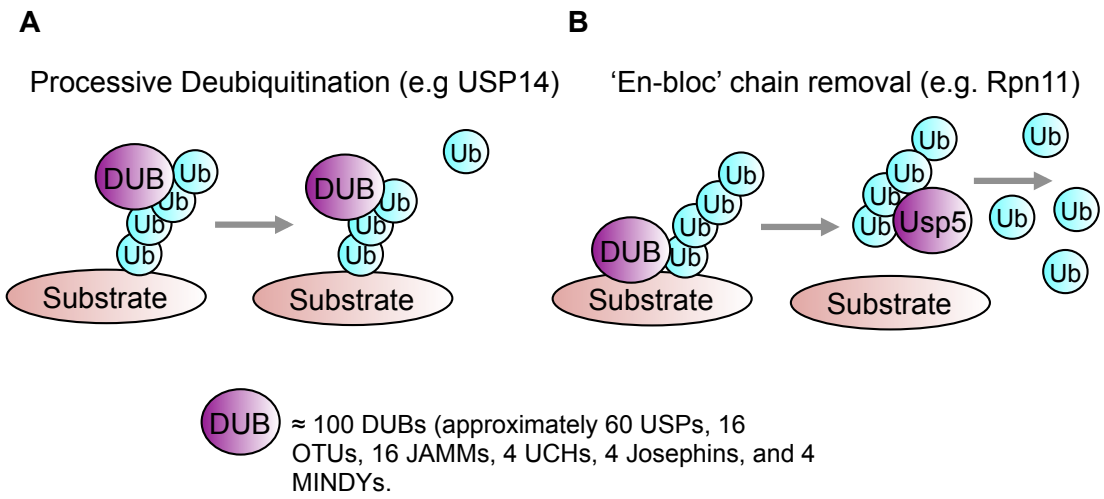

Figure 1.2: Deubiquitination. Schematic of the removal of ubiquitin chains by deubiquitination. **(A)** Most DUBs remove chains in a processive manner, such the proteasome-associated DUB USP14. **(B)** Some DUBs can remove the whole ubiquitin chain, 'en-bloc'. A well validated example is the proteasome-associated DUB, Rpn11. The polyubiquitin chain is disassembled by DUBs that recognize the free C-terminus (e.g. USP5). The approximate number of mammalian DUBs are also indicated.

1.2 The Proteasome.

The 26S proteasome is a large, 2.5MDa, degradative complex within the cell, composed of the 20S catalytic chamber and the 19S regulatory particle (**Figure 1.3**)**.** The proteasome recognizes ubiquitinated substrates, which bind to the 19S regulatory particle (Peth et al., 2010). The ubiquitin chains are then removed by proteasome-associated DUBs (Finley, 2009), and the protein unfolded in an ATP-dependent process, prior to opening of the 20S gate, and translocation into the 20S catalytic chamber (**Figure 1.3**) (Peth et al., 2010; Smith et al., 2007; Smith et al., 2011), where proteolysis takes place. The resulting polypeptides are released within the cell to be recycled, but an additional important function of the proteasome is to provide peptides that are trimmed to 9-13 amino acids in length and loaded onto MHC Class I molecules to be presented on the cell surface for immune surveillance (Kisselev et al., 1999; Rock et al., 2002).

1.2.1 Proteasome composition

The proteasome consists of a 20S catalytic subunit and a regulatory 19S cap (**Figure 1.3**). There is a gate between the subunits, which allows transmission of unfolded substrates into the 20S catalytic chamber. This gate is in a closed conformation when substrates are not bound to the 19S, and is only opened following activation of the AAA ATPases in the 19S ring. In addition, the proteasome binds several DUBs and UBPs, which can modulate the binding of ubiquitinated substrates and disassembly of the polyubiquitin chains.

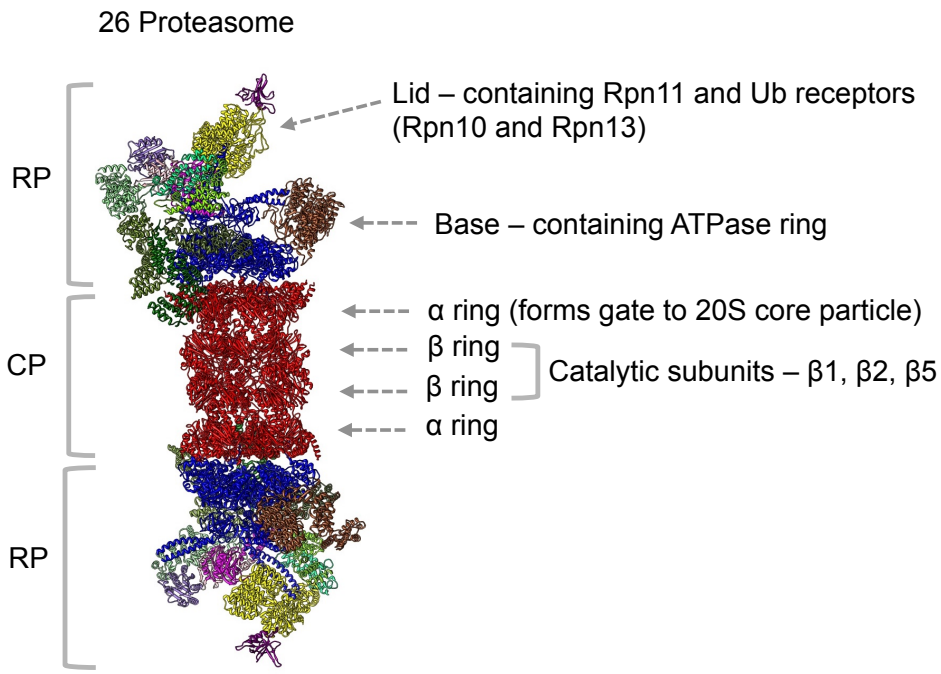

Figure 1.3: The 26S Proteasome. Ribbon cartoon structure of the 26S proteasome based on the *S. Cerevisiae* cryo-EM structure by Beck et al (Beck and Baumeister, 2016) of the removal of ubiquitin chains by deubiquitination. The proteasome comprises a 2.5MDa complex of the 19S regulatory particle (RP) and the 20S catalytic core particle (CP). Ubiquitin receptors are present in the RP lid. The ATPase subunits in the base control gate opening of the 20S α-ring. Peptidase activity occurs in the β-rings and is encoded in the three subunits (β1, β2, β5). The DUB Rpn11 forms part of the lid. Ubp6 (USP14) was not resolved in this structure. The other mammalian DUB, Uch37, is not present in yeast.

1.2.2 Functions of the 19S regulatory particle.

The 19S cap is formed of a base, containing the ATPase subunits, and the lid, which binds polyubiquitinated substrates via two ubiquitin receptors, Rpn10 and Rpn 13 (**Figure 1.3**) (Husnjak et al., 2008; Peth et al., 2010; Schreiner et al., 2008).

The 19S lid is composed of nine subunits, Rpn3, 5, 6, 7, 8, 9, 11, 12 and 15. Rpn11 is a JAMM metalloprotease which combines with Rpn8 to form a heterodimer with DUB activity (Pathare et al., 2014; Worden et al., 2014) and is responsible for deubiquitination of substrates. Rpn11 is thought to cleave polyubiquitin chains proximally from the ubiquitinated substrate prior to unfolding and translocation to the 20S, enabling rapid degradation of the substrate (Verma et al., 2002; Yao and Cohen, 2002).

The 19S base contains six AAA-ATPase subunits (termed Rpt1-6), two scaffolding proteins (Rpn 1 and 2), and ubiquitin binding receptors (Rpn10 and Rpn 13) (**Figure 1.3**). Rpn10 was the first ubiquitin receptor to be identified in the 26S proteasome (Deveraux et al., 1994), however deletion mutants of Rpn10 in yeast were still viable indicating that there were other ubiquitin receptors within the proteasome (van Nocker et al., 1996). Subsequently, other proteasome-associated UBPs were identified in yeast, including Rpn13 (Husnjak et al., 2008), Rpt5 (Lam et al., 2002) and Sem1 (Paraskevopoulos et al., 2014). Rpn1 was also identified as being responsible for binding and recruitment of ubiquitinated substrates (Elsasser et al., 2002), but it was only recently demonstrated that Rpn1 not only binds ubiquitin via its UBD but also binds the UBL domain of a DUB, Ubp6 (USP14 in mammals), by another Rpn1 UBL-binding site, facilitating substrate deubiquitination (Shi et al., 2016).

The ATPase subunits of the 19S base catalyse the unfolding of the protein substrate, the opening of the narrow gate into the 20S and the translocation of the unfolded substrate into the 20S catalytic chamber in an ATP-dependent process (Smith et al., 2005).

Up to three DUBs are known to associate with the proteasome: Rpn11, USP14 (Ubp6 in yeast), and Uch37. Rpn11 forms a core component of the 19S as discussed above (**Figure 1.3**). The functions of Uch37, which is not found in less diverse organisms such as yeast, are obscure. USP14, which is always found bound to proteasomes, is only active when associated with the complex (Leggett et al., 2002) and seems to be involved in the processive removal of ubiquitin molecules from the distal end of chains. Whether USP14 is rate-limiting for proteasome-mediated degradation or promotes substrate degradation remains unclear. The Finley group show removal of USP14 increases protein degradation of Cyclin B1 and other substrates, and that an USP14 inhibitor can promote the removal of aggregate prone proteins (Lee et al., 2016; Lee et al., 2011). However, Peth et al showed that USP14 is required for activation of the AAA ATPases and gate opening following deubiquitination of the protein substrate (Peth et al., 2009). Thus, while USP14 is clearly required for proteasome-mediated degradation, the complex nature of its functions remain to be fully determined.

1.2.3 Mechanisms of catalytic action within the 20S

The 20S core particle is responsible for the catalysis of proteins and is composed of four stacked heptameric rings (**Figure 1.3**). The outer rings contain the structural α-subunits which form a narrow entry channel which control substrate entry into the catalytic core (Groll et al., 2000). The requirement for entry into the 20S is governed by the gate, and only de-ubiquitinated, unfolded polypeptides are able to pass into the catalytic chamber. The flux of small fluorescent tri-peptides through the gate and their subsequent cleavage can be used in *in vitro* assays as a measure of gate opening (Peth et al., 2009).

The two inner rings contain the catalytic β-subunits (β1, β2 and β5) (**Figure 1.3**), which are caspase, trypsin and chymotrypsin like peptidases that degrade the substrate into small peptides. These peptides are then further degraded by intracellular proteases, or can be presented at the cell surface by MHC Class I, enabling the immune system to survey the intracellular protein content of cells (Rock et al., 1994).

1.2.4 Recognition of ubiquitinated proteins by the 26S proteasome

It is well established that the canonical signal for proteasomal degradation is K48-linked polyubiquitin chains (Thrower et al., 2000). However, the proteasome in isolation does not seem to have the ability to distinguish between different polyubiquitin linked chains (Hofmann and Pickart, 2001; Kim et al., 2007; Saeki et al., 2009). Isolated proteasomes bind to K48 and K63-linked chains *in vitro* and degrade the substrates. Thus Rpn10 and Rpn13 do not appear to have any lysine linkage specificity. However, in cells, K63-polyubiquitinated conjugates are protected from proteasomal degradation by K63-selective UBPs, such as the ESCRT0 complex, which bind strongly to the conjugates and block their binding to the 19S (Nathan et al., 2013). Interestingly, prior to my studies, it was not known whether other ubiquitin lysine linkages, such as K11, could bind to the 26S proteasome.

Aside from specific recognition of ubiquitin chains, proteasome associated proteins may be able to promote ubiquitin chain formation on certain substrates. In yeast, the proteasome-associated ubiquitin ligase, Hul5

(mammalian orthologue, UBE3C), can extend the ubiquitination of bound ubiquitinated substrates by acting as an E4 (Crosas et al., 2006). Furthermore, Ubp6 (USP14 orthologue) preferentially deubiquitinates substrates modified by Hul5, suggesting that Hul5 and Ubp6 may function in opposition to each other to modify proteasome-associated degradation of certain substrates (Crosas et al., 2006).

1.2.5 What are the minimal requirements to signal proteasome-mediated degradation?

Until recently, it is was thought that a chain of four ubiquitins was the minimum linkage length required for proteolysis by the proteasome (Thrower et al., 2000). However, this has recently been disputed, and may depend on the nature of the substrate or the number of ubiquitin chains. The Ciechanover group showed that a single ubiquitin moiety can facilitate the degradation of several protein substrates *in vitro* (Shabek et al., 2012). Furthermore, recent studies have shown that multiple monoubiquitination of cyclin B1 and the NF-κB precursor, p105 (Dimova et al., 2012; Kravtsova-Ivantsiv et al., 2009) can trigger proteasomal degradation or proteasomal processing. Single molecule studies (Lu et al., 2015) confirm these findings and go on to explore the requirement of several short polyubiquitin chains as a more efficient signal for proteasome-mediated degradation than a single tetraubiquitin chain. However, it is important to note that multiple monoubiquitination of other cell cycle substrates, securin and geminin, did not allow degradation (Lu et al., 2015) suggesting that proteasome-mediated degradation is not solely ubiquitin linkage specific and is dependent on intrinsic properties of the protein substrate.

The Matouschek lab have shown that an ubiquitin chain is not sufficient to signal proteasome-mediated degradation without the presence of an unfolded region within the protein substrate (Prakash et al., 2004; Yu et al., 2016). Binding of the ubiquitinated substrate occurs via the ubiquitin chain but the proteasomal degradation is initiated at a disorded region within the protein (Prakash et al., 2004; Takeuchi et al., 2007). Interestingly, proteins with UBL domains that lack initiation sites are spared degradation by the proteasome. For example, the

proteasome shuttling factor, Rad23, binds K48-linked ubiquitinated substrates and shuttles them to the proteasome allowing the substrate to be degraded, however Rad23 is spared from degradation due to the lack of a sufficient unstructured region to act as an initiation site (Fishbain et al., 2011).

1.3 Lysine-11 polyubiquitin chains.

K11-linked polyubiquitin chains are of interest as they are the third most abundant linkages in cells (5-10% in humans, 20-30% in yeast) (Jacobson et al., 2009; Xu et al., 2009), have a unique structure compared to K48, K63 or linear-linked chains (Castaneda et al., 2013), and have putative roles in many cellular pathways (**Figure 1.4**). The best characterized role for K11-linkages is in the cell cycle. In mitosis, the anaphase promoting complex/cyclosome (APC/C) E3 ligase catalyses polyubiquitin chain formation on cell cycle proteins, cyclinB1 and securin, signalling the degradation of these mitotic regulators (Min and Lindon, 2012; Pines, 2011). In addition K11-chains have been shown to accumulate in cells released from mitotic arrest, when the APC/C is most active (Matsumoto et al., 2010). *In vitro* studies have identified that several E2 enzymes are required for the ubiquitination of APC/C substrates. Either UbcH10 or UbcH5 are required to initiate ubiquitination of CyclinB1, and the polyubiquitin chain formed is then extended by the K11-specific E2 enzyme, Ube2S (Garnett et al., 2009; Jin et al., 2008). Therefore, it was initially thought that K11-chains were required for the degradation of cell cycle checkpoint proteins. Interestingly however, knockdown of Ube2S by siRNA-depletion in HeLa cells only delayed exit from mitosis when drug-induced perturbations (e.g. monastrol) of the cell cycle were used, and Ube2S was not required for normal mitosis (Garnett et al., 2009). In addition, Ube2S is not necessary for degradation of ubiquitinated CyclinB1 in *Xenopus* cell extracts, as multiple monoubiquitination of CyclinB1 was sufficient to initiate its proteasome-mediated degradation (Dimova et al., 2012). It is possible that K11-chains are required for degradation, but in conjunction with K48-chains. Recent *in vitro* studies showed that branched K11/K48-chains formed on cell cycle substrates, Nek2A and CyclinA, facilitated proteasomal degradation (Meyer and Rape, 2014).

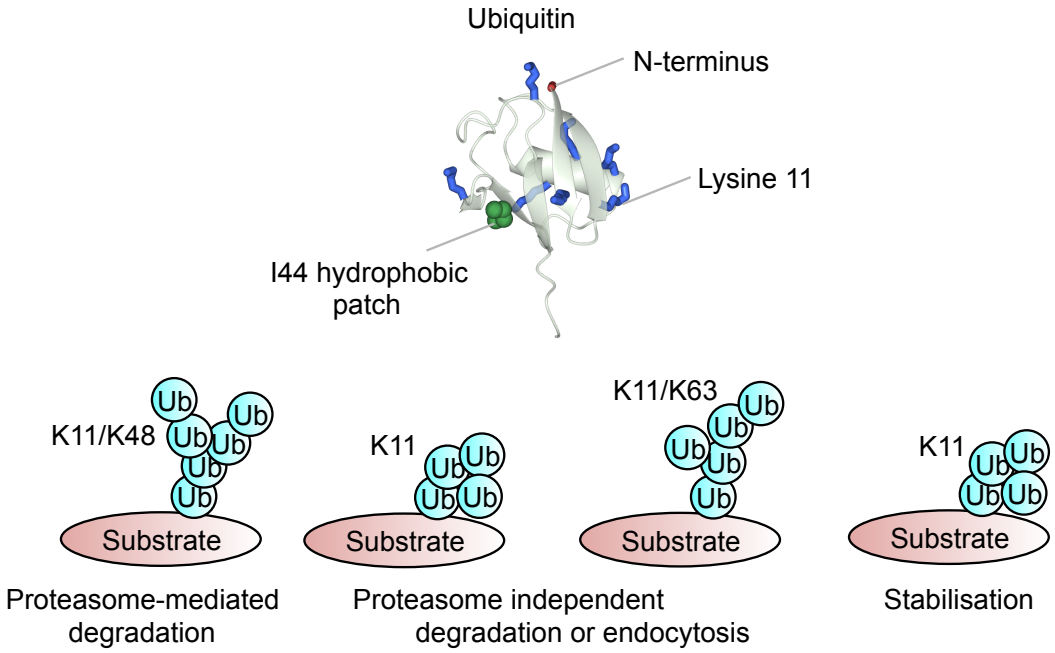

Figure 1.4: K11-polyubiquitin chains and their potential functions. Schematic of the potential outcomes of modifications with K11-linked ubiquitin chains. The position of K11 within the ubiquitin molecule is shown. K11-linked ubiquitin may be involved in proteasome-mediated degradation, proteasome-independent degradation, endocytosis or stabilisation of the protein substrate.

In contrast with the presumed proteasome-mediated degradative role of K11-linkages in the cell cycle, K11-polyubiquitination has been observed in other cellular processes, including ER-associated degradation (ERAD) (Xu et al., 2009), the hypoxia response (Bremm et al., 2014), and even stabilizing proteins such as β-catenin (Dao et al., 2012). Therefore, it is important to establish whether K11-chains are a signal for proteasomal degradation, and if not, to establish how K11-polyubiquitin chains mediate cellular outcomes. I was particularly interested in exploring the hypoxia response pathway, as this was a major focus of the Nathan lab.

1.4 The oxygen sensing pathway

Oxygen is an essential molecule for life and it is therefore important for cells to be able to respond swiftly to changes in oxygen availability. Metazoans have developed an evolutionary conserved mechanism to respond to oxygen

availability, dependent on the Hypoxia Inducible transcription Factors (HIFs) which, under conditions of low oxygen tension (hypoxia,) activate genes involved in glucose uptake, angiogenesis, and redox homeostasis to promote cell survival (Benita et al., 2009; Manalo et al., 2005). Since the identification of these transcription factors nearly thirty years ago, it has become apparent that HIFs are not only involved in a physiological response to promote cell survival and oxygen delivery to tissues, but are also implicated in hereditary cancer syndromes, tumorigenesis, pulmonary hypertension and modulation of immune responses (Kaelin, 2008; Maxwell and Ratcliffe, 2002). Moreover, the regulation of HIFs in aerobic conditions is poorly understood. Consequently, it is of interest to understand how HIFs are tightly regulated.

1.4.1 Hypoxia Inducible transcription Factors upregulate gene expression in hypoxia

HIFs consist of a basic helix-loop-helix motif and a PER-ARNT-SIM domain (Wang and Semenza, 1995). There are three different isomers of HIF: HIF1, HIF2 and HIF3. HIF1 and HIF2 have the same domain architectures, and are post translationally regulated similarly, whereas HIF3 encodes a truncated form of the transcriptional activating domains, incapable of activating genes to the same extent as the other isoforms (**Figure 1.5**). HIF1 is ubiquitously expressed, whereas HIF2 is more specific, being localized in blood vessels, lungs, liver, kidneys, interstitial cells and the neural crest (Wiesener et al., 2003). However, HIF1 and HIF2 can be expressed in the same cells, where they can differentially activate target genes. The mechanism for the selective activation of HIF2 target genes is not known. HIF1 was first implicated in the regulation of oxygen responses, when it was identified as a transcription factor which bound to the erythropoietin (EPO) gene promoter under hypoxic conditions, activating EPO transcriptional activity (Semenza, 1994). How HIF1 activity was regulated by oxygen, at that time, was unclear.

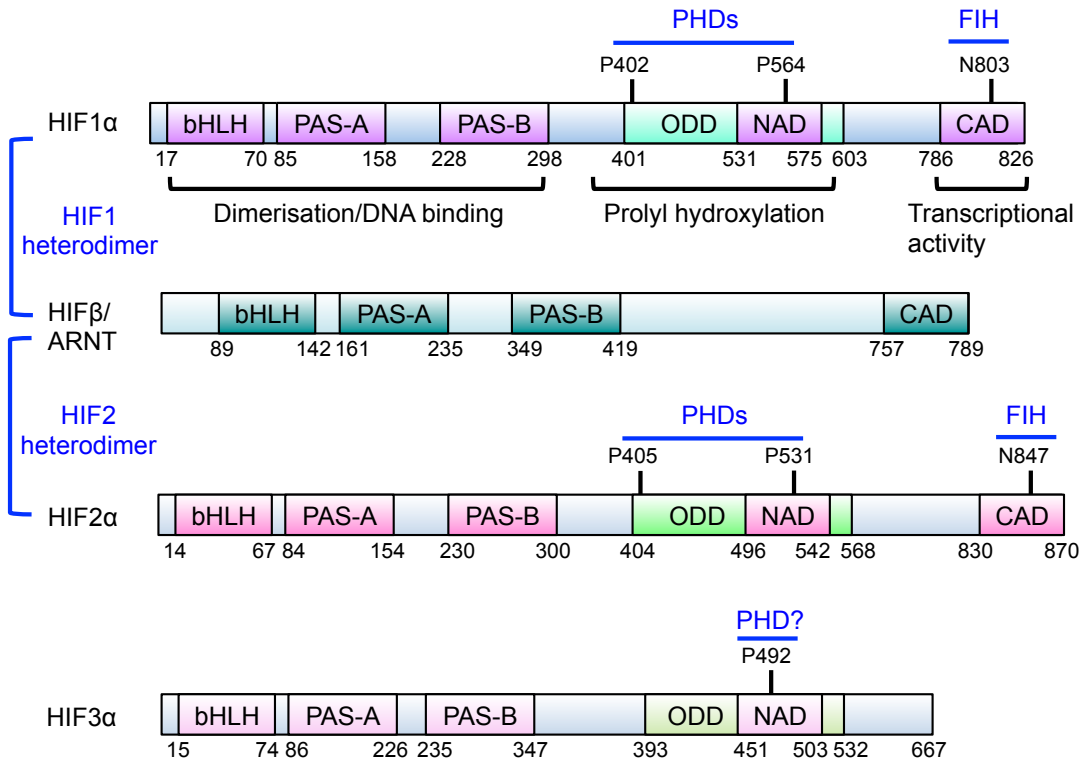

Figure 1.5: The hypoxia inducible transcription factors. Schematic illustrating the domain architecture of the HIF subunits. HIF1α and HIF2α share a similar domain architecture with the bHLH-PAS domains (DNA binding), the ODD and the N- and C-activating domains (NAD and CAD). Both HIF1α and HIF2α form a heterodimer with HIFβ (ARNT). The prolines hydroxylated by PHDs are indicated. FIH hydroxylates a conserved asparagine within the CAD (N803 and N847) to regulate transcriptional activity. HIF3α has many isoforms, which may encode the bHLH-PAS domains and a putative ODD. No CAD has been identified. It is postulated that P492 is hydroxylated by PHDs but this remains controversial.

The first purification of HIF identified two proteins of 120 and 92kDa corresponding to an α and β subunit, respectively (Wang and Semenza, 1995). Later, it was discovered that HIFβ (aryl hydrocarbon receptor nuclear translocator (ARNT)) is constitutively expressed in normoxia and can participate in other transcriptional responses, whereas HIFα (referring to both HIF1α and HIF2α isoforms) forms the regulatory component (discussed in **1.4.2** below).

During hypoxia, HIFα binds with HIFβ to form a heterodimer which translocates to the nucleus and binds to a HIF Response Element, a consensus sequence of 5'-RCGTG-3' in the promoter of hypoxia-responsive genes (Benita et al., 2009). Between one and two hundred genes are upregulated by binding of the HIF heterodimer to the HRE in target genes, including those responsible for

stimulating angiogenesis, such as the Vascular Endothelial Growth Factor (VEGF) (Kelly et al., 2003; Pugh and Ratcliffe, 2003). Studies in arterial endothelial cells (ECs) using a constitutively active form of HIF1α, have shown that targets of HIF include transcription factors, cytokines, prostaglandins and collagens, enabling tissue reperfusion when oxygen is scarce (Manalo et al., 2005). HIF1 also acts as a metabolic regulator, coordinating a change from oxidative metabolism to glycolysis by increasing expression of glucose transporters (GLUT1), glycolytic enzymes, and enzymes associated with the tricarboxylic acid (TCA) cycle (e.g. Lactate Dehydrogenase (LDHA) and pyruvate dehydrogenase kinase) (Semenza, 2012).

1.4.2 Hypoxia Inducible transcription Factors are regulated by hydroxylation and ubiquitination

HIFs have been shown to be highly sensitive to oxygen concentration, increasing as oxygen concentrations decrease between 2 and 1% and reaching a peak at 0.5% oxygen concentration (Jiang et al., 1996), and their cellular abundance is controlled by post-translational regulation of the HIFα subunit.

In normoxia, HIFα is degraded in a two stage process involving the prolyl hydroxylation of two conserved proline residues in the oxygen degradation domain of HIF1α (Bruick and McKnight, 2001; Epstein et al., 2001) which allows recognition of these hydroxylated prolines by the Von Hippel Lindau E3 ligase complex, VHL (Maxwell et al., 1999) (**Figure 1.6**). VHL subsequently polyubiquitinates three conserved lysine residues in the HIF1α ODD (Paltoglou and Roberts, 2007; Tanimoto et al., 2000), leading to proteasome-mediated degradation of HIF1α and thereby preventing undesirable activation of the hypoxic response during conditions of normoxia.

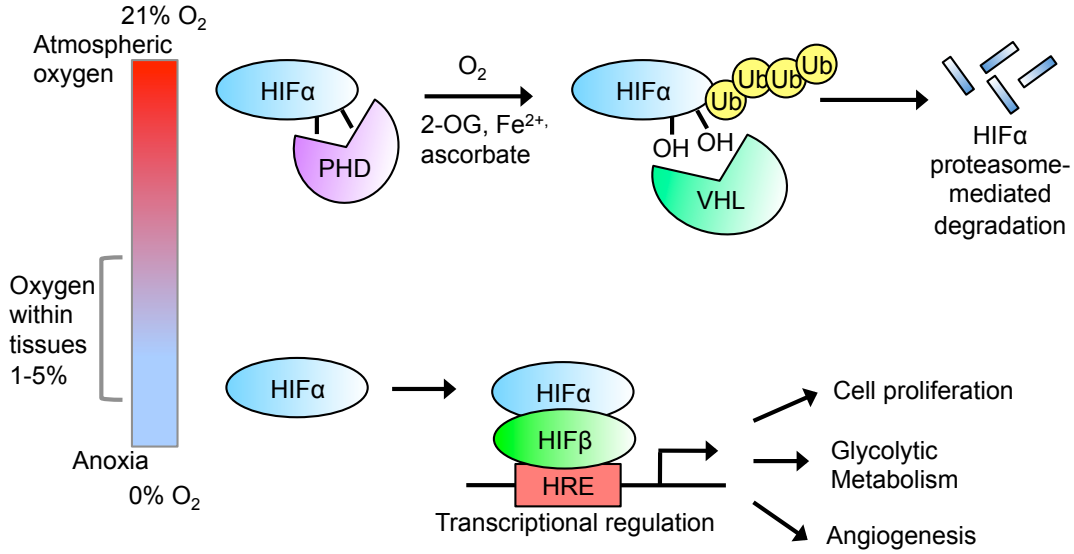

Figure 1.6: Regulation of HIF stability by prolyl hydroxylation and ubiquitination. Schematic illustrating the regulation of the HIFα subunit by prolyl hydroxylation and ubiquitination. When oxygen is abundant HIFα undergoes prolyl hydroxylation by the PHDs. Prolyl hydroxylated HIFα is recognized by the VHL E3 ligase which ubiquitinates HIFα leading to its rapid proteasome-mediated degradation. When oxygen is scarce, PHDs are no longer active and HIFα is stabilized. HIFα then forms a heterodimer with HIFβ, translocates to the nucleus and activates genes containing HREs. PHD activity is not only dependent on oxygen, but also requires 2-OG, ferrous iron and ascorbate. It is also noteworthy that oxygen concentrations in tissues are much lower than atmospheric oxygen.

Interestingly, the ubiquitin post-translational modification of HIF1α was identified prior to the identification of HIF1α prolyl hydroxylation by PHD enzymes. As discussed, HIF1α was first shown to be involved in the transcriptional regulation genes by examining the hypoxic activation of EPO (Semenza, 1994) and p53 (An et al., 1998). By expressing specific regions of HIF1α in HEK293 cells and measuring degradation by pulse chase, Huang et al were able to identify the oxygen sensitive region of HIF1α, termed the oxygen dependent degradation domain (Huang et al., 1998). They identified that amino acids 401 to 603 of HIF1α contained two PEST-like sequences (two proline, glutamic acid, serine, threonine) that were required for proteasome-mediated degradation of the α subunit in normoxia (Huang et al., 1998).

Subsequently, the E3 ligase required for the ubiquitination and degradation of HIF1α was identified by the Ratcliffe group, as the product of the

Von Hippel-Lindau (VHL) tumour suppressor gene, pVHL (Maxwell et al., 1999). VHL disease is a hereditary cancer syndrome characterised by angiogenic tumours which show features in common with activation of hypoxia inducible genes (Iliopoulos et al., 1995). Maxwell et al showed that renal carcinoma cells deficient in the VHL gene (RCC4 cells) stabilized HIF1α and this was reversed by expression of VHL in RCC4 cells. Furthermore, HIF1α and HIF2α were found to associate with VHL by immunoprecipitation, following treatment with proteasome inhibitors or under hypoxic conditions (Maxwell et al., 1999), suggesting that VHL was required for the ubiquitination of HIFα. Biochemical studies by the Kaelin and Ratcliffe groups and others showed that VHL associates with Elongins A and B, and cullin-2 (Cul-2) (Kamura et al., 1999; Maxwell et al., 1999; Pause et al., 1997) thereby forming an SCF (Skp-1-Cullin-F-box protein) E3 ligase complex (Hershko and Ciechanover, 1998). The E2 enzyme used in these studies was UbcH5, however the E2 enzyme required for VHL ubiquitination in cells is not known.

The first lysine within the HIF1α ODD observed to be modified by VHL was lysine 532 (K532) (using Flag-tagged HIFα mutants in HEK293 cells) (Tanimoto et al., 2000). Subsequently, two other lysine residues, K538 and K547, were found to be modified by VHL (Paltoglou and Roberts, 2007). Indeed, it seems that all these lysines are required for efficient ubiquitination and proteasome-mediated degradation of HIF1α, as the ODD was only fully stabilized when point mutations were made in each of the three lysines (Paltoglou and Roberts, 2007). Interestingly, Paltoglou et al also identified an ODD degradation product when VHL-mediated degradation was impaired suggesting that there may be a VHL-independent mechanism of HIF1α degradation (Paltoglou and Roberts, 2007).

It was noted that HIF was stabilised not only by hypoxia, but also by iron chelation and cobalt ions, suggesting that a ferro-protein oxygen sensor maybe involved in HIF regulation. In addition, the inhibition of HIF degradation by 2-oxoglutarate (2-OG, also known as α-ketoglutarate)- analogues, the requirement for oxygen, and the binding of VHL to an ODD domain containing proline residues (Ivan et al., 2001; Jaakkola et al., 2001; Masson et al., 2001) suggested

that prolyl hydroxylation by a 2-oxoglutarate dependent dioxygenase maybe required for HIF regulation.

As HIFs are conserved in all metazoans, it was possible to explore their regulation in less diverse organisms, and rapidly identify the dioxygenases required for HIFα degradation. A database analysis in *Caenorhabditis elegans (C. elegans)* identified a conserved 2-oxoglutarate dioxygenase enzyme, egg-laying-defective 9 (EGL-9, EGLN), whose structural predictions suggested that it could bind 2-OG and Fe^{2+} and has the characteristic β-barrel jelly roll motif, common to 2-oxoglutarate dioxygenases. Worms containing inactivating mutations in EGL-9 stabilised HIF1. In addition, recombinant HIF1 incubated with lysates containing either overexpressed or recombinant EGL-9 bound VHL. These reactions were dependent on the addition of Fe^{2+} and 2-OG, and inhibited by hypoxia and cobalt (Epstein et al., 2001).

Concurrently, studies in drosophila identified several 2-oxoglutarate dependent dioxygenases which have human homologues. Recombinant proteins of these five homologues were incubated with a biotinylated HIF1αODD$^{556-574}$ peptide in the presence of Fe^{2+}, ascorbate and 2-OG, and one homologue bound VHL assessed by a ^{35}S-VHL pull down assay (described in **Chapter 5.1**). This 2-oxoglutarate dependent dioxygenase was named HIF prolyl hydroxylase (HPH-1, later named prolyl hydroxylase domain-containing enzyme 1 (PHD1)) and found to have two related paralogs, HPH-2 and 3 (PHD2 and PHD3), which bound VHL under similar conditions (Bruick and McKnight, 2001). When recombinant PHD was incubated with HIF1 peptide, a 16kDa modification was produced, which corresponded to the size of the hydroxylation of HIF1α by mass spectrometry. This hydroxylation reaction was enhanced by addition of Fe^{2+}, ascorbate and 2-OG and inhibited by the hypoxia mimic, cobalt (Bruick and McKnight, 2001), consistent with the known cofactors for 2-OG dependent dioxygenases.

In combination, these studies demonstrated that the regulation of HIF1α in normoxia was dependent on prolyl hydroxylation of two conserved proline residues, Pro402 and Pro564 (**Figure 1.5**), enabling binding of the VHL E3 ligase complex and subsequent ubiquitination of one of three conserved lysine residues, K532, K538 or K547, leading to proteasome-mediated degradation of HIF1α.

1.4.3 The Prolyl Hydroxylase Enzymes

While three PHDs have been identified in humans, PHD2 is the predominant enzyme involved in HIF1α regulation. RNAi-mediated depletion of PHD2 results in increased HIF1α protein expression and activation of HIF1α target genes (Berra et al., 2003). Loss of PHD2 in mice is lethal due to heart or placental defects, but PHD1 and PHD3 null mice are viable (Takeda et al., 2006). Furthermore, PHD2 is ubiquitously expressed whereas PHD1 and 3 expression is more limited, with PHD1 being predominantly expressed in the testes and PHD3 in the heart (Appelhoff et al., 2004; Lieb et al., 2002).

The structure of the PHD enzymes incorporates a two-histidine-one-carboxylate motif which coordinates a catalytic Fe^{2+} iron in its centre (Epstein et al., 2001) and the crystal structure of PHD2 has been resolved (McDonough et al., 2006; Wilkins and Abboud, 2016) (**Figure 1.7**). There are two 2-OG binding sites and one O_2 binding site (Kaelin and Ratcliffe, 2008). The prolyl hydroxylation reaction results in the splitting of O_2, hydroxylation of HIF1α, oxidative decarboxylation of 2-OG to form succinate, and the release CO_2 (**Figure 1.7**). The importance of 2-OG and Fe^{2+} for PHD activity is demonstrated by the use of competitive inhibitors for 2-OG binding, such as the 2-OG analogue dimethyloxalylglycine (DMOG), and the use of the iron chelator, desferrioxamine (DFO).

PHD mutations have been identified as a cause of human disease, including familial erythrocytosis in which patients with a P317R mutation on PHD2 have a substantial loss of function of the PHD2 enzyme resulting in an elevated haematocrit, but normal EPO, and requiring frequent venesection (Percy et al., 2006). Interestingly, mutations in VHL are also linked to erythrocytosis, in particular in the Chuvash population in Russia, but these patients have high EPO levels in addition to a high haematocrit, suggesting that the mechanism of erythrocytosis is different from that of PHD2 mutations (Percy et al., 2003).

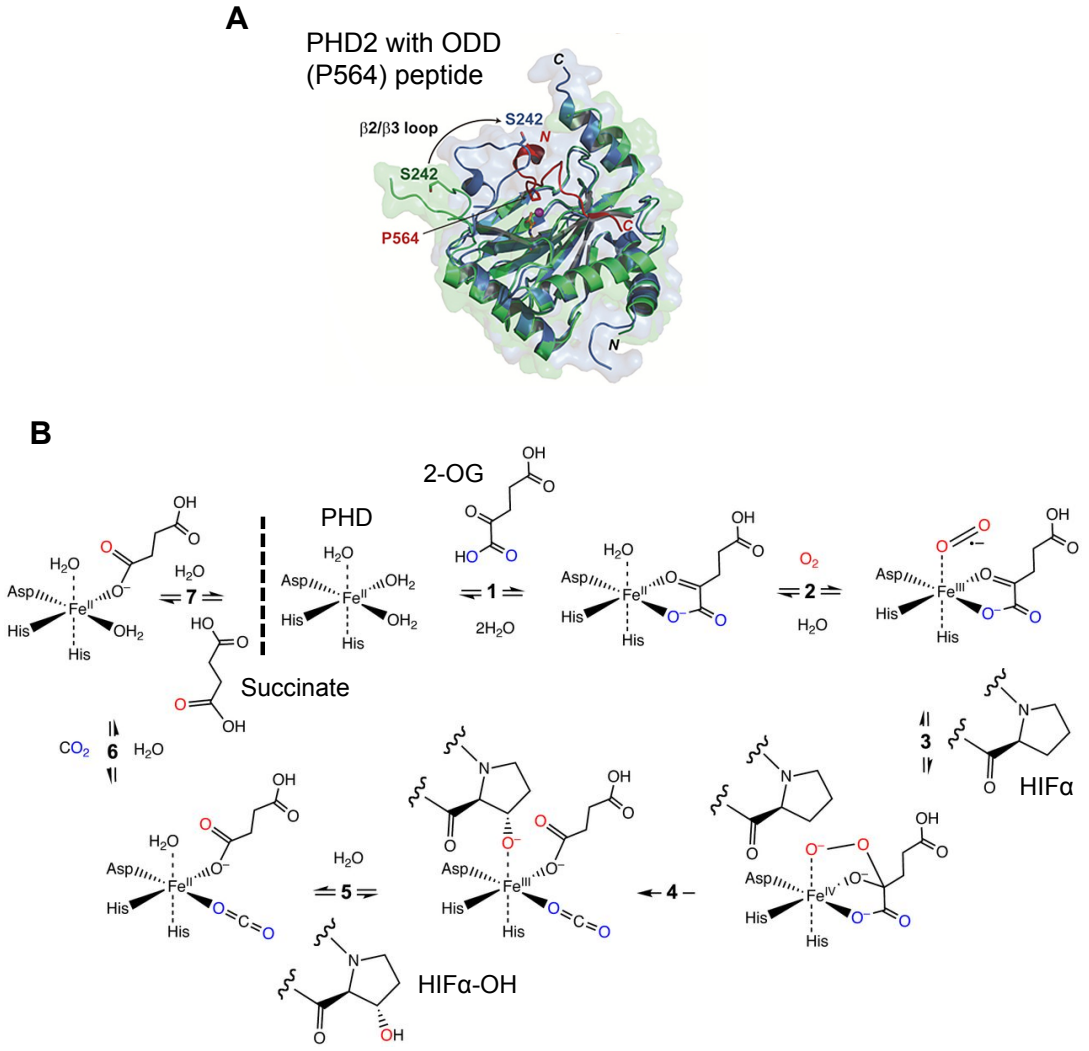

Figure 1.7: PHDs and their mechanism of action. **(A)** Ribbon structural diagram of PHD in complex with the ODD of HIF1α (P564 region peptide). Apo PHD2 is shown in green, PHD2 in complex with ODD is shown in blue. The ODD peptide is shown in red. (*Adapted from (Wilkins and Abboud, 2016)*). **(B)** PHD Enzymatic reaction: (1) The ferrous iron (Fe^{2+}) bound to PHD reacts with 2-oxoglutarate (2-KG). (2) oxygen reacts with the Fe^{2+} and HIF-1α, to form an iron-peroxyhemiketal bicyclic complex. (4) The oxygen is then cleaved, resulting in the hydroxylation of HIF1α. (5) Decarboxylation of 2-OG occurs and the prolyl hydroxylated HIFα is released. (6) carbon dioxide (CO_2) and (7) succinate (from the decarboxylated 2-OG) are then released. The PHD can then recycle and bind 2-OG again. (*Adapted from (Peters et al., 2015)*).

PHD proteins are themselves regulated by SIAH (Seven In Absentia Homolog), a RING E3 ligase (Nakayama and Ronai, 2004) which also regulates an asparagine hydroxylase that controls HIF activation, Factor Inhibiting HIF (FIH) (Fukuba et al., 2007). However, despite the ability of SIAH ligases to mediate the proteasomal degradation of only PHD1 and 3, not PHD2, expression of SIAH2 leads to HIF1α stabilisation in U2OS and HEK293 cells (Moller et al., 2009). In

addition, a small protein inhibitor, derived from the *Drosophila* protein Phyllopod (PHYL), has been shown to bind SIAH leading to reduced degradation of PHD3, increased HIF1α stabilisation and reduced HIF target gene activation (Moller et al., 2009).

1.4.4 The roles of HIFs in physiological contexts and in disease.

The most well described functions of HIFs relate to their activation of genes involved in metabolism, angiogenesis, redox homeostasis and pH regulation (Benita et al., 2009; Manalo et al., 2005). However, they are increasingly implicated in cell fate determination and regulation of immune responses (Maltepe et al., 2005; Mutoh et al., 2012; Palazon et al., 2014). While a detailed analysis of all the physiological functions of HIFs is beyond the scope of this thesis, it is of relevance to discuss the role of HIFs in physiological regulation of metabolism and the role of HIFs in cancer.

In normoxic conditions, oxidative phosphorylation allows generation of ATP from glucose in the mitochondria. However, when oxygen is reduced, cells switch to glycolysis (Semenza, 2012) either in order to limit cellular damage from reactive oxygen species (Zhang et al., 2008) or due to the decrease in oxygen availability. This physiological response to hypoxia is necessary to enable cell survival and a major function of HIFs is to upregulate genes involved in glucose uptake and redox homeostasis, allowing this switch to glycolysis (Benita et al., 2009; Manalo et al., 2005). HIF1 mediates the upregulation of: (i) glucose transporters (GLUT1) and glycolytic enzymes which convert glucose to pyruvate (ii) pyruvate dehydrogenase kinase (PDHK), which prevents conversion of pyruvate to Acetyl Coenzyme A (Acetyl CoA) by inhibition of pyruvate dehydrogenase (PDH) thereby preventing entry of Acetyl CoA into the TCA cycle in mitochondria, and (iii) lactate dehydrogenase (LDH), which converts pyruvate to lactate (Semenza, 2013). HIF1 also upregulates genes which enable selective mitochondrial autophagy, BNIP3 (Zhang et al., 2008) and BNIP3L (Bellot et al., 2009), thereby reducing the availability of mitochondria for oxidative phosphorylation. These HIF mediated modifications in energy metabolism

prevent the oxidation of proteins, lipids and nucleic acids by reactive oxygen species (ROS), which would lead to cell destruction and, ultimately cell death.

The first indication that HIFs were important in tumour formation, related to the identification of HIF activation in renal cell carcinomas (Kondo et al., 2002) (**discussed in 1.4.7**). Indeed, over 90% of renal cell carcinomas have mutations in VHL (Cowey and Rathmell, 2009). Subsequent studies in other hereditary tumour conditions also suggested that HIFs were important for tumour formation, such as mutations in the TCA cycle enzymes succinate dehydrogenase (SDH), fumarate hydratase (FH) and isocitrate dehydrogenase (IDH) (Hewitson et al., 2007a), primarily through metabolic activation of HIF1α (**discussed in 1.4.6**). However, these germline mutations may also affect other 2-oxoglutarate dependent dioxygenases, which may contribute to tumorigenesis (**discussed in 1.4.5**). Thus, whether HIFs can really be termed oncogenes is debatable, as in some cases tumour suppressor functions have been observed, whereby deletion of HIF1α lead to increased tumour growth of ES cells injected into mice (Carmeliet et al., 1998).

1.4.5 PHDs as members of the 2-OG dependent dioxygenase family

While PHDs are mainly involved in HIF regulation, they form part of a large group of 2-OG dependent dioxygenases (2-OG-DDs) of which there are more than 60, which have diverse biological roles. All 2-OG-DDs are characterised by a double-stranded β helix fold (jelly roll) and a Fe^{2+} binding motif, and their enzymatic activity relates to an oxygen-dependent reaction in which O_2 is split into two atoms, one resulting in oxidation of a substrate and the other enabling oxidative decarboxylation of 2-OG to form succinate and CO_2 (Loenarz and Schofield, 2008).

The first 2-OG-DD identified was collagen prolyl hydroxylase (CPH) (Hutton et al., 1967). CPH catalyses prolyl-4-hydroxylation of specific proline-containing motifs in collagen which leads to stabilisation of a collagen triple helix (Radmer and Klein, 2006). Interestingly, the requirement for ascorbate (vitamin C) as a cofactor explains the incidence of scurvy in those lacking vitamin C and the resulting connective tissue damage. A further prolyl hydroxylase catalyses

prolyl-3-hydroxylation of collagen causing destabilisation of the collagen triple helix (Myllyharju and Kivirikko, 2004).

More recently, important roles for 2-OG-DDs have been identified in the epigenetic modification of genes by demethylation of histones. Histone methylation, by histone methyl transferases, mostly occurs on lysine residues of chromatin and results in transcriptional silencing or activation, thereby modifying gene expression (Klose et al., 2006). This methylation can be mono, di or tri-methylation. JumonjiC (JmjC) domain-containing histone demethylases (JHDMs), which are members of the 2-OG-DD family, form the largest group of histone demethylases, catalysing the removal of all three states of methylation, by binding Fe^{2+} and 2-OG and hydroxylating the methyl group on chromatin which is released as formaldehyde (Klose et al., 2006).

FIH is a JmjC domain-containing protein which can hydroxylate asparagine residues, including the HIF1α asparagine 803 (Lando et al., 2002). This asparagine hydroxylation prevents HIF1α from binding the co-activators p300 and CREB binding protein (CBP) inhibiting transcriptional upregulation of HIF1 target genes (Loenarz and Schofield, 2008)

Further evidence of the importance of 2-OG-DDs is evidenced by their role in DNA demethylation or repair. DNA methyl transferases (DNMTs) covalently modify the DNA base, cytosine, by forming 5-methylcytosine (5mC). This epigenetic modification results in a transcriptionally repressed state. Recent work has identified that Ten-eleven translocation (TET) enzymes are members of the 2-OG-DD family, capable of catalysing the oxidation of 5mC to 5-hydroxymethylcytosine (5hmC). Subsequent oxidation by TET enzymes can lead to 5-formyl cytosine (5fC) and 5- carboxylcytosine (5caC), which may all be recognised by different DNA binding proteins (Kohli and Zhang, 2013).

While TETs and JHDMs require oxygen for catalytic activity it has been debated whether they respond to changes in oxygen availability in cells. Originally, it was assumed that TETs and JHDMs functioned at lower oxygen tensions than HIFs. However, recently Thienpont et al, have shown that TETs are sensitive to oxygen availability and that decreased availability of oxygen leads to decreased TET activity, independent of levels of HIF or competing metabolites (Thienpont et al., 2016).

1.4.6 Metabolic regulation of PHDs and other 2-OG-dependent dioxygenases

While the oxygen sensitivity of different 2-OG-DDs is still debated, it is increasingly evident that they are susceptible to changes in oxidative phosphorylation and TCA molecule metabolites.

Oxidative phosphorylation occurs in mitochondria. Under aerobic conditions, glucose is converted to pyruvate and oxidatively decarboxylated to form Acetyl CoA. This enters the tricarboxylic acid (TCA) cycle in which ATP is generated from Acetyl CoA by a series of oxidation-reduction reactions (**Figure 1.8**). A four carbon molecule, oxaloacetate, initiates the first step in the TCA cycle by condensing with a two carbon Acetyl CoA unit to form citrate. The 6 carbon citrate is oxidatively decarboxylated to form 5 carbon 2-OG, forming NADH and releasing CO_2. This oxidative decarboxylation occurs again converting 5 carbon 2-OG to 4 carbon succinate, with the formation of NADH and release of CO_2. Oxaloacetate is regenerated from succinate with the formation of NADH, $FADH_2$ and GTP. Electrons have therefore been removed from Acetyl CoA and transferred to NADH and $FADH_2$, these are then released by the electron transport chain via membrane proteins which generate a proton gradient across the membrane which enables formation of ATP from ADP and phosphate.

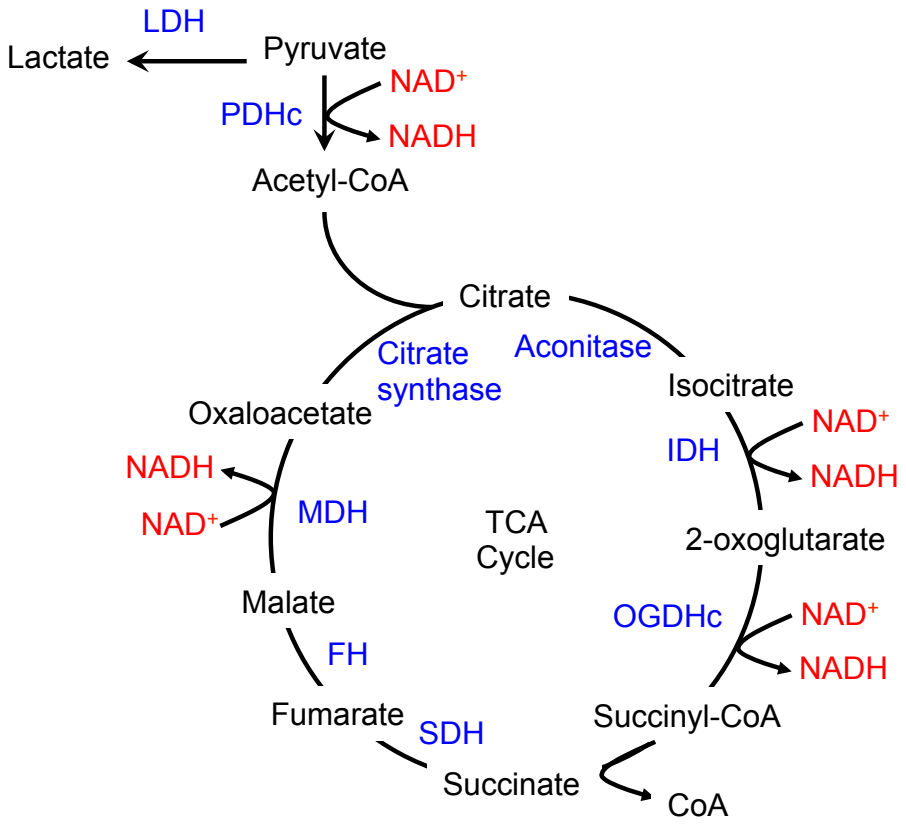

Figure 1.8: The TCA cycle. Schematic representation of the TCA cycle. Essentially, the oxidation of Acetyl-CoA drives NADH and small molecule metabolite precursors (e.g. succinate) for oxidative phosphorylation. NADH is produced by three enzymes within the TCA cycle: isocitrate dehydrogenase (IDH), the 2-oxoglutarate dehydrogenase complex (OGDHc), and malate dehydrogenase (MDH). NADH is also released by the pyruvate dehydrogenase complex (PDHc) with the conversion of pyruvate to acetyl-CoA. LDH=lactate dehydrogenase, FH=fumarate hydratase, SDH=succinate dehydrogenase.

As 2-OG is central to the TCA cycle, it is possible that alterations in TCA enzymes change the cellular abundance of 2-OG and modulate PHD and other 2-OG-DD activity. To explore this possibility, the Schofield group performed biochemical experiments to investigate whether TCA intermediates are able to bind to PHD2 similarly to 2-OG. TCA intermediates, including fumarate and succinate, were incubated with recombinant $PHD2^{181-426}$ and Fe^{2+} and the complexes formed were analysed by native Electrospray Ionisation MS (ESI-MS). These experiments showed that all TCA intermediates except oxaloacetate and pyruvate were able to form a stable complex with the PHD2-HIF1αODD,. However, when competition assays were performed in the presence of 2-OG,

only fumarate and succinate could compete with 2-OG for active binding sites (Hewitson et al., 2007a).

In support of these biochemical findings, human germline mutations in TCA cycle enzymes, such as SDH, FH and IDH have been linked to tumour formation, potentially through their metabolic activation of HIFs or inhibition of other 2-OG-DDs. Mutations in SDH are associated with development of phaechromocytoma, paraganglionaoma (Eng et al., 2003; Pollard et al., 2005) renal cell carcinoma and papillary thyroid cancer (Neumann et al., 2004). Mutations in SDH, which catalyses the conversion of succinate to fumarate, lead to accumulation of succinate and subsequently HIF1 stabilisation in normoxia (Selak et al., 2005). Inhibition of SDH using SiRNA in HEK293T cells showed stabilisation of HIF1α and activation of the HIF1α target gene BNIP3. *In vitro* prolyl hydroxylation assays using recombinant HIF1αODD, cell extracts, cofactors, and addition of either succinate or the iron chelator, DFO, showed by immunoblot that increasing concentrations of succinate inhibited the hydroxylation of HIF1α. Hence, SDH mutations lead to inhibition of PHD2, causing HIF1α stabilization thereby enabling angiogenesis and the formation of angiogenic tumours (Selak et al., 2005).

Mutations in FH, which catalyses the conversion of fumarate to malate, are linked to leiomyomatosis and renal cell carcinoma (Pollard et al., 2005). As fumarate was able to inhibit PHD2 activity in 2-OG turnover assays (Hewitson et al., 2007a), it was possible that FH mutations lead to tumorigenesis by inhibition of PHD2 causing HIF1α stabilization, similarly to succinate. However, the Frezza group have recently shown that mutations in FH lead to epigenetic modification involving the inhibition of TET-mediated demethylation of the regulatory region of an antimetastatic mRNA, thereby increasing cancer metastasis, independent of HIF1 (Sciacovelli et al., 2016).

Mutations in IDH1 and IDH2, the enzyme which catalyses the conversion of isocitrate to 2-OG, are commonly present in gliomas and also occur in acute myeloid leukaemia. IDH mutations have a reduced ability to catalyse the conversion of isocitrate to 2-OG, thereby decreasing PHD activity and stabilizing HIF1α, (Zhao et al., 2009). However, Dang et al, found that certain glioblastoma IDH mutations (R132H) also led to the spurious formation of a metabolite of

unknown physiological function, the D enantiomer of 2-hydroxyglutarate (D-2-HG) (Dang et al., 2009). Paradoxically, this IDH1 R132H mutation resulted in decreased levels of HIF1α and HIF2α (Koivunen et al., 2012), as the increased levels of D-2-HG increased PHD2 activity but inhibited other 2-OG-DDs (Koivunen et al., 2012).

The identification of D-2-HG in tumours has led to considerable interest in enantiomers of this metabolite. 2-hydroxyglutarate (2-HG) can exist in both the L and D form in metazoans. The metabolite has traditionally been regarded as a by-product of 2-OG metabolism under conditions of oxidative damage, as human germline mutations in the dehydrogenases of 2-HG (L-2-HGDH and D-2-HGDH) cause inborn errors of metabolism characterized by neurological defects and urinary excretion of 2-HG (Oldham et al., 2015). Interestingly, approximately half of all patients with D-2-HG aciduria have mutations in IDH2 resulting in the formation of D-2-HG from 2-OG, rather than mutations in D-2-HGDH (Kranendijk et al., 2012). However L-2-HG aciduria has only been described in patients with mutations in L-2-HGDH.

Following the identification that D-2-HG can alter the activity of 2-OG-DDs, biochemical studies on the enantiomeric forms were undertaken. Studies have shown that both D-2-HG and L-2-HG act as inhibitors of 2-OG-DDs, including the TET methyl cytosine hydroxylases, collagen prolyl-4 hydroxylases and FIH (Chowdhury et al., 2011; Figueroa et al., 2010; Xu et al., 2011). However, the 2-HG enantiomers had opposing effects on PHD enzymatic function, with D-2-HG increasing PHD2 activity, and L-2-HG marginally decreasing PHD2 function (Koivunen et al., 2012). The reasons for these findings are not fully understood but the Schofield group have suggested that non-enzymatic catalysis of D-2-HG to 2-OG may occur *in vitro* (mediated by ferrous-ferric iron and reducing agents such as ascorbate) promoting PHD function (Tarhonskaya et al., 2014).

Several recent cell based studies confirmed the biochemical observations that L-2-HG could modulate the activity of some 2-OG-DDs, and interestingly identified a role for L-2-HG in hypoxia. Metabolomic analysis of pulmonary arterial and smooth muscle cells in hypoxia showed an increase in 2-OG and L-2-HG (Oldham et al., 2015), and this L-2-HG accumulation in hypoxia was due to conversion of 2-OG to L-2-HG by lactate dehydrogenase (Intlekofer et al., 2015).

However, neither group identified a role for L-2-HG modulating a HIF response in cells, and prior to our studies, the role of the 2-HG enantiomers in the HIF pathway remained controversial.

1.4.7 Does VHL have additional functions outside of the HIF pathway?

The efficient VHL-mediated degradation of HIF in normoxia is highly important to prevent unwanted activation of hypoxia-responsive genes (Benita et al., 2009; Berra et al., 2001). Moreover, the identification of germline mutations in VHL and cancer somatic mutations highlight the dominant role of this ligase in regulating HIFs.

Von Hippel-Lindau (VHL) disease is a dominantly inherited cancer syndrome characterised by angiogenic tumours including renal cell carcinomas, haemangioblastomas, phaeochromocytomas and pancreatic islet tumours (Kaelin, 2008). Hereditary VHL disease is characterised clinically as type 1, 2A, 2B and 2C, where type 1 patients have low risk of phaechromocytoma whereas type 2 have high risk (Kaelin, 2008). In addition, type 2 is subdivided into 2A with low risk of renal cell carcinoma (RCC), type 2B with high risk of RCC and type 2C with phaechromocytoma alone (Cowey and Rathmell, 2009). Interestingly, studies suggest that deregulation of HIF2α rather than HIF1α is associated with VHL-null RCC tumorigenesis (Kaelin, 2008), as tumour formation is suppressed in VHL-null RCCs depleted of HIF2α (Kondo et al., 2003). Conversely, overexpression of a HIF2α mutant (P531A), which cannot be bound by VHL, induced tumour formation in VHL reconstituted RCCs (Kondo et al., 2002). However, in families with type 2C VHL disease, characterised by phaeochromocytoma alone, HIF regulation is unaffected (Clifford et al., 2001; Hoffman et al., 2001), suggesting that VHL may have additional targets to HIFs. Furthermore, the observations that PHD mutations activate HIF target genes but do not lead to tumour formation supports the notion that VHL must have additional functions aside from HIF regulation.

Several studies have attempted to assign novel functions to VHL to explain these observations. One possible mechanism is that VHL is required to inhibit Akt kinase activity. Akt is a serine-threonine kinase which promotes

cancer survival and proliferation, including in renal cell carcinomas where VHL is defective (Hager et al., 2009). Guo et al showed that Akt undergoes prolyl hydroxylation by PHD and the subsequent binding of VHL inhibits Akt kinase activity (Guo et al., 2016). In addition, VHL has been implicated in lactate sensing (Lee et al., 2015). Lee et al have shown that lactate, an anaerobic metabolite, can promote a HIF-independent hypoxic response. In normoxia, N-myc downstream-regulated gene 3 protein (NDRG3) is hydroxylated and ubiquitinated by PHD2 and VHL, leading to its proteasome-mediated degradation. However, in hypoxia, lactate accumulates via anaerobic respiration and binds NDRG3 preventing its degradation. NDRG3 then binds c-Raf leading to activation of the Raf-ERK pathway thereby triggering angiogenesis and cell growth in response to hypoxia (Lee et al., 2015). It is still possible that VHL may have additional functions outside of HIF and lactate signalling, relating to its ability to recognise prolyl-hydroxylated motifs in proteins.

1.4.8 Does proteasome independent degradation of HIFα occur?

The proteasomal degradation of HIF1α by VHL ubiquitination is well characterised, however a longstanding, intriguing observation is that HIF1α is stabilised by Bafilomycin A (Baf A), a lysosomal inhibitor which acts by inhibition of the V-ATPase (Lim et al., 2006). It has been suggested that this HIF1α stabilisation by Baf A is mediated by the V-ATPase binding to VHL (Lim et al., 2007), mitochondrial uncoupling (Zhdanov et al., 2012) or chaperone-mediated autophagy (Bremm et al., 2014; Ferreira et al., 2015; Hubbi et al., 2014; Hubbi et al., 2013; Selfridge et al., 2016). However, it is difficult to reconcile this hypothesis with the observations that HIFα is completely stabilised by proteasome inhibition.

In addition to the proteasome-independent degradation of HIFα, there is evidence that VHL may not be the only ligase implicated in regulation of the HIF response as Ferreira et al, suggest that HIF1 may be lysosomally degraded in a VHL-independent fashion by the E3 ligase, CHIP (Stub1), leading to CMA (Ferreira et al., 2015). This observation suggests that ubiquitinated HIFα may be prone to aggregrate formation, and in support of this the Deshaies lab observed

that P97, the AAA ATPase required for extracting ubiquitinated proteins from membrane or complexes, was required for HIF1α degradation (Alexandru et al., 2008). It is therefore plausible that HIF1α is not only degraded in a proteasome-independent manner, but that many other ubiquitin enzymes may also be involved in its regulation.

1.5 Aims of this thesis

My project aims were to determine how different types of K11-polyubiquitin conjugates interact with the 26S proteasome, and to examine whether K11-linkages are recognised by specific UBPs. Furthermore, I wanted to identify the functional outcome of K11-chains by focussing on the hypoxia inducible transcription factor (HIF) pathway. Specifically, my aims were to:

I) Establish *in vitro* systems to generate K11-polyubiquitin chains.

II) Determine if K11-linked polyubiquitin chains are a signal for proteasomal degradation.

III) Elucidate which UBPs bind to lysine-11 linked polyubiquitin chains.

IV) Establish *in vitro* assays to measure HIFα prolyl hydroxylation and ubiquitination.

V) Determine which ubiquitin chain types were formed on HIF1α in normoxia.

Chapter 2: Materials and Methods

2.1 Antibodies and Reagents

The following primary antibodies were used: Mouse monoclonal to Ub (P4D1, Santa Cruz); mouse monoclonal to proteasome 20S α subunits (MCP231, Enzo Life Sciences); mouse monoclonal to cyclin B1 (BD Pharmingen), mouse monoclonal to cdc27 (AF3.1, Santa Cruz); rabbit polyclonal to USP5 (Bethyl Laboratories), mouse monoclonal to Rpn10 (S5a-−18, Enzo Life Sciences); rabbit monoclonal to UBQLN1 (Cell Signaling); mouse monoclonal to ubiquitin (P4D1, sc-8017 Santa Cruz Biotechnology); mouse monoclonal to ubiquitin (FK2, ST-1200 Calbiochem,); affinity purified rabbit polyclonal antibodies to MyosinVI and Tax1BP1 (generated by the Buss laboratory (Buss et al., 1998; Morriswood et al., 2007; Sahlender et al., 2005)); rabbit polyclonal to hydroxyl-proline HIF1α (3434, Cell Signaling); mouse monoclonal to HIF1α (610959, BD Transduction laboratories); rabbit polyclonal to HIF1α (sc-10790, Santa Cruz); rabbit polyclonal to OGDH (HPA020347, Atlas); rabbit polyclonal to Lipoic acid (437695, Calbiochem); mouse monoclonal to βactin (A228, Sigma); rabbit polyclonal to PHD2 (NB100-137, NovusBio); rabbit polyclonal to HIF2α (ab199, Abcam).

The following secondary antibodies were used: Goat anti-mouse HRP (115-035-146, Jackson); goat anti-rabbit HRP (111-035-045, Jackson).

The following reagents were used: Ubiquitin (Boston Biochem); Methyl ubiquitin (Boston Biochem); MG132 (Sigma Aldrich,); Bafilomycin A1 (Alfa Aesar, J61835); DMOG (Sigma-Aldrich, D6395); DFO (Sigma-Aldrich, D9533); (D)-2-HG (Sigma-Aldrich, H8378); (L)-2-HG (Sigma-Aldrich, 90790); α-ketoglutaric acid (Sigma-Aldrich, K1128); Sodium oxamate (Sigma-Aldrich, O2751); Iron II Choride (Sigma-Aldrich, 372870).

2.2 Molecular Biology

2.2.1 Plasmids.

The following plasmids were kind gifts from Fred Goldberg: pET26bHis10-UIM2-S5a (UIM of Rpn10/S5a), pDEST15-UBL-hHR23B, pGEX GST-E6AP, pGEX GST-Nedd4, pGEX4 T2 GST-RAD23B, pET15b-E1, pET15b-His-Ubch5b (Besche et al., 2009; Nathan et al., 2013).

pGEX-6P-1 GST-AMSH (gift from Sylvie Urbe), pET28his-Ube2S (gift from Mark Kirschner), pET28a HA-WT Ncyclin B1-6His pET28a and HA-WT Ncyclin B1 K64 -6His (gifts from Randall King), pGEX PreScission (gift from Lauren Jackson), pCDNA3 HIF1α-HA (gift from Patrick Maxwell), and pHRSIN-pSFFV-HIF2α-Puro (made by Peter Bailey, Nathan lab). pET47b KanR N term His tag 3C and pET49b KanR N term GST tag 3C (gift from Vangelis Christodoulou and Katrin Rittinger).

2.2.2 Plasmids generated using standard restriction enzyme cloning.

pGEX-6P-1 GST-Ube2SΔ. His-Ube2S was a gift from Marc Kirschner (Harvard Medical School). GST-Ube2SΔ was formed by cloning DNA encoding residues 1 to 196 of Ube2S into the bacterial expression vector pGEX-6P-1, using the following primers: Ube2S BamH1 For CGGGA TCCAACTCCAACGTGGAGAACC and Ube2S Not1 Rev TTGCGGCCGCCTACTTGGCCATGGGACCCTCA.

All PCRs were performed according to the manufacturer's protocols using Phusion (NEB) polymerase. The following reactions were typically used.

5X Phusion GC buffer	4μl	1X
10mM dNTPs	0.4μl	200μM each
template DNA	0.5μl	
Forward primer (10μM)	1μl	0.5μM
Reverse primer (10μM)	1μl	0.5μM
DMSO	0.6μl	3%
Phusion DNA polymerase (NEB)	0.2μl	0.02U/μl

Correct insertions were identified by restriction digest and verified by sequencing (Source Bioscience). The pCR TOPO vectors were then digested with the respective restriction enzymes and the inserts ligated into the pGEX-6P-1 backbone (antarctic phosphatase treated) following gel purification using the Roche rapid ligation kit:

0.5μl rapid T4 ligase
5μl 2x buffer
3.5μl insert
1μl vector

pGEX-6P-1 GST-Ube2SUBD was generated by James Nathan (Grice et al., 2015) using the UBD from USP5, similarly to the methods described by Bremm et al (Bremm et al., 2010).

GST-FAM115A or His-FAM115A constructs. FAM115A full length (FL), the flavodoxin-like fold (FD) and putative protease domain (M60) were amplified by PCR from the IMAGE clone template pOTB7 FAM115A (IMAGE ID 3346754, Source Bioscience).

For the GST-tagged versions in pGEX-6P-1 a 5' BamHI site and a 3' NotI site were used. For the His-tagged versions in pET15b a 5' NdeI site and a 3' BamHI site were used. The PCR products were ligated into pCR TOPO Blunt (Invitrogen) as a subcloning and sequencing vector. Correct insertions were identified by restriction digest and verified by sequencing (Source Bioscience). The pCR TOPO vectors were then digested with the respective restriction enzymes and the inserts ligated into the pGEX-6P-1 or PET15b backbone (antarctic phosphatase treated) following gel purification using the Roche rapid ligation kit.

2.2.3 Ligation Independent Cloning (also described in Chapter 5.2.1)

All the primers designed for Ligation Independent Cloning are listed in **Appendix 1.**

GST or His tagged FAM115A. Primers were designed with extensions homologous to the LIC vector, pET47b KanR N term His tag 3C or pET49b KanR pET49b Kan^R N term GST tag 3C. Forward primer: 5' CAG GGA CCC CGT-specific FAM115A sequence 3' and reverse primer: 5' GGC ACC AGA GCGTTA–specific FAM115A sequence 3'. Primers were designed to two regions of FAM115A: the FD-like region and M60 region. This resulted in 48 primer pairs for each region. These were separated by 1% agarose DNA gel electrophoresis at 100V and analysed by ChemiDoc. These primer pairs were expanded by sequential PCR. 10µg LIC vector was linearised using 50U KpnI (NEB), 50U SacI (NEB), 1X NEB 1.1 buffer (NEB) in 100µl reaction at 37°C for 3 hr. Both LIC vector and PCR products were PCR purified (Qiagen QIA Quick spin column kit) according to manufacturer's instructions. Both the linearised vector and PCR product was T4 DNA polymerase treated as follows: 0.01pmol PCR product in EB buffer (10mM Tris-HCl pH8.0), 1X T4 DNA Polymerase Buffer (NEB), 6U T4 DNA Polymerase (NEB) and 2.5mM dATP (NEB) was incubated at 22°C 30 min, 75°C 20 min in a PCR thermocycler; 1.5µg linearised vector, 1X T4 DNA Polymerase buffer (NEB), 3U T4 DNA Polymerase (NEB) and 2.5mM dTTP (NEB) was incubated as described for PCR insert above. The LIC vector and PCR products were then annealed as follows; 50ng vector was added to 0.02 pmol insert and incubated at 22°C for 5 min in a PCR thermocycler then 6.2mM EDTA was added and the mixture incubated for a further 5min. As there were several inserts, this was performed in a 96 well format. Annealed vector and insert were then transformed into BL21 DE3* Gold *E. coli* as described below.

His-HIF1α^{ODD}. His-HIF1α^{ODD} primers were designed with extensions homologous to the pET47b LIC vector. Forward primer: 5' CAG GGA CCC CGT-specific HIF1α sequence 3' and reverse primer: 5' GGC ACC AGA GCGTTA-specific HIF1α sequence 3'. Primers were designed to include the Oxygen Dependent Degradation domain and this resulted in 8 primer pairs. The vector was

linearised, vector and PCR products purified, T4 DNA polymerase treated, and annealed using methods described above.

GST-HIF1α^{ODD}. Primers were designed with extensions homologous to the pET49b LIC vector. Forward primer: 5' CAG GGA CCC CGT-specific HIF1α sequence 3' and reverse primer: 5' GGC ACC AGA GCGTTA-specific HIF1α sequence 3'. Primers were designed to include the Oxygen Dependent Degradation domain and this resulted in 8 primer pairs. The vector was linearised, vector and PCR products were purified, T4 DNA polymerase treated, and annealed using methods described.

His-HIF2α^{ODD}. HIF2α primers were designed with extensions homologous to the pET47b LIC vector. Forward primer: 5' CAG GGA CCC CGT-specific HIF2α sequence 3' and reverse primer: 5' GGC ACC AGA GCGTTA–specific HIF2α sequence 3'. Primers were designed to include the Oxygen Dependent Degradation domain and this resulted in 8 primer pairs. The vector was linearised, vector and PCR products were purified, T4 DNA polymerase treated, and annealed as described.

2.3 Biochemistry

2.3.1 SDS-PAGE and immunoblotting

Proteins were visualised by heating with 6x SDS loading buffer at 90°C for 5 min and separating by SDS-PAGE electrophoresis using Tris Glycine buffer at 200V. Total protein was analysed using Simply Safe Blue Coomassie Stain (Thermofisher).

Immunoblotting was performed by transferring protein from SDS-PAGE gel to PVDF membrane at 100V for 1 hr and visualising specific proteins by incubation with primary antibody conjugated to Horse Radish Peroxidase (HRP) or subsequent incubation with secondary antibody conjugated to HRP as specified in the text. The membrane was incubated with SuperSignal West Pico or Dura Enhanced Chemiluminescent Substrate (Thermofisher) for 5 min,

washed twice with 0.2% PBST for 5 min and chemifluorescence visualised by radiography using X-ray film (Fuji Film).

2.3.2 High throughput protein expression of GST-FAM115A in E. coli using LIC and protein purification

GST-FAM115A. pET47b GST-FAM115A was transformed into BL21 DE3* Gold *E. coli* at 4°C for 10min, 42°C for 25 sec, 4°C 30 sec and then SOC medium added and the culture incubated 37°C for 1 hr in a shaking incubator. Cultures were then plated onto warmed agar plates containing 30µg/ml kanamycin at 37°C for 18 hr. Two colonies were grown per construct in deep well blocks in enriched media (10mg/ml N-Z-amine AS, 5mg/ml yeast extract, 50mM $MgSO_4$, 50mM PO_4, 50mM NH_4Cl, 5mM Na_2SO_4, 0.5% glycerol, 0.05% glucose) and protein expression was induced using 0.5mM IPTG at 20°C overnight. Cultures were lysed *in situ* using lysozyme and DNAaseI and lysates added to filter columns capable of binding His, GST and Strep tags. Bound proteins were washed and eluted before protein concentration was assessed by SDS-PAGE and stained with Coomassie.

2.3.3 Bacterial protein expression and purification.

GST-E6AP. pGEX GST-E6AP was transformed into BL21 DE3* *E. coli* as described, and plated onto warmed agar plates containing 100µg/ml ampicillin 37°C incubator overnight. Two colonies were grown in 5ml LB, 100µg/ml ampicillin at 37°C for 7 hr in shaking incubator. 5 ml culture was added to 50 ml LB, 100µg/ml ampicillin at 37°C overnight in shaking incubator. 10 ml overnight culture was added to 1l LB, 100µg/ml ampicillin at 37°C in shaking incubator until OD 0.4-0.6, measured by nanodrop. Protein synthesis was then induced with 0.1mM IPTG 16°C overnight. Cultures were centrifuged 4,500rpm 10 min at 4°C and pellets washed in PBS, 1mM DTT, transferred to 50ml falcon and centrifuged at 3,750rpm at 4°C for 30min (Beckmann 8:1000), before being stored at -80°C. The cell pellet was thawed on ice and resuspended in 20ml PBS, 1mM DTT. Cells were vortexed to ensure they were fully resuspended and 30ml PBS, 1mM DTT added. 50ml resuspended cells were lysed in cell disruptor 30,000 PSI resulting in 100ml final volume. Lysed cells were centrifuged at

30,000rpm at 4°C for 1 hr (Beckmann 45Ti). Supernatants were passed through a 45µM filter and incubated with 3ml equilibrated GSH Sepharose slurry (1:1 resin: PBS, 1mM DTT) for 2 hr at 4°C on rotator. Purification was continued in 4°C cold room and the resin/ filtered lysate suspension was then passed over a 20 ml filter column (Biorad), and the flow through (FT) collected. The resin was washed in 3 x 20ml PBS with 1mM DTT, followed by 2 x 20ml TBS (1mM DTT_. Finally, the washed resin with E6AP bound was resuspended in 3.5ml TBS, with 1mM DTT, and 10% glycerol. 200l aliquots were stored at -80°C.

GST-Nedd4. pGEX GST-Nedd4 was transformed, expressed and purified as described for ***GST-E6AP*** above.

His-UbcH5b. His-UbcH5b was transformed and expressed as described for ***GST-E6AP*** to the point of cell lysis, with the following exception: protein expression was induced with 0.5mM IPTG for 3 hr at 37°C in shaking incubator. Cell pellets were lysed in Binding Buffer (25mM Hepes pH 7.5, 500mM NaCl, 1mM DTT, 20mM imidazole) in the cell disruptor as described for GST-E6AP. Lysed cells were centrifuged at 30,000rpm at 4°C for 1 hr (Beckmann 45Ti). Supernatants were passed through a 0.45µm filter and incubated with 2ml equilibrated NiNTA resin in 100ml bottle with magnetic stirrer at 4°C for 2 hr. Purification was continued in 4°C cold room. The resin/filtered lysate suspension was passed over a 20ml filter column (Biorad) and the flow through (FT) collected. Resins were washed in 20ml Elution Buffer 50mM (EB: 25mM Hepes pH 7.5, 500mM NaCl, 1mM DTT, 0.025% NP-40, 50mM imidazole) to elute bacterial chaperones. UbcH5b was eluted in 12ml EB 100mM (25mM Hepes pH 7.5, 500mM NaCl, 1mM DTT, 0.025% NP-40, 100mM imidazole) and 1ml fractions collected in 1.5ml eppendorfs until no protein was no longer detected in the eluate (tested by Bradford reagent (Biorad)). This procedure was repeated with EB 200mM (25mM Hepes pH 7.5, 500mM NaCl, 1mM DTT, 0.025% NP-40, 200mM imidazole) and 1ml fractions collected in 1.5ml eppendorfs. Finally, the resin was washed in EB 500mM (25mM Hepes pH 7.5, 500mM NaCl, 1mM DTT, 0.025% NP-40, 500mM imidazole) to remove all bound proteins. Protein concentration was assessed by SDS-PAGE and fractions containing His-UbcH5b

at around 17kDa were pooled in 10,000MWCO Snakeskin dialysis membrane (Pierce) and dialysed against 1l HEPES buffer (20mM HEPES pH 7.5, 10% glycerol, 150mM NaCl, 5mM $MgCl_2$, 1mM DTT) overnight 4°C with magnetic stirrer and repeated for 2 hr in 1l fresh HEPES buffer the following day. Protein purity was assessed by SDS-PAGE, protein concentration was assessed by nanodrop, and aliquots were stored at -80°C.

His-Ube2S. His-Ube2S was transformed, expressed and purified as described for ***His-UbcH5b***.

GST-tagged Ube2SΔ and Ube2SUBD. A truncation mutant of Ube2S, or a similar truncation fused to the UBD of USP5 were expressed in BL21 DE3* *E. coli* and induced using 0.1mM IPTG 16°C O/N. GST-Ube2SΔ was purified as for GST-E6AP. For the Ube2SUBD protein, the cells were lysed in 270mM Sucrose, 50mM Tris pH7.5, 1mM DTT and 1 tablet Roche EDTA free protease cocktail in 50ml using a cell disruptor (30,000Psi lysis, 15,000Psi washes), and centrifuged at 30,000rpm for 45 min at 4°C. The supernatants were filtered through a 0.2µm filter and incubated with 2 ml equilibrated GSH Sepharose resin (GE Healthcare) 2 hr 4°C. The resins were then washed with 100ml high salt buffer (500mM NaCl, 25mM Tris-HCl pH7.5, 1mM DTT) and 100ml low salt buffer (150mM NaCl, 25mM Tris-HCl pH7.5, 1mM DTT) and incubated with 1.2mg/ml PreScission protease (GE Healthcare) on rotator 4°C overnight. The suspension was applied to a 20ml Biorad column and the PreScission-cleaved Ube2SUBD was collected. The resin was washed with 5ml low salt buffer and the eluate collected until no further protein was present (assessed by Bradford reagent (Biorad)). The eluted and cleaved Ube2SUBD was concentrated to half original volume using Vivaspin 10,000MWCO column and assessed by nanodrop and SDS-PAGE. Aliquots were stored at -80°C. This technique was modified from Bremm et al, (Bremm et al., 2010).

GST-AMSH. pGEX6P1-AMSH was a kind gift from Sylvie Urbe (University of Liverpool). The protein was expressed and purified as for ***GST-Ube2SΔ***, and PreScission protease cleavage was used to cleave the N-terminal GST tag.

GST-CyB1-NT^{K64}. An N-terminal peptide of Cyclin B1 with a single lysine at 64 and GST tag (CyB1-NT^{K64}) was generated from the CyB1-NT^{K64}-His tagged vector, which was a gift from Randall King (Harvard Medical School)(Dimova et al., 2012). This construct was transformed and expressed in BL21 DE3* *E. coli* and the cells were induced using 0.5mM IPTG 37°C for 3hr. The cells were lysed in 25mM Hepes pH7.4, 500mM NaCl, 1mM DTT, 0.025% NP40 and 20mM imidazole using cell disruptor, (30,000Psi lysis, 15,000Psi washes) and centrifuged 30,000rpm 45min 4°C. The supernatant was filtered through a 0.2µm filter and CyB1-NT^{K64} purified using a HT Trap crude 3ml column (GE Healthcare), at 0.5ml/min into 25mM Hepes pH7.4, 500mM NaCl, 1mM DTT, 0.025% NP40 and 500mM Imidazole. 0.5ml fractions were collected in a 96 well plate and protein concentration was assessed by SDS-PAGE. Fractions containing CyB1-NT^{K64} at 36kDa, were pooled and dialysed against 20mM Hepes pH 7.2, 10% glycerol, 150mM NaCl, 5mM $MgCl_2$ and 1mM DTT at 4°C using 3,000MWCO Snakeskin dialysis tubing (Pierce.) CyB1-NT^{K64} was concentrated using Vivaspin 15,000MWCO centrifugal filter columns (Millipore) until desired concentration achieved and assessed by nanodrop and SDS-PAGE. Aliquots were stored at -80°C.

GST-PreScission. pGEX PreScission was a kind gift from Lauren Jackson (University of Vanderbilt). The protein was transformed, expressed and purified as described for ***GST-CyB1-NT^{K64}*** above.

His-HIF1α solubility testing. Two colonies were grown per construct in 5ml LB broth with 50µg/ml kanamycin and protein synthesis induced using either 0.5mM IPTG at 37°C for 3h or 0.1mM IPTG at 20°C overnight. Pre and post-induction cultures were centrifuged and cell pellets lysed using freeze/thaw lysis in 100µl *E. coli* lysis buffer (20mM Tris-HCl pH8.0, DNAaseI (Sigma-Aldrich), lysozyme (Sigma-Aldrich).) The lysate was then divided in two: 50µl was kept as the whole lysate and 50µl was centrifuged 14,000rpm 5min to separate soluble and insoluble fractions. All samples were analysed by SDS-PAGE and stained

with Coomassie blue. ***His-HIF1α$^{ODD530-652}$*** was chosen for large-scale purification due to its solubility and size.

His-HIF1α$^{ODD530-652}$. A His-tagged protein encoding residues 530-652 of hHIF1α was expressed in BL21 DE3* *E. coli* and induced using 0.5mM IPTG 37°C for 3hr. Cells were lysed in TBS (20mM Tris-HCl pH 7.4, 150mM NaCl, 1mM DTT) in 50ml using a cell disruptor, (30,000Psi lysis, 15,000Psi washes) and centrifuged at 30,000 rpm for 45min at 4°C. The supernatants were filtered through a 0.2µm filter and incubated with 500µl equilibrated NiNTA resin 2 hr 4°C on a rotator. The suspension was applied to 20ml filter column (Biorad) and resins were washed in 20 ml TBS. Protein was eluted in 15ml TBS with 200mM imidazole and 1ml fractions were collected. Protein was then eluted in 15 ml TBS with 500mM imidazole and the eluate collected until no further protein was present (assessed by Bradford reagent (Biorad)). Protein purity was assessed by SDS-PAGE. Fractions containing His-HIF1α$^{ODD530-652}$ at between 16 and 22kDa, were pooled and dialysed against TBS at 4°C using 10,000MWCO Snakeskin dialysis tubing (Pierce.) His-HIF1α$^{ODD530-652}$ was concentrated using Vivaspin 15,000MWCO centrifugal filter columns (Millipore) until desired concentration achieved and assessed by nanodrop and SDS-PAGE. 10% glycerol was added to the protein before aliquoting and storage at -80°C.

GST-HIF1α solubility testing. Two colonies were grown per construct, expressed, lysed and analysed by SDS-PAGE as described for ***His-HIF1α solubility testing*** above. ***GST-HIF1α$^{ODD401-652}$*** was chosen for large-scale purification due to its solubility and size.

GST-HIF1α$^{ODD401-652}$. A GST-tagged protein encoding residues 401-652 of hHIF1α was expressed in BL21 DE3* *E. coli* and induced using either 0.1mM IPTG 16°C O/N or 0.5mM IPTG 37°C for 3 hr. Cells were lysed in PBS, 5mM $MgCl_2$, 1mM DTT in cell disruptor and centrifuged as described above. The supernatant was filtered through 0.45µm filter and GST-HIF1α$^{ODD401-652}$ purified using a GST column (GE Healthcare), at 0.5ml/min into 10mM GSH, PBS, 1mM DTT. 0.5ml fractions were collected in a 96 well plate and protein concentration was

assessed by SDS-PAGE. Fractions containing GST-HIF1α$^{ODD401-652}$ at between 64 and 98kDa, were pooled and dialysed against 20mM Tris pH 7.4, 10% glycerol, 150mM NaCl, 1mM DTT at 4°C using 10,000MWCO Snakeskin dialysis tubing (Pierce.) GST-HIF1α$^{ODD401-652}$ was measured, concentrated and stored as described for ***His-HIF1α$^{ODD530-652}$*** above.

His-HIF2α$^{ODD381-655}$. A His-tagged protein encoding residues 381-655 of human HIF2α was expressed and purified as described above for ***His-HIF1 α $^{ODD530-652}$*** above.

His-E1. pET15b-E1, a kind gift from Fred Goldberg, was expressed, lysed and centrifuged in TBS, as described for ***His-HIF1α$^{ODD530-652}$***. The lysate was then adjusted with a conjugation buffer (20mM Tris-HCl, 20mM KCl, 5mM $MgCl_2$, 1mM DTT, 5mM ATP) to bind to 1ml equilibrated Ub-agarose (Sigma) (30 min, 4°C on a rotator). The resin was washed with 2.5ml 50mM Tris, pH 7.5, 5ml 50mM Tris, pH 7.5, 250mM KCl and then 2.5ml 50mM Tris, pH 7.5, to remove unbound or catalytically inactive E1. To elute the catalytically active E1, the resin was incubated with 3ml 50mM Tris, 2mM AMP, 2mM PPi (disodium pyrophosphate, both made to 0.2M stocks) for 10min on column and the eluate collected. This was repeated. Finally, the resin was washed in 2.5ml 50mM Tris followed by 3ml 0.1M Tris, pH 9.0, 10mM DTT to ensure full elution of the E1. Protein was analysed by SDS-PAGE and eluates containing His-E1 were pooled and dialysed against 500ml 40mM Tris pH 8.0, 2mM DTT at 4°C using 3,000MWCO Snakeskin dialysis tubing (Pierce.) overnight and then repeated in the morning. Concentration was assessed by nanodrop and SDS-PAGE. 10% glycerol was added to the protein before aliquoting and storage at -80°C.

The following proteins were expressed and purified by the Buss and Kendrick-Jones' labs:

His-TAX1BP1. His-tagged hTAX1BP1 (aa291-747) was expressed and purified as described previously (Morriswood et al., 2007).

His-MyosinVI CBD. His-tagged hMyosinVI cargo binding domain (CBD, aa 1034-1253) was purified as described previously (Spudich et al., 2007) however

the NiNTA column was washed with PBS with 100mM imidazole pH7.4 and eluted in PBS with 300mM imidazole pH7.4.

GST-MyosinVI CBD. GST-tagged hMyosinVI cargo binding domain (CBD, aa 1034-1253) was purified as described previously for GST-tagged Myosin fusion proteins (Buss et al., 1998) and purified on glutathione sepharose 4B (GE Healthcare) according to manufacturer's instructions.

2.3.4 In vitro autoubiquitination reaction

***E6AP autoubiquitination*.** GST-tagged E6AP was ubiquitinated using ubiquitin (50μM), E1 (100nM), UbcH5b (400nM), 4mM ATP and 1mM DTT in TBS for 1hr. The resins were washed 5 x 1ml of TBS (50mM Tris-HCl, pH7.5, 150mM NaCl and 1mM DTT). The reaction was stopped with sample buffer and the autoubiquitination analysed by SDS-PAGE and immunoblotting.

Ube2S autoubiquitination.GST-Ube2SΔ was ubiquitinated using 50nM E1, 4mM ATP, 400nM AMSH and 50μM Ub in conjugation buffer (150mM NaCl, 50mM Tris pH 7.4, 1mM DTT, 1mM $MgCl_2$) for 4hr or O/N. The resins were washed 5 x 1ml of TBS (50mM Tris-HCl, pH7.5, 150mM NaCl and 1mM DTT.) Ubiquitination was analysed by SDS-PAGE and immunoblotting.

Cyclin B1 ubiquitination. GST-CyB1-NT^{K64} (3μM) was ubiquitinated using E1 (300nM), Ube2C (2.5μM), Ube2S (0.9μM), ubiquitin (150μM), 20μl APC/C /cdc27 beads, UBAB buffer (25mM Tris-HCl pH7.4, 50mM NaCl, 10mM $MgCl_2$, and 100mM DTT) and 1.5μl energy mix (375mM creatinine phosphate, 50mM ATP, pH8, 50mM $MgCl_2$.) The ubiquitinated GST-CyB1-NT^{K64} was then bound to glutathione Sepharose resin, washed and analysed by SDS-PAGE and immunoblotting.

Alternatively, 5μM GST-CyB1-NT^{K64} was ubiquitinated using recombinant APC/C (kind gift from David Barford, (Zhang et al., 2013)) using a reaction containing the following: 40mM Tris (pH 7.4), 10mM $MgCl_2$, 0.6mM DTT, 250nM E1, 125nM to 1.25μM Ube2C, 900nM Ube2S, 40nM APC/C, 2mM Cdh1, 50μM Ub, 5mM ATP, and 0.25mg/ml BSA. Reaction mixtures were incubated at 37°C for up to 1 hr. The ubiquitinated GST-CyB1-NT^{K64} was then bound to glutathione resin,

washed, and analyzed by SDS-PAGE and western blotting. Ubiquitin linkages formed on GST-CyB1-NT^{K64} were measured by MS.

2.3.5 K11-polyubiquitin chain purification from Ube2SUBD autoubiquitination reaction.

K11-polyubiquitin chains were purified from an Ube2SUBD autoubiquitination reaction based on methods published by Bremm et al (Bremm et al., 2010)). GST-Ube2SUBD was ubiquitinated using 250nM E1, 4.8μM Ube2SUBD, 3mM Ub, 400nM AMSH and 10mM ATP 37°C for 18hr. 5ml of this autoubiquitination reaction were incubated with 60mM DTT 10min on ice to stop the ubiquitination reaction and release non-covalently bound polyubiquitin chains from the UBD. 70ml 50mM NH_4Ac pH4.5 was added to the ubiquitination reaction for 30min on ice to precipitate all proteins except for ubiquitin. Precipitates were removed by passing through a 0.2μM filter and ubiquitin chains were separated using cation exchange chromatography using a Mono-S 5/50 GL column (GE Healthcare), at 0.5ml/min and eluted using 50mM NH_4Ac pH4.5, 1M NaCl at linear gradient in upflow 0-60% Buffer B1 (50mM NH_4Ac pH4.5, 1M NaCl) over 44 column volumes. 0.5ml fractions were collected in a 96 well plate. Polyubiquitin chains were assessed by SDS-PAGE and pooled Ub_4 chains dialysed against 20mM Tris-HCl pH7.4, 1mM DTT at 4°C using 3,000MWCO Snakeskin dialysis tubing (Pierce.) Ub_4 chains were concentrated using Vivaspin 15,000MWCO centrifugal filter columns (Millipore) 500rpm at 4°C until desired concentration achieved and assessed by nanodrop and SDS-PAGE.

2.3.6 Mammalian 26S proteasome purification

Proteasome isolation. The hHR23B-Ubl method was used to extract functional 26S proteasomes from cells (Besche et al., 2009). 2g rabbit skeletal muscle were homogenised in 20ml binding buffer (25mM Hepes, 5mM $MgCl_2$, 1mM DTT, 1mM ATP 10% glycerol and 150mM NaCl), and the insoluble material was removed by low speed centrifugation (15min. 3000rpm at 4°C.) The

supernatant was ultracentrifuged for 1hr at 36,000rpm at 4°C to remove the microsomal fraction. The supernatant was filtered through 0.45µm filter and the cleared cell lysate supplemented with 4mg GST-Ubl and 1ml of equilibrated GSH Sepharose (GE Healthcare.) The suspension was rotated for 2h at 4°C and then poured into a 20ml Econo-Pac column (Biorad.) The Sepharose resin was washed with 3 x 25ml of binding buffer. To elute the proteasomes, the resin was agitated in 500µl of 2mg/ml His-UIM in the binding buffer supplemented with 1mM ATP and incubated for 15min. The eluate was collected and the elution step repeated. To remove the His-UIM the combined eluates were incubated for 20 min at 4°C with equilibrated-NiNTA (Qiagen.) The NiNTA was removed by spinning the eluate through a 0.22µm centrifugal filter unit (Millipore) at 11,000rpm 1min. The eluate containing 26S proteasomes were stored at -80°C.

Measurement of proteasome activity. Suc-LLVY-AMC was purchased from Bachem. Purified proteasomes were incubated with the peptide in a buffer containing 50 mM Tris pH 7.4 with 40 mM KCl, 5 mM MgCl2, 1 mM ATP, and 1 mM DTT. Kinetic fluorescence was measured in triplicate in a 96-well format (Molecular Devices). Proteasome composition was assessed by analysis of 20nM 26S proteasomes on native gels (NuPage, Invitrogen) in a buffer containing 50mM Tris-HCl pH8, 5mM $MgCl_2$, 1mM ATP, 1mM DTT and 50µM Suc-LLVY-amc, incubating at 37°C for 30 min and measuring LLVY-AMC in-gel cleavage using Fuji LAS 3000.

2.3.7 Proteasome binding of ubiquitin conjugates and measurement of 26S activity

The measurements of proteasomes bound to polyubiquitin conjugates were based on methods described by the Nathan lab and others (Nathan et al., 2013). Rabbit 26S proteasomes (10nM) were incubated with polyUb resin-bound conjugates (20nM) in the presence of a proteasome binding buffer (50mM Hepes-KOH pH8, 250mM Potassium acetate, 5mM $MgCl_2$, 0.1% TritonX-100, 2mM DTT, 0.2mg/ml BSA and 2mM ATP), and rotated for 20 min at 4°C. Unbound 26S particles were removed by washing with 400µl binding buffer and 1ml wash buffer (50mM Tris/HCl pH 7.5, 10mM $MgCl_2$, 1mM DTT and 1mM ATP)

at 5,000rpm for 1 at min 4°C. Proteasome activity was measured with 100μM of the fluorescent substrate LLVY-AMC (Bachem) in proteasome reaction buffer (50mM Tris/HCl pH 7.5, 10mM $MgCl_2$, 40mM NaCl, 1mM DTT and 1mM ATP). Cleavage of the peptide was monitored at λ_{ex} 380nm, λ_{em} 460nm 37°C for 60min and expressed as arbitrary fluorescent units (AU).

2.3.8 Competition assay to measure K48 or K11 tetraubiquitin binding to 26S proteasomes.

Rabbit 26S proteasomes (10nM) were incubated with polyUb resin-bound conjugates (20nM) and 75nM, 150nM or 300nM K48 or K11 tetraubiquitin in the presence of binding buffer (50mM Hepes-KOH pH8, 250mM Potassium acetate, 5mM $MgCl_2$, 0.1% TritonX-100, 2mM DTT, 0.2mg/ml BSA and 2mM ATP), and rotated for 20 min at 4°C. 26S particles bound to K48 or K11 tetraubiquitin and unbound 26S particles were removed by washing with 400μl binding buffer (without BSA) and 1ml wash buffer (50mM Tris/HCl pH 7.5, 10mM $MgCl_2$, 1mM DTT and 1mM ATP) as described previously . Proteasome activity was measured by cleavage of the fluorescent substrate LLVY-AMC.

2.3.9 Binding assay to measure lysine-63 or lysine-11 tetraubiquitin conjugate binding to MyosinVI CBD or Tax1BP1

His-Tax1BP1 (500nM) or His-MyosinVI CBD (500nM) were incubated with Ni-NTA agarose resin (Qiagen) in the presence of Tris binding buffer (25mM Tris-HCl pH7.4, 250mM NaCl, 0.1% Triton, 1mM DTT, 0.25mg/ml BSA) and rotated for 30min at 4°C. Increasing concentrations of lysine-63 or lysine-11 tetraubiquitin conjugates were added (25, 50 or 100nM) and incubated at 4°C for 30min on a rotator. Unbound proteins were removed by washing five times with Tris binding buffer and proteins visualised by Western blotting.

2.3.10 Competition assay to measure lysine-63 tetraubiquitin conjugate binding to MyosinVI CBD or Tax1BP1

GST-MyosinVI (300nM) was incubated with Glutathione Sepharose 4B (GE Healthcare) and lysine-63 tetraubiquitin (150nM) in the presence of Tris binding buffer and rotated for 30min at 4°C. The resins were then washed five times before incubating with increasing concentrations of Tax1BP1 (150nM, 300nM, 600nM, 1.2μM, 2.4μM) in the presence of Tris binding buffer and rotated for 30min at 4°C. The resins were then washed five times and proteins visualised by Western blotting.

2.3.11 In vitro hydroxylation assay of HIF1α or HIF2α

1μM HIF1α$^{ODD530-652}$ or 100nM HIF2α$^{ODD381-655}$ was incubated with 50μl HeLa cell extract (see **2.4**) in Tris Buffer (20mM Tris (pH7.4), 5mM KCl, 1.5mM $MgCl_2$, 1mM DTT) for 15 min at 37°C. The reaction was stopped by the addition of SDS loading buffer and the proteins were separated by SDS-PAGE. Hydroxylation was measured using the hydroxyl-proline specific antibody. Measurements of DMOG or L-2-HG were performed similarly except the lysate were pre-incubated with the compounds for 10min at 37°C or 4°C respectively and HeLa lysates pre-incubated with the same volume of reaction buffer (20mM Hepes (pH7.5), 5mM KCl, 1.5mM $MgCl_2$) for 10min at 4°C.

2.3.12 In vitro ubiquitination assay of HIF1α

13.5μM HIF1α$^{ODD401-652}$ was incubated with 500μl washed GSH resin (Tris buffered saline (TBS): 50mM Tris (pH7.5), 150mM NaCl, 1mM DTT) and incubated 1 h 4°C on a rotator followed by centrifuging 10,000rpm 1 min 4°C. Supernatant was aspirated and sample taken. Resin was washed x5 in TBS 500rcf 2min 4°C and resuspended in TBS to 500μl final. 200μl resin was incubated with 250μl HeLa lysate and TBS added to 1ml final. 500μl resin/lysate mixture was taken as 0 timepoint and 500μl was incubated for 18 h at 37°C. Each resin/lysate mixture was passed over a 10ml filter column (Biorad) to separate

resin from flow through (FT), and the FT was collected. Resins were washed x4 in 10ml TBS, 0.5% NP40 and 1 wash TBS without detergent. SDS-loading buffer was added to FT and resins samples, and proteins were separated by SDS-PAGE. Ubiquitination was visualised using a ubiquitin specific antibody. Experiments using addition of ubiquitination machinery were performed similarly except 50nM E1, 5μM ubiquitin or ubiquitin aldehyde, 4mM ATP with or without 2.5μM UbcH5b were added to HIF1α$^{ODD401-652}$ with HeLa lysate prior to incubation. Experiments using proteasome inhibition were performed similarly except 50μM MG132 was added to HeLa lysate prior to incubation with HIF1α$^{ODD401-652}$.

2.4 Cell Biology

2.4.1 Cell culture

HeLa cells were grown in DMEM (Sigma) supplemented with 10% fetal calf serum (FCS, PAA), 50 IU/ml penicillin and 50μg/ml streptomycin (Sigma). HeLa cells treated with proteasome inhibitors were grown similarly except with addition of 5μM MG132, 4μM lactacystin or 20nM Bortezomib/Velcade for 18 hr.

2.4.2 Cell lysis for in vitro hydroxylation and ubiquitination reactions

HeLa cell lysates were prepared for the *in vitro* hydroxylation reaction from 1 x 10^8 cells using two rounds of freeze/thaw lysis in 2ml lysis buffer (20mM Hepes (pH7.5), 5mM KCl, 1.5mM $MgCl_2$). Lysates were passed through a 21G needle eight times followed by two passes through a 26G needle and centrifuged at 14,000rpm for 30 min at 4°C. Supernatants were pooled, aliquoted and stored at -80°C. HeLa cell lysates were prepared for the *in vitro* ubiquitination from 1 x 10^8 cells in 2ml lysis buffer (50mM Tris-HCl pH7.4, 150mM NaCl, 5mM $MgCl_2$, 0.5% NP40, PMSF, Roche cocktail), incubated on ice for 30 min and centrifuged at 14,000rpm for 30 min at 4°C. Supernatants were pooled, aliquoted and stored at -80°C.

2.4.3 Immunoprecipitation of HIF1α

HIF1α was immunoprecipitated from 1 x10^6 or 1 x 10^8 HeLa cells with or without proteasome inhibition for 18 hr. Cells were incubated with lysis buffer (LB: 50mM Tris pH7.4, 150mM NaCl, 5mM $MgCl_2$, 1mM DTT, Benzonase, 1% NP40, PMSF, Roche) for 30 min at 4°C on a rotator. Lysed cells were centrifuged (4,000rpm 15min 4°C) and the cell pellet/debris removed. 10% of the supernatant was stored as total cell lysate (TCL) and the remaining lysate was pre-cleared by incubating with Protein G magnetic dynabeads (Thermo Fisher), equilibrated in LB (30min 4°C on rotator). Supernatants were separated from the dynabeads using a magnet, and then incubated with Protein G dynabeads conjugated to HIF1α mouse antibody (3 hr 4°C on a rotator). The protein G beads were again immobilised using a magnet and washed x 5 in wash buffer (WB: 50mM Tris pH 7.4, 150mM NaCl, 5mM $MgCl_2$, 1mM DTT, 0.1% Triton X) and 1 wash in WB without detergent. Immunoprecipitated proteins were eluted in 2X SDS loading buffer. Proteins were separated by SDS-PAGE and HIF1α stabilisation was measured using a HIF1α specific antibody.

2.5 Mass Spectrometry

All MS was performed by the CIMR core facility (Robin Antrobus) or by Mike Weekes (Steve Gygi lab, Harvard Medical School/CIMR) according to the following protocols.

Proteins were resolved using a 4-12% pre-cast polyacrylamide gel and the lanes were cut into equal size chunks with proteins reduced, alkylated and digested in-gel. Tryptic peptides were analysed by LC-MS/MS using a Q Exactive coupled to an RSLCnano 3000. Peptides were resolved and sprayed using a 50cm EASY spray column with MSMS acquired by top 6 DDA. Data was processed in Proteome Discoverer 1.4 using the Sequest search engine. Searches were performed against a Uniprot human database (20,176 entries, downloaded 03/06/14) with Cam C as a fixed modification, oxidised M, GlyGly K, deamidated N/Q as variable modifications and a maximum of 2 missed cleavages. Peak area detection was enabled with peptides reporting average area of the three most abundant of each detected species. Peptides were filtered to 0.01 FDR and

identified branch sites were expressed as a percentage of the summed intensity of all quantified ubiquitin peptides.

AQUA mass spectrometry. The polyubiquitinated Ube2SΔ gel piece was sliced into 3 parts and each slice was destained and dehydrated in acetonitrile. Proteins were then digested in-gel with Trypsin for 3 hr. Ubiquitin AQUA analysis was performed as previously described (Kirkpatrick et al., 2006). Briefly, peptides were eluted, and peptide amount estimated. AQUA peptides were mixed at 600fmol per microgram Ube2SΔ peptide, and the entire samples were analysed on a Q Exactive mass spectrometer equipped with an Agilent 1100 binary pump and a Famos microautosampler. Peptides were separated using a gradient of 6 to 28% Acetonitrile in 0.125% Formic acid over 120 minutes. Peptides were detected in the Orbitrap by means of a data- dependent top-20 method. Extracted ion chromatograms were generated using Xcalibur v2.2 software (Thermo). Chromatographic co-elution of heavy and light peptide pairs and accurate peak integration were manually confirmed. The abundance of each peptide was determined by taking the ratio of the integrated areas for the light sample peptide versus the heavy AQUA internal standard peptide (Kirkpatrick et al., 2006). The percentage K11-linkages was calculated as (fmol K11) / (fmol K6 + K11 + K27 + K29 + K33 + K48 + K63).

Chapter 3: Results 1, K11-polyubiquitin chains as a signal for proteasome-mediated degradation.

3.1 Introduction

K11-polyubiquitin chains are the third most abundant linkage within the cell and have been shown to be involved in cell cycle progression and intracellular signaling (Jin et al., 2008; Wickliffe et al., 2011; Williamson et al., 2009b). K11-chains are also thought to signal protein degradation by both proteasome and proteasome-independent means, however it is not known how these linkages are recognised by the 26S. To understand how K11-ubiquitin chains are recognized, and ultimately to determine their functions, it was necessary to establish *in vitro* methods to form both free and substrate-bound K11-polyubiquitin chains.

To allow measurement of proteasome binding and activity *in vitro*, it was important to purify mammalian proteasomes and quantify their activity. The Nathan lab has developed methods to quantitatively measure the binding of pure mammalian proteasomes to different polyubiquitin chains types (Nathan et al., 2013). This approach compares the binding of polyubiquitin chains on substrate proteins to isolated mammalian 26S proteasomes by measuring the peptidase activity of the proteasomes bound to the chains.

I chose this *in vitro* approach, as it allowed me to compare differences in binding of different polyubiquitin chain types directly to the proteasome independent of cellular factors, such as proteasome shuttling factors or ubiquitin binding proteins, which may enhance or decrease this binding (Nathan et al., 2013). In addition, it allowed the formation of chains of a defined length.

In this Chapter, I outline the methods to generate K11 and K48-linked polyubiquitin chains and measure their binding to the proteasome. First, I describe the formation of substrate-bound homotypic K11-linked polyubiquitin chains on the E2 enzyme, Ube2S, and K48-linked chains on the E3 ligase, E6AP. To enable direct comparison of free polyubiquitin chains of the same length, I

describe the formation of free homotypic K11-linked ubiquitin tetramers. Subsequently, I measure the binding of free and substrate-bound K11 or K48-linked polyubiquitin chains in order to determine which chain type binds more strongly to the proteasome. Finally, I explore whether homotypic or heterotypic K11-polyubiquitin chains formed on a physiological cell cycle substrate, CyclinB1, signal proteasome-mediated degradation.

3.2 Results.

3.2.1 Formation of homotypic lysine 11-linked chains on the E2 enzyme Ube2S.

To measure the direct binding of K11-chains to the proteasome and other interacting proteins, it was first necessary to generate pure K11-chains on a single lysine residue on a substrate protein. Therefore, I developed a system to form K11-chains on the E2 enzyme, Ube2S. This E2 enzyme is unusual in that it can autoubiquitinate without requiring an E3 ligase (Wickliffe et al., 2011; Wu et al., 2010). To prevent the formation of multiple monoubiquitinated species, I made a GST-tagged Ube2S mutant construct, in which the lysine rich tail had been removed leaving a single terminal lysine, 197. I transformed this GST-Ube2SΔ into DE3* *E. coli* using standard methods and induced protein synthesis with 0.5mM IPTG 37°C 3 hr. Analysis of pre and post-induction samples showed a clear band at around 50kDa in the post-induction samples (**Figure 3.1A**), indicating expression of the GST-Ube2SΔ protein. After lysis of these bacteria and removal of cell debris by centrifugation and filtration, I incubated the cleared lysate with GSH Sepharose resin. I washed the resin to leave the resin-bound GST-Ube2SΔ protein. Analysis by SDS-PAGE showed GST-Ube2SΔ migrated at 50kDa with few other faster migrating species, likely to be truncations of the GST-Ube2SΔ (**Figure 3.1B**).

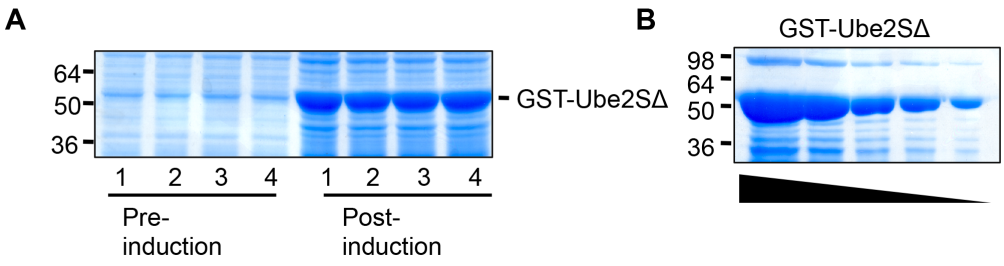

Figure 3.1: Expression and purification of GST-Ube2SΔ. GST-tagged Ube2SΔ was expressed in *E. coli*, purified on glutathione sepharose beads and separated by SDS-PAGE before staining with Coomassie blue. **(A)** Coomassie stained gel of GST-Ube2SΔ induction. *Numbers refer to 4 separate clones (10μl sample added)* **(B)** Coomassie stained gel of GST-Ube2SΔ purification. *20, 10, 5, 2.5 and 1.25μl samples added.*

Having purified the truncated GST-Ube2SΔ construct, I went on to establish ubiquitination assays. I incubated the resin-bound GST-Ube2SΔ with recombinant E1, ubiquitin, ATP, and AMSH at 37°C overnight, enabling polyubiquitin chain formation on the GST-Ube2SΔ (**Figure 3.2A**). The presence of the de-ubiquitinating enzyme, AMSH, within the reaction should cleave the K63 chains that can be formed by Ube2S truncations (Bremm et al., 2010), increasing the purity of K11-chain formation. Subsequent washing of the ubiquitinated resin removed unbound components of the reaction, leaving resin-bound polyubiquitinated GST-Ube2SΔ shown in the Coomassie stained gel (**Figure 3.2B**). Mass spectrometry (MS) analysis of the polyubiquitinated GST-Ube2SΔ (performed by Robin Antrobus) confirmed that these chains were formed on the single terminal lysine 197 of GST-Ube2SΔ (**Figure 3.2C**). To further exclude the possibility of multiple monoubiquitination on GST-Ube2SΔ, I ubiquitinated GST-Ube2SΔ as described, but used methyl ubiquitin (Ub^{Me}, Boston Biochem), which prevents polyubiquitin chain formation. The reaction was terminated by the addition of SDS loading buffer, and the ubiquitination of GST-Ube2SΔ measured by immunoblot. This showed a single ubiquitinated GST-Ube2SΔ species (**Figure 3.2D**) confirming that only a single lysine residue within GST-Ube2SΔ could be modified by ubiquitination.

To determine the ubiquitin linkage purity of the polyubiquitin chains on Ube2SΔ, we used Absolute Quantification (AQUA) mass spectrometry (MS), which uses linkage specific ubiquitin standards (New England Biolabs) to measure the levels of the different linkages within the polyubiquitin chains formed on GST-Ube2SΔ. Polyubiquitinated GST-Ube2SΔ was formed as described and analysed by MS AQUA (performed by Mike Weekes, Harvard Medical School/CIMR). This showed 92% purity of the K11-polyubiquitin chains formed (**Figure 3.2E**).

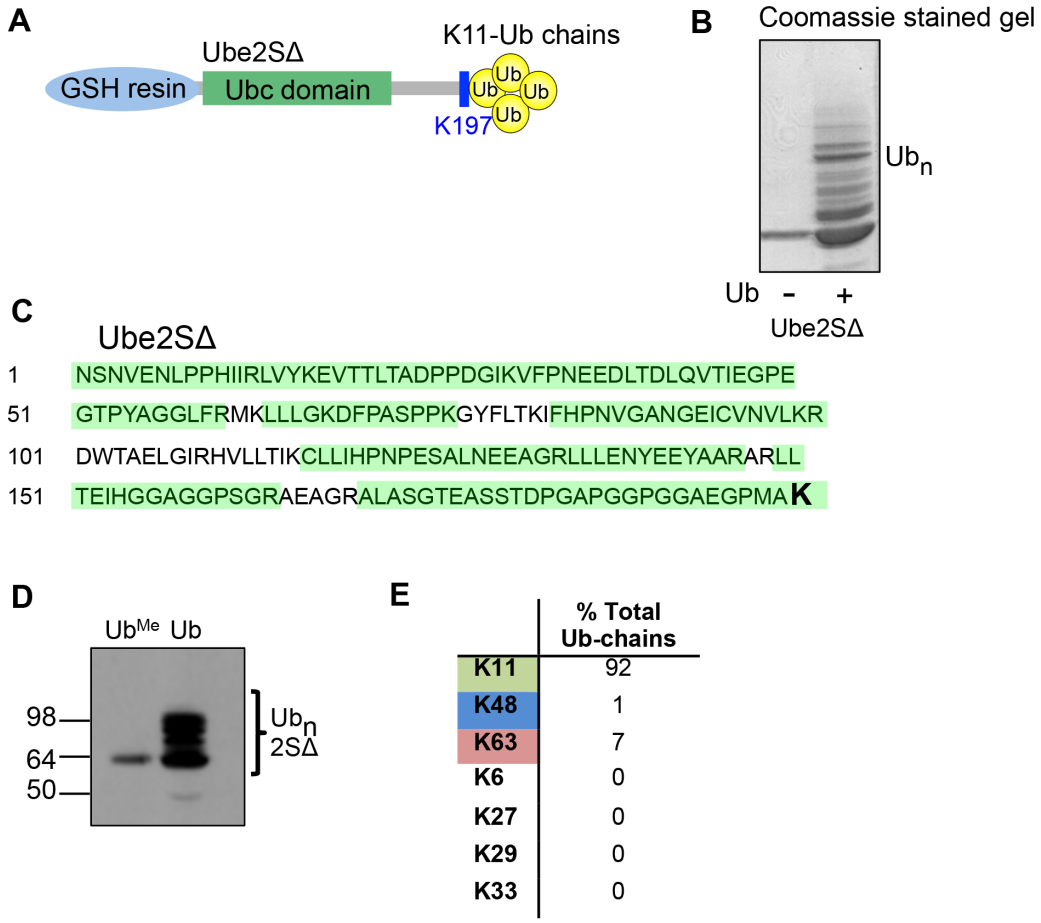

Figure 3.2: Formation of homotypic K11-linked polyubiquitin chains on Ube2SΔ. (A) Schematic of polyubiquitinated Ube2SΔ with K11-linked chains. **(B)** Polyubiquitination of Ube2SΔ. GST-Ube2SΔ resin was incubated with E1, ATP and ubiquitin overnight, the resin washed and ubiquitinated Ube2SΔ visualised by Coomassie staining. **(C, D)** K197 is the lysine modified by ubiquitination. Polyubiquitinated GST-Ube2SΔ resin was separated by SDS-PAGE and analysed by MS/MS or immunoblot for ubiquitin. **(E)** K11-linked polyubiquitin chains are formed on Ube2SΔ. The ubiquitination reactions described were subjected to AQUA MS to analyse the different ubiquitin linkages (Mike Weekes, Harvard Medical School/CIMR). *Ub=ubiquitin, Ub^{Me}=methyl ubiquitin.*

3.2.2 Formation of K11-linked tetraubiquitin chains.

Although the GST-Ube2SΔ polyubiquitination reactions generated pure K11-linked linkages, the chains were of undefined length. To compare the binding of K11-polyubiquitin chains to other ubiquitin linkages (e.g. K48 and K63) it was necessary to generate K11-linked chains of a fixed length. K48 and K63-linked tetraubiquitin (Ub_4) chains were commercially available, but this was not the case for K11-linkages. I therefore generated pure, free K11-linked chains

based on methods described by Bremm et al. (Bremm et al., 2010). Free K11-linked chains are formed during the autoubiquitination reaction of Ube2S, and the yield of these free chains can be increased by using a Ube2S fused to the ubiquitin binding domain (UBD) of USP5 (Bremm et al., 2010) (**Figure 3.3A**). Therefore, the UBD domain of USP5 was first cloned into our truncated Ube2S construct (by James Nathan) and I transformed this GST-tagged Ube2SUBD into BL21 DE3* *E. coli* as described. Protein synthesis was induced with 0.1mM IPTG 16°C overnight. Analysis of pre and post-induction samples showed a band at around 50kDa in the post-induction samples compared to the pre-induction (**Figure 3.3B**), indicating expression of the GST Ube2SUBD protein. After lysis of these bacteria, I incubated the cleared lysate with GSH Sepharose resin, then washed the resin with a high salt buffer and then low salt buffer to remove contaminants. Analysis by SDS-PAGE showed that GST-Ube2SUBD migrated at 50kDa (**Figure 3.3C**). The GST tag was removed by incubating the resin-bound GST-Ube2SUBD with GST-PreScission (1.2mg/ml) and the soluble Ube2SUBD eluted. SDS-PAGE analysis of the resin and eluate showed cleaved Ube2SUBD at 36kDa (**Figure 3.3D**).

Next, soluble K11-linked ubiquitin chains were generated by incubating the Ube2SUBD with E1, ubiquitin, ATP and cleaved AMSH at 37°C overnight as described in **3.2.1**. The autoubiquitination reaction was terminated by addition of 60mM DTT, which helps release the non-covalently bound K11-chains from the active cysteine of the Ube2S and the UBD (**Figure 3.3E, lane 2**). The Ube2SUBD and E1 were precipitated by addition of 50mM NH_4Ac pH4.5, and the K11-linked chains isolated using cation exchange chromatography. 0.5ml fractions were collected and analysed by SDS-PAGE. The fractionation of tri and tetra-ubiquitinated (Ub_4) species is shown (**Figure 3.3F**). Fractions from each chain length were pooled and dialysed into 20mM Tris pH 7.4. Finally, the Ub_4 chains were concentrated and the chain length verified by Coomassie staining (**Figure 3.3G**) and immunoblot (**Figure 3.3H**) compared to the commercial K48-linked tetraubiquitin. Having generated the K11-linked tetraubiquitin (K11-Ub_4) it was important to verify that these chains are linked though K11. Therefore, quantitative MS was performed (Robin Antrobus, CIMR), which showed K11-linkages of high purity (**Figure 3.3I**).

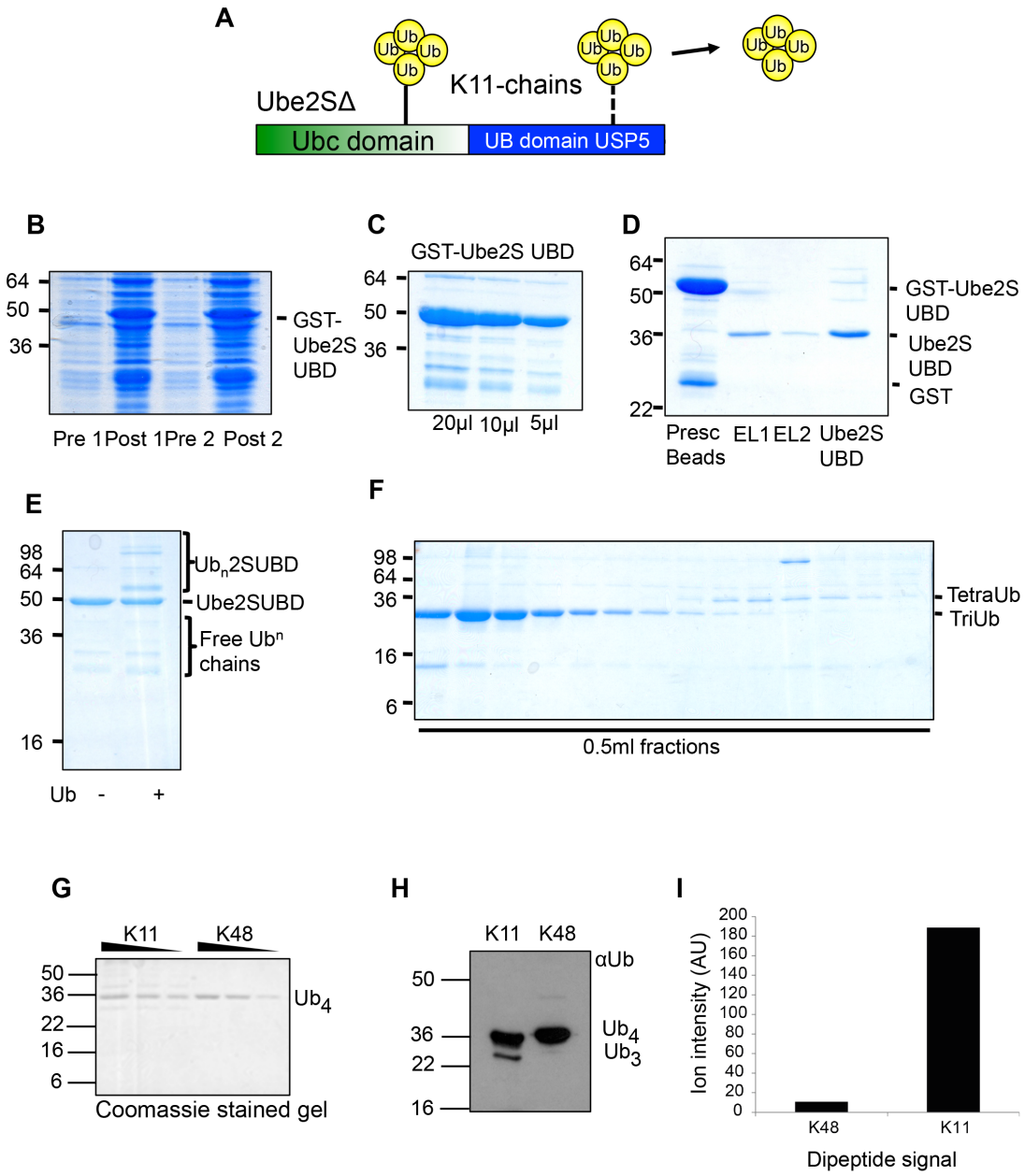

Figure 3.3: Formation of K11-tetraubiquitin chains using GST-Ube2SUBD. **(A)** Schematic of the ubiquitination reaction. **(B)** GST-Ube2SUBD induction in *E. Coli*. **(C)** GST-Ube2SUBD purification on GSH resin. **(D)** PreScission cleavage of GST-Ube2SUBD. The resin bound GST-Ube2SUBD was incubated with GST-PreScission and the free Ube2SUBD concentrated from the flow through. **(E)** Ube2SUBD autoubiquitination reaction illustrated in **(A).** **(F)** Fractions containing K11-Ub_4 separated using cation chromotography. **(G-I)** Analysis of the K11-Ub_4. The K11-Ub_4 was concentrated and compared to commercial K48-Ub_4 using SDS-PAGE and Coomassie staining **(G)** or immunoblot for ubiquitin **(H).** Chain linkage was analysed by quantitative MS using ion intensity (Robin Antrobus, CIMR) **(I).**

3.2.3 Do homotypic K11-linked polyubiquitin chains bind to the mammalian proteasome?

Mammalian proteasomes were isolated from rabbit muscle using the method described by Besche et al. (Besche et al., 2009). Briefly, the rabbit muscle was homogenized and proteasomes extracted by incubating the lysate with the Ubl of hHR23B bound to GST (GST-hHR23B Ubl). This ubiquitin like (Ubl) domain binds with high affinity to the Rpn10 and Rpn13 receptors on the 19S. The 26S proteasomes were eluted with an excess of a His-tagged UBD, the ubiquitin interacting motif (UIM) of Rpn10. This UBD was subsequently removed with NiNTA resin, leaving pure 26S proteasomes (Besche et al., 2009). I confirmed the structural integrity of the purified proteasomes by native gel with fluorescent substrate overlay (LLVY-AMC) which showed clear bands corresponding to doubly and singly-capped 26S proteasome (**Figure 3.4A**). I also confirmed the functional activity of the 26S by cleavage of the chymotrypsin-like fluorescent substrate, LLVY-AMC (**Figure 3.4B**).

Having purified the mammalian proteasome, I could then compare the binding of homotypic K11-linked chains to K48-linked polyubiquitin chains, the canonical signal for proteasomal degradation. K48-linked polyubiquitin chains were formed by incubating GST resin-bound E6AP with E1, the E2 UbcH5b, ubiquitin and ATP (**Figure 3.4C**). E6AP is a HECT E3 ligase that forms pure K48-linked polyubiquitin chains (Kim et al., 2007). The resin-bound K11 or K48-linked polyubiquitin chains were incubated with 20nM proteasomes at 4°C for 30min, washed to remove unbound proteasomes, and the proteasomes bound measured by the cleavage of the fluorescent proteasome substrate LLVY-AMC at 37°C (Peth et al., 2010). Surprisingly, I found that the K11-linked chains formed on Ube2SΔ did not bind to the proteasome in comparison to K48-linked polyubiquitin chains (**Figure 3.4D**).

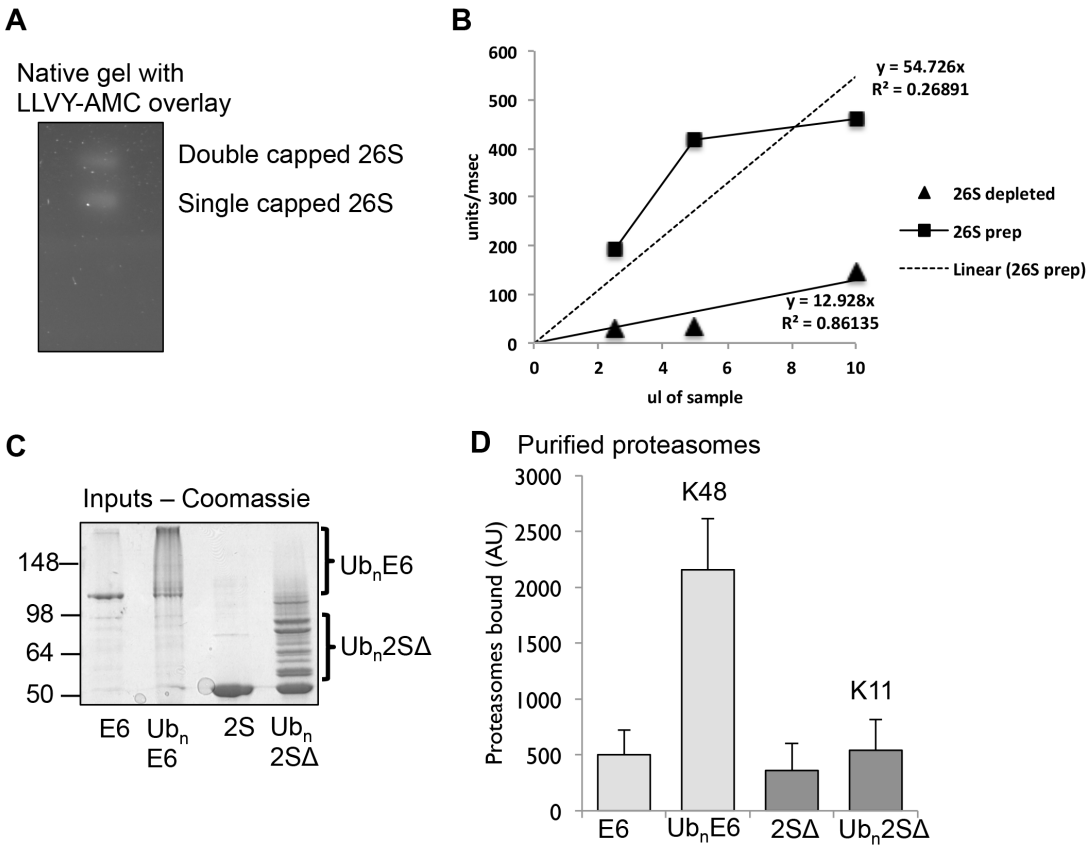

Figure 3.4: Homotypic K11-polyubiquitin chains on UBE2SΔ do not bind the proteasome. **(A, B)** Isolation of mammalian proteasomes from rabbit muscle. 26S proteasomes were isolated from muscle extracts using the GST-Ubl method and the purity and activity were measured by native gel electrophoresis **(A)** and LLVY-AMC cleavage **(B).** In-gel proteasome activity was measured by incubating the gels in a Tris buffer containing 1 mM ATP, 5mM $MgCl_2$, and 50μM Suc-LLVY-AMC at 37°C for 30 min **(A)**. Peptidase activity of the proteasomes (26S) was measured by LLVY-AMC cleavage (black squares), and a standard curve generated (linear 26S prep). LLVY-AMC peptidase activity of the rabbit muscle lysate depleted of proteasomes (black triangles) was also measured to assess the efficiency of the proteasome purification **(B)**. **(C, D)** binding to polyubiquitinated GST-Ube2SΔ or GST-E6AP. Coomassie stained gel of *in vitro* autoubiquitination reaction showing polyubiquitin chain formation on Ube2SΔ and E6AP **(C).** GST-bound K11-chains (Ub_n2SΔ) or K48-chains (E6AP) were incubated with purified mammalian proteasomes and proteasomes bound were measured by LLVY-AMC cleavage **(D).** *Mean±SEM, 3 experimental replicates.*

3.2.4 K11-linked tetraubiquitin cannot displace K48-polyubiquitin chains binding to the proteasome.

Although K11-linked chains on Ube2SΔ do not bind strongly to the proteasome, this finding may be accounted for by the difference in substrate used to generate the K11- and K48-linked chains or a difference in polyubiquitin chain length formed on Ube2SΔ and E6AP. Therefore, I compared the binding of K11- and K48-Ub_4 to the proteasome using a competition assay developed by Peth et al (**Figure 3.5A**) (Peth et al., 2010). I incubated resin-bound ubiquitinated GST-E6AP (**Figure 3.5B**) with either proteasomes alone or with proteasomes and increasing concentrations of K11-Ub_4 or K48-Ub_4 at 4°C. I then washed the resin-bound ubiquitin conjugates, and quantified the proteasomes bound by cleavage of LLVY-AMC fluorescent substrate (**Figure 3.5C**) Increasing concentrations of K48-Ub_4 competed with the resin-bound K48-linked chains to bind proteasomes, such that at 300nM K48-Ub_4, proteasomes bound to polyubiquitinated E6AP were reduced by about 70%. (**Figure 3.5C**). However, K11-Ub_4, at concentrations up to 300nM, did not prevent proteasomes binding to polyubiquitinated E6AP (**Figure 3.5C**). Thus, K11-linked chains bind more weakly than K48-linked chains to proteasomes.

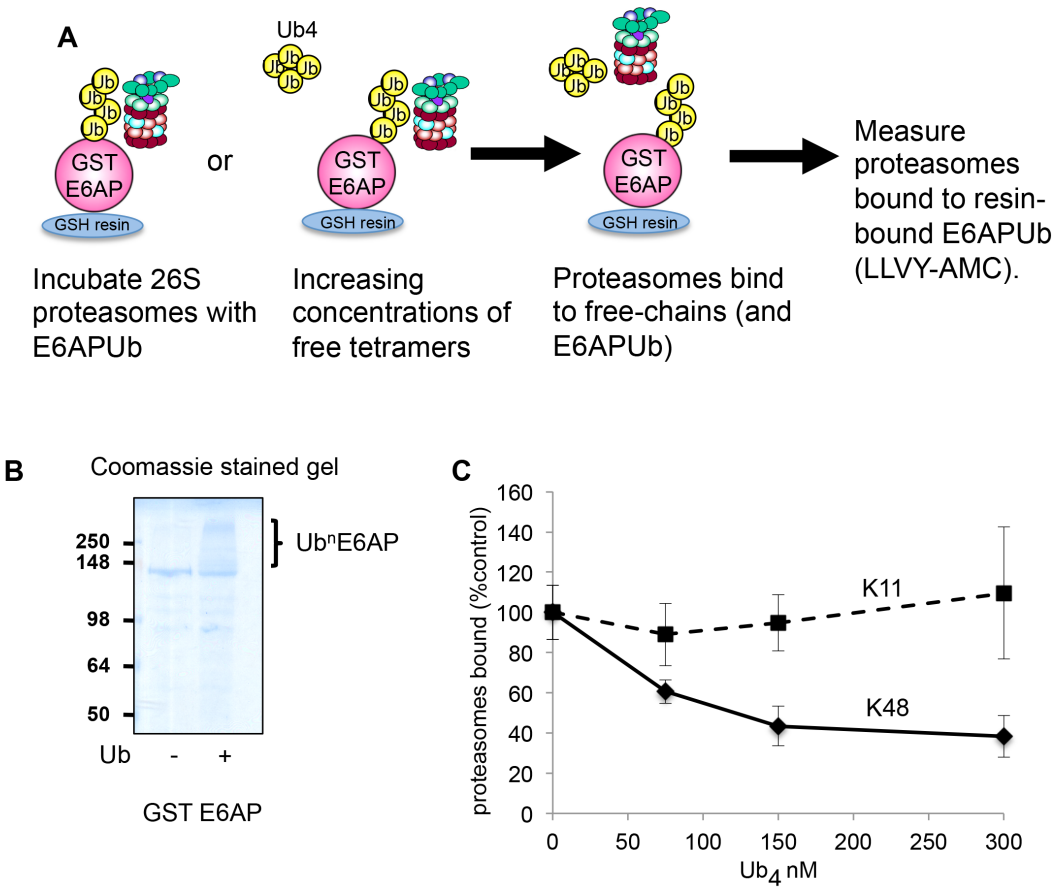

Figure 3.5: Free K11-ubiquitin tetramers do not compete with K48-ubiquitin tetramers for binding to bind 26S proteasomes. **(A)** Schematic of 26S proteasome binding competition assay. Polyubiquitinated resin-bound GST-E6AP **(B)** were incubated with K11 or K48-Ub_4, the resins washed and proteasomes bound to polyubiquitinated E6AP measured by LLVY-AMC cleavage **(C)**. *Means±SEM of 4 experiments.*

3.2.5 Homotypic and heterotypic K11-linked polyubiquitin chains differ in their ability to bind to the proteasome.

While homotypic K11-linked polyubiquitin chains did not bind to the proteasome, it was important to determine whether this was true for other K11-ubiquitinated substrates. In addition, K11-linked polyubiquitin chains of mixed (heterotypic) linkages exist in cells, and may be the dominant species formed by the APC/C (Meyer and Rape, 2014). Therefore, I wanted to establish methods to generate different types of K11-linked polyubiquitin chains on the physiological substrate, Cyclin B1, and measure their ability to bind to the proteasome.

(i) Formation of K11 polyubiquitin chains on Cyclin B1 using immunoprecipitated APC/C.

I first attempted to form K11-chains on cyclin B1, using semi-purified APC/C from HeLa cells arrested in mitosis, according to published methods (Williamson et al., 2009a). I used a Cyclin B1 N-terminal mutant construct (CyB1-NT^{K64}, a kind gift from Randall King) in which all lysines have been mutated to arginines except for lysine 64, to prevent the formation of multiple monoubiquitination (Dimova et al., 2012). I modified this construct to encode a GST tag at the N-terminus and a His tag at the C-terminus, for use in our proteasome binding assays. I purified this protein as described (see methods **2.2**) and verified the purity of the protein SDS-PAGE and Coomassie staining (**Figure 5.6A**). Although there were some truncated products (**Figure 5.6B**), the purity was sufficient for my subsequent experiments.

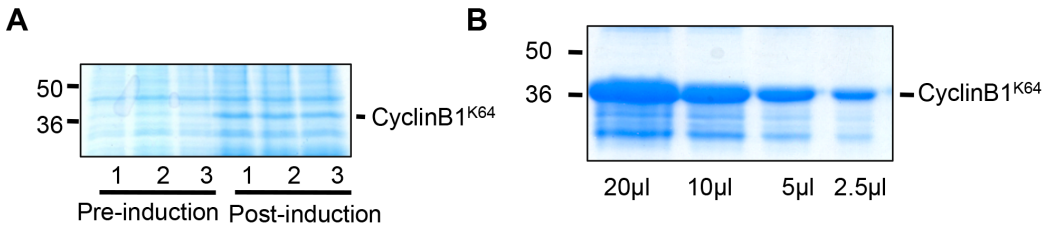

Figure 3.6: Expression and purification of GST-CyB1-NT^{K64}. GST-tagged CyB1-NT^{K64} was expressed in *E. coli*, purified on glutathione sepharose beads and separated by SDS-PAGE before staining with Coomassie blue. **(A)** Coomassie stained gel of GST-CyB1-NT^{K64} induction. *Numbers correspond to litres of culture.* **(B)** Coomassie stained gel of GST-CyB1-NT^{K64} purification.

The APC/C was immunoprecipitated according to published methods from HeLa-S cells released from a nocodazole arrest (cells prepared by James Nathan) (Williamson et al., 2009a). I then incubated the CyB1-NT^{K64} in an *in vitro* autoubiquitination reaction containing E1, ubiquitin, Ube2C, Ube2S, resin-bound semi-purified APC/C and ATP at 37°C (**Figure 3.7A**). To separate the resin-bound APC/C which may itself be ubiquitinated, I centrifuged the suspension using a 0.2µm filter column and collected the flow through (FT). This FT was then incubated with equilibrated GSH resin to bind the polyubiquitinated GST-tagged K64 CyclinB1 (**Figure 3.7A**) The suspended resin was analysed by

immunoblot with a ubiquitin antibody to assess CyB1-NT^{K64} ubiquitination. This showed polyubiquitination of CyB1-NT^{K64} Ube2C (**Figure 3.7B, lane 2**) and chain elongation, presumably with K11-linkages, in the presence of Ube2S, (**Figure 3.7B, lane 3**).

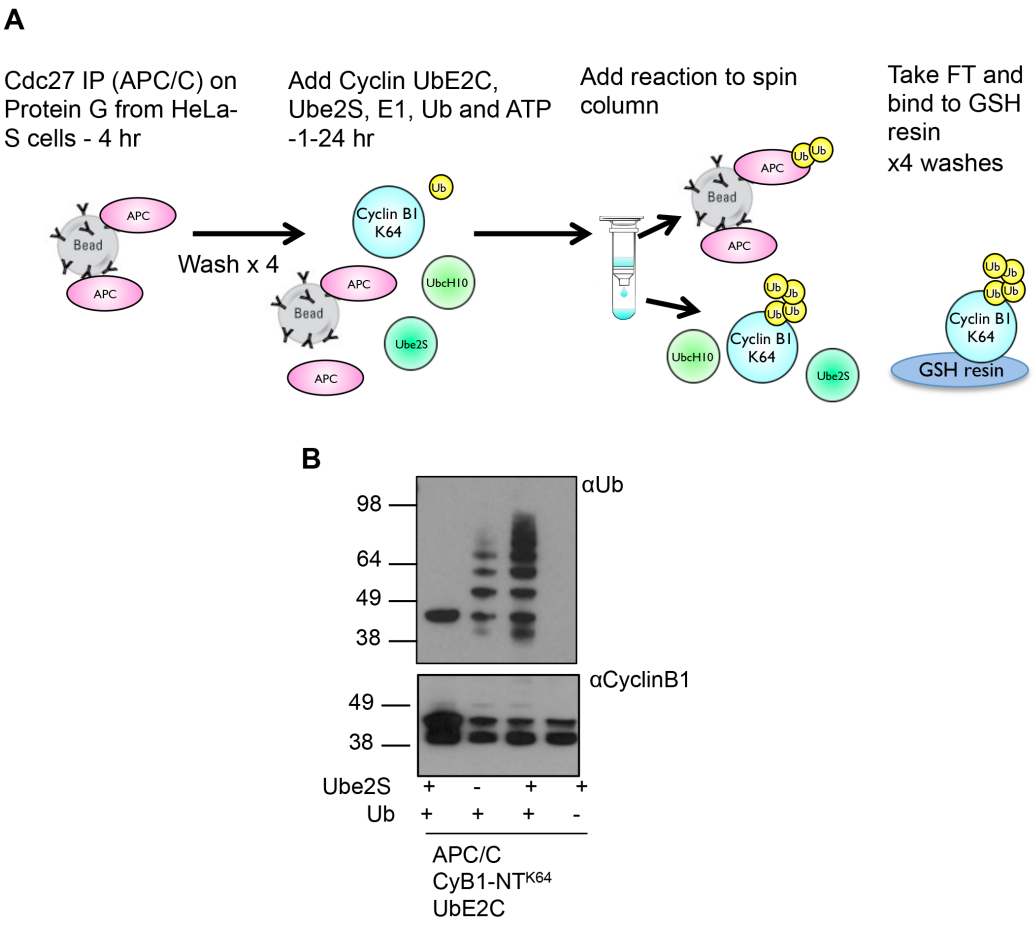

Figure 3.7: Polyubiquitination of GST-CyB1-NT^{K64} using immunoprecipitated APC/C from HeLa-S cells. **(A)** Schematic of ubiquitin chains formed on resin-bound cyclinB1^{K64}. **(B)** Immunoblot of polyubiquitin chains formed on GST-CyB1-NT^{K64} with Ube2C and Ube2S. *Two forms of cyclin B1 are observed, which does not seem to be dependent on ubiquitination.*

Although this approach was successful in forming polyubiquitin chains on CyB1-NT^{K64}, ubiquitination was very variable between experiments and optimisation using different time points and temperatures showed that CyB1-NT^{K64} was degraded during long incubations. Indeed, MS analysis of the immunoprecipitated APC/C showed that it contained multiple E3s, DUBs and proteasome subunits (data not shown). The variability in ubiquitination of CyB1-NT^{K64} and complexity of the immunoprecipitated APC/C made this approach

difficult to interpret. It was therefore important to establish a cleaner system to generate ubiquitinated CyB1-NT^{K64}. This required human recombinant APC/C, which was kindly provided by David Barford (Laboratory of Molecular Biology, Cambridge) (Zhang et al., 2013).

(ii) Formation of K11-polyubiquitin chains on Cyclin B1 using human recombinant APC/C.

Human recombinant APC/C provided the opportunity to form homotypic K11, heterotypic K11/K48 or homotypic K48-chains on CyB1-NT^{K64} and compare the binding and degradation of these different chains by the proteasome. Therefore, GST bound CyB1-NT^{K64} was ubiquitinated using human recombinant APC/C, E1, two E2s (Ube2C and Ube2S), and different ubiquitins (wildtype ubiquitin, K48-only ubiquitin (Ub^{K48}), K11-only ubiquitin (Ub^{K11}) or methyl-ubiquitin (Ub^{Me})) to form homotypic K11 or K48-linked chains, as well as heterotypic polyubiquitin chains (experiments performed with James Nathan) (**Figure 3.8A**). The resin-bound polyubiquitinated CyB1-NT^{K64} was then washed and ubiquitination measured by immunoblot. Monoubiquitination of CyB1-NT^{K64} was observed with Ub^{Me} (**Figure 3.8B**) confirming that a single lysine of CyB1-NT^{K64} is modified. Homotypic K11-chains were formed with Ub^{K11} (**Figure 3.8B**) and homotypic K48-chains with Ub^{K48} (**Figure 3.8D, lane 4**). Low concentrations of Ube2C (125nM) formed monoubiquitinated CyB1-NT^{K64} (**Figure 3.8B**), but these chains were elongated in the presence of Ube2S (**Figure 3.8B**). The polyubiquitin chains formed on CyB1-NT^{K64} were analysed by quantitative MS, and showed that low concentrations of Ube2C with Ube2S formed heterotypic K11 and K48-chains whereas high concentration Ube2C with Ube2S formed polyubiquitin chains forming several different linkages (**Figure 3.8C**). Interestingly, the homotypic and heterotypic K11-chains were similar in length, but the homotypic K48-chains were a little shorter (**Figure 3.8D**).

Having established a system to form different polyubiquitin chains on CyB1-NT^{K64}, we could then measure the ability of these conjugates to bind proteasomes. Resin-bound homotypic K11, heterotypic K11/K48 or homotypic K48-polyubiquitin chains were incubated with purified mammalian proteasomes at 4°C for 30 min, and the proteasomes bound measured by LLVY-AMC cleavage.

Minimal binding of homotypic K11-chains to the proteasome was observed, similarly to polyubiquitinated Ube2SΔ (**Figure 3.4**). In comparison, homotypic K48-polyubiquitin chains bound strongly to the proteasome. The heterotypic K11/K48-linked chains bound to the proteasomes, but less strongly than the homotypic K48-chains (**Figure 3.8E**). Thus, while homotypic K11-chains did not bind to proteasomes, heterotypic K11/K48-chains could associate with the 26S.

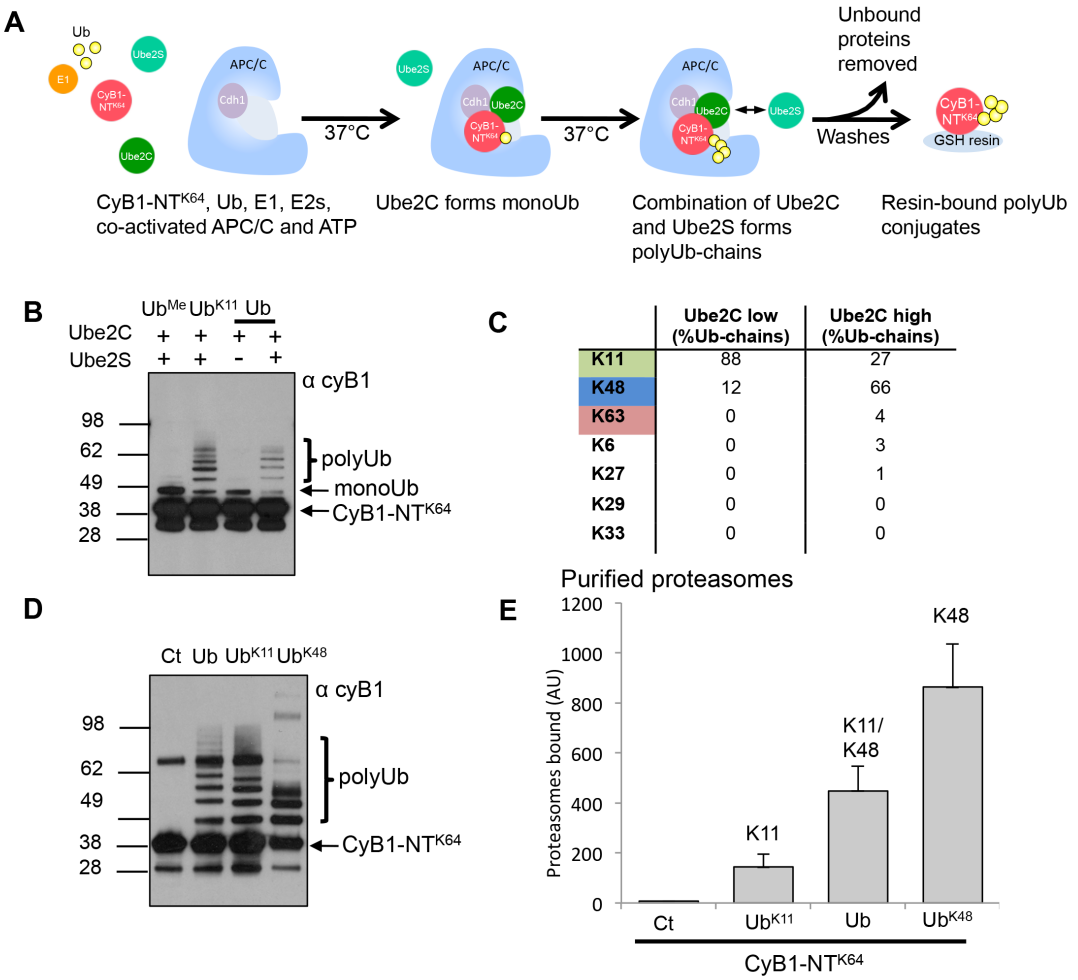

Figure 3.8: Heterotypic K11-polyubiquitin chains on cyclin B1 bind to the proteasome. **(A-C)** Synthesis of homotypic and heterotypic K11/K48-polyUb chains on CyB1-NT^{K64} using human recombinant APC/C. Resin-bound CyB1-NT^{K64} was incubated with co-activated APC/C, Ub (Ub, Ub^{Me} and Ub^{K11}), and E2s (Ube2C and Ube2S) for 1 hr at 37°C, washed and ubiquitination of CyB1-NT^{K64} measured by immunoblot for cyclin B1 **(B).** Quantification of the Ub-linkages formed was measured by MS **(C). (D, E)** Heterotypic but not homotypic K11-polyubiquitin chains bind to the proteasome. CyB1-NT^{K64} was ubiquitinated with Ub^{K11} and Ub^{K48} to form homotypic polyUb chains or ubiquitinated with wildtype ubiquitin, forming K11/K48 heterotypic polyubiquitin chains **(D).** These ubiquitin conjugates were incubated with purified proteasomes and 26S proteasomes bound to the chains measured by LLVY-AMC cleavage **(E).** *Means±SEM of 3 experiments. Ct=control*

3.2.6 Heterotypic K11/K48-linked chains facilitate proteasome-mediated degradation of cyclin B1.

I had shown that the proteasome did not bind to homotypic K11-linked chains but did bind to heterotypic K11/K48 and homotypic K48-chains to different extents. How would this difference in binding affect the proteasomal degradation of the ubiquitinated substrate? To measure the ability of the proteasome to degrade polyubiquitinated CyB1-NT^{K64}, the homotypic K11, heterotypic K11/K48 or homotypic K48-chains were incubated with purified mammalian 26S proteasomes at 37°C for the indicated times (**Figure 3.9A, B**) (these experiments were conducted with James Nathan). CyB1-NT^{K64} degradation was visualized by immunoblot (**Figure 3.9A, B)** and quantified by densitometry (**Figure 3.9C**). Analyses of 4 experiments showed that about 80% of CyB1-NT^{K64} modified with homotypic K48-chains was degraded by 90 min, whereas homotypic K11-chains were only weakly degraded (20% by 90 min). CyB1-NT^{K64} modified with heterotypic K11/K48-chains was degraded, but less so than CyB1-NT^{K64} modified with homotypic K48-chains (60% by 90 min) (**Figure 3.9C**).

Interestingly, although the homotypic K11-chains did not stimulate significant proteasomal degradation of CyB1-NT^{K64}, the proteasome-associated DUBs could still disassemble the polyubiquitin chains (**Figure 3.9A, B**). Homotypic K48 and heterotypic K11/K48-chains are deubiquitinated to 3 ubiquitins by the proteasome whereas homotypic K11-chains are deubiquitinated to only 4 ubiquitins.

To further examine the ability of the proteasome to disassemble polyubiquitin chains, I measured the cleavage of K11-Ub$_4$ and K48-Ub$_4$ by the proteasome. Equal concentrations of either K11-Ub$_4$ or K48-Ub$_4$ were incubated with purified mammalian proteasomes for 0, 30 or 60 min and the deubiquitination analysed by immunoblot (**Figure 3.9D**). While both K48 and K11-Ub$_4$ were disassembled by the proteasome, the K48-chains were cleaved more rapidly. Thus, while homotypic K11-chains did not bind strongly to mammalian proteasomes, the 26S associated DUBs could still disassemble these chains, potentially protecting them from degradation. Alternatively, heterotypic

K11/K48-chains were sufficient to promote the degradation of a ubiquitinated substrate.

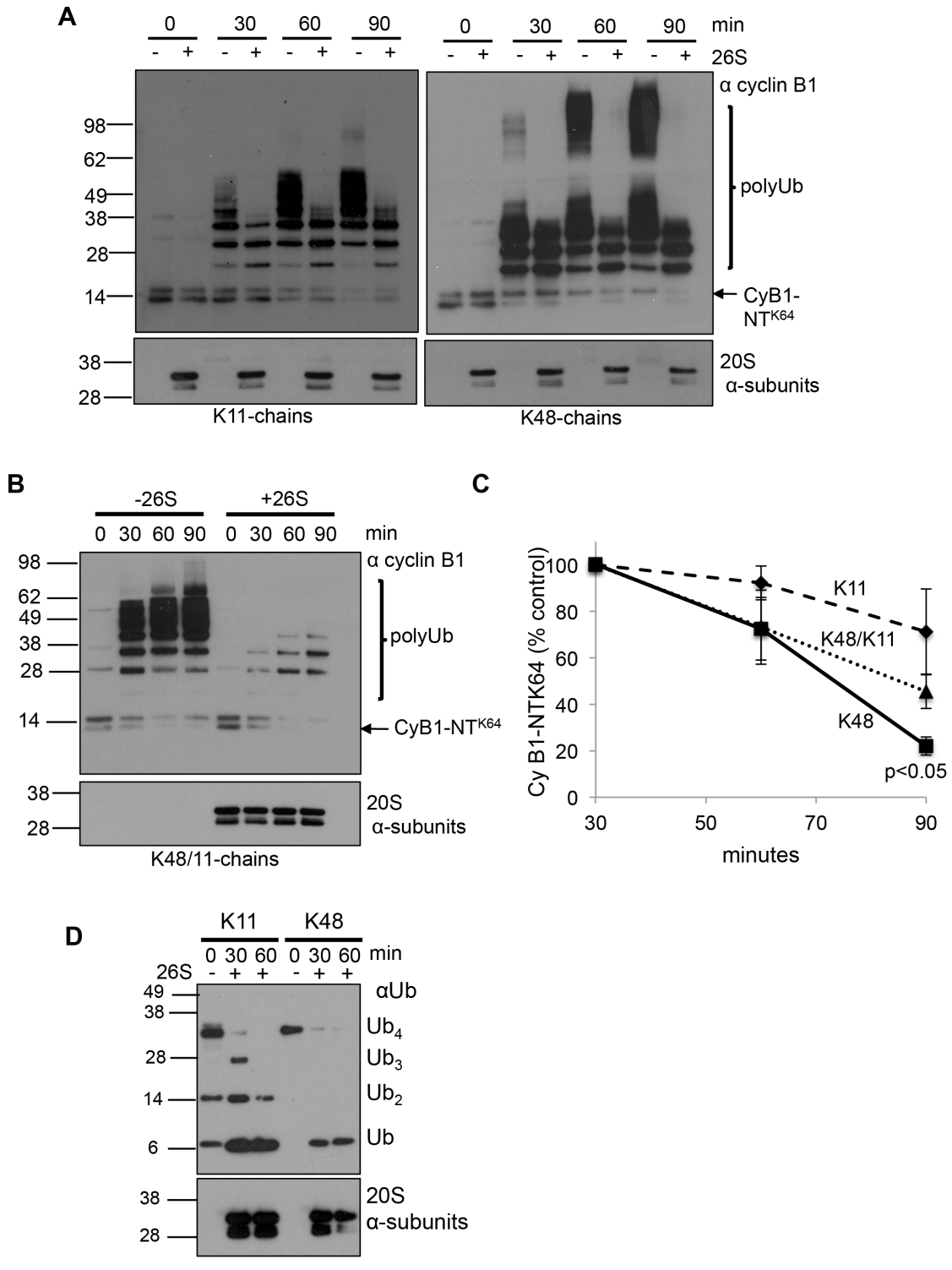

Figure 3.9: Homotypic K11-polyubiquitin is not efficiently degraded by mammalian proteasomes. **(A-C)** HA-tagged CyB1-NT^{K64} was incubated with co-activated APC/C, E1, E2s (Ube2C and Ube2S) and Ub, forming homotypic K11- and K48-polyUb chains (using Ub^{K11} and Ub^{K48}) or heterotypic K11/K48-polyUb chains (using wildtype Ub). 26S proteasomes were added to the reactions and the samples incubated at 37°C. The reactions were terminated by the addition of SDS loading buffer at 0, 30, 60 and 90 min/ ubiquitination and degradation of measured by Immunoblot for cyclin B1 were used to measure degradation of CyB1-NT^{K64} **(A, B)** and graphical presentation of the means ± SEM of densitometric evaluation of the immunoblots from 4 separate experiments are shown **(C).** Degradation of CyB1-NT^{K64} was measured from 30 min, as time was needed to allow for ubiquitination of cyclin B1.Densitometry of the the cumulative ubiquitinated and non-ubiquitinated species of cyclin B1 was used to measure the effect of adding the proteasome. Immunoblots for the 20S α-subunits and the APC/C subunit cdc27 were used as loading controls. **(D)** Homotypic K11- and K48-free polyUb chains are disassembled by proteasome associated DUBs. 150nM K11-Ub_4 and K48-Ub_4 were incubated with 20nM proteasomes at 37°C. The reactions were terminated by the addition of SDS loading buffer at 0, 30, and 60 min, and disassembly of the chains visualised by immunoblot for Ub. Immunoblots for the 20S α-subunits served as loading controls.

3.3 Discussion

By examining direct binding of purified mammalian proteasomes I have shown that homotypic K11-chains bind weakly to the proteasome in comparison with K48-chains. This represents a potentially novel mechanism of the proteasome itself distinguishing between different chain types.

We also showed that the proteasome differentiates between homotypic and heterotypic K11-polyubiquitin chains. Heterotypic K11/K48-chains not only bound to the proteasome but also resulted in a degradative outcome for the polyubiquitinated substrate, cyclin B1. Therefore, it is possible that different polyubiquitin chain conformations, as illustrated by homotypic and heterotypic K11-chains, increases the diversity of ubiquitin signals targeting substrates to the proteasome, which may be important for regulating protein breakdown.

3.3.1 Does the topology of homotypic chain linkages account for their weak proteasomal binding?

The finding that K11-polyubiquitin chains did not bind to proteasome was unexpected, as previous studies had not identified any chain linkage specificities by ubiquitin receptions with the 19S. To ensure that my initial observations were not due to the conformations of K11-polyubiquitin chains on Ube2S, I went on to examine free K11-ubiquitin chains and K11-polyubiquitinated cyclin B1. Together, these experiments clearly show that the proteasome ubiquitin receptors do not bind strongly to K11-conjugates, which suggests that the structural conformations of K11-ubiquitin linkages are distinct from that of K48-ubiquitin chains. Subsequently, another group has confirmed observed similar findings for K11-polyubiquitin chains on GFP, supporting our findings that homotypic K11-chains are not a signal for proteasome-mediated degradation (Martinez-Fonts and Matouschek, 2016)

The structure of K11-ubiquitin dimers has been resolved by several groups, and while this clearly reveals a structure distinct from other known

ubiquitin linkages, such as K48 and K63, there is lack of agreement as to the position of the hydrophobic I44 binding patch, the recognition site on ubiquitin for UBPs. Resolved structures of K11-ubiquitin dimers have different ubiquitin-ubiquitin orientations, depending on the experimental methods used, and crucially that the hydrophobic I44 binding region of ubiquitin is exposed in one crystal structure (Bremm et al., 2010), and buried in another (Matsumoto et al., 2010). Furthermore, Nuclear Magnetic Resonance (NMR) data and Small Angle Neutron-scattering (SANS) data shows that the structure of K11-dimers is distinct from the crystal structures (Castaneda et al., 2013). In addition, Castaneda et al show that increasing salt concentration brings the hydrophobic patches of the two ubiquitins closer to each other, which is not seen with K48 or K63 dimers (Castaneda et al., 2013). Interestingly, the Fushman and Glickman groups also show that the UBA2 domain of hHR23A (which is thought to shuttle ubiquitinated proteins to the proteasome for degradation) binds K48 dimers more strongly than K11 ubiquitin dimers, as a single molecule of UBA cannot interact with both hydrophobic regions of the K11 ubiquitin dimers at the same time, which is the case for K48 ubiquitin dimers (Mansour et al., 2014). Therefore, it is possible that the compact K11 dimer formation and orientation of the two ubiquitin molecules may prevent the I44 hydrophobic region being available to proteasomal receptors. Whether K11-polyubiquitin conjugates directly associate with proteins such as hHR23A and other putative 'proteasome shuttling' proteins was important to examine (**see Chapter 4**).

3.3.2 Heterotypic K11/K48-chains allow binding and substrate degradation by the proteasome.

The presence of a relatively low percentage of K48-polyubiquitin linkages within the K11-polyubiquitin chains allowed proteasome binding and substrate degradation. Presumably, the presence of K48-linkages within the heterotypic chains may open this chain formation exposing the hydrophobic binding surface of ubiquitin to proteasome receptors and shuttling factors. Alternatively, it is possible that short regions of K48-ubiquitin linkages within a mixed chain are sufficient for proteasome binding. So far, it is not possible to distinguish between

these possibilities, as the structures of mixed ubiquitin linkages have not been resolved. However, my findings are consistent with the studies of Meyer et al, where they identified K11/K48-heterotypic chains on cell cycle substrates, facilitating their proteasome-mediated degradation (Meyer and Rape, 2014). However, one important difference with our studies is that Meyer et al conclude that K11/K48-polyubiquitin chains are superior signals for proteasome-mediated degradation compared to K48-linked chains, which we did not observe.

It is likely that heterotypic K11-polyubiquitin chains have different functions depending on the linkages involved. Heterotypic K11/K63 chains were identified on Major Histocompatibility Complex (MHC) Class I molecules when they are polyubiquitinated by the Kaposi Sarcoma associated herpes virus E3 ligase, K5 (Boname et al., 2010). These mixed chains resulted in the internalisation of MHC Class I from the cell surface, rather than degradation by the proteasome (Boname et al., 2010). How the conformation and linkages within K11-polyubiquitin chains alters the recognition and outcome for the ubiquitinated substrate may account for the diversity of functional outcomes of K11-linkages in different pathways (Bremm et al., 2014; Dao et al., 2012; Dynek et al., 2010; Qin et al., 2014). However, further studies are needed to determine the structures of the K11-heterotypic chains, and it would be intriguing to visualise the alteration that K48, or indeed other ubiquitin linkages within a heterotypic chain, make to the binding surfaces revealed to the proteasome and UBPs within the cell.

3.3.3 What is the optimal signal for proteasome-mediated degradation of cyclin B1?

Until recently, it was widely accepted that the shortest polyubiquitin chain required for recognition by the proteasome and to signal degradation was four ubiquitins, linked by lysine 48 linkages (Thrower et al., 2000) but our studies and those of others (Dimova et al., 2012; Kravtsova-Ivantsiv et al., 2009; Meyer and Rape, 2014) raise the possibility that the ubiquitin signals for proteasome degradation may be more diverse.

Two labs have recently shown that multiple monoubiquitination may signal proteasome degradation (Dimova et al., 2012; Kravtsova-Ivantsiv et al., 2009). The Ciechanover lab shows that multiple monoubiquitination of the p105 NF-κB precursor may be sufficient to signal proteasomal degradation (Kravtsova-Ivantsiv et al., 2009). NF-κB activation requires partial proteasomal degradation of one of its precursors, p105, to form p50. This requires phosphorylation of the p105 protein by IκB kinase (Myllyharju and Kivirikko) which allows recognition and polyubiquitination of p105 by the SCF E3 ligase, βTrCP and leads to partial proteasomal degradation of p105 to leave p50. The Ciechanover lab proposes a phosphorylation independent proteasomal degradation mechanism using a S927A p105 mutant in which the serine phosphorylated by IKK and recognised by βTrCP (Heissmeyer et al., 2001; Lang et al., 2003; Salmeron et al., 2001) is mutated to an alanine. In a cell free system, they show that this ^{35}S-labelled mutant is degraded to form p50 in the presence of E1, E2, WT ubiquitin and a crude reticulocyte fraction that lacks ubiquitin, and this degradation is impaired in the presence of MG132. In addition, they show that the S927A p105 mutant can be degraded to form p50 in the presence of ubiquitin mutants which cannot form polyubiquitin chains (methyl ubiquitin (Ub^{Me}), and Ub^{KO} (ubiquitin in which all lysine residues have been mutated)) or an ubiquitin mutant unable to form K48-linked chains (Ub^{K48R}), albeit to a lesser extent than with WT ubiquitin. This data does support the hypothesis that multiple monoubiquitination of S927A p105 mutant can signal proteasomal degradation to p50, although chains formed with WT Ub still appear to be a more efficient degradation signal. The Ciechanover lab went on to show that S927A p105 mutant was degraded to form p50 in a yeast system expressing Ub^{KO} similarly to one expressing WT Ub. In mammalian HEK293T cells co-expressing Flag p105 and either WT Ub or Ub^{KO}, p105 was processed similarly. However, the polyubiquitin conjugates visualised in these cells were certainly of lower molecular weight but not necessarily monoubiquitinated as endogeous ubiquitin is present in these cells in addition to the overexpressed Ub^{KO}. In addition, p105 is expressed not the S927A p105 mutant, therefore the ubiquitination visualised may be due to phosphorylation and βTrCP catalysed polyubiquitination to form short chains and was able to bind proteasomal subunits similarly.

The King and Finley labs also suggest that multiple monoubiquitination may be a proteasome degradation signal for Cyclin B1 (Dimova et al., 2012). Dimova et al added a ^{35}S-labelled N-terminal fragment of CyclinB1 (cyc-B1-NT) to mitotically-arrested Xenopus extracts treated with ubiquitin vinyl sulphone (UbVS,) an isopeptidase inhibitor which prevents ubiquitin recycling, and showed that cyc-B1-NT degradation was reduced by 90-95%. Addition of wildtype ubiquitin restored cyc-B1-NT degradation however addition of K11, K48 or K63 mutants and methyl ubiquitin restored the degradation of cyc-B1-NT to a lesser extent. Degradation still occurred, indicating that polyubiquitin chain formation was not essential for cyc-B1-NT degradation. As the cyc-B1-NT contained a limited number of lysines, the King lab went on to investigate whether the number of lysines available for ubiquitination affected the enhanced degradation seen with polyubiquitinated cyc-B1-NT versus the monoubiquitinated substrate. Using the Xenopus system described above they measured the degradation of full-length CyclinB1 versus CyclinB1 mutants (in which one or more of four lysines had been mutated to arginine). Interestingly full length CyclinB1 was degraded similarly with the addition of exogenous WT Ub, Ub^{11R}, Ub^{triR} or Ub^{Me} indicating that monoubiquitinated CyclinB1 supported proteasomal degradation. However, the $CyclinB1^{K64only}$ mutant, in which only a single lysine was available for ubiquitination, showed significantly reduced degradation with the addition of Ub^{11R}, Ub^{triR} or Ub^{Me} compared with WT Ub. This data indicates that when there is multiple monoubiquitination of CyclinB1 this may act as a proteasome degradation signal and raised the question of whether polyubiquitin chain linkage determined degradation by the proteasome, or whether the density of ubiquitin on the 19S was more important.

To explore this further, the Kirschner and Finlay labs developed single molecule assays that enabled comparison of the proteasomal degradation of cyclin B1 modified with a single ubiquitin tetramer versus two dimers (Lu et al., 2015). Lu et al used purified APC/C to conjugate pre-formed K48 dimers or tetramers onto an N terminal fragment of CyclinB1 ($CyclinB1^{Nterm}$) and separated the di or tetraubiquitinated conjugates by electrophoresis. These conjugates were incubated with purified proteasomes, which had been salt washed to remove USP14, preventing deubiquitination of the tetramers to dimers.

Quantification of the rate of degradation of CyclinB1^{Nterm} by autoradiography showed that CyclinB1^{Nterm} ubiquitinated with two K48 dimers was degraded more rapidly than one ubiquitinated with a single K48 tetramer, and this was superior to K11-ubiquitin chains. Interestingly, the Kirschner and Finley labs also compared the proteasomal degradation of Securin modified with K48 or K11-linked dimers, and showed that K48-linked dimers resulted in more rapid degradation than K11 (Lu et al., 2015), agreeing with our findings that K11 ubiquitination is a weaker proteasomal degradation signal than K48. The physiological benefit of forming non-proteasomally degraded K11-conjugates on cell cycle substrates is not yet clear, but they may serve to prime cyclin B1 for subsequent K48 mediated degradation.

Whether the ubiquitin signal is the only requirement for degradation is brought into question by the Matouschek lab who suggest that an unfolded region in the substrate is also needed and that proteins can be degraded either from C to N or from N to C terminus (Prakash et al., 2004). While they have not directly examined cyclin B1, the Matouschek lab formed a model two domain protein consisting of dihydrofolate reductase (DHFR) and the ribonuclease, barnase. Incubation with purified proteasomes allowed quantification of degradation of the two-domain protein by autoradiography, and interestingly, the two-domain protein could be completely degraded regardless of which protein was adjacent to the ubiquitination signal. The Matouschek lab went on to design a protein lacking an unstructured region which consisted of a tetra-ubiquitin tag attached to the N-terminus of DHFR. This protein was degraded inefficiently by the proteasome. However, when an unstructured region was attached either to the C-terminus or between the ubiquitin tag and the DHFR, the protein was rapidly degraded, providing evidence that an unstructured region of 20 amino acids was sufficient to allow degradation of the DHFR (Prakash et al., 2004). While unfolded regions of Cyclin B1 have not been determined, the N-terminal region of Cyclin B1 (1-64) is predicted to be disorded, and is also the site of ubiquitination. It is therefore likely that disorder in the N-terminus of cyclin B1 contributes to its recognition by the proteasome, in addition to modification by polyubiquitination. Moreover, my findings highlight that the

nature of the polyubiquitin chain can directly alter the affinity of the polyubiquitin chain on Cyclin B1 for the proteasome ubiquitin receptors.

3.4 Summary

In this chapter, I determined if K11-linked polyubiquitin chains were recognised by the proteasome and whether they acted as a signal for proteasomal degradation. I generated both free and substrate-bound K11 and K48-linked polyubiquitin chains using *in vitro* autoubiquitination of the E2 enzyme, Ube2S, and E3 enzyme, E6AP, respectively, and purified mammalian proteasome from rabbit muscle. Using an *in vitro* binding assay to compare binding of the substrate-bound polyubiquitin chains to purified proteasomes, I showed that K11-linked polyubiquitin conjugates did not bind the proteasome compared to K48-linked chains. Furthermore, K11-linked ubiquitin tetramers were not able to displace K48-linked polyubiquitin conjugates from purified 26S proteasomes, confirming that K11-linked chains bound more weakly to the proteasome than K48-linked polyubiquitin chains. To determine the relevance of these findings to known K11-polyubiquitinated substrates, we compared the ability of homotypic versus heterotypic polyubiquitin chains on Cyclin B1 to bind the proteasome. Homotypic K11-linked chains on Cyclin B1 were unable to bind the proteasome whereas heterotypic K11/K48-linked chains facilitated proteasome-mediated degradation, albeit less efficiently than homotypic K48-linked chains. Thus, while homotypic K11-linked polyubiquitin chains are not a signal for proteasome-mediated degradation, heterotypic K11/K48-linked chains are recognised by the proteasome and enable degradation of the polyubiquitinated substrate, Cyclin B1.

Chapter 4: Results 2, Identification of K11-ubiquitin binding proteins.

4.1 Introduction

4.1.1 The recognition of K11-linked polyubiquitin chains by ubiquitin binding proteins

To date, no specific UBPs have been identified for K11-ubiquitin chains. It had been suggested that the Rad23 protein, hHR23A binds to K11-polyubiquitinated Cyclin B1 and shuttle it to the proteasome (Jin et al., 2008). However, these observations may relate to Rad23 proteins associating with heterotypic K11/K48-polyubiquitin chains on cyclin B1 rather than homotypic K11-linked polyubiquitin linkages. Therefore, it was of interest to explore whether there were UBPs that bound specifically to K11-linked polyubiquitin chains or whether there were proteasome-associated shuttling factors which enabled K11-linked polyubiquitin chain binding to the proteasome.

In this chapter, I first examine how known proteasomal shuttling proteins bind to substrate-bound K11-linked polyubiquitin chains, before describing how mass spectrometry analysis of K11-linked polyubiquitin chains incubated with cell lysates can be used to identify potential novel K11-specific UBPs. I then investigate whether a novel protein, FAM115A (identified by mass spectrometry), is able to bind directly to K11-linked polyubiquitin chains using bacterial expression of the recombinant protein. Lastly, I focus on other UBPs found to bind to K11-linked polyubiquitin chains by mass spectrometry, and determine how Tax1 Binding Protein 1 (TAX1BP1, also known as T6BP1), and myosin VI bind to K11 and K63–linked polyubiquitin chains.

4.2 Results

4.2.1 Ubiquitin binding proteins involved in shuttling proteins to the proteasome do not bind K11-polyubiquitin chains.

Rpn10 and the Rad23 proteins (hHR23A and hHR23B) are the predominant UBPs thought to shuttle polyubiquitinated proteins to the proteasomes (Elsasser et al., 2004; Husnjak et al., 2008; Peth et al., 2010; Schreiner et al., 2008). To determine whether homotypic K11-chains are directed to the proteasome by associating with these proteasome shuttling factors, I measured the binding of polyubiquitinated GST-Ube2SΔ and GST-E6AP to either the proteasomal subunit Rpn 10 or purified hHR23A. The polyubiquitin conjugates were incubated with the His-tagged UIM of Rpn10 or full-length hHR23A for 1 hr at 4°C, the resins washed and the bound UBPs visualized by immunoblot (**Figure 4.1A**). While His-UIM bound to polyubiquitinated E6AP, minimal binding to the K11-conjugates was observed. HHR23A only bound to polyubiquitinated E6AP and not the K11-chains on Ube2SΔ. I repeated this binding experiment using recombinant hHR23B (**Figure 4.1B**) which, similarly to hHR23A, only bound to polyubiquitinated E6AP.

Having used recombinant proteins to investigate polyubiquitin chain binding, I went on to investigate whether the K11 and K48-chains associate with proteasome shuttling factors from cell lysates (**Figure 4.1C, D**). Polyubiquitinated GST-Ube2SΔ and GST-E6AP were incubated with HeLa cell lysates for 1hr at 4°C, the resins washed and proteins bound to the polyubiquitin conjugates visualized by immunoblot (**Figure 4.1C, D**). Rpn10, hHR23A and B bound to polyubiquitinated E6AP but not polyubiquitinated Ube2SΔ, consistent with the assays using the recombinant proteins. I also immunoblotted for another proteasome shuttling factor, Ubiquilin (UBQLN1), which contains an ubiquitin like domain (Ubl) and a ubiquitin associated domain (Ko et al., 2004). Similarly to the Rad23 proteins, UBQLN1 only bound to the K48-polyubiquitin chains.

While the proteasome shuttling factors demonstrated clear specificity for K48-linked polyubiquitin conjugates, it was important to determine whether the

K11-chains could bind other UBPs in cell lysates. Therefore, I probed the blots for the UBP, USP5, a deubiquitinating enzyme that can bind both K48 and K63-linked chains (Nathan et al., 2013). USP5 bound to both polyubiquitinated E6AP and Ube2SΔ, confirming that the K11-chains can be recognized by other UBPs.

Although the proteasome shuttling factors did not bind to the K11-chains, it remained possible that the Rad23 proteins, in complex with 19S, may increase the binding of K11-chains to the proteasome. To address this, I used K11-chains formed on GST-Ube2SΔ and K48-chains formed on GST-E6AP in the proteasome binding assay (**Figure 3.4**), but now in the presence of recombinant hHR23A. After 1hr incubation at 4°C, I washed the resins, and assessed the proteasomes bound to the polyubiquitin chains by LLVY-AMC cleavage. Polyubiquitinated E6AP bound strongly to the proteasome, and this binding is increased in the presence of hHR23A (protein purified by James Nathan) (**Figure 4.1E**), as previously reported (Nathan et al., 2013). However, hHR23A did not affect the ability of K11-chains on Ube2SΔ to bind to proteasomes (**Figure 4.1E**). Thus, Rad23 proteins, in complex with the 26S proteasome, did not facilitate the binding of K11-linked polyubiquitin conjugates to the proteasome.

Could there be other factors within cell lysate that affect the binding of K11-chains to the proteasome? To examine this, I incubated the K11-chains formed on GST-Ube2SΔ and K48-chains formed on GST-E6AP with Hela cell lysates, removed unbound proteins by sequential wash steps, and measured the binding of endogenous proteasomes within the cell extract to the polyubiquitin chains. The K48-linked polyubiquitin conjugates bound strongly to the endogenous proteasomes, however, the K11-chains only bound weakly to proteasomes (**Figure 4.1F**). Therefore, there did not seem to be other cellular factors that facilitated the binding of K11-linked polyubiquitin chains to the proteasome.

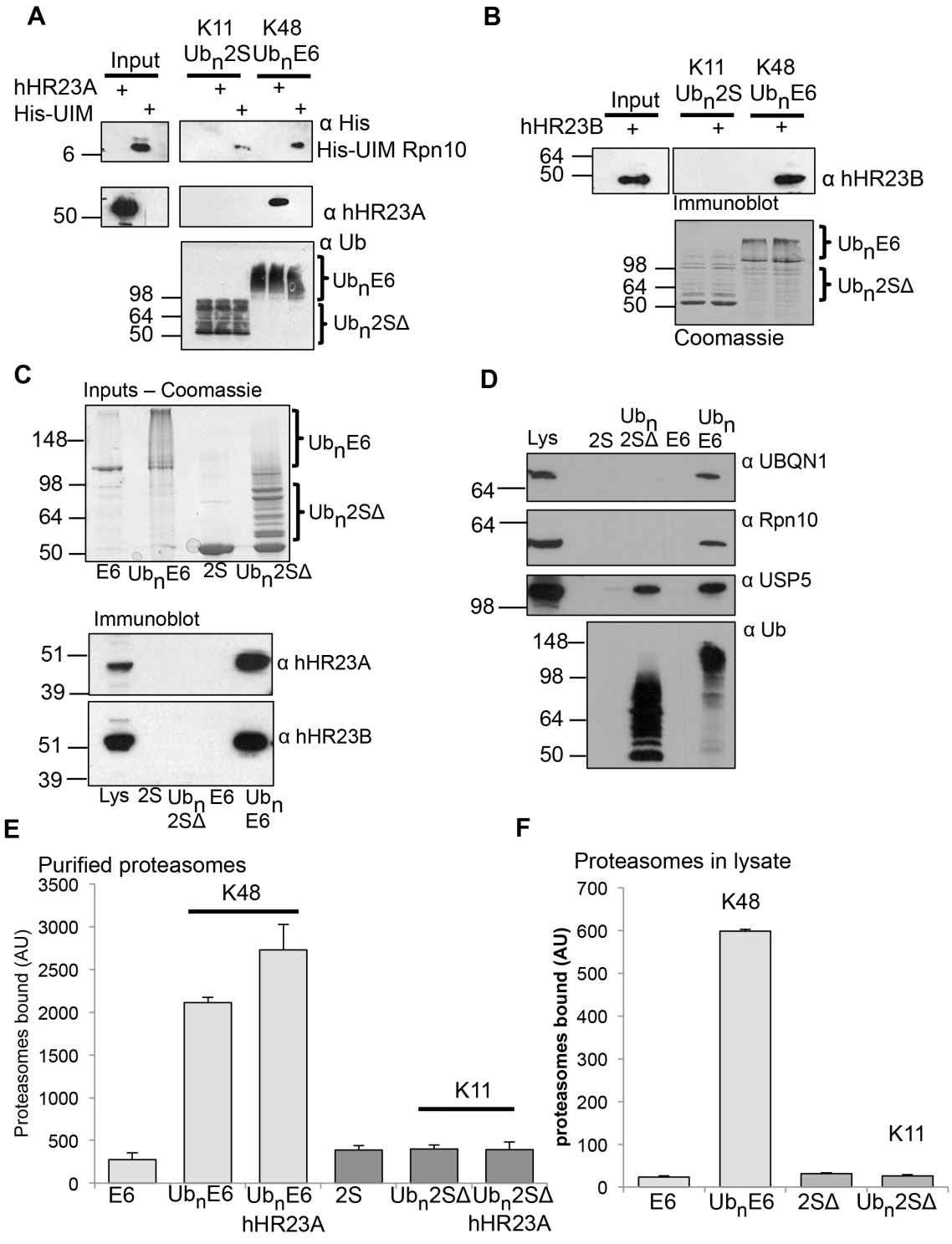
A
Input
K11 Ub$_n$2S
K48 Ub$_n$E6
hHR23A
His-UIM
α His
His-UIM Rpn10
α hHR23A
α Ub
Ub$_n$E6
Ub$_n$2SΔ
B
Input
K11 Ub$_n$2S
K48 Ub$_n$E6
hHR23B
α hHR23B
Immunoblot
Ub$_n$E6
Ub$_n$2SΔ
Coomassie
C
Inputs – Coomassie
Ub$_n$E6
Ub$_n$2SΔ
E6 Ub$_n$E6 2S Ub$_n$2SΔ
Immunoblot
α hHR23A
α hHR23B
Lys 2S Ub$_n$2SΔ E6 Ub$_n$E6
D
Lys
Ub$_n$2S
Ub$_n$2SΔ
E6
Ub$_n$E6
α UBQN1
α Rpn10
α USP5
α Ub
E
Purified proteasomes
Proteasomes bound (AU)
K48
K11
E6
Ub$_n$E6
Ub$_n$E6 hHR23A
2S
Ub$_n$2SΔ
Ub$_n$2SΔ hHR23A
F
Proteasomes in lysate
proteasomes bound (AU)
K48
K11
E6
Ub$_n$E6
2SΔ
Ub$_n$2SΔ

Figure 4.1: Proteasome-associated ubiquitin binding proteins preferentially bind K48-chains compared to K11-polyubiquitin chains. **(A, B)** Polyubiquitinated-E6AP and Ube2SΔ were incubated with 100nM Rpn10-UIM, hHR23A **(A)** or hHR23B **(B)** for 30 min at 4°C, washed and the bound proteins visualised by immunoblot for His (Rpn10) or hHR23A/B. Ubiquitination of E6AP and Ube2SΔ was confirmed by immunoblot for ubiquitin **(A)** or Coomassie **(B). (C, D)** Proteasome associated UBPs in cell extracts do not bind homotypic K11-chains. Polyubiquitinated-E6AP and Ube2SΔ were incubated with HeLa cell extracts for 30min at 4°C, washed and the bound proteins visualised by immunoblot for hHR23A and B **(C)**, or Rpn10, UBQLN1 and USP5 **(D).** Ubiquitination of E6AP and Ube2SΔ was confirmed by Coomassie **(C)** or immunoblot for ubiquitin **(D). (E)** Resin-bound polyUb-E6AP and Ube2SΔ were incubated with purified proteasomes, or with 26S particles and 300nM hHR23A. The bound proteasomes were measured by LLVY-AMC cleavage. **(F)** Proteasomes in cell lysates bind to K48-polyUb chains but not K11-chains. Resin-bound polyubiquitinated-E6AP and Ube2SΔ, and non-modified controls were incubated with HeLa lysates for 30 min at 4°C and the bound proteasomes measured. *Values are means ± SEM from three experimental replicates.*

4.2.2 Mass spectrometry approach to identify proteins that associate with K11-linked polyubiquitin chains.

Although K11-chains do not seem to bind the proteasome-associated UBPs or shuttling factors, they must be recognized by other UBPs to facilitate their functional outcomes in cells. We were also interested to determine whether there are UBPs that demonstrate linkage specificity for K11-chains, as has been shown for K48 and K63-linkages (Nathan et al., 2013). Therefore, to identify UBPs that bound K11-chains, we incubated polyubiquitinated GST-Ube2SΔ with HeLa cell lysates for 1hr at 4°C, extensively washed the resins, separated the proteins bound to the polyubiquitin conjugates by SDS-PAGE and visualized the bound proteins by Coomassie staining (these experiments were conducted with James Nathan). The gels were then analysed by MS/MS (**Table 4.1**). Polyubiquitinated E6AP was used as a control for identifying K48-selective UBPs.

The predominant proteins identified to be K48-specific were components of the 26S proteasome and associated UBPs. No proteasome subunits were observed to bind to the K11-conjugates, consistent with the proteasome binding experiments (**Chapter 3**). However, several proteins that bound to K11-ubiquitin linkages were identified. The most abundant protein by MS was an uncharacterized 102kDa protein, FAM115A. Other proteins that bound to K11-linkages are shown in **Table 4.1**. These included proteins with known UBDs, such as myosin VI, TAX1BP1 and Epsin 2; DUBs, including USP4, 11, and 15, which are a subgroup of USPs that contain a DUSP (domain present in ubiquitin-

specific proteases) (Harper et al., 2011). Several proteins bound to both K48 and K11-linked polyubiquitin chains, including the DUB USP5, which I had previously shown bound both chain types (**Figure 4.1D**).

As FAM115A was an uncharacterized protein, which potentially bound selectively to K11-linked polyubiquitin chains, I was keen to explore whether this was indeed a K11-specific UBP.

	K48 specific	K11 specific	Both K48 and K11
UBPs	3	5 (myosin VI, **Epsin 2**, Tax1BP, Tollip and UBXN1)	2 (WRNIP, TOM1L2)
Ubl-UBA proteins	2	0	0
E3 ligases	2	2 (NCCRP1/f box, RNF126)	2 (HUWE1, UBR4)
DUBs	3	4 (**USP15,** USP4, USP11, USP19)	2 (USP5, USP13)
26S components	14	0	2 (Alpha 4 and Rpt1)
P97 components	5	0	0
Uncharacterised	3	4 (**FAM115A, ANKRD13A,** PAIP1/PABC)	0

Table 4.1: Identification of ubiquitin binding proteins that bind to homotypic K11-linked ubiquitin chains. Polyubiquitinated GST-E6AP (K48-chains) or GST-Ube2SΔ (K11-chains) were incubated with A431 cell extracts at 4°C for 2 hr, the resins washed and the proteins bound to the resins separated by SDS-PAGE and analysed by MS/MS. The table summarises the proteins identified with more than 2 peptides.

4.2.3 Is FAM115A a novel K11-selective ubiquitin binding protein?

Bioinformatic analyses of FAM115A showed that it is predicted to be a soluble protein that is evolutionary conserved from zebrafish to humans. Using the Phyre2 structural prediction programme (Kelley et al., 2015), FAM115A is predicted to encode a flavodoxin-like fold at its N-terminus, and a C-terminal region that shows high structural homology to the aminopeptidase domain of ERAP1 (endoplasmic reticulum aminopeptidase 1) (**Figure 4.2A, B**), a single-pass type II ER membrane that cleaves the amino terminus of peptides to load onto MHC Class I (Chang et al., 2005). This ERAP1 like domain is also similar to a peptidase domain initially identified in bacteria (M60 domain) (Nakjang et al.,

2012) (**Figure 4.2B**). However, FAM115A encodes an arginine instead of a histidine in the predicted catalytic site that co-ordinates the zinc molecule (**Figure 4.2B**), and therefore may be catalytically inactive as a peptidase.

Initial experiments (conducted by James Nathan) suggested that FAM115A may bind to K11-polyubiquitin conjugates, as A431 cells stably expressing HA-FAM115A bound polyubiquitinated GST-Ube2SΔ resins more strongly than polyubiquitinated GST-E6AP (**Figure 4.2C**).

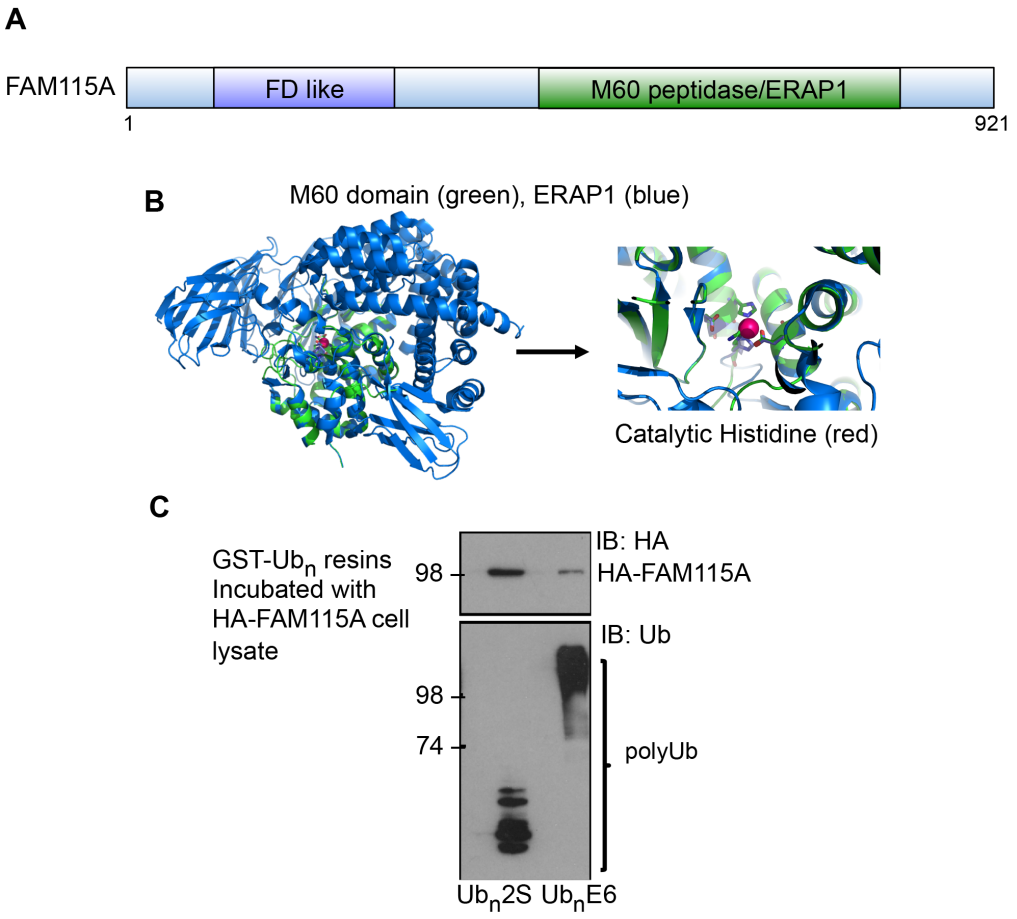

Figure 4.2: FAM115, a putative K11-ubiquitin binding protein. **(A)** Schematic of FAM115A protein (human) indicating the flavodoxin like region (FD like) and the M60 peptidase domain (M60/ERAP1). **(B)** Schematic ribbon diagram of the predicted M60/ERAP1 (green) like structure compared to ERAP1 (blue). The catalytic histidine (Maltepe et al.) in ERAP1 is indicated (images prepared by Roger Dodd, CIMR). **(C)** Association of HA-FAM115A from cell lysates with polyubiquitin conjugates (James Nathan, CIMR). HA-FAM115A was expressed in A431 cells, immunopurified and incubated with either ubiquitinated E6AP or Ube2S in vitro 1h 4° and the resins washed x4 TBS 1% NP40.

To examine whether FAM115A directly bound to the K11-polyubiquitin conjugates, it was important to generate recombinant FAM115A. Therefore, I made GST and His-tagged constructs of full-length FAM115A (FL), the flavodoxin-like fold (FD) and putative protease domain (M60). I transformed these constructs into DE3* *E. coli* using standard methods and induced protein synthesis with 0.5mM IPTG 37°C 3hr. These proteins were highly expressed in the bacteria but unfortunately were not soluble. I tested several His- and GST-tagged constructs, different *E. coli* strains (BL21, Rosetta, C41 and C43) different induction temperatures (16°C, 25°C, 37°C) and many different buffers for lysis, but only low concentrations of proteins were achieved with a GST-tagged construct of the M60 domain, and this rapidly aggregated in solution or remained on the resin after GST-PreScission cleavage (**Figure 4.3A-C**).

In a final attempt to purify FAM115A I used the Ligation Independent Cloning (LIC) system established by Dr Katrin Rittinger's group (National Institute for Medical Research/Francis Crick Institute), as a high throughput method to screen up to 96 different constructs at a time, testing for protein expression and solubility (**Chapter 2.3.1**). The advantage of this system is that one can make multiple peptides for each protein of interest, which may have differently solubility characteristics depending on the amino acid sequence. Therefore, working with Vangelis Christodoulou in Dr Rittinger's group at the NIMR, I designed primers for 48 FAM115A peptides, amplified the DNA by PCR and used LIC to insert the DNA into a LIC vector with an N-terminal His tag. These vectors were then transformed into BL21DE3* Gold *E. coli* and protein expression induced with 0.5mM IPTG overnight. Solubility of the peptides was assessed by SDS-PAGE and Coomassie staining. Although all constructs expressed successfully in *E. coli,* the peptides were either insoluble or migrated at the incorrect predicted size (probably truncated). Thus, bacterial expression of FAM115A was unsuccessful, and so far I have been unable to test whether it directly binds to K11-linked polyubiquitin chains.

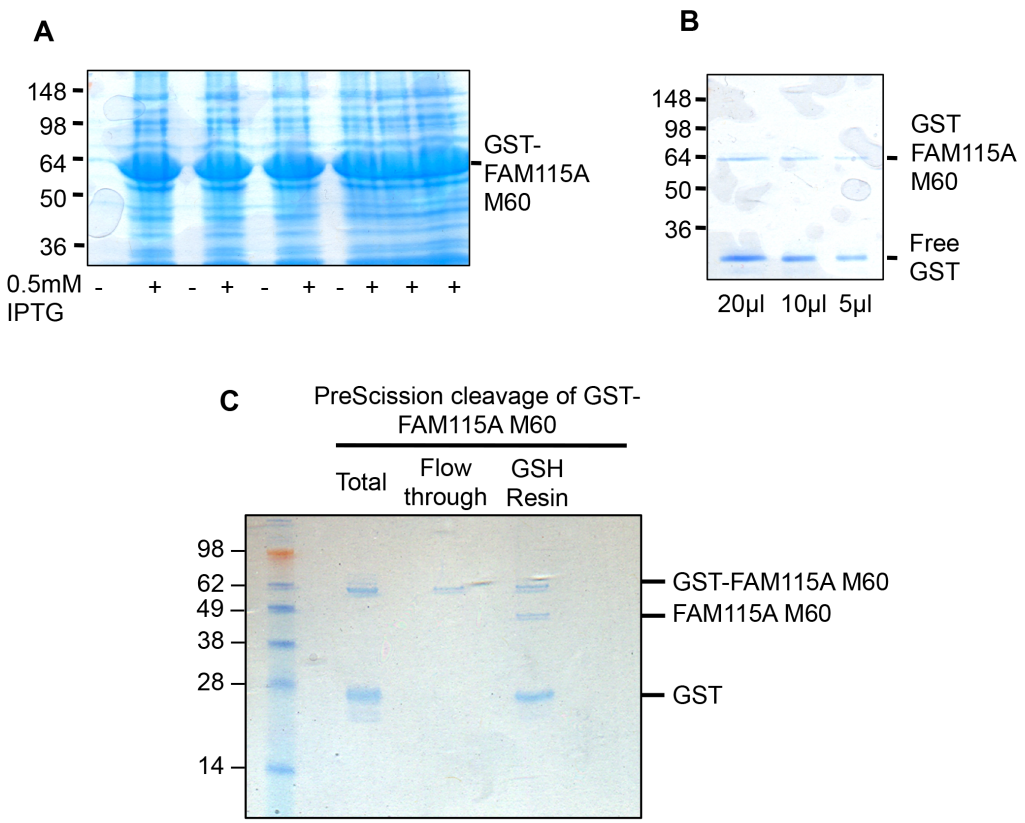

Figure 4.3: Expression of GST-FAM115A M60 in E. Coli. **(A-C)** GST-tagged FAM115A M60 was induced in *E. coli* with 0.5mM IPTG and expression in the total cell extracts measured by Coomassie staining **(A).** The GST-FAM115A M60 protein was then purified on glutathione sepharose beads and separated by SDS-PAGE before staining with Coomassie blue **(B).** PreScission cleavage of GST-FAM115A M60 on GSH resin overnight, analysed with Coomassie blue staining **(C).** The total reaction, flow through (unbound GST-FAM115A) and resin bound (GST-FAM115A, cleaved FAM115A, and free GST) are indicated.

4.2.4 Do ubiquitin binding proteins involved in mitophagy, TAX1BP1 and myosin VI, bind to K11 polyubiquitin chains?

While it proved difficult to examine if FAM115A was a K11-specific UBP, several other proteins that were enriched for K11-linked polyubiquitin conjugate binding were of interest (**Table 4.1**). The identification of the autophagy receptors, TAX1BP1 and Myosin VI, as putative K11-linkage selective UBPs from our mass spectrometry results (**Table 4.1**) were intriguing, and I studied this further as part of a collaboration with Folma Buss' group (CIMR).

Prior mass spectrometry based studies showed that K11-linked ubiquitin linkages increased during mitophagy (Cunningham et al., 2015), suggesting that K11-linked polyubiquitination is involved in this specialised form of autophagy. TAX1BP1 was also known to be recruited by the ubiquitin kinase PINK1 when mitophagy is induced (Lazarou et al., 2015). Furthermore, a ubiquitin binding domain in myosin VI that binds to K11, K63 and K29 dimers had been identified (He et al., 2016). Therefore, using recombinant TAX1BP1 and Myosin VI from Dr Buss and Dr Kendrick-Jones (**Chapter 2.3.2**) I aimed to examine how these proteins bind to K11-polyubiquitin chains and whether K11-polyubiquitin chains have a functional role in the binding of TAX1BP1 to myosin VI.

Do Myosin VI and TAX1BP1 bind to K11 and K63-linked ubiquitin tetramers in vitro? In order to measure whether K11 or K63-linked tetraubiquitin conjugates would bind to myosin VI CBD or TAX1BP1, it was first necessary to generate an *in vitro* binding assay. I used homotypic K11-linked tetramers that I had generated previously (**Chapter 3**) and recombinant His-TAX1BP1 and His-myosin VI cargo binding domain (CBD), containing the MyUb ubiquitin binding site recently identified as a novel ubiquitin binding domain which includes the RRL motif, responsible for binding autophagy receptors including TAX1BP1 (Morriswood et al., 2007). These proteins were designed and purified by Prof. John Kendrick-Jones (LMB). First, equal concentrations of the His-TAX1BP1 or His-Myosin VI CBD were immobilised on NiNTA agarose resin at 4°C for 30min on a rotator in the presence of Tris binding buffer (TBB) and then the resins washed to remove unbound proteins. The resin-bound His-TAX1BP1 or His-myosin VI CBD was then incubated alone or with increasing

concentrations of K11 or K63-tetramers for 30min at 4°C on a rotator, and unbound tetramers (Ub^4) removed by washing in TBB. Bound proteins were visualised by immunoblot using antibodies to TAX1BP1, myosin VI or ubiquitin respectively (**Figure 4.4A-C**). Interestingly, I found that His-TAX1BP1 or His-myosin VI CBD were able to bind both K11 and K63-Ub^4, however only weak binding to K11 Ub^4 was observed (**Figure 4.4A, B**).

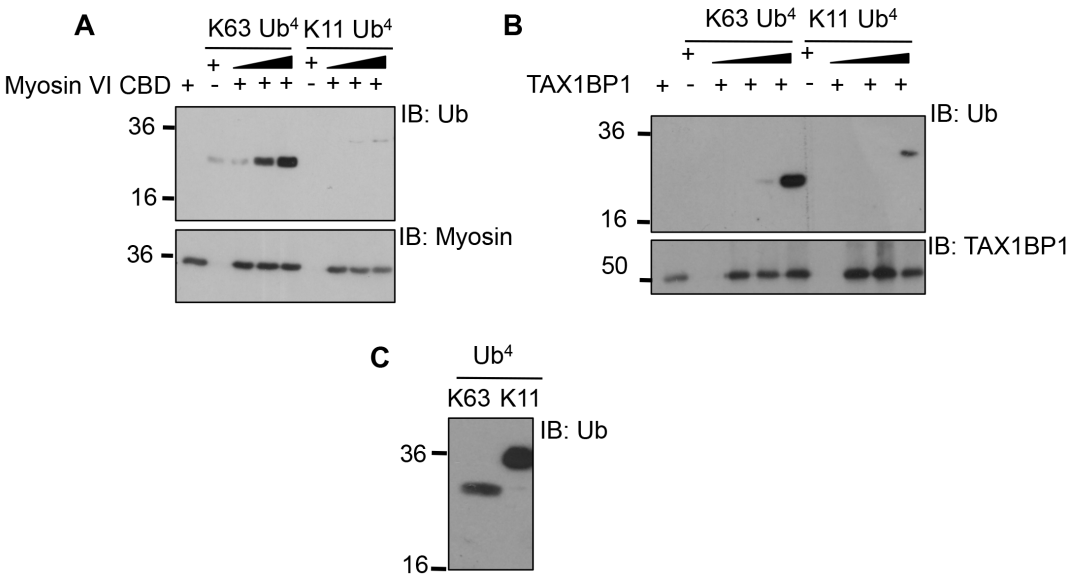

Figure 4.4: MyosinVI CBD and Tax1BP1 bind to K63 and K11 ubiquitin tetramers in vitro. **(A, B)** His-tagged MyosinVI cargo binding domain (CBD) **(A)** His-tagged Tax1BP1 (C-terminal half) (**B**) were bound to NiNTA resin and incubated with increasing concentrations of K63 or K11 tetra-ubiquitin (Ub^4) and then washed to remove unbound Ub^4. Bound proteins were visualised by immunoblot using antibodies against ubiquitin **(A, B**) and MyosinVI **(A)** or TaxBP1 **(B**). **(C)** Equal amounts of K63 or K11 Ub^4 were visualised by immunoblot using an antibody against ubiquitin (FK2).

Competition assay to measure K63 and K11 tetraubiquitin conjugate binding to Myosin VI CBD or TAX1BP1 in vitro. Myosin VI not only binds ubiquitin but can also bind TAX1BP1 (Morriswood et al., 2007; Sahlender et al., 2005). However, the myosin VI binding domains for ubiquitin and TAX1BP1 overlap (Tumbarello et al., 2015). Therefore, I wanted to determine whether ubiquitin or TAX1BP1 bound preferentially to myosin VI, or whether the

complex of TAX1BP1 with Myosin VI had a high affinity/avidity for K63 or K11-polyubiquitin chains.

Recombinant GST-myosin VI CBD was incubated with Glutathione Sepharose resin with either K11 or K63 ubiquitin tetramers for 30 min at 4°C on a rotator. Unbound proteins were removed by several washes in TBB. The resin-bound myosin VI and ubiquitin tetramers were then incubated with or without increasing concentrations of His-TAX1BP1, and bound proteins were visualised by immunoblot using antibodies to GST, ubiquitin or TAX1BP1 respectively (**Figure 4.5**).

Unfortunately, minimal binding of the K11-polyubiquitin chains to Myosin VI was observed, and TAX1PB1 did not alter the binding of Myosin VI to the ubiquitin chains (data not shown). However, interestingly, while the concentration of K63 Ub^4 bound to myosin VI remained the same with increasing concentrations of TAX1BP1 (**Figure 4.5, middle panel**), more TAX1BP1 bound to the GST-Myosin VI CBD when K63 Ub^4 was added (**Figure 4.5, lower panel**). Therefore, TAX1BP1 bound to Myosin VI CBD more strongly in the presence of K63-Ub^4, rather than displacing the ubiquitin chains, suggesting that a Myosin VI-K63Ub^4-TAX1BP1 complex was formed.

I attempted to repeat these experiments with higher concentrations of K11-Ub^4, but it was not possible to generate sufficient recombinant K11-Ub^4 for the competition assay. Therefore, it is probable that K11-linked polyubiquitin conjugates have a low affinity or avidity for the Myosin VI UBD, and are of less importance than K63-ubiquitin linkages in mitophagy.

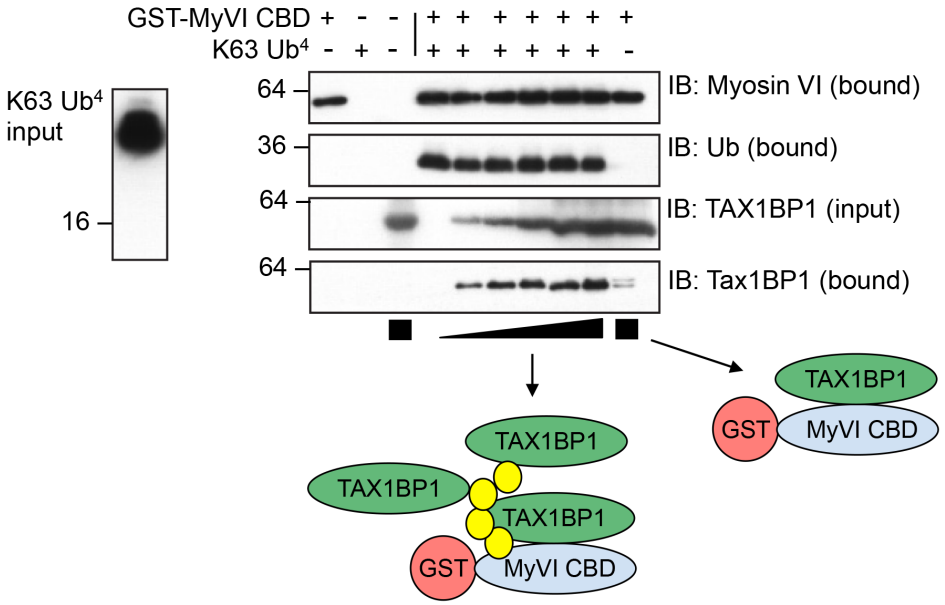

Figure 4.5: K63 tetramers form a complex with MyosinVI CBD and TAX1BP1. GST-tagged Myosin VII CBD (MyVI CBD, blue) and K63 tetra-ubiquitin (Ub^4) chains (yellow) were incubated with glutathione sepharose resin (GSH, red). The resins were washed and then incubated with increasing amounts of His-tagged TAX1BP1 (C-terminal half, green). The samples were analysed by immunoblotting with antibodies against GST to detect Myosin VI, bound ubiquitin (P4D1), and bound His-TAX1BP1. As controls, GST-MyosinVI CBD, K63 Ub^4, and His-TAX1BP1 were individually incubated with GSH sepharose to determine if there was any non-specific binding. GST-MyosinVI CBD and His-TAX1BP1 were also incubated together to demonstrate direct binding. Inputs of K63 Ub^4 and His-TAX1BP1 are also shown (TAX1PB1 input). *Representative of four independent experiments.*

4.3 Discussion

4.3.1 Is FAM115A a K11-linked polyubiquitin selective UBP?

It is very likely that K11-selective UBPs exist, particularly as they are required for other ubiquitin linkages in cells. The Rad23 proteins have been shown to bind K48-linked polyubiquitin chains and shuttle them to the proteasome (Elsasser et al., 2004; Nathan et al., 2013), whereas the ESCRT0 proteins Hrs and STAM1, preferentially bind K63-linkages, blocking their binding to the proteasome and instead diverting them to the ERAD pathway (Nathan et al., 2013; Ren and Hurley, 2010). Our mass spectrometry experiments identified several proteins that potentially bind selectively to K11-linked polyubiquitin chains, and I initially focused on FAM115A, as it was an uncharacterised protein that bound more strongly to K11-chains compared with K48-chains when immunopurified from cell lysates. Unfortunately these studies have been difficult to pursue, as I was unable to purify FAM115A in *E. coli* despite many attempts, and therefore could not determine whether FAM115A bound K11-chains directly. In addition, other members of the Nathan group attempted several approaches to examine if FAM115A is important in cell cycle regulation, and found that overexpression or depletion of FAM115A had no effect on the exit of cells from mitosis, cyclin B1 ubiquitination or proteasomal degradation.

During our investigations, FAM115A was reported to act as a membrane associated protein for temperature control channels, and was renamed TCAF-1 (TRPM8 Channel Associated Factor 1) (Gkika et al., 2015). TRPM8, a cold sensor, interacted with FAM115A using GST-pulldown assays. Cell surface biotinylation experiments showed that over expression of TCAF-1 resulted in increased TRPM8 levels at the cell surface, and siRNA-mediated depletion of TCAF-1 decreased conductance activity of the TRPM8 channel. Although the studies support the association of FAM115A/TCAF-1 with TRPM8, this study gives no additional insights into its putative role as a K11-UBP. Further attempts of purification of FAM115A could have been pursued, such as using a baculovirus expression system. However, this process would be a significant and high risk undertaking, given that the interaction we observed with HA-FAM115A and K11-linked chains was from cell lysate and maybe indirect.

4.3.2 Is the binding of K11-linked chains to TAX1BP1 and myosin VI of importance in mitophagy?

Both TAX1BP1 and myosin VI bound K11-linked chains, albeit weakly when compared to K63-linked chains. These findings are consistent with the work of the Polo lab, who show that Myosin VI can bind to K11, K63 and K29-linked di-ubiquitin (He et al., 2016). However, whether binding of these UBPs to K11-linked ubiquitin chains is a biological relevance to mitophagy remains to be determined.

Studies from the Harper group suggest that only K63 chains are essential (Ordureau et al., 2015) and that ubiquitin density at the mitochondrial membrane is likely to be important (Ordureau et al., 2014). By quantifying ubiquitin chains formed on mitochondria following mitochondrial depolarisation (Ordureau et al., 2014), the Harper group found that depolarisation leads to the formation of multiple different chain linkages (K6, K11, K48 and K63) on mitochondrial outer membrane proteins (Ordureau et al., 2014). Subsequently, they identified that mitochondria isolated from Ub^{K6R} or Ub^{K63R} replacement cells showed a reduction in mitophagy (Ordureau et al., 2015), indicating the importance of K63-linkages. Although a decrease in mitophagy was observed with Ub^{K11R}, the difference was not significant (Ordureau et al., 2015). Therefore, while it is also possible that K11-chains have a specific role in mitophagy, it is evident that K63-linkages are more important. This is also supported by my findings that more TAX1BP1 is recruited to Myosin VI when it is bound to K63-polyubiquitin conjugates (**Figure 4.5**). However, it would be of interest to examine if heterotypic K11/K63-chains are involved in mitophagy or have higher affinity or avidity for TAX1BP1 or myosin VI. Furthermore, as other groups have shown an involvement of K11-linkages in Beclin-1 degradation and autophagy (Jin et al., 2016), it will be important to determine the conformation of the chains involved.

4.3.3 Could other proteins that bound to polyubiquitinated Ube2S selectively bind K11-chains?

Several of the proteins listed in **Table 4.1** may be involved in the recognition of polyubiquitin chains, and potentially may bind K11-conjugates. For example, Ankyrin Repeat Domain 13 (ANKRD13) consists of three ankyrin repeats in the N-terminus and three or four UIMs in the C-terminus, depending on the isoform. ANKRD13 has been identified as a regulator of EGFR endocytosis from the plasma membrane via K63-polyubiquitination (Tanno et al., 2012). HeLa cells stimulated with Epidermal Growth Factor (EGF) showed that ANKRD13 A, B and D proteins bound K63-polyubiquitinated EGFR (Tanno et al., 2012). However, the role of K11-ubiquitination was not explored. In addition, the Komada lab recently identified ANKRD13 as a novel Valosine Containing Protein (VCP)-interacting protein on the endosome, which binds K63-polyubiquitinated Cav-1, leading to its lysosomal trafficking (Burana et al., 2016). As three of the proteins identified from our mass spectrometry analysis have been associated with both K63- and K11-chains (TAX1PB1, Myosin VI and ANKRD13), it is possible that the UBPs we identified have a preference for heterotypic K11/K63-linked chains on Ube2S. Indeed, our AQUA experiments showed that 92% of the linkages are lysine 11 but the remaining 8% may form heterotypic chains (**Chapter 3**). One mechanism to investigate this further would be to vary the concentrations of AMSH in the ubiquitin reaction to generate K11-homotypic or K11/K63-heterotypic chains on Ube2S and compare whether this alters the proteins bound to the polyubiquitin conjugates.

4.3.4 What are the biological roles of K11-linked polyubiquitin chains in cells?

Our experiments could provide a rationale for the observed proteasome-dependent and independent outcomes of K11-linked polyubiquitination that have been described.

Firstly, K11-linkages within a polyubiquitin chain may protect the substrate from proteasome mediated-degradation, as suggested by the studies of the Wnt/β-catenin pathway (Dao et al., 2012). The Druker and Bagby groups

(Dao et al., 2012) investigated whether the E3 ligase Fanconi anaemia complementation group L (FANCL), had an important role in maintaining haematopoietic stem cells. They showed that cells overexpressing FANCL ubiquitinated β-catenin, surprisingly lead to its stabilisation, not degradation. Using ubiquitin mutants, a K11-only mutant ubiquitin lead to stabilisation of β-catenin, almost to the same extent as wildtype ubiquitin. This suggests that when FANCL ubiquitinates β-catenin with K11-chains the protein is stabilised (Dao et al., 2012), supporting our findings that K11-linked polyubiquitination of a substrate is an inefficient signal for proteasomal degradation.

The ability of K11-linked polyubiquitination to stabilise proteins is also supported by Qin et al, in their studies on MITA (Mediator of IRF3 Activation), a protein involved in the innate interferon response to viral infection (Qin et al., 2014). The E3 ligase, Ring Finger protein (RNF) 5, ubiquitinates MITA with K48-chains signalling its proteasomal degradation (Zhong et al., 2009), whereas K63-linked polyubiquitination of MITA by TRIM56 and TRIM32 positively regulates type IFN induction (Zhang et al., 2012). Recently, however, Qin et al showed that an RNF26 ubiquitinates MITA with K11-chains during viral infection, which stabilises MITA (Qin et al., 2014). Interestingly, overexpression of RNF26 within cells led to autophagy-mediated degradation of MITA, which suggests there is a link between K11-linked polyubiquitination and proteasome-independent degradation.

The involvement of the K11-specific DUB, Cezanne (also known as OTUB7B) in the non-proteasomal degradation of HIF1α (Bremm et al., 2014) also supports a role for K11-chains in proteasome-independent degradation. The Komander group showed that knockdown of Cezanne decreased HIF1α levels in both normoxia and hypoxia. In addition, in cells where Cezanne was depleted, the proportion of K11-ubiquitin linkages (assessed by linkage specific antibodies) on HIF1α increased. However, this ubiquitinated HIF1α in Cezanne deficient cells did not increase following proteasome inhibition (Bremm et al., 2014). As the Nathan group has a particular interest in the hypoxia response pathway, I was keen to explore the role of K11-polyubiquitin and proteasome-independent degradation of HIFα further (**Chapter 5**).

4.4 Summary

In this chapter, I showed that the known proteasomal shuttling factors, Rpn10, Rad23 A and B and UBQLN1, were unable to bind K11-linked chains in comparison to K63-linked chains using an *in vitro* binding assay. However, the non-specific UBP, USP5, did bind both K11 and K63-Ub^4. Using a MS approach, we identified several proteins from cell lysates that putatively bound selectively to K11-linked polyubiquitin conjugates. I showed that the top candidate protein, FAM115A, was able to bind K11-linked polyubiquitin chains in cell extracts. However, it was not possible to determine whether this interaction was direct, as I was not able to recombinantly express FAM115A. Subsequently, I showed that two mitophagy receptors, MyosinVI and TAX1BP1, bound K11-linked chains, but more weakly than K63-linked chains. In addition, I found that K63- but not K11-ubiquitin tetramers formed a complex with MyosinVI and TAX1BP1. Together, these studies demonstrate that K11-polyubiquitin conjugates can be recognised by UBPs, but a K11-selective UBP remains elusive.

Chapter 5: Results 3, Mechanisms of HIFα prolyl hydroxylation

5.1 Introduction

My biochemical studies identified clear differences in the recognition of homotypic and heterotypic K11-ubiquitin linkages by the proteasome. These findings were surprising, given that K11-chains had previously been thought to have a major role in the cell cycle. Furthermore, although my biochemical studies on the ubiquitin receptors, TAX1BP and Myosin VI, suggested that K11-linked chains may have a role in mitophagy, they demonstrated very weak binding compared to K63-linked chains. Therefore, I wanted to explore the functional outcome of K11-ubiquitin chains in other cellular responses and focused on the HIF pathway.

Two prior studies predicted a role for K11-linkages in HIF regulation: (i) The K11-selective DUB Cezanne had been shown to be involved in the non-proteasomal degradation of HIF (Bremm et al., 2014), and the K11 E2, Ube2S, regulated HIF levels, putatively through ubiquitination of the VHL E3 ligase (Jung et al., 2006). A further reason for exploring the HIF pathway was that the Nathan group had recently uncovered novel metabolic mechanisms of HIF activation, independent of oxygen availability and potentially also independent of proteasome-mediated degradation. Stephen Burr (PhD student, Nathan lab) had undertaken forward genetic screens in aerobic conditions and identified genes involved in the TCA cycle (the 2-oxoglutarate dehydrogenase complex (OGDHc)) (**Figure 5.3**) and vacuolar-ATPase (V-ATPase) (**Figure 5.7**) that increased HIFα stability, but the mechanism was not known and it was possible that K11-linked polyubiquitin chains may be involved. Therefore, I wanted to establish an *in vitro* system to explore HIFα ubiquitination.

As the constitutive turnover of HIFα requires a two-step process, involving the initiation of ubiquitination via HIFα prolyl hydroxylation and its subsequent ubiquitination, this chapter focuses on establishing an *in vitro* assay

of HIFα prolyl hydroxylation, while the ubiquitination of HIFα is addressed in **Chapter 6**.

Previous assays of HIFα prolyl hydroxylation have used either direct or indirect measurements of PHD activity, typically using small HIF peptides, radio-labelling and the addition of excess cofactors to stimulate HIF hydroxylation (Hewitson et al., 2007b). While these techniques inform on the specificity and site of HIF prolyl hydroxylation, a major limitation is that they are not able to determine how changes in the cell (i.e. metabolite levels) directly affect HIFα hydroxylation. Therefore, I aimed to establish a novel assay that enabled quantification of PHD activity on the HIFα protein, using cell lysates without the addition of exogenous co-factors, providing a unique tool to elucidate the prolyl hydroxylation and subsequent ubiquitination of HIFα. Moreover, I wanted to use this assay to help uncover how HIFs can be regulated by small molecule metabolites.

Here, I first describe the generation of a recombinant HIF1α protein followed by the development of an *in vitro* assay to measure the prolyl hydroxylation of HIF1α under normoxic conditions, without the addition of exogenous cofactors. I use this assay to determine the effect of changes in cellular metabolites on HIF1α hydroxylation, and confirm that disrupting the OGDHc, prevents HIF1α prolyl hydroxylation. I also investigate how TCA small molecule metabolites can alter PHD activity. I subsequently use this assay to determine how HIF1α can be regulated in a seemingly proteasome-independent manner, and demonstrate that prolyl hydroxylation may be altered by inhibiting the main proton pump involved in lysosomal degradation, the Vacuolar ATPase (V-ATPase). Lastly, I develop an *in vitro* assay for HIF2α prolyl hydroxylation, and compare the metabolic regulation of prolyl hydroxylation between the two HIFα isoforms.

5.2 Results

5.2.1 Establishing an in vitro assay to determine hydroxylation of HIF1α: generation of a HIF1α recombinant protein.

To measure the hydroxylation and ubiquitination of HIFα *in vitro*, it was first necessary to generate a HIF1α recombinant protein that included the Oxygen Dependent Degradation Domain, which encodes the prolines and lysines modified by hydroxylation and ubiquitination respectively. Previous studies of HIFα prolyl hydroxylation had only used small peptides containing a single prolyl hydroxylated residue, and it was therefore unclear whether the whole ODD of HIF1α would be soluble in bacteria. To rapidly test the solubility of different HIF1α constructs I used a Ligation Independent Cloning (LIC) system, developed by Vangelis Christodoulou in Katrin Rittinger's lab (Francis Crick Institute) (**Figure 5.1A**). Eight HIF1α^{ODD} constructs were amplified by PCR and, using LIC, expressed in DE3* *E. coli* using standard methods (**Figure 5.1B, Appendix 1**). Protein synthesis was induced with either 0.5mM IPTG 37°C 3 hr or 0.1mM IPTG 25°C overnight. Pre and post-induction samples were centrifuged to separate soluble from insoluble protein and analysis by SDS-PAGE allowed me to identify which post-induction samples displayed clear bands indicating expression of soluble His-tagged HIF1α^{ODD} protein. The HIF1α$^{ODD530\text{-}652}$ protein was the most suitable for the subsequent assays, due to its small size and solubility (**Figure 5.1C**). However, His-HIF1α$^{ODD530\text{-}652}$ migrated between 16 and 22kDa (**Figure 5.1C**), which is slower than would be predicted for its molecular weight of 14kDa. I therefore analysed the pure protein by MS (Robin Antrobus, CIMR proteomics facility), and confirmed that it encoded the correct protein sequence.

In order to generate biochemical amounts of the His-HIF1α$^{ODD530\text{-}652}$ protein, I grew 2l of DE3* *E. coli* expressing the construct and induced protein synthesis with 0.5mM IPTG 37°C 3 hr. I initially attempted purification of the His-HIF1α$^{ODD530\text{-}652}$ protein using Fast Protein Liquid Chromatography (FPLC), however the protein failed to bind the NiNTA column (data not shown). This was possibly due to a partially exposed His tag within the folded protein. As an

alternative approach, I incubated the bacterial lysates with NiNTA resin for 2 hr, hypothesizing that a prolonged incubation step would allow the His-HIF1α$^{ODD530-652}$ protein to bind to the resin. This method improved protein binding and allowed elution of the HIF1α protein from the resin (**Figure 5.1D**), generating pure His-HIF1α$^{ODD530-652}$ protein for the hydroxylation and ubiquitination assays (**Figure 5.1D**).

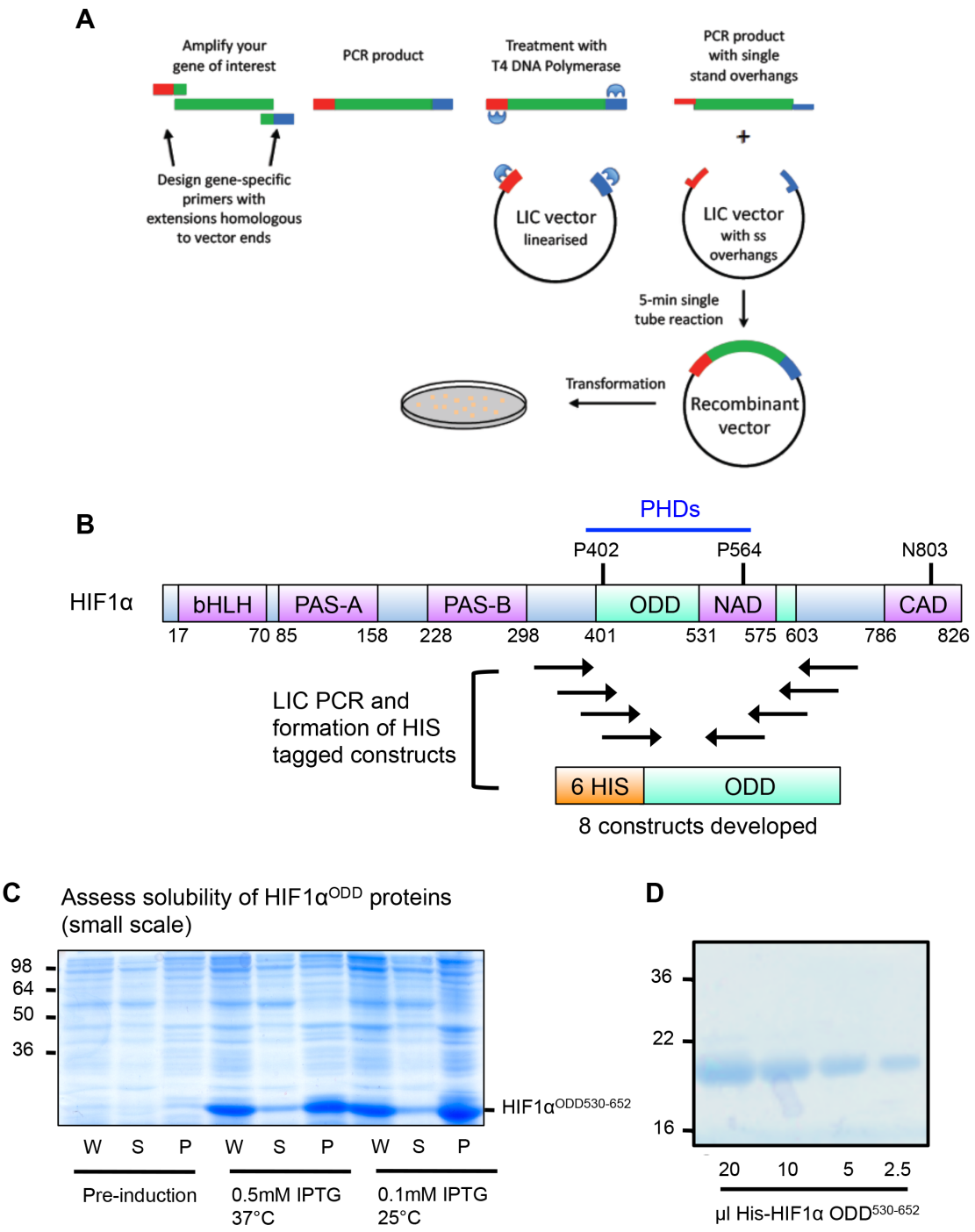

Figure 5.1: Generation of a HIF1α protein for use in the *in vitro* assay using ligation independent cloning. **(A)** Schematic of Ligation Independent Cloning technique (LIC) courtesy of Vangelis Christodoulou (Katrin Rittinger lab, Francis Crick Institute). **(B)** Schematic of LIC of the HIF1α^{ODD}. The two prolines that can be hydroxylated by the PHDs are highlighted. Eight constructs were amplified by LIC and cloned into a 6xHis expression vector. **(C)** Small-scale solubility assays were performed to identify the HIF1α^{ODD} protein best suited for the hydroxylation assay. Coomassie-stained gel shows solubility assay of HIF1α$^{ODD530-652}$ protein selected. W – whole sample, S- supernatant (soluble fraction), P- pellet (insoluble fraction). **(D)** Dilution series of the purified HIF1α^{ODD} protein selected, separated by SDS-PAGE and stained with Coomassie blue.

5.2.2 The HIF1α^{ODD} protein is hydroxylated in vitro in a PHD2 dependent manner without the addition of exogenous cofactors.

Prior studies typically used recombinant HIF1α peptides with the addition of exogenous co-factors, but I wanted to establish a system that would allow prolyl-hydroxylation, and ultimately ubiquitination, directly from a cell lysate. Therefore, I first isolated HeLa cell lysates that would provide a source of the prolyl hydroxylase enzyme, PHD2, and the essential cofactors for HIF1α hydroxylation, Fe^{2+} and 2-OG. Based on my prior studies using cell lysates as a source of the APC/C, I lysed 1 x 10^8 HeLa cells using freeze/thaw lysis in a hypotonic buffer, followed by mechanical needle lysis, separated the supernatants using centrifugation and collected these supernatants. I also obtained lysates from HeLa cells that had been depleted of PHD2 using CRISPR Cas9 genome editing (PHD2 null cells generated by Stephen Burr).

The prolyl hydroxylation assay was performed by incubating the HeLa lysates with 100nM of the His-HIF1α$^{ODD530-652}$ recombinant protein for 15 min at 37°C in TBS (**Figure 5.2A**), and the samples analysed by immunoblot for HIF1α, PHD2, β-actin, and a hydroxyl-proline specific antibody (OH-HIF1α) (**Figure 5.2B**). A single migrating species was identified by the HIF1α antibody, corresponding to the His-HIF1α$^{ODD530-652}$ protein. However, the hydroxyl-proline specific antibody (OH-HIF1α) only detected the HIF1α protein following 15 min incubation with the HeLa cell lysate. Furthermore, the levels of the prolyl-hydroxylated His-HIF1α$^{ODD530-652}$ were reduced in the PHD2-depleted cell extract, consistent with the antibody specifically recognising the prolyl-hydroxylated species (**Figure 5.2B**). These experiments confirmed that the His-HIF1α$^{ODD530-652}$ protein could be prolyl-hydroxylated *in vitro*, in a PHD2 dependent manner, without the use of exogenous cofactors.

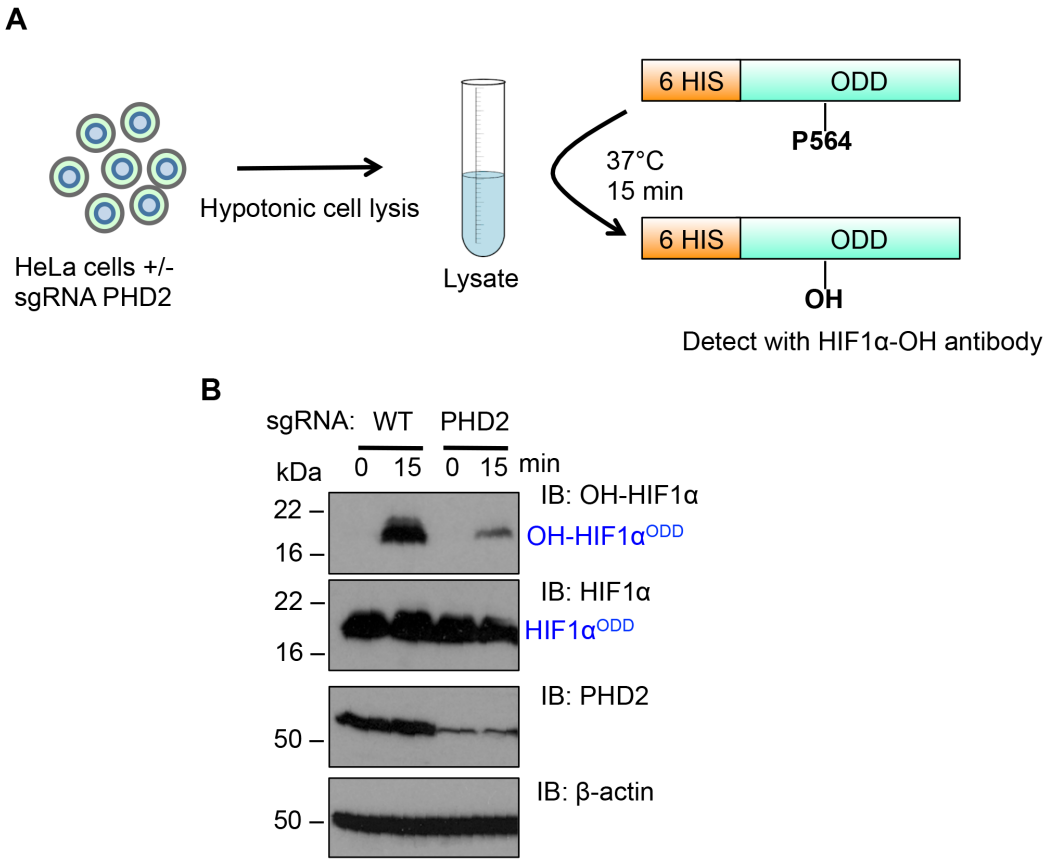

Figure 5.2: The HIF1α^{ODD} protein is hydroxylated *in vitro* in a PHD2 dependent manner without the addition of exogenous cofactors. **(A)** Schematic of the *in vitro* hydroxylation assay: 1 x 10^8 wildtype HeLa cells were lysed using freeze/thaw lysis in a hypotonic buffer. Lysates were also obtained from HeLa cells depleted of PHD2 using CRISPRCas9 genome editing (sgRNA). Supernatants were collected and incubated with the His-HIF1α^{ODD} recombinant protein for 15 min at 37°C. Prolyl-hydroxylation was detected using a hydroxyl-proline specific antibody (OH-HIF1α). **(B)** Hydroxylation of the His-HIF1α$^{ODD530-652}$ using wildtype and PHD2 depleted HeLa cell lysates. Prolyl hydroxylation was measured by immunoblot and compared to total His-HIF1α^{ODD} levels. β-actin served as a loading control.

5.2.3 HIF1α prolyl hydroxylation is prevented when the OGDHc is disrupted.

Next, I wanted to explore whether this hydroxylation reaction could be used to elucidate how HIF1α can be stabilised in aerobic conditions. In particular, this assay could help to explain the recent finding in the Nathan group that HIF1α was stabilised in aerobic conditions when the OGDHc was disrupted.

Using a forward genetic screen in near-haploid KBM7 cells, Stephen Burr (Nathan lab) identified two mitochondrial genes, oxoglutarate dehydrogenase (OGDH) and lipoic acid synthase (LIAS), whose deletion results in HIF1α stabilisation (**Figure 5.3A**) (Burr et al., 2016). OGDH is a core component of the oxoglutarate dehydrogenase complex (OGDHc), which catalyses the conversion of 2-OG to succinate in the TCA cycle (**Figure 5.3B, C**). The OGDHc has three subunits and one of these subunits (Dihydrolipoamide S-Succinyltransferase, DLST) requires lipoylation with lipoic acid for catalytic activity (**Figure 5.3C).** Therefore, we had genetic evidence that both OGDH and LIAS were required for catalytic activity of the OGDHc, which Stephen Burr went on to confirm (Burr et al., 2016). However, the mechanism for HIF1α stabilisation was not clear, and whether this prevented HIF1α prolyl hydroxylation (**Figure 5.3D**), ubiquitination or proteasome-mediated degradation was not known.

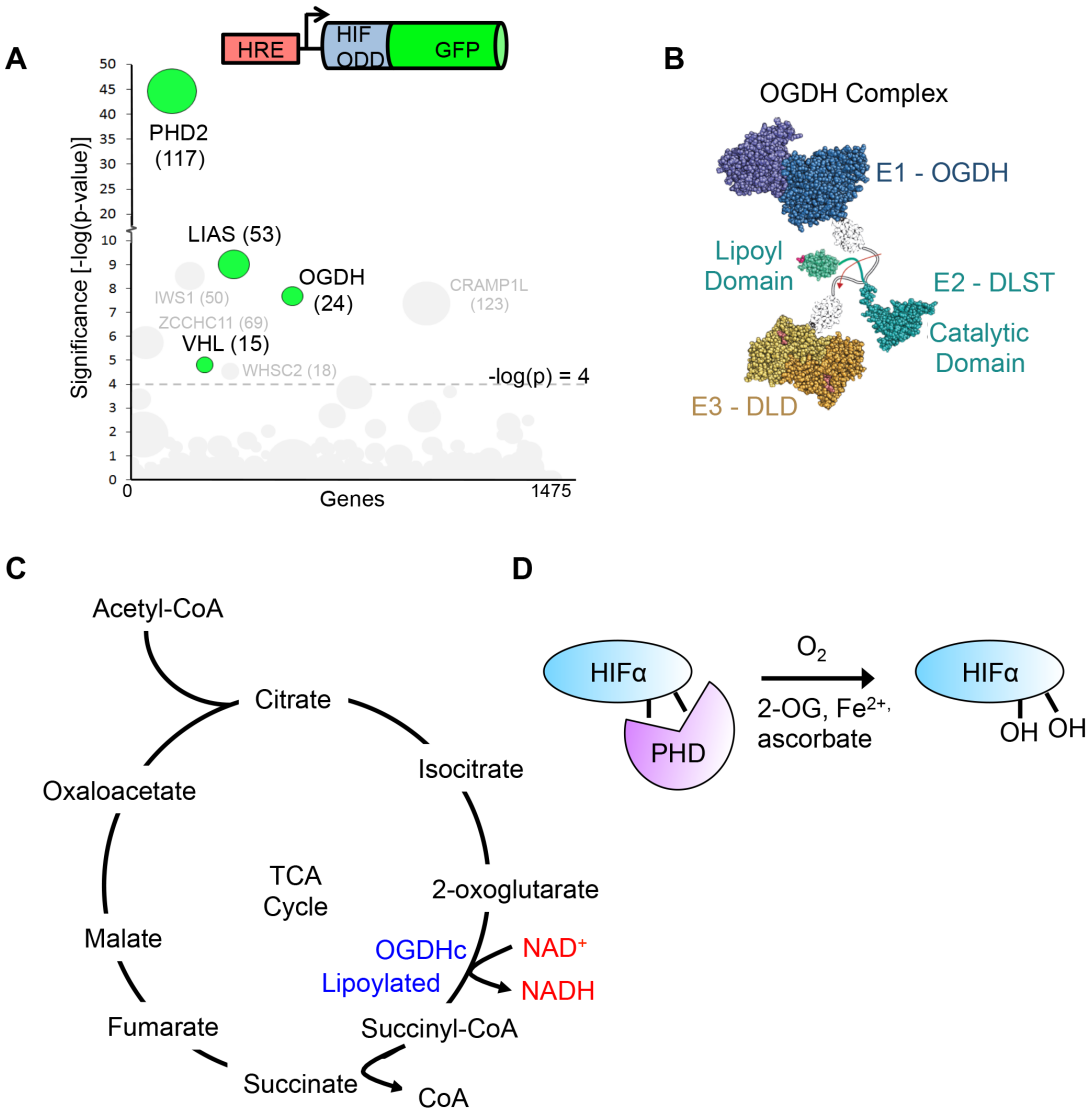

Figure 5.3: A KBM7 forward genetic screen identifies OGDH and LIAS as regulators of HIF1α stability. **(A)** Schematic of KBM7 HIFα-GFP reporter construct and results of the genetic screen by Stephen Burr (Nathan lab). KBM7 HIFα-GFP reporter cells were transduced with a gene-trapping retrovirus. Mutagenised GFP^{HIGH} cells were selected by FACS and the gene-trapping insertions mapped by Illumina HiSeq. The bubble plot of enriched genes in the GFP^{HIGH} population compared to unsorted mutagenised control KBM7 cells is shown. Bubble size is proportional to the number of independent inactivating gene-trap integrations identified (shown in brackets). **(B)** Structure of the OGDHc, showing OGDH and the lipoylated DLST (lipoylated by LIAS). **(C)** TCA schematic highlighting the OGDHc. **(D)** HIFα prolyl hydroxylation reaction, which requires 2-OG for catalytic activity. ***A, B,*** *adapted from (Burr et al., 2016).*

To test if OGDH or LIAS were required for HIF1α prolyl hydroxylation, I used HeLa cells from OGDH or LIAS CRISPR-Cas9 knockout (KO) clones (validated by Stephen Burr (Burr et al., 2016)) and measured prolyl hydroxylation of His-HIF1α$^{ODD530-652}$ (**Figure 5.4A**). HIF1α prolyl hydroxylation was observed after 15 min in the wildtype HeLa lysates incubated with the His-HIF1α$^{ODD530-652}$ protein, similarly to my initial optimisation experiments. Moreover, a PHD2 null clone completely prevented prolyl hydroxylation of the HIF1α protein (**Figure 5.4B, C**), confirming that PHD2 is the main PHD for HIF1α in HeLa cells. Incubating the wildtype HeLa lysate with the well-validated PHD inhibitor, Dimethyloxalolylglycine (DMOG,) for 10 min 37°C prior to the hydroxylation assay also prevented His-HIF1α$^{ODD530-652}$ prolyl-hydroxylation **(Figure 5.4B),** again confirming the specificity of my assay. Two null OGDH (**Figure 5.4B**) and LIAS (**Figure 5.4C**) clones were examined respectively, and in all cases demonstrated decreased levels of prolyl hydroxylation compared to the wildtype cells. Indeed, in two of the clones prolyl hydroxylation was not detected. The variability in levels of the hydroxylated HIF1α protein in the OGDH and LIAS null clones suggests that they are not directly involved in catalytic activity but alter the levels of metabolites, that may interfere with 2-OG dependent dioxygenase activity. However, it was clear that deletion of OGDH or LIAS led to inhibition of the prolyl hydroxylation of HIF1α *in vitro*.

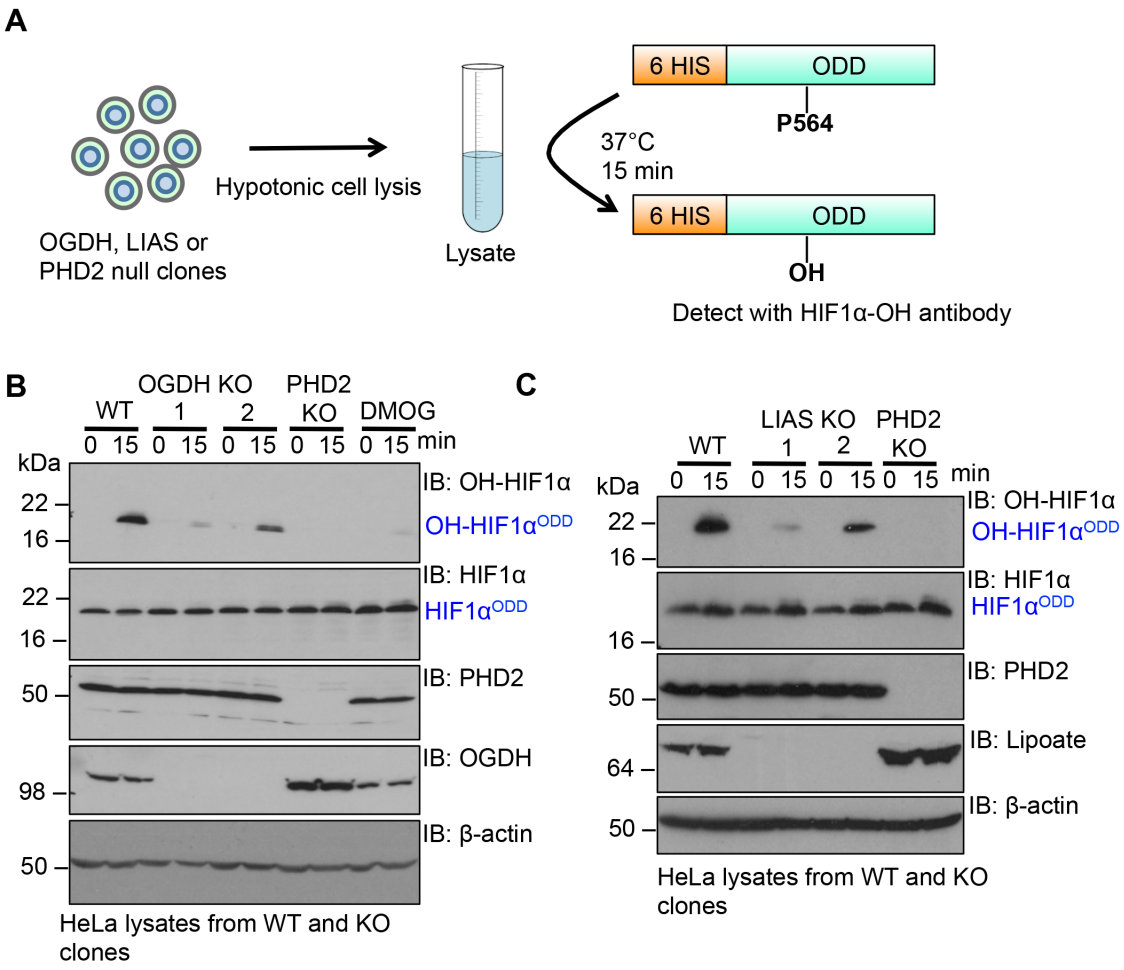

Figure 5.4: HeLa cells extracts depleted of mitochondrial enzymes OGDH or LIAS inhibit HIF1α^{ODD} prolyl hydroxylation. **(A)** Schematic showing the HIF1α hydroxylation assay with lysates from OGDH, LIAS or PHD2 knockout (KO) clones. **(B, C)** Immunoblots of prolyl hydroxylated and total His-HIF1α$^{ODD530-652}$ in WT, OGDH null **(B)**, LIAS null **(C)** or PHD2 null **(B, C)** lysates. OGDH or LIAS loss (lipoate antibody detects lipoyl moiety on OGDHc) was confirmed by immunoblot. β-actin served as a loading control.

5.2.4 HIF1α prolyl hydroxylation is impaired by the small molecule metabolite, L-2-hydroxyglutarate.

The most likely explanation for the inhibition of PHD activity following OGDH or LIAS depletion related to changes in small molecule metabolite levels when the TCA cycle was disrupted. Several TCA metabolites, such as succinate, are known to inhibit prolyl hydroxylation by directly competing for 2-OG binding

to PHDs (Selak et al., 2005). This oxygen-independent stabilisation of HIF1α drives a transcriptional HIF response and promotes tumour metastases (Kaelin, 2008; Maxwell and Ratcliffe, 2002). Whole cell metabolite studies (performed by Stephen Burr, Nathan lab, and Sofia Costa, Frezza lab) showed that succinate was not increased in the LIAS and OGDH null cells, and in fact was barely detectable. However, one metabolite was markedly increased in the OGDH and LIAS null clones, 2-hydroxyglutarate (Burr et al., 2016).

2-HG is a chiral compound that exists in both L-2-HG and D-2-HG forms in cells, previously implicated in altering the activity of 2-OG dependent dioxygenases. However, it was controversial whether both enantiomers inhibit or activate the PHD enzymes, or whether 2-HG can accumulate to a sufficiently high level in cells to inhibit 2-OG dependent dioxygenases (Chowdhury et al., 2011; Tarhonskaya et al., 2014; Xu et al., 2011).

To investigate whether the levels of small molecule metabolites altered prolyl-hydroxylation in my assay, I first determined whether succinate, which had previously been shown to inhibit PHD activity, prevented prolyl-hydroxylation. HeLa lysates were incubated with increasing concentrations of succinate for 10 min at 37°C, before incubating with the His-HIF1α$^{ODD530-652}$ peptide for 15 min at 37°C (**Figure 5.5A**), and analysis by immunoblot as previously described (**Results 5.2.2**). DMOG was used as a control, as described previously. While total levels of HIF1α$^{ODD530-652}$ remained constant between the samples, prolyl-hydroxylated His-HIF1α$^{ODD530-652}$ decreased with increasing concentrations of succinate, compared with WT HeLa lysate (**Figure 5.5A**). Interestingly, relatively high levels of succinate (5-10mM) were required to inhibit the prolyl-hydroxylation. This compares similarly to the *in vitro* prolyl hydroxylation assay performed by Selak et al, in which concentrations of 5mM succinate were shown to inhibit hydroxylation of HIF1α (Selak et al., 2005).

Next, I wanted to explore whether the 2-HG enantiomers altered prolyl hydroxylation of the HIF1α$^{ODD530-652}$ protein. HeLa cell lysates were pre-incubated with either L-2-HG or D-2-HG before adding to the HIF1α$^{ODD530-652}$ peptide for 15 min at 37°C (DMOG was used as a control for prolyl-hydroxylation inhibition) (**Figure 5.5B, C**). Increasing concentrations of the L-2-HG enantiomer reduced prolyl-hydroxylation of the HIF1α$^{ODD530-652}$ peptide, similarly to the

addition of DMOG, however addition of the D-2HG enantiomer had no effect (**Figure 5.5B, C**). Interestingly, higher levels of D-2-HG actually increased prolyl hydroxylation of HIF1α$^{ODD530-652}$ (**Figure 5.5B, right panel**), consistent with a prior report showing that D-2-HG may activate the HIF response (Koivunen et al., 2012; Losman et al., 2013). However, this did not reach statistical significance when examined in several biological replicates (**Figure 5.5C**).

It was noteworthy that inhibition of PHD activity occurred at relatively low levels L-2-HG (0.5-1mM), making this a plausible inhibitor of PHDs when the OGDHc was impaired. In fact, subsequent studies by Stephen Burr demonstrated that L-2-HG can accumulate to 1mM in cells when OGDHc activity is impaired, in support of this *in vitro* assay (Burr et al., 2016).

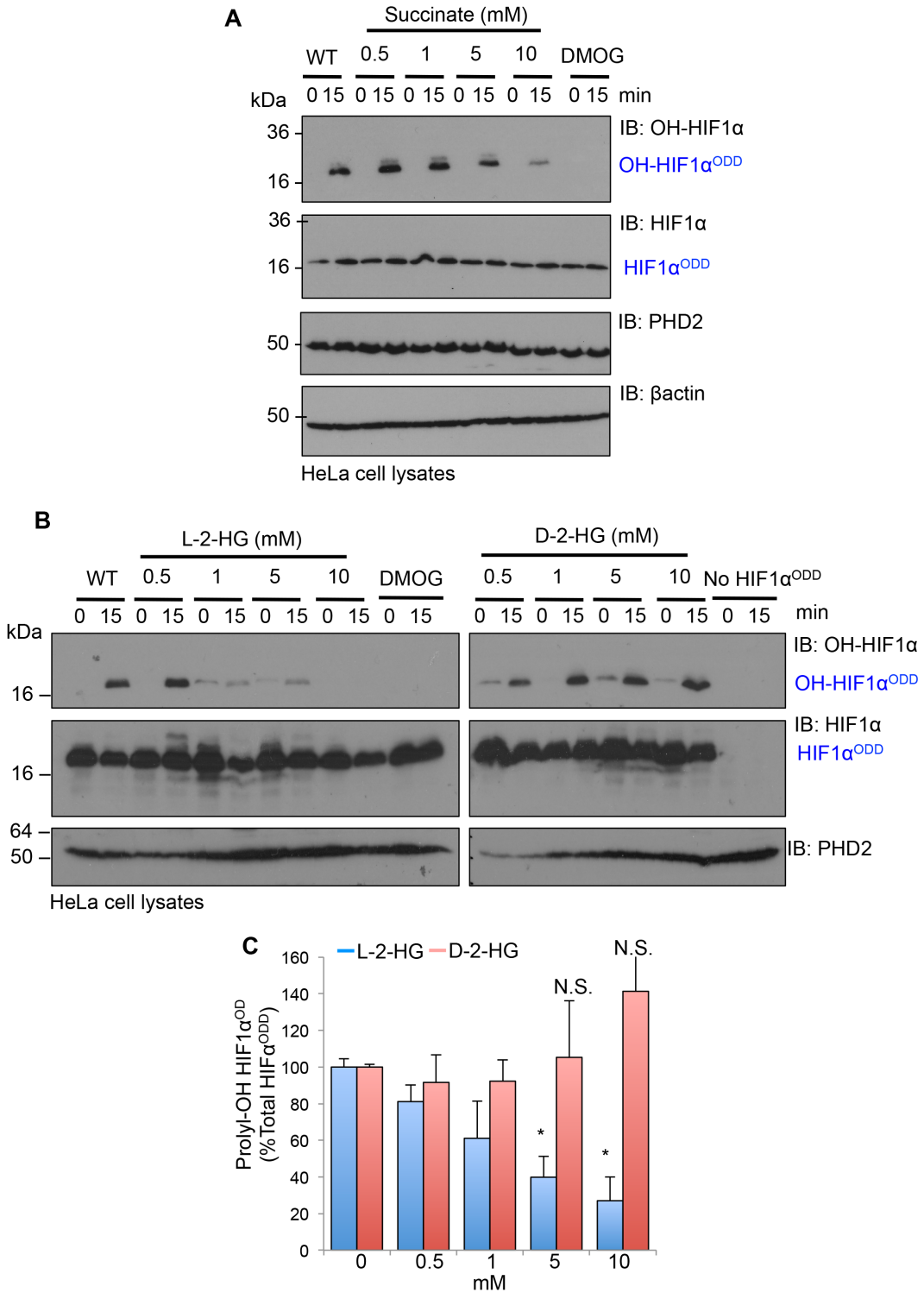

Figure 5.5: HIF1α hydroxylation is regulated by succinate and the 2-hydroxyglutarate enantiomers. **(A)** Prolyl hydroxylation of His-HIF1α$^{ODD530-652}$ in wildtype (WT) HeLa lysates with or without the addition of succinate or DMOG. The hydroxylation assay was performed as previously described. **(B,C)** Prolyl hydroxylation of His-HIF1α$^{ODD530-652}$ in HeLa cell lysates with the addition of either L-2-HG or D-2-HG. Representative immunoblots are shown **(B)**. Quantification using ImageJ software of three replicates. *Mean±SEM, *p<0.05. N.S. = not significant.*

5.2.6 Addition of 2-OG inhibits HIF1α hydroxylation and cannot restore PHD2 activity when the OGDHc is disrupted.

In principle, small molecule metabolite inhibition of PHDs should be reversible, following the addition of sufficient 2-OG. Therefore, excess 2-OG should be able to restore HIF1α prolyl hydroxylation when L-2-HG has accumulated following disruption of the OGDHc (**Figure 5.6A**). Using either WT HeLa lysate or lysates from OGDH or PHD2 KO null clones, I first confirmed that His-HIF1α$^{ODD530\text{-}652}$ prolyl hydroxylation was reduced in the OGDH KO's **Figure 5.6B**), consistent with my prior findings. Next, I examined if the addition of 2-OG restored HIF1α hydroxylation in the OGDH null lysates (**Figure 5.6C, D**)**.** Surprisingly, WT HeLa lysate showed decreased prolyl-hydroxylation of the His-HIF1α$^{ODD530\text{-}652}$ protein with pre-incubation of 2-OG, similar to the inhibition observed with DMOG or in the PHD2 KO clone (**Figure 5.6C**)**.** Furthermore, the addition of 2-OG to the OGDH KO clone decreased prolyl hydroxylation further after 15 min (**Figure 5.6D**). However, I did observe some restoration of prolyl hydroxylation in the OGDH null lysates, particularly with 1 and 5 mM, at the 0 min sample (**Figure 5.6D**), suggesting that addition of 2-OG may have very transient effects on restoring prolyl hydroxylation.

As 2-OG is converted to L-2-HG in cells by the enzymes Lactate Dehydrogenase (LDHA) and Malate Dehydrogenase 1 and 2 (MDH 1/2) (Intlekofer et al., 2015; Oldham et al., 2015), it was possible that the inhibition of HIF1α hydroxylation by 2-OG was due to the rapid conversion of 2-OG to L-2-HG in the cell lysates. Indeed, in related studies, Stephen Burr had shown that inhibition of LDHA with oxamate prevented the formation of L-2-HG when OGDHc activity was impaired, and restored HIF1α degradation (Burr et al., 2016). Furthermore, the conversion of 2-OG to L-2-HG within the lysate may explain why hydroxylation was observed in the 0 min samples in the OGDH null cells, but not after a 15 min incubation (**Figure 5.6D**).

Therefore, I examined whether the addition of oxamate to the OGDH cell lysate restored prolyl hydroxylation. However the addition of oxamate to cell lysates altered the pH of the reaction to such an extent (indicated by the colour change on the loading buffer) that proteins precipitated from the reaction and it

was not possible to determine whether any inhibition of HIF1α hydroxylation was due to the activity of oxamate or to the pH change and protein precipitation in the reaction (data not shown). Thus, the reason for inhibition of prolyl hydroxylation following 2-OG remains unclear, but it may be due to conversion to L-2-HG.

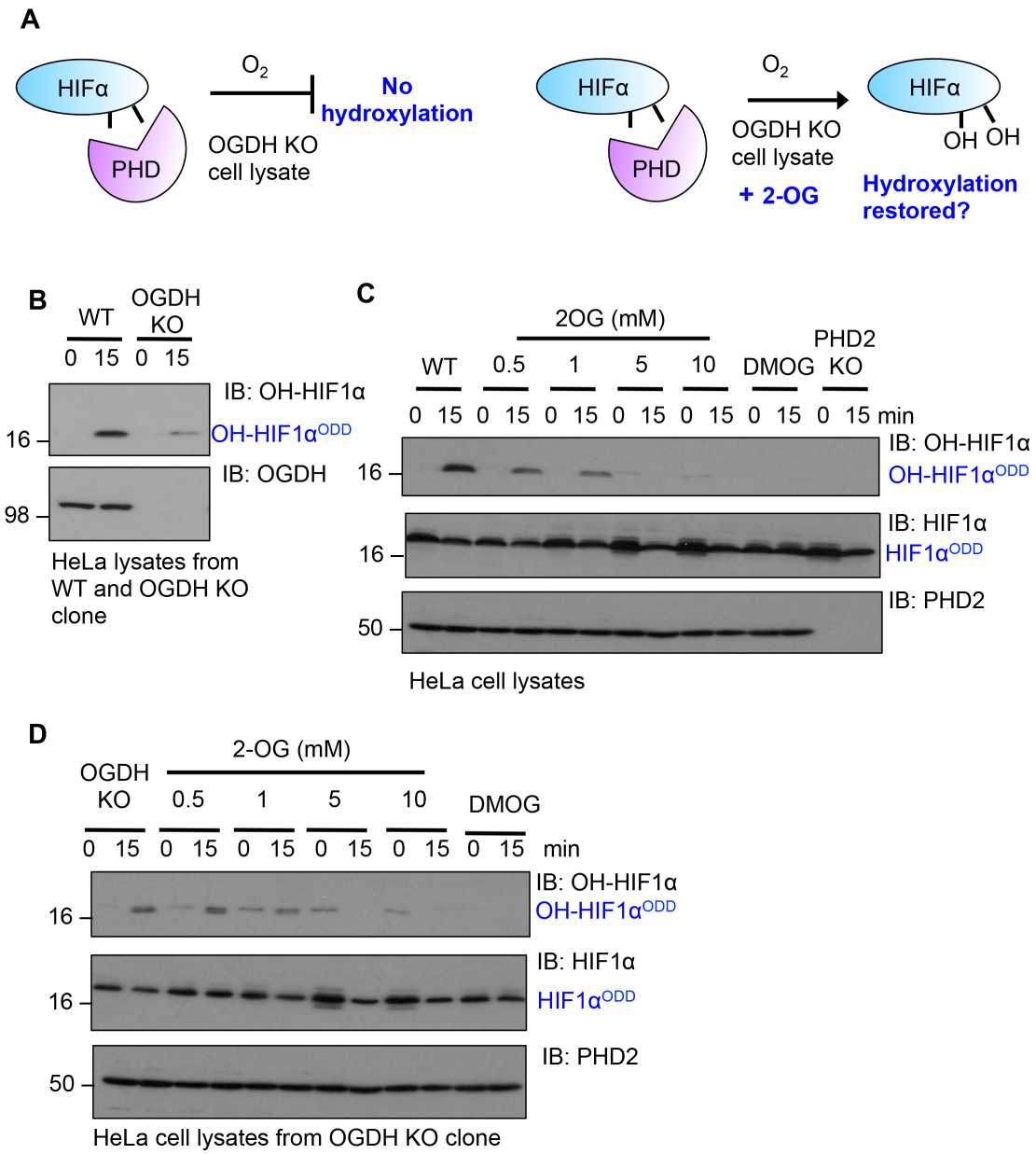

Figure 5.6: Addition of 2-OG inhibits HIF1α^{ODD} hydroxylation and cannot restore PHD2 activity when the OGDH complex is disrupted. **(A)** Schematic of the experimental outline, showing HIF1α hydroxylation assay with the addition of 2-OG (0.5-10mM) in the OGDH KO clone. **(B)** Immunoblot of prolyl hydroxylated His-HIF1α$^{ODD530-652}$ in HeLa lysates from WT cells and an OGDH KO clone. **(C, D)** Immunoblot of prolyl hydroxylated and total His-HIF1α$^{ODD530-652}$ with increasing concentrations of 2-OG in WT **(C)** or OGDH null **(D)** cells. PHD2 null cells or DMOG treated lysates were used as controls for inhibition of HIF1α prolyl-hydroxylation.

5.2.7 Inhibition of the Vacuolar H+ATPase prevents HIF1α hydroxylation via depletion of intracellular iron.

Studies using disruption of the OGDHc highlighted the ability of the *in vitro* approach to directly measure the effects of metabolic changes on prolyl-hydroxylation and HIF1α stabilisation. However, I was also keen to explore whether this assay could be informative in other situations where HIF1α stabilisation has been observed but the mechanism was not known. An interesting observation from the forward genetic screen in near-haploid cells using the HIFα fluorescent reporter was that gene-trap mutations in the vacuolar ATPase (V-ATPase) stabilised HIF1α, but this was not dependent on lysosomal degradation (Burr et al., 2016; Miles et al., 2017) (**Figure 5.7**). Indeed, stabilisation of HIF1α by inhibition of the V-ATPase with Bafilomycin A had been shown by several groups previously, although the mechanism was unclear (Bremm et al., 2014; Ferreira et al., 2015; Hubbi et al., 2013; Lim et al., 2007; Selfridge et al., 2016; Zhdanov et al., 2012). My *in vitro* assay provided an opportunity not only to determine whether deletion of the V-ATPase subunit genes would directly inhibit the prolyl hydroxylation of HIF1α *in vitro,* but also to assist in identifying the mechanism by which this inhibition occurs.

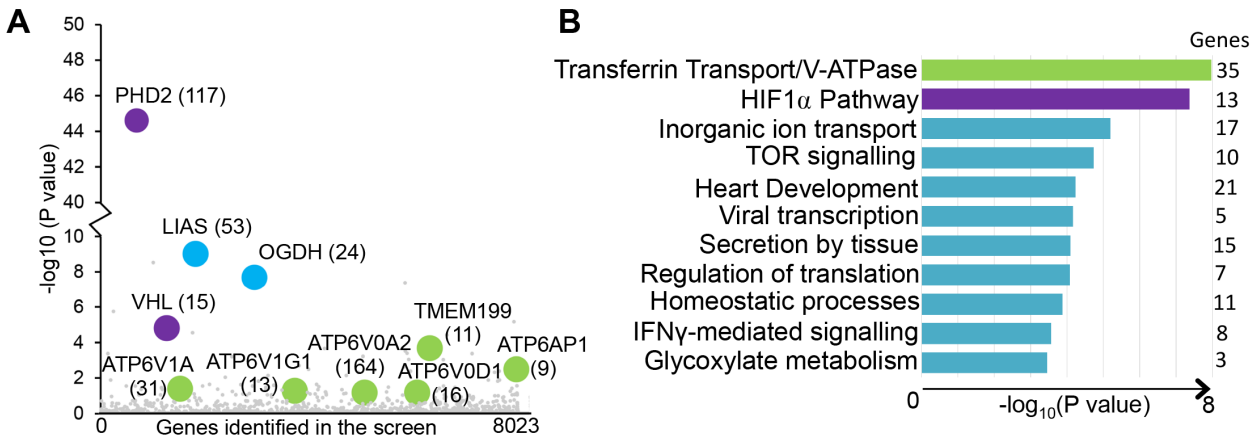

Figure 5.7: A KBM7 forward genetic screen identifies V-ATPase subunits as regulators of HIF1α stability. **(A)** Results of the genetic screen by Stephen Burr. KBM7 HIFα-GFP reporter cells were transduced with a gene-trapping retrovirus. Mutagenised GFP^{HIGH} cells were selected by FACS and the gene-trapping insertions mapped by Illumina HiSeq. The bubble plot of enriched genes in the GFP^{HIGH} population compared to unsorted mutagenised control KBM7 cells is shown. **(B)** Gene-ontology pathway analysis of genes most enriched for gene-trapping insertional mutations in the genetic screen. *Adapted from (Miles et al., 2017).*

To investigate how inhibition of the V-ATPase may alter the hydroxylation of HIF1α I treated HeLa lysates with 10nM Bafilomycin A (BafA) overnight, harvested the cells, lysed them as described (**Results 5.2.2**), and compared the levels of His-HIF1α$^{ODD530-652}$ prolyl-hydroxylation in BafA treated or untreated HeLa lysates (**Figure 5.8A, B).** The levels of prolyl-hydroxylated His-HIF1α$^{ODD530-652}$ were markedly reduced in the BafA treated cell extract, similar to the levels observed when DMOG was added to the hydroxylation reaction. As a further control, I treated cells with 100μM of the iron chelator desferrioxamine (DFO) overnight, which inhibited prolyl-hydroxylation similarly to the BafA treated cells (**Figure 5.8C**). Thus, V-ATPase inhibition decreases the activity of prolyl-hydroxylation in the cell extracts.

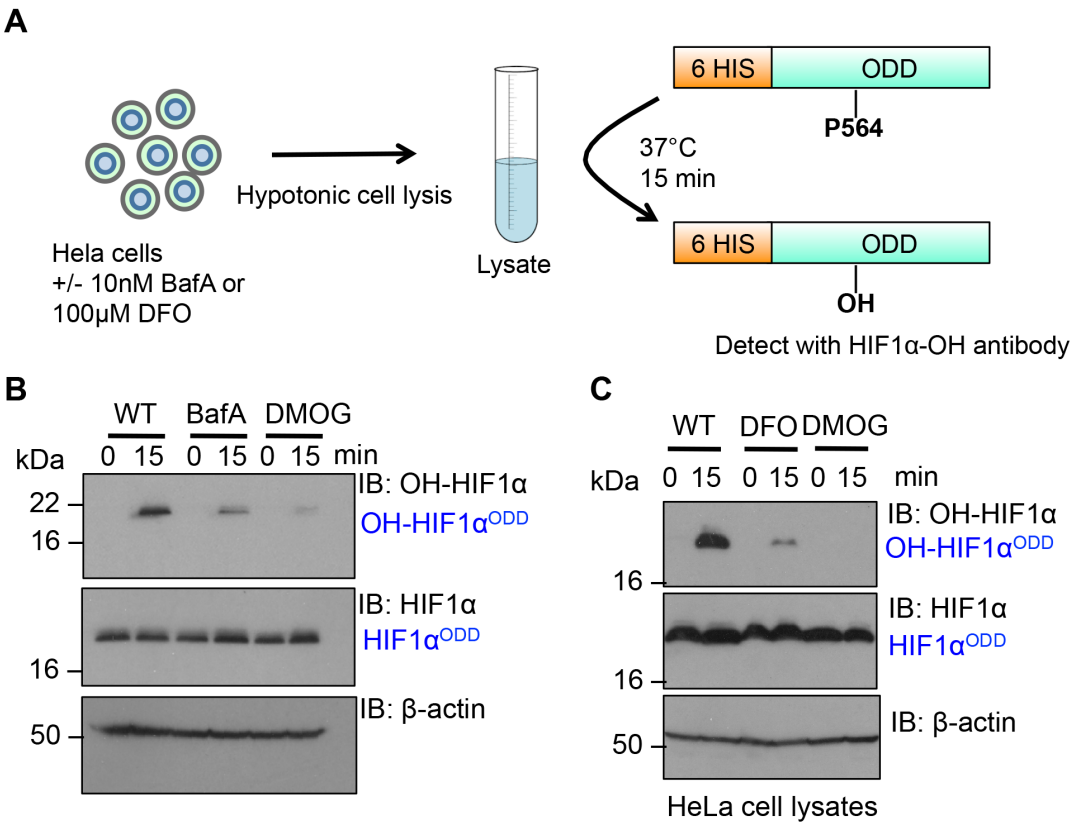

Figure 5.8: Inhibition of the V-ATPase prevents the prolyl hydroxylation of the HIF1α^{ODD}. (A) Schematic showing the prolyl hydroxylation of the HIF1α^{ODD} with HeLa cell extracts, treated with either BafA or DFO prior to lysis. **(B, C)** Immunoblots of His-HIF1α$^{ODD530-652}$ prolyl hydroxylation using cells treated with BafA **(B)** or DFO **(C)** prior to lysis. DMOG was added to the cell extracts during the hydroxylation reaction as a control.

As there was no change in the overall level of PHD2 in Hela cells treated with V-ATPase inhibitors (Anna Miles, PhD student, Nathan lab (Miles et al., 2017)), it was likely that changes in essential cofactors were responsible for the decreased PHD activity. No significant alterations in 2-OG abundance were observed (Stephen Burr, data not shown). Moreover, while the V-ATPase can affect pH, the assay was buffered in TBS at pH 7.4, making changes in pH unlikely to account for the PHD inhibition observed. We therefore focused on iron as this is an essential cofactor for PHDs, and several prior studies implicated the V-ATPase in iron metabolism: (1) Iron is taken up in its ferric form bound to transferrin, and Kozik et al had previously shown that V-ATPase inhibition impairs transferrin clathrin-mediated endocytosis (Kozik et al., 2013), (2) acidification of endosomes is required for the conversion of ferric to ferrous iron by ferroreductases (Dautry-Varsat et al., 1983; Straud et al., 2010), and (3) the release of iron from ferritin stores is dependent on a specialised form of autophagy (ferritinophagy) which requires V-ATPase acidification of the lysosome (Mancias et al., 2014).

Therefore, I examined if iron supplementation to cell extracts treated with BafA prior to lysis restored prolyl-hydroxylation of the His-HIF1α$^{ODD530-652}$ protein (**Figure 5.9A**). $FeCl_2$ was first prepared in hypoxic conditions to prevent oxidisation and then added to the WT, BafA or DFO cell lysates, and prolyl-hydroxylation of His-HIF1α$^{ODD530-652}$ measured as described. While the addition of ferrous iron had no effect on the hydroxylation of the His-HIF1α$^{ODD530-652}$ protein in the untreated lysates (**Figure 5.9B, C**), it increased prolyl-hydroxylation of His-HIF1α$^{ODD530-652}$ in the BafA treated lysate (**Figure 5.9B**), consistent with the restoration of PHD activity. To confirm that iron supplementation could overcome intracellular iron depletion, I repeated the experiments using cells treated with DFO prior to lysis. Similarly to the BafA treated cells, ferrous iron supplementation could overcome the loss of intracellular iron, and restored prolyl-hydroxylation of His-HIF1α$^{ODD530-652}$ (**Figure 5.9C**), demonstrating that altering iron levels can directly affect PHD activity in the *in vitro* assay. These findings were observed with several

experimental replicates (**Figure 5.9D**), and together, these results show that V-ATPase inhibition prevents prolyl-hydroxylation by depleting cellular iron levels.

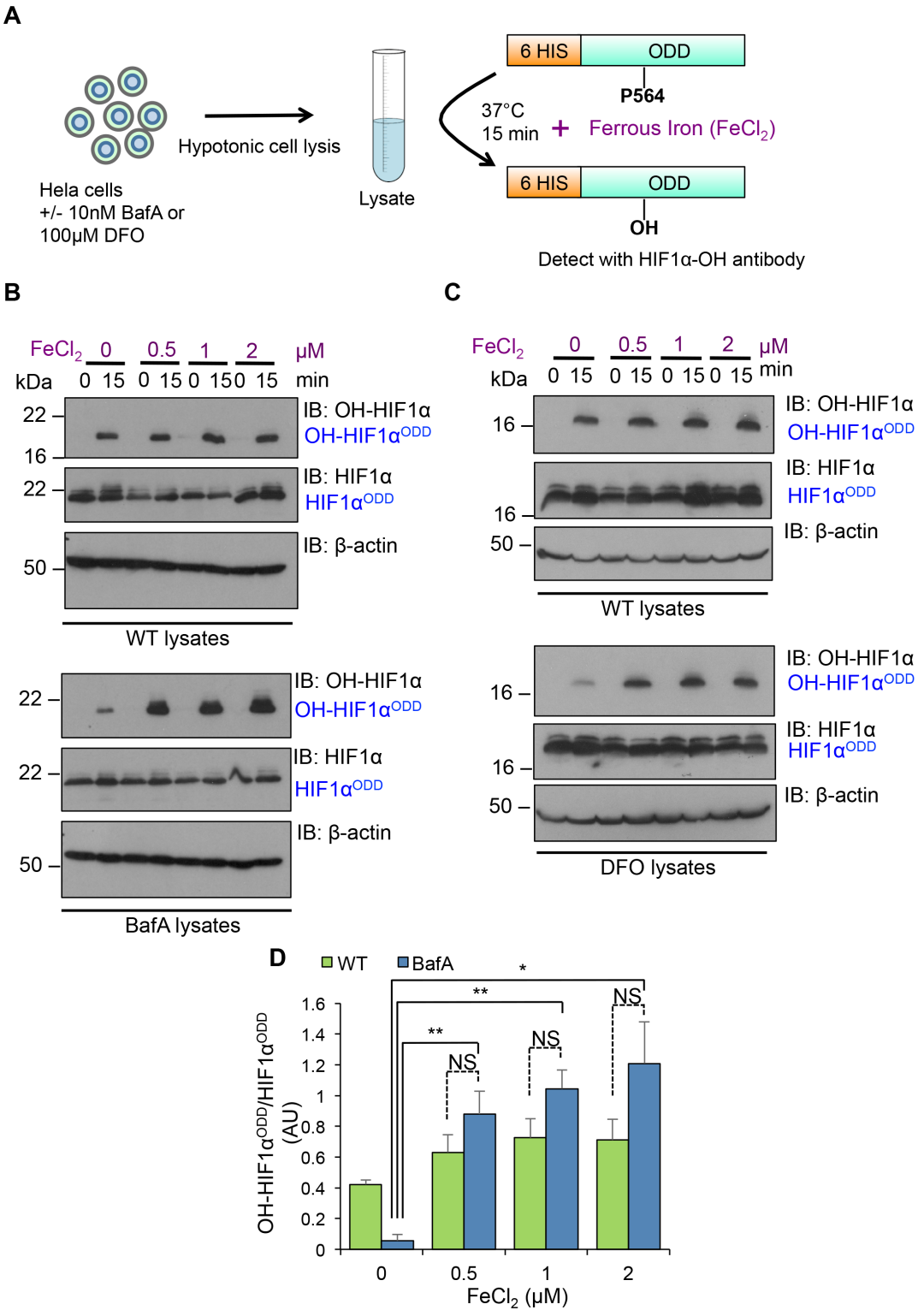

Figure 5.9: Ferrous iron restores prolyl hydroxylation of the HIF1α^{ODD} following V-ATPase inhibition with BafA. **(A)** Schematic showing the hydroxylation of HIF1α^{ODD} with HeLa cell lysates treated with either BafA or DFO, and iron supplementation ($FeCl_2$). **(B, C)** Immunoblots of His-HIF1α$^{ODD530-652}$ prolyl hydroxylation using cells treated BafA **(B)** or DFO **(C)** with or without addition of ferrous iron. **(D)** Quantification of three experimental replicates of **(B)** using ImageJ. *Mean±SEM, *p<0.05, **p<0.01 N.S. = not significant.*

5.2.8 Establishing an in vitro assay to determine hydroxylation of HIF2α.

Having demonstrated that an *in vitro* assay of HIF1α prolyl hydroxylation could be used to explore and identify new mechanisms for HIF1 activation, I was keen to see if similar techniques could be used to examine hydroxylation of the other main isoform, HIF2α. While HIF1α is ubiquitously expressed, HIF2α is limited to certain cell types (eg. renal cells, endothelial cells) (Ema et al., 1997; Flamme et al., 1997; Tian et al., 1997). However, little is known about the regulation of HIF2α under normoxic conditions.

I first generated a HIF2α recombinant protein that included the either one or both of the proline residues that have been identified as being hydroxylated by PHD2, Pro405 and Pro531, by sequence similarity to HIF1α. Eight constructs were generated using Ligation Independent Cloning (LIC) (**Figure 5.10A**) and the protein was purified as described previously (**Results 5.2.2.**) I chose to use the His- HIF2α$^{381\text{-}655}$ construct for the hydroxylation assay as this was soluble (**Figure 5.10B, C**) and included both proline residues known to be hydroxylated (**Figure 5.10A**).

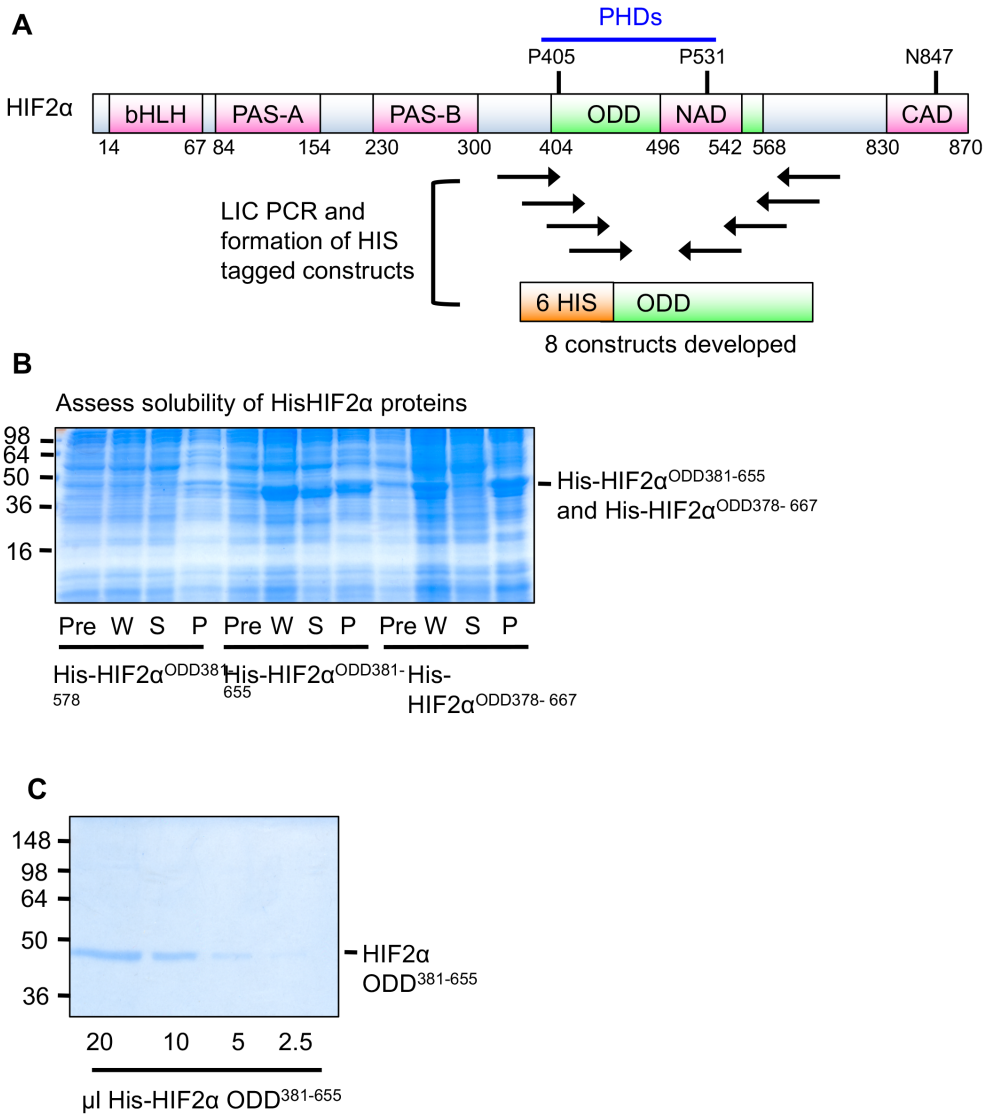

Figure 5.10: Generation of a HIF2α protein for use in the *in vitro* assay using ligation independent cloning. **(A)** Schematic of LIC of the HIF2α ODD. The two prolines that can be hydroxylated by the PHDs are highlighted. Eight constructs were amplified by LIC and cloned into a 6xHis expression vector. **(B)** Small-scale solubility assays were performed to identify the HIF2α^{ODD} protein best suited for the hydroxylation assay. Coomassie-stained gel shows solubility assay of three HIF2α^{ODD} protein constructs. W – whole sample, S- supernatant (soluble fraction), P- pellet (insoluble fraction). **(C)** Dilution series of the purified His-HIF2α$^{ODD381-655}$protein selected, separated by SDS-PAGE and stained with Coomassie blue.

5.2.9 The HIF2α^{ODD} protein is hydroxylated in vitro in a PHD2 dependent manner.

A HIF2α specific hydroxyl-proline antibody was not commercially available, but given the similarities between the HIFα isoforms it was possible that the antibody would cross-react with the hydroxylated HIF2α peptide.

Therefore, I first determined if the His-HIF2α$^{381-655}$ recombinant protein could be hydroxylated in the presence of HeLa cell lysates in a PHD2 dependent manner (**Figure 5.11A**), without the addition of cofactors as I had shown for HIF1α (**Results 5.2.3**)**.** WT HeLa lysates were incubated with the His-HIF2α$^{381-655}$ peptide for 15 min at 37°C and DMOG was used as a control (**Figure 5.11B**). Samples were analysed by immunoblot for HIF2α, β-actin, and a hydroxyl-proline specific antibody (OH-HIFα) (**Figure 5.11B**). A single migrating HIF2α species was identified by immunoblot, corresponding to His-HIF2α$^{381-655}$ peptide in all samples (**Figure 5.11B**). Probing with the OH-HIFα antibody identified a single band after 15 min incubation with WT lysate (**Figure 5.11B**). Furthermore, no hydroxylation was observed at the 0 time points or after 15 min incubation with DMOG. Thus, the OH-HIFα antibody successfully detected HIF2α prolyl-hydroxylation.

Next, I examined whether small molecule metabolites could impair HIF2α prolyl hydroxylation and focused first on succinate (**Figure 5.11C**). Pre-incubation with high concentrations succinate (5 to 10 mM) inhibited HIF2α prolyl-hydroxylation (**Figure 5.11C**), suggesting that succinate regulates both HIF1α and HIF2α hydroxylation similarly.

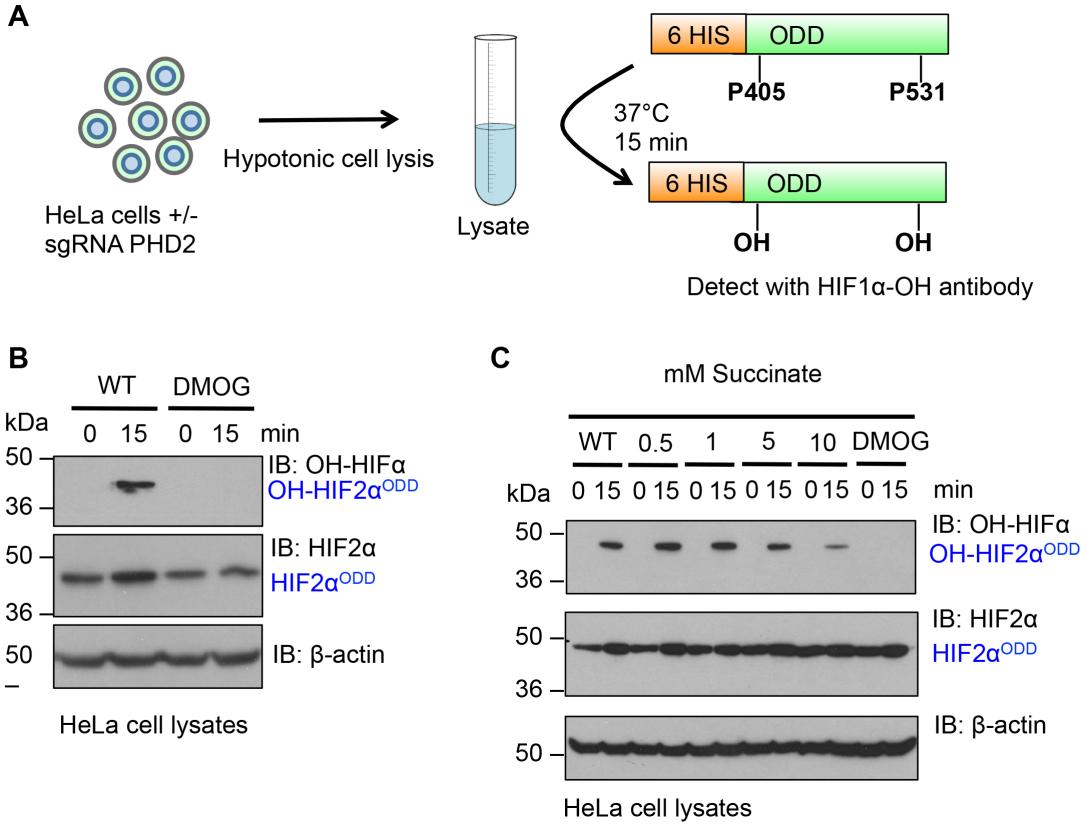

Figure 5.11: The HIF2α^{ODD} protein is hydroxylated *in vitro* in a PHD dependent manner. **(A)** Schematic of the *in vitro* hydroxylation assay, illustrating the His-HIF2α$^{ODD381-655}$ protein. **(B)** Immunoblot of total or prolyl hydroxylated His-HIF2α$^{ODD381-655}$ using wildtype HeLa lysates with or without addition of DMOG to the reaction. **(C)** Prolyl hydroxylation of HIF2α$^{ODD381-655}$ with wildtype HeLa lysates with or without increasing concentrations of succinate (0.5-10mM) or DMOG. β-actin served as a loading control.

5.2.10 HIF2α prolyl hydroxylation is impaired when the OGHDc is disrupted, and by the accumulation of L-2-HG

Having established an *in vitro* assay of HIF2α prolyl hydroxylation, which robustly reproduced published findings, I tested whether HIF2α hydroxylation was inhibited by deletions of OGDH and LIAS, or by the addition of L-2-HG, as had been identified for HIF1α.

First, I performed the HIF2α assay as described using HeLa cell lysates from OGDH, LIAS or PHD2 KO clones (**Figure 5.12A, B**). Prolyl hydroxylation of the His-HIF2α$^{381-655}$ protein was observed after 15 min incubation with WT lysate (**Figure 5.12A, B**), but to a lesser extent in the OGDH (**Figure 5.12A**) or LIAS (**Figure 5.12B**) KO lysates. No hydroxylation was detected after 15 min in

the PHD2 null lysate (**Figure 5.12A, B**). While these findings are similar to those observed for HIF1α (**Figure 5.4**), the levels of prolyl hydroxylation were slightly higher in the HIF2α assay, although it is not known if only one or both of the prolyl hydroxylation sites within HIF2α are recognized by the antibody.

To determine the effect of the 2-HG enantiomers on HIF2α hydroxylation I incubated the His-HIF2α$^{381-655}$ peptide with Hela lysates treated with increasing concentrations of L-2-HG or D-2-HG as described previously. His-HIF2α$^{381-655}$ prolyl hydroxylation was inhibited with increasing concentrations of L-2-HG (**Figure 5.12C, left panel**). However, L-2-HG did not inhibit HIF2α hydroxylation to the same level as observed with HIF1α, as even 10mM L-2-HG did not fully prevent prolyl hydroxylation. Interestingly, there was also a slight inhibition of His-HIF2α$^{381-655}$ hydroxylation with increasing concentrations of D-2-HG (**Figure 5.12C, right panel**), which had not been observed with HIF1α (**Figure 5.5B, C**). Thus, while impaired OGDHc activity and L-2-HG accumulation inhibits HIF2α prolyl-hydroxylation, this is to a lesser extent than HIF1α.

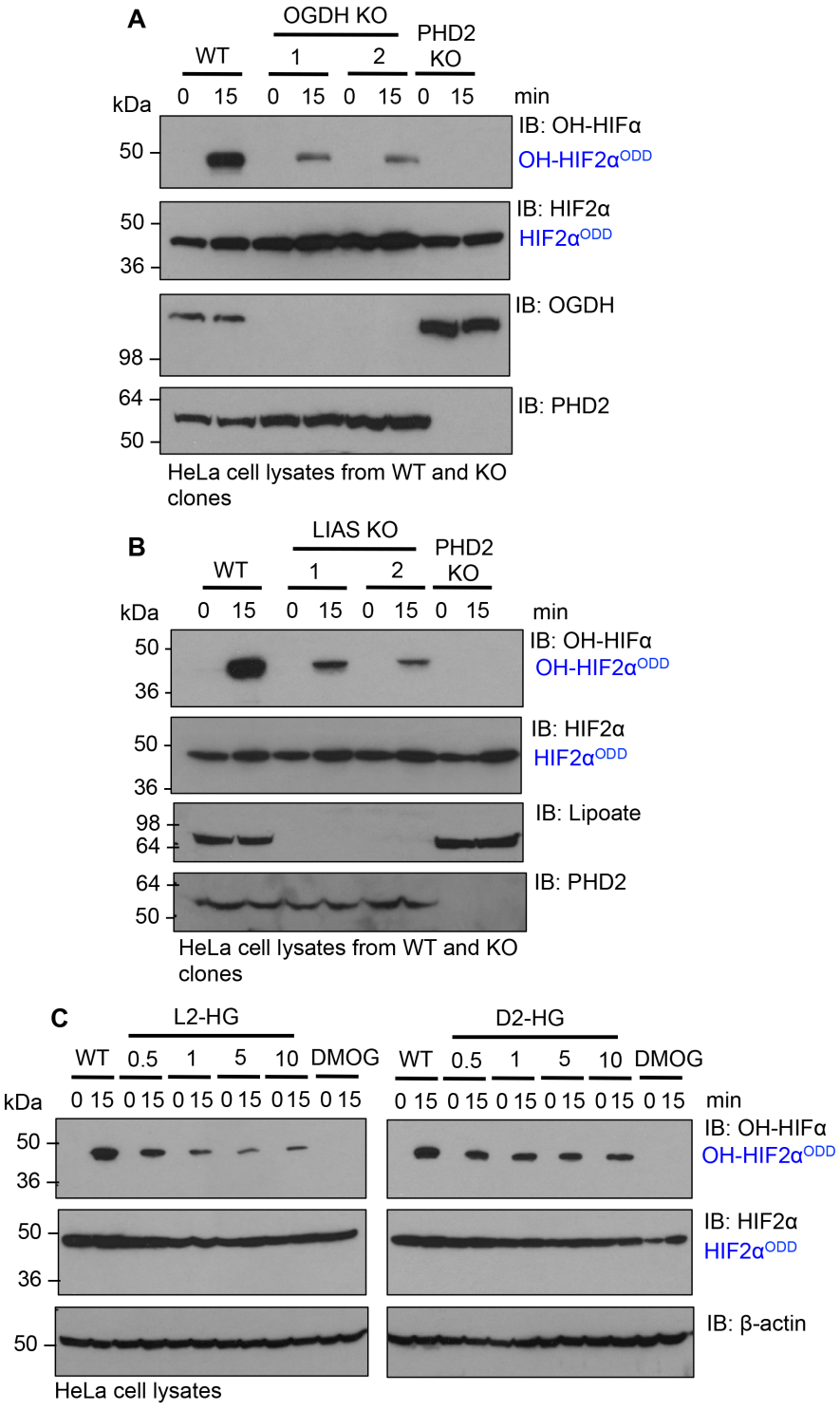

Figure 5.12: HIF2α^{ODD} prolyl hydroxylation is inhibited when the OGDHc is disrupted or following treatment with 2-HG. **(A, B)** Immunoblot of prolyl hydroxylated and total HIF2α$^{ODD381-655}$ with lysates from OGDH **(A)**, LIAS **(B)** or PHD2 **(A, B)** KO clones. **(C)** Immunoblot of prolyl hydroxylated and total HIF2α$^{ODD381-655}$ with HeLa cell lysates treated with increasing concentrations of L-2-HG (left) or D-2-HG (right) (0.5-10mM). The addition of DMOG served as a control for PHD inhibition. β-actin was used as a loading control.

5.2.11 V-ATPase inhibition depletes intracellular iron and prevents HIF2α hydroxylation.

Next, I examined whether HIF2α hydroxylation would be affected by intracellular iron depletion, similarly to HIF1α. I first treated HeLa cells with or without DFO (100μM) overnight and then incubated the cell lysates with the His-HIF2α$^{ODD381-655}$ protein before measuring prolyl hydroxylation by immunoblot (**Figure 5.13A**). The addition of DMOG to the hydroxylation reaction served as a control for PHD activity. The DFO treated lysate almost completely inhibited His-HIF2α$^{ODD381-655}$ prolyl hydroxylation in comparison with untreated HeLa cells (**Figure 5.13A**).

Having demonstrated that the HIF2α prolyl hydroxylation was susceptible to iron chelation, I examined if V-ATPase inhibition prevented HIF2α prolyl hydroxylation and whether this could be reversed with ferrous iron supplementation (**Figure 5.13B**). I treated HeLa cells with BafA (10nM) or DFO (100μM) overnight, lysed the cells, and incubated the extracts with or without iron chloride. While the addition of ferrous iron had little effect on the hydroxylation of His-HIF2α$^{ODD381-655}$ in the WT lysate, 0.5nM $FeCl_2$ completely restored prolyl hydroxylation in the BafA and DFO treated lysates (**Figure 5.13B),** similar to the findings with HIF1α prolyl hydroxylation (**Figure 5.9**). Thus, inhibition of the V-ATPase depletes cellular iron and decreases the prolyl hydroxylation of HIF1α and HIF2α similarly.

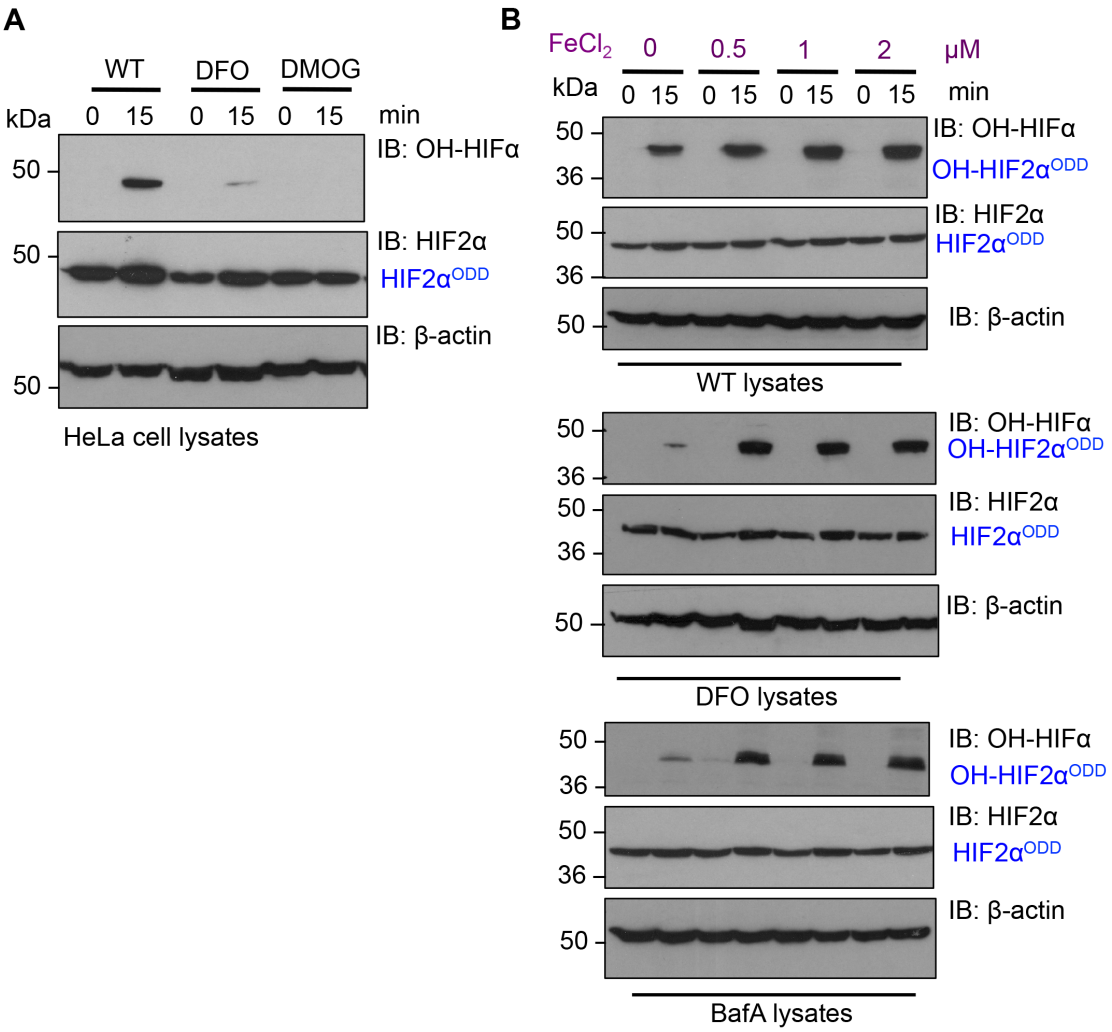

Figure 5.13: Ferrous iron restores prolyl hydroxylation of the HIF2α^{ODD} following V-ATPase inhibition with BafA. **(A)** Immunoblots of His-HIF2α$^{ODD381-655}$ prolyl hydroxylation using cells treated with or without DFO prior to lysis. DMOG was added to the reaction as a control for PHD activity. **(B)** HeLa cells were treated with or without BafA (10nM) or DFO (100μM) overnight and then lysed. The cell extracts were then incubated with His-HIF2α$^{ODD381-655}$ with or without addition of increasing concentrations of ferrous iron ($FeCl_2$) as shown.

5.3 Discussion

The balance between HIF1α stabilisation and degradation provides an intrinsic mechanism for the cellular response to oxygen and nutrient availability. In normoxia, the rapid proteasomal degradation of HIFα prevents unwanted activation of hypoxia-responsive genes. This degradation is mediated by HIF prolyl hydroxylation and subsequent ubiquitination by the E3 ligase complex, VHL, leading to proteasome-mediated degradation. Ultimately, I aimed to identify the ubiquitin chains and other enzymes involved in HIF degradation, however prolyl hydroxylation is required to initiate this ubiquitination and I was keen to identify factors controlling this initiation step before proceeding to evaluate ubiquitination.

5.3.1 In vitro prolyl hydroxylation of HIFs using cell extracts

Prior assays of HIFα prolyl hydroxylation have used both direct and indirect measurements of PHD activity. Epstein et al, utilised 1-^{14}C to radiolabel 2-OG and measure ^{14}C-CO_2 release when incubated with a small HIF1α peptide, recombinant PHD2, exogenous Fe^{2+}, ascorbate and DTT (Epstein et al., 2001). Thus, measurement of ^{14}C-CO_2 allowed an indirect quantification of PHD2 activity. With modifications to this assay, the hydroxylated HIF1α peptide could also be collected and analysed by LC/MS (Hewitson et al., 2007a; McNeill et al., 2005) allowing direct measurement of HIF1α hydroxylation. An alternative approach is the pVHL capture assay (Tuckerman et al., 2004), in which the binding of a radiolabelled-pVHL to the hydroxylated proline of a biotinylated HIF1α peptide was measured. However, as all these approaches require exogenous cofactors and PHD2, the effects of changes in whole cell lysates affecting metabolites or iron levels could not be assessed.

The development of an *in vitro* hydroxylation reaction, using only a recombinant HIFα peptide and whole cell lysates enables the quantification of HIFα prolyl hydroxylation without the need for addition of exogenous cofactors in a short, 15 min reaction. This has several advantages over previous assays, as radioactivity or purification of PHDs is not required. Moreover, as exogenous

cofactors are not added, the effect of changes in levels of cofactor or other metabolites on HIFα hydroxylation can be determined. A further benefit is the use of HIFα itself as a measure of prolyl-hydroxylation, rather than indirect readouts such as VHL binding.

There are several limitations to my approach. I used a hydroxyl-proline specific antibody, which does not provide an absolute quantification of prolyl hydroxylation, as it is dependent on the affinity of the antibody for the HIFα protein. An alternative strategy would be to use the migration properties of hydroxylated HIFα following electrophoresis, as previously used by Selak et al (Selak et al., 2005). MS of the HIFα protein could be used to determine HIFα hydroxylation, but this would have made the assay more laborious and more expensive.

In addition, the $HIF1\alpha^{ODD}$ protein used encoded amino acids 530-652 and therefore incorporated only one of the prolines (Pro564) hydroxylated by PHDs. However, prior studies have shown that both prolyl hydroxylation sites, Pro564 and Pro402, can function independently, to bind VHL and undergo ubiquitination (Masson et al., 2001), although most assays of PHD activity have typically used very small HIF1α peptides (10-12mer) encoding Pro564 only (Hewitson et al., 2007a). Therefore, it may be important to measure prolyl hydroxylation in a HIF1α protein with both prolines, similarly to the HIF2α protein used in my assays. Indeed, the presence of two prolines in the HIF2α ODD may explain why L-2-HG inhibition was less efficient compared to HIF1α prolyl hydroxylation.

All PHDs may be involved in HIFα hydroxylation but as PHD2 is the major enzyme implicated in the hydroxylation of HIF1α (Berra et al., 2003), prior assays have mainly focussed on this isoform. Hela cells encode all three PHDs (unpublished data, Nathan lab), and it was therefore interesting that depletion of PHD2 alone was sufficient to prevent both HIF1α and HIF2α prolyl hydroxylation. These findings suggest that PHD1 and PHD3 do not have a major role in constitutive HIFα turnover, and it will be of interest to explore the specific effects of their loss on HIFα prolyl hydroxylation.

5.3.2 Inhibition of prolyl hydroxylation by impaired OGDHc activity and L-2-HG formation

I show that the hydroxylation of HIF1α under aerobic conditions is highly regulated by the availability of TCA metabolites, succinate, 2-OG and L-2-HG, and by two mitochondrial enzymes OGDH and LIAS. Together with Stephen Burr's cell biology studies, my *in vitro* assay allowed us to build a model whereby disrupting the OGDHc leads to the reversible stabilisation of HIF1α through the accumulation of L-2-HG and inhibition of the PHDs (**Figure 5.14**).

In cells, depletion or inhibition of the three main enzymes involved in L-2-HG formation, LDHA, MDH1 and MDH2, decreased L-2-HG formation and promoted HIF1α turnover (Burr et al., 2016). However, *in vitro*, I was not able to restore prolyl hydroxylation of HIF1α in the OGDH or LIAS null cells. Several explanations may account for this discrepancy. It is possible that 2-OG is converted to L-2-HG within the lysate, during the incubation at 37°C. My attempts to prevent this by the addition of oxamate were not successful. An alternative approach would be to use antibody-depletion to remove LDHA or MDH from the lysate, thereby preventing L-2-HG formation.

Alternatively, L-2-HG may not compete directly with 2-OG for binding to PHDs but instead function as an allosteric inhibitor of prolyl hydroxylation. Intriguingly, the L-2-HG inhibits PHDs at relatively low concentrations (0.5-1mM) compared to the levels of 2-OG in cells (>10mM). It would therefore be interesting to directly measure the ability of L-2-HG to bind and inhibit a recombinant PHD2 protein, and to measure if L-2-HG can dissociate 2-OG from the enzyme.

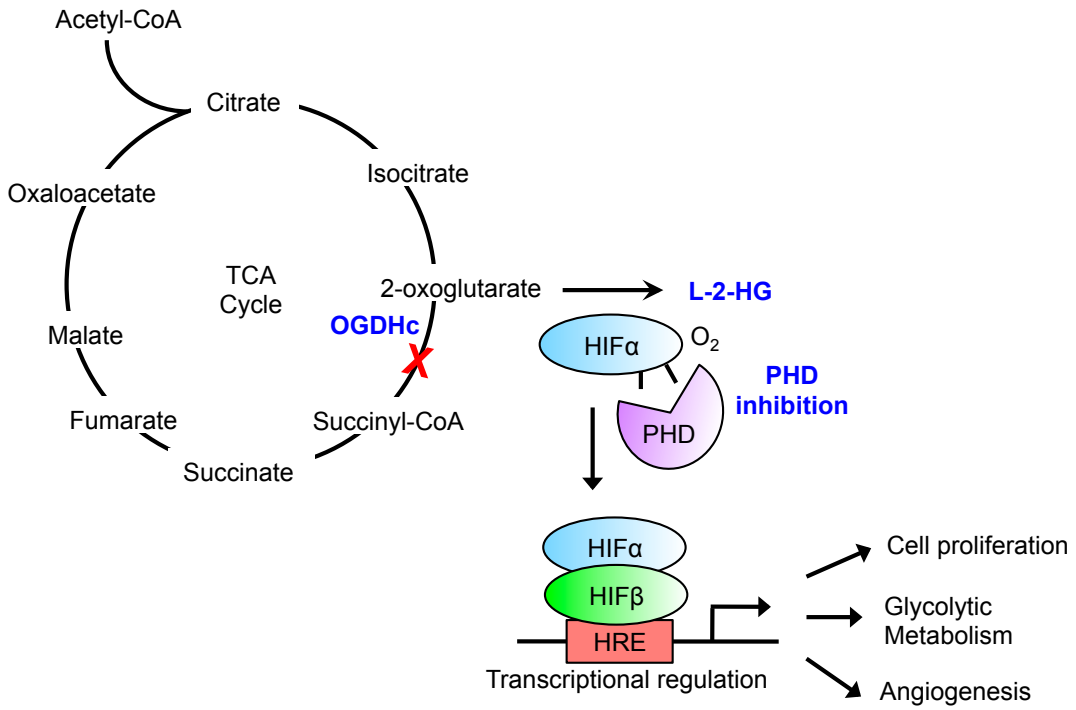

Figure 5.14: Disrupting the OGDHc leads to the accumulation of L-2-HG and activation of the HIF response. Schematic of the proposed model leading to HIF activation when the OGDHc is disrupted. The accumulation of 2-OG is converted to L-2-HG (dependent on LHDA and MDH1/2). L-2-HG inhibits PHD activity even in the context of high 2-OG levels, leading to stabilisation of the HIFα subunit. The HIF heterodimeric complex can then form. *Based on model detailed in (Burr et al., 2016).*

5.3.3 Inhibition of prolyl hydroxylation by intracellular iron depletion

I show that inhibition of the V-ATPase leads to HIF1α stabilisation by inhibition of HIF1α prolyl hydroxylation and this can be restored by the addition of Fe^{2+}. Together with Annie Miles' (PhD student, Nathan lab) cell biology studies, my *in vitro* assay allowed us to develop a model in which inhibition of the V-ATPase restricts iron uptake, reducing the free pool of intracellular iron and stabilizing HIFα by inhibition of prolyl hydroxylation (**Figure 5.15**).

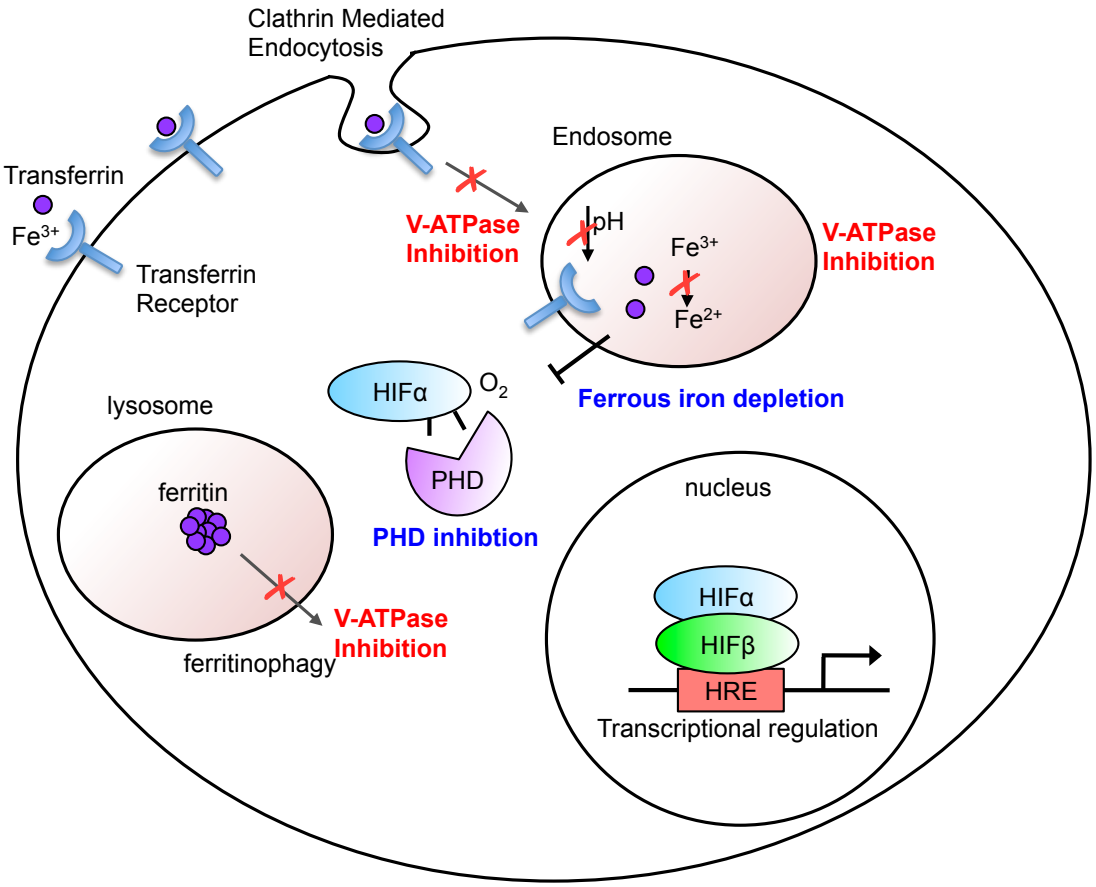

Figure 5.15: V-ATPase inhibition leads to intracellular iron depletion and activation of a HIF response. Schematic of the proposed model leading to HIF activation when the V-ATPase is inhibited. Inhibition of the V-ATPase prevents acidification of the endosomes and lysosomes, which prevents the conversion of ferric to ferrous iron, and the release of iron stores by ferritinophagy. Prolonged V-ATPase inhibition also leads to cholesterol depletion and a decrease in clathrin-mediated endocytosis, thereby also contributing to intracellular iron depletion through decreased transferrin trafficking. *Based on my studies and the work of Anna Miles and Stephen Burr *(Miles et al., 2017)*

As the PHD2 enzyme is dependent upon Fe^{2+} for its activity (Epstein et al., 2001) it is interesting that the chelation of iron from cell lysates did not prevent the re-activation of PHD2 once Fe^{2+} was restored. In addition, it has been suggested that Fenton chemistry is responsible for non-enzymatic catalysis of D-2-HG to 2OG *in vitro* promoting PHD function (Tarhonskaya et al., 2014) however, the use of a wildtype lysate control shows no increase in hydroxylation with increasing Fe^{2+} indicating that Fenton chemistry is not occurring at significant levels at the concentrations of Fe^{2+} used in these reactions.

Finally, I observed that lysates treated with BafA lead to inhibition of HIF2α hydroxylation which was restored by the addition of Fe^{2+}. Similarly to HIF1α, the reduction of Fe^{2+} caused by V-ATPase inhibition or iron chelation lead to PHD2 inhibition due to lack of the co-factor. As the hydroxylation of both HIF1 and HIF2α is catalyzed by PHD2, the findings are unsurprising but revealing as HIF2α hydroxylation had not been previously investigated and further validates the robustness and reproducibility of these *in vitro* assays, which can now test hydroxylation of two HIFα isoforms.

5.3.4 Comparison of HIF1α and HIF2α prolyl hydroxylation

The development of the HIF2α hydroxylation assay allowed me to determine whether there were differences in the hydroxylation of HIF1α versus HIF2α, particularly as HIF2α has more a limited range of tissue expression, and little is known about the normoxic regulation of HIF2α. While overall, the findings were similar between the HIF1α and HIF2α assays, there were a few interesting observations.

Lysates lacking either OGDH, LIAS or PHD2 led to inhibition of HIF2α hydroxylation, as did the TCA metabolite succinate and the 2-OG derivative L-2-HG. However, the level of HIF2α hydroxylation remained higher in the OGDH and LIAS null cells, compared to the HIF1α peptide. While the presence of two proline residues in the HIF2α peptide may partially explain these findings, it is possible that HIF2α prolyl hydroxylation is less susceptible to L-2-HG inhibition. Physiologically, this may be important for differentially regulating the stability of HIFα subunits to fine-tune the HIF response.

Interestingly, lysates treated with the 2-HG enantiomer D-2-HG slightly enhanced hydroxylation of the $HIF1\alpha^{ODD}$ protein whereas similar concentrations led to a slight decrease in $HIF2\alpha^{ODD}$ hydroxylation. The effect of D-2-HG on HIFα hydroxylation has been contentious within published literature (Koivunen et al., 2012; Tarhonskaya et al., 2014) and the reason for the differences observed in these assays are not yet clear (see also **Chapter 7**).

5.4 Summary

In this chapter, I focused on an alternative pathway where K11-linked chains had been implicated, the HIF response. I established *in vitro* assays to measure the initiation step of HIFα ubiquitination, prolyl hydroxylation. Using cell extracts and recombinant HIFα proteins I demonstrated that HIFα prolyl hydroxylation could be rapidly quantified, without the addition of exogenous cofactors. In particular, I identified that the TCA metabolite, L-2-HG, was able to inhibit HIF1α hydroxylation and that deletion of the mitochondrial enzyme genes OGDH and LIAS led to HIF1α stabilisation by inhibiting the prolyl hydroxylation of the $HIF1\alpha^{ODD}$. I also showed that inhibition of the V-ATPase lead to HIF1α stabilisation due to depletion of cellular iron, and that HIF1α hydroxylation was restored by addition of the Fe^{2+}. Development of a HIF2α *in vitro* hydroxylation assay showed that prolyl hydroxylation of the $HIF2\alpha^{ODD}$ was inhibited in a similar manner to HIF1α. However, D-2-HG led to a slight increase of HIF1α hydroxylation, but a moderate decrease of HIF2α hydroxylation. Together, these findings demonstrate the initiation step of HIF ubiquitination can be regulated by diverse cellular processes, and that endogenous levels of small molecule metabolites are critical in regulating HIFα prolyl hydroxylation. Having established a robust method to prolyl hydroxylate HIFα, I now aimed to use this approach to explore the ubiquitination of HIF1α.

Chapter 6: Results 4, Can HIF1α ubiquitination be reconstituted *in vitro*?

6.1 Introduction

HIF1α is one of the most short-lived proteins in cells (approximately 5 minutes)(Salceda and Caro, 1997) and its rapid proteasome-mediated degradation is dependent on its ubiquitination by the VHL E3 ligase complex. However, it is intriguing that HIF1α still has a short half-life of approximately 1 hr following VHL depletion (Maxwell et al., 1999) and is still ubiquitinated (Cockman et al., 2000), suggesting that factors aside from VHL may be involved in its ubiquitination and/or degradation. Furthermore, it is possible that HIF1α is regulated by several different polyubiquitin modifications, analogous to the NFκB pathway, where K63 or linear ubiquitin linkages mediate NF-kB signalling (Deng et al., 2000; Shimizu et al., 2015) independently of degradation. Thus, I was keen to explore if I could identify the types of ubiquitin linkages formed on HIF1α, and whether this would give some insights into VHL or proteasome-independent regulation of HIF1α stability.

Prior studies of HIF1α ubiquitination typically used radiolabelling and expression of a small HIF1α peptide (Cockman et al., 2000). These studies were instrumental in identifying a role for VHL, but the types of ubiquitin chains formed were not examined. Indeed, examining ubiquitin lysine linkages using radiolabelling techniques is challenging, as the samples are not suitable for mass spectrometry analysis of the ubiquitin chains formed. Therefore, I wanted to explore if I could adapt the hydroxylation assay to measure HIFα ubiquitination, and use this system to determine the ubiquitin linkages formed, particularly as generating biochemical quantities of ubiquitinated HIF1α had not been previously attempted.

In this chapter, I have taken two approaches to investigate the ubiquitination of HIF1α: (1) by using the HIF1α prolyl hydroxylation assay to initiate ubiquitination on the HIF1α ODD ($HIF1\alpha^{ODD}$), and (2) by

immunoprecipitating endogenous HIF1α in an attempt to identify new ubiquitin enzymes involved in HIFα signalling.

6.2 Results

6.2.1 Establishing an in vitro assay to determine ubiquitination of HIF1α.

The *in vitro* assay to quantify prolyl hydroxylation of HIF1α had proved extremely valuable in elucidating mechanisms of HIF1α stabilisation (Burr et al., 2016; Miles et al., 2017), but had not yet identified HIF1α ubiquitination. Indeed, it was somewhat surprising that I had not observed any ubiquitination or degradation of the His-HIF1α$^{ODD530-652}$ protein, given that it contains all three lysines known to be ubiquitinated by VHL (K532, K537 and K548) (Paltoglou and Roberts, 2007; Tanimoto et al., 2000). It was possible that a 15 min reaction was of insufficient length to ubiquitinate the His-HIF1α$^{ODD530-652}$ protein. However, I did not observe any ubiquitination or decreased protein levels using longer reaction times (data not shown).

Prior studies showed that both proline residues and all three lysine residues of HIF1α maybe required for efficient ubiquitination (Paltoglou and Roberts, 2007). As the His-HIF1α$^{ODD530-652}$ protein lacked the initial prolyl hydroxylation site (P402), it was possible that a HIF1α^{ODD} construct encoding all three lysine residues and both proline residues would be required to visualise ubiquitination. Therefore, I designed a construct encoding all these residues, His-HIF1α$^{ODD380-652}$, and purified the recombinant protein (**Figure 6.1A**). This longer HIF1α^{ODD} construct was rapidly hydroxylated (**Figure 6.1B**), similarly to His-HIF1α$^{ODD530-652}$protein (**Figure 5.2**).

As there is no antibody specific to ubiquitinated HIF1α available, identification of ubiquitination on the HIF1α^{ODD} would require isolation of the recombinant ubiquitinated protein and identification of the ubiquitinated residues and chains by probing with ubiquitin antibodies or using mass spectrometry. His-tagged proteins require isolation using NiNTA resin, which often undergoes non-specific binding (**Figure 6.1B, *band**). Therefore, I also designed and generated a GST-tagged HIF1α^{ODD} that encoded the required proline (P402, P654) and lysine (K532, K537 and K548) residues (GST-HIF1α$^{ODD401-652}$) that bound GSH Sepharose (**Figure 6.1C**), without the problems of non-specific binding. Importantly, GST-HIF1α$^{ODD401-652}$ was hydroxylated

when incubated with HeLa cell extracts, similarly to the His-tagged construct (**Figure 6.1D**).

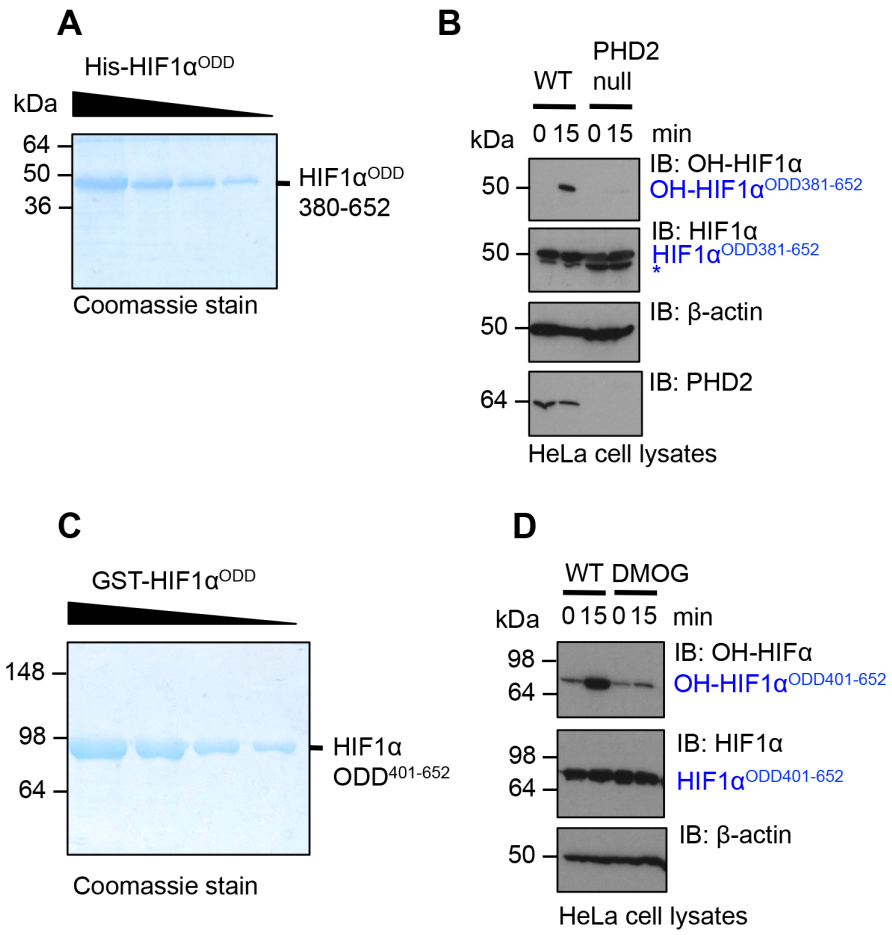

Figure 6.1: Generation of HIF1α recombinant proteins for an *in vitro* ubiquitination assay. **(A)** Dilution series of the His-tagged HIF1αODD$^{380-652}$ protein, separated by SDS-PAGE and stained with Coomassie blue. **(B)** Hydroxylation of the His-HIF1αODD$^{380-652}$ using HeLa cell lysate and PHD2 depleted HeLa cell lysate (*non-specific band). **(C)** Dilution series of the GST-tagged HIF1αODD$^{401-652}$ protein, separated by SDS-PAGE and stained with Coomassie blue. **(D)** Hydroxylation of the GST-HIF1αODD$^{401-652}$ using HeLa cell lysates with or without DMOG treatment.

Having generated new HIF1α^{ODD} constructs I could proceed with the *in vitro* ubiquitination assay, as shown in **Figure 6.2**. Briefly, 100nM GST-HIF1α$^{ODD401-652}$ was pre-incubated with GSH Sepharose resin for 30 min at 4°C. The resins were then washed in TBS to remove unbound protein and incubated with cell lysate for 18 hr at 37°C in a shaking incubator. As it was possible that the lack of ubiquitination seen in my hydroxylation assays (**Chapter 5**) may have

been due to insufficient E1, E2, ubiquitin or ATP in the cell lysate, these were added to the overnight reaction (50nM E1, 2.5μM UbcH5b, 5μM ubiquitin and 4mM ATP) (**Figure 6.2**). Samples were taken at the start of the reaction or after 18 hr, and passed over a 10ml Biorad column at 4°C to separate resin bound GST-HIF1α$^{ODD401-652}$ from the flow through (FT), and analysed by immunoblot or Coomassie staining.

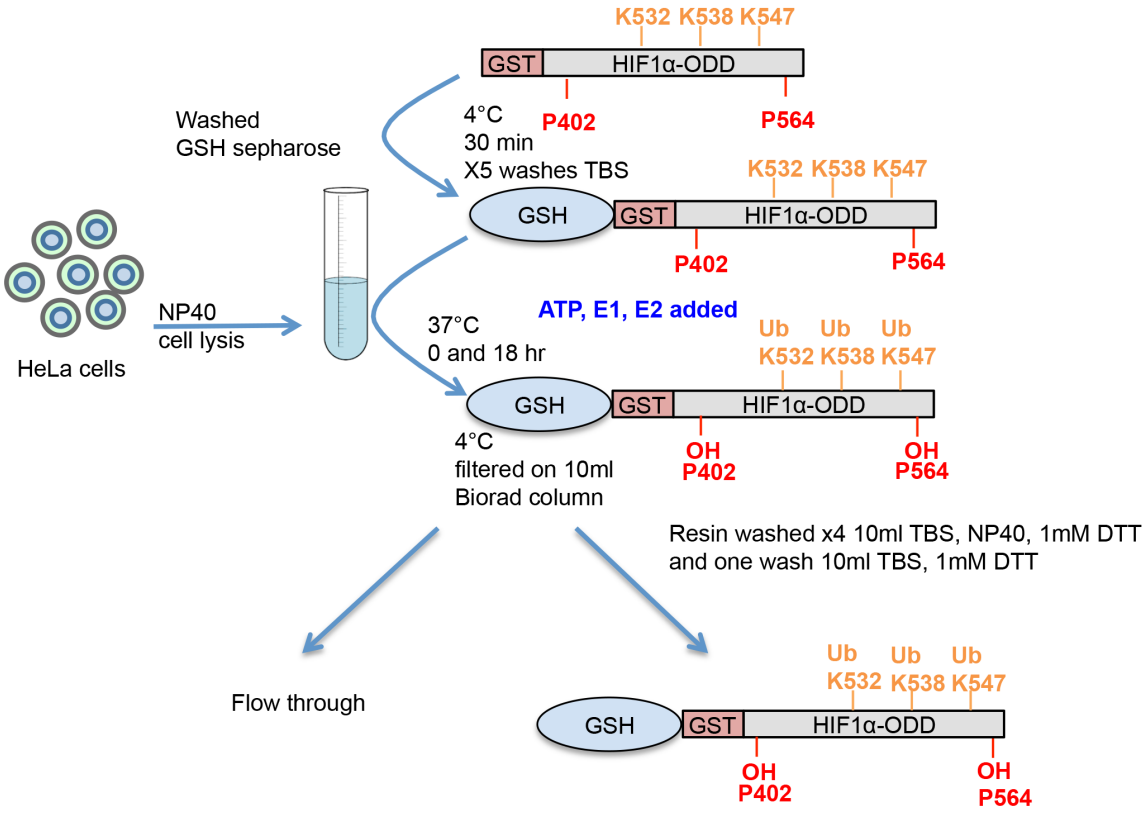

Resin and flow through analysed by immunoblot and Coomassie

Figure 6.2: The *in vitro* ubiquitination assay. Schematic of the *in vitro* prolyl-hydroxylation and ubiquitination assay. The proline (P) and lysine (K) residues predicted to be hydroxylated and ubiquitinated are shown.

A single HIF1α species was identified using the HIF1α antibody in the resin-bound samples at just above 64kDa, corresponding to the GST-HIF1α$^{ODD401-652}$ peptide (**Figure 6.3A, top panel**). However, this band was also clearly identified in the FT samples, indicating that not all GST-HIF1α$^{ODD401-652}$ remained resin-bound once lysate was added (**Figure 6.3A, bottom panel)**. There was also faint band (**Figure 6.3A, *band**) present above the 64kDa band in both resin and flow through after 18 hr (long exposure), which was not present at the start that may correspond to monoubiquitination of GST-HIF1α$^{ODD401-652}$. Interestingly, when the resin-bound samples were probed with the ubiquitin specific antibody, a protein smear above 100 kDa was identified (**Figure 6.3B, left panel**), which was only present after 18 hr incubation, suggesting that the GST-HIF1α$^{ODD401-652}$ protein undergoes polyubiquitination. As expected, the flow through samples showed abundant ubiquitination at both 0 hr and 18 hr. However, more ubiquitination was observed after 18 hr, suggesting that the addition of E1, E2, ubiquitin and ATP promoted general E2 and E3 ligase activity in the cell extract **(Figure 6.3B, C, right panels**).

Next, I attempted to visualise whether the ubiquitinated GST-HIF1α$^{ODD401-652}$ could be observed by Coomassie Blue staining (**Figure 6.3C**). The resin-bound GST-HIF1α$^{ODD401-652}$ was clearly observed at 0 hr but barely detectable at 18 hr, with a very faint slower migrating ubiquitinated species observed **(Figure 6.3, left panel**). It was possible that the level of ubiquitinated GST-HIF1α$^{ODD401-652}$ was below the detection limit for the Coomassie staining, or that GST-HIF1α$^{ODD401-652}$ was degraded by endogenous proteasomes within the cell extract. To test this latter hypothesis, I repeated the 18 hr ubiquitination reaction in the presence of a proteasome inhibitor (50μM MG132), however no increase in the GST-HIF1α$^{ODD401-652}$ band intensity was observed (data not shown).

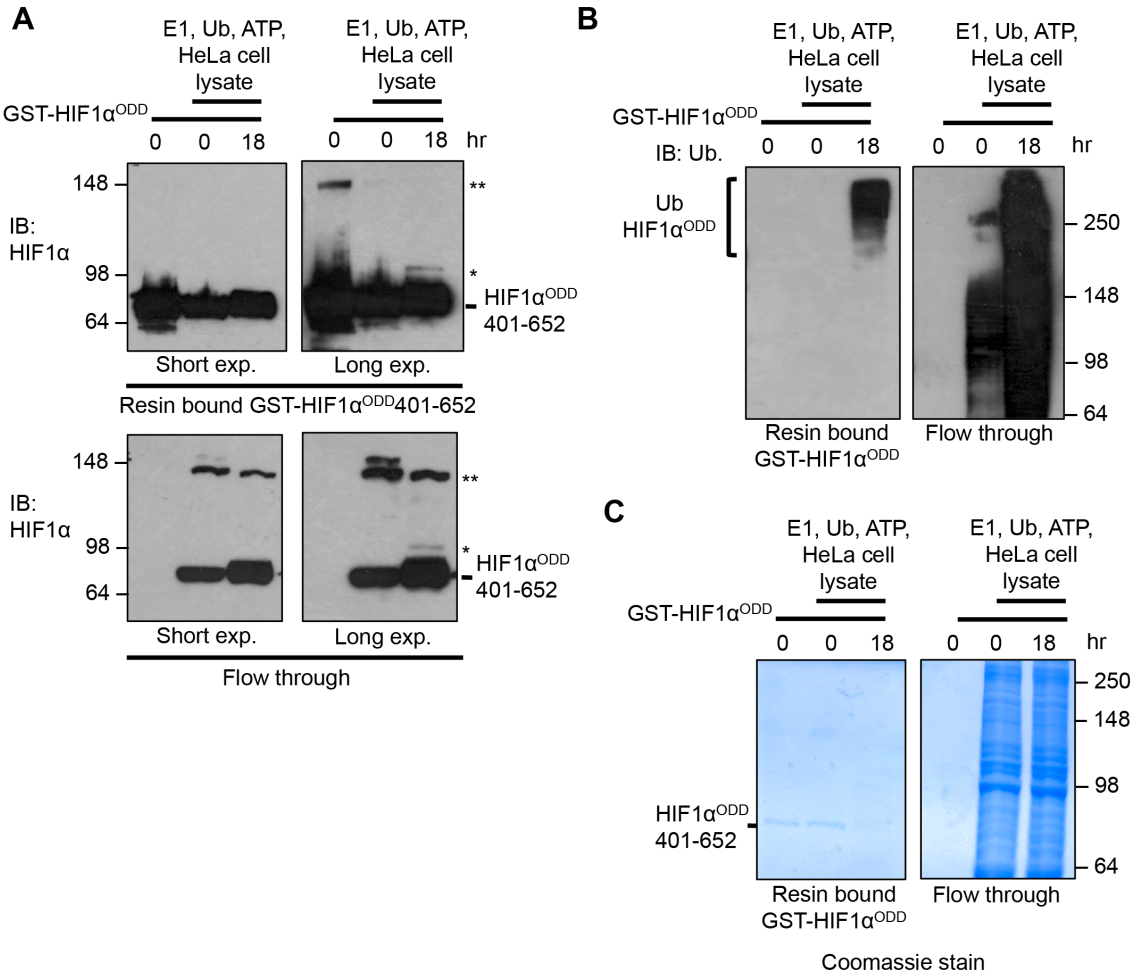

Figure 6.3: *In vitro* ubiquitination assay using the GST-tagged HIF1αODD$^{401-652}$ recombinant protein with the addition of E1, E2, Ub, ATP and HeLa lysates. (A, B) Immunoblots of resin-bound GST-HIF1αODD$^{401-652}$ and flow through from the *in vitro* ubiquitination reaction using antibodies specific to HIF1α **(A)** and ubiquitin **(B)** *band may correspond to monoubiquitinated GST-HIF1αODD$^{401-652}$, **band may correspond to dimerised GST-HIF1αODD$^{401-652}$ or endogenous HIF1α. Long and short exposures of the HIF1α immunoblots are shown. **(C)** Coomassie-stained SDS-PAGE gels of resin-bound GST-HIF1αODD$^{401-652}$ and FT from the *in vitro* ubiquitination assay.

6.2.2 Are ubiquitin chains formed on GST-HIF1α^{ODD} rapidly disassembled by DUBs?

While these initial experiments were encouraging, the levels of ubiquitinated HIF1α were barely detectable, and insufficient for mass spectrometry analysis. Therefore, I sought alternative explanations for the inefficient ubiquitination. Within the cell extract, it was possible that ubiquitin chains formed on GST-HIF1α$^{ODD401-652}$ were formed but then rapidly disassembled by DUBs. Indeed, a prior *in vitro* study using a radiolabelled HIF1α peptide required the addition of ubiquitin aldehyde (which inhibits isopeptidase activity through modification of the ubiquitin c-terminal carboxyl residue to an aldehyde) to visualise HIF1α ubiquitination (Cockman et al., 2000). Therefore, I repeated the ubiquitination reaction with the addition of 5μM ubiquitin aldehyde. After 18 hr incubation at 37°C, I observed higher molecular weight species of GST-HIF1α$^{ODD401-652}$ using the HIF1α antibody with addition of either ubiquitin or ubiquitin aldehyde (**Figure 6.4, top right**). Immunoblotting using the ubiquitin specific antibody showed an ubiquitin ladder was present only when ubiquitin aldehyde was used (**Figure 6.4, bottom right**) which would correspond to GST-HIF1α$^{ODD401-652}$ ubiquitination. However, this was not reproducibly visible on a Commassie gel (data not shown) and was not suitable for mass spectrometry analysis. Thus, while there is some improvement in the ubiquitination with ubiquitin aldehyde, the assay was still not suitable to examine the types of ubiquitin chains formed on the HIF1α^{ODD}.

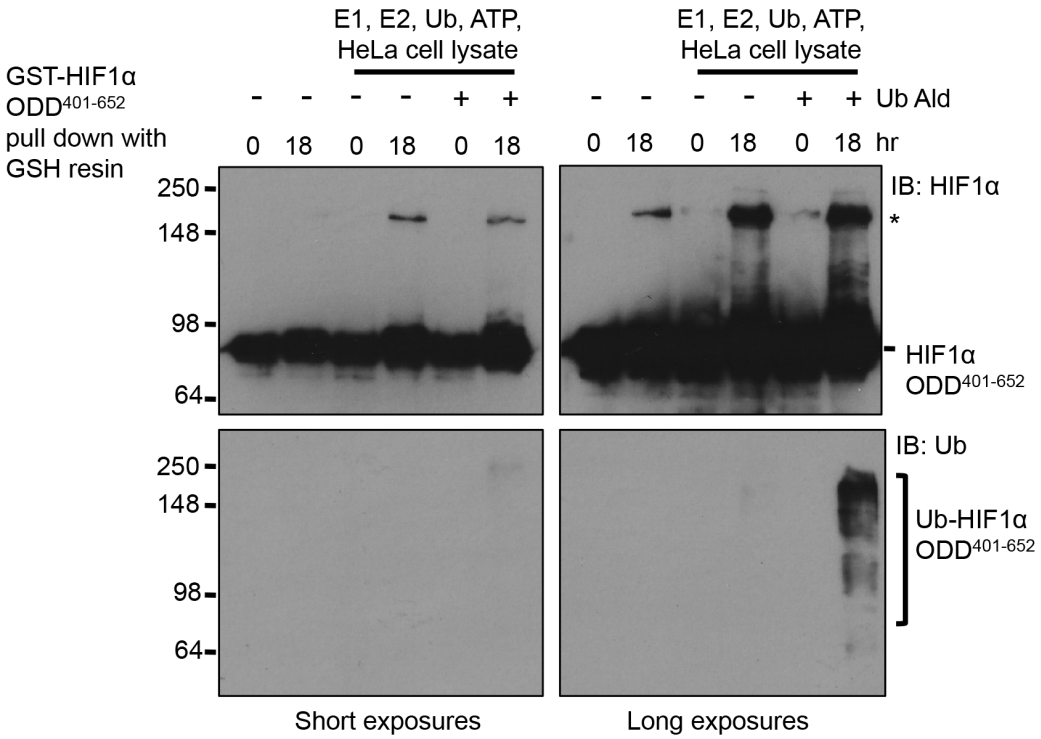

Figure 6.4: HIF1α^{ODD} *in vitro* ubiquitination assay with DUB inhibition. GST-HIF1α$^{ODD401-652}$ was incubated with E1, E2 (Ubch5b), ATP, and ubiquitin (Ub) as previously described, with or without the addition of 5μM ubiquitin aldehyde (Ub Ald). Immunoblots of resin-bound GST-HIF1α$^{ODD401-652}$ from the *in vitro* ubiquitination reaction using antibodies specific to HIF1α (top panels) and ubiquitin (bottom panels) are shown. *possible HIF1α^{ODD} dimerisation.

6.2.3 Identifying ubiquitination of endogenous HIF1α.

It had proven challenging to reconstitute HIF1α^{ODD} ubiquitination using the *in vitro* assay of HIFα hydroxylation. In particular, I was not able to generate sufficient ubiquitinated HIF1α for mass spectrometry analysis. Furthermore, the initial aim of this experimental approach was to use the cell extracts without the addition of ubiquitin, E1 or E2 enzymes, which may alter the ubiquitin linkages formed. Therefore, as an alternative strategy I examined if I could isolate ubiquitinated endogenous HIF1α directly from cells.

As HIF1α should be stabilised in cells during aerobic conditions by proteasome inhibition, I examined if I could immunoprecipitate endogenous

HIF1α in cells to isolate the ubiquitinated HIF1α, with the ultimate aim of using mass spectrometry to identify the ubiquitin chains formed.

To test the efficiency of endogenous HIF1α stabilisation, I first incubated 1 x 10^6 HeLa cells with or without different proteasome inhibitors (5μM MG132, 4μM Lactacystin or 20nM Velcade (Bortezomib)) overnight, and measured HIF1α stabilisation by immunoblot (**Figure 6.5A, B**). Lactacystin is an irreversible proteasome inhibitor, whereas MG132 and Velcade are reversible inhibitors that preferentially target the chymotrypsin-like activity of the proteasome. HIF1α was stabilised following MG132 treatment, with higher molecular weight species possibly corresponding to HIF1α ubiquitination (**Figure 6.5A, B**). Surprisingly, other proteasome inhibitors at concentrations known to inhibit the proteasome (data not shown) had no effect on HIF1α levels (**Figure 6.5A**) and it may be of interest in future studies to explore why MG132 seems to preferentially stabilise the protein.

Having verified that proteasome inhibition lead to the accumulation of HIF1α, I examined if I could detect endogenous HIF1α ubiquitination by immunoprecipitation (**Figure 6.5A, C**). HIF1α was readily detected in the IP samples following MG132 treatment, and a higher molecular weight ladder was visible, potentially consistent with ubiquitination (**Figure 6.5A, C**). However some HIF1α degradation products were observed (**Figure 6.5C, *bands**) and no polyubiquitination was detected (**Figure 6.5C, lower right panel**). I scaled up the experiment to attempt to generate sufficient samples for mass spectrometry quantification, using 1 x 10^8 HeLa cells with or without 5μM MG132 treatment overnight. While HIF1α stabilisation was again observed, ubiquitinated HIF1α was barely detectable by Coomassie staining (data not shown), and when subjected to mass spectrometry, the HIF1α protein was not identified.

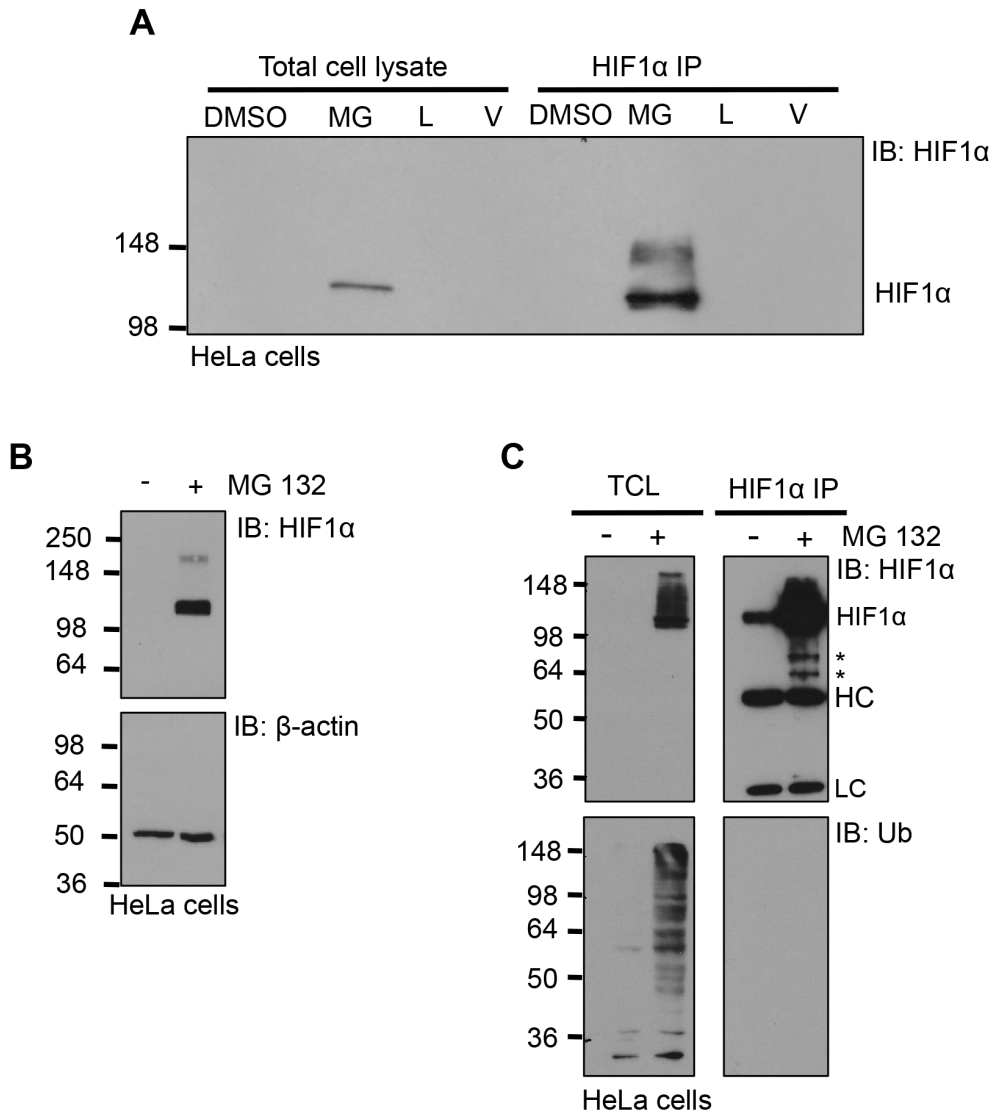

Figure 6.5: Immunoprecipitation of endogenous HIF1α following proteasome inhibition. **(A-C)** Immunoblots of total cell lysates and immunoprecipitated HIF1α. **(A)** 1x10^6 HeLa cells were treated with or without proteasome inhibitors overnight (MG132 (MG), 5μM, lactacystin (L), 4μM, or Velcade (V), 20nM). Cells were lysed in 1% NP40 and 10% of the reaction was taken for the total cell lysate (TCL). The rest of the sample was immunoprecipitated for HIF1α. **(B)** Immunoblot of HIF1α in HeLa cells with or without overnight treatment with MG132 (5μM). β-actin served as a loading control. **(C)** HIF1α was immunoprecipitated in HeLa cells treated with 5μM MG132 overnight and the immunoprecipitated samples were probed for HIF1α or ubiquitin. *HC, heavy chain, LC, light chain. *HIF1α species that may represent ubiquitination.*

The reasons for failing to detect HIF1α by mass spectrometry were not clear. It is possible that there was insufficient protein from the IP, but this seems unlikely based on previous sample analysis for other proteins in the Nathan lab. It has also been reported previously that HIF1α is difficult to detect by mass spectrometry (Doreen Cantrell, personal communication), which concurs with the Nathan lab's experience. An alternative approach would be to use overexpressed HIF1α, but we find that this leads to HIF1α stabilisation, presumably by overcoming the cellular hydroxylation machinery, and it is therefore unclear how informative this would be on understanding the mechanisms of HIF1α ubiquitination. Therefore, I have decided not to pursue these *in vitro* approaches further, and instead will focus my future work on a forward genetic screens to uncover novel ubiquitin enzymes involved in the HIF response (**Chapter 7, future directions**).

6.3 Discussion

Most prior studies of HIFα ubiquitination have relied on reconstitution of with small HIFα peptides and radiolabelling. Here, I attempted to generate biochemical amounts of polyubiquitinated HIF1α to explore the types of ubiquitin linkages involved, but unfortunately these were not successful. Indeed, it was surprising that HIF1α ubiquitination was difficult to detect, given that I had successfully generated a robust assay for HIFα prolyl hydroxylation.

6.3.1 Why was it difficult to detect HIF1α ubiquitination?

A major limitation in my ubiquitin assays may be the level of ubiquitin E3 ligases within the cell extract. An intrinsic feature of E3 ligases is their ability to rapidly autoubiquitinate, which usually leads to their degradation. It is possible that VHL was destabilized by the lysis conditions or there was insufficient VHL (or other E3 ligases) within the cell extracts to ubiquitinate HIF1α. For example, Kamura et al observed HIF1α ubiquitination in vitro, but this required purifying HIF1α and the VHL complex from baculovirus and incubating with recombinant E1, E2 (Ubc5a) and ubiquitin (Kamura et al., 2000). However, as my aim was to identify enzymes and ubiquitin chains involved in HIF1α, I required a system in which VHL was not added, as this may dictate the ubiquitin chains formed and prevent identification of other enzymes.

Cockman et al did observe ubiquitination of HIF1α without the addition of E1 or E2 enzymes, by using radiolabelled HIF1α peptides purified from reticulocyte lysates and incubating them with extracts from COS7 cells or RCC4 cell lysates (renal cell carcinoma with VHL mutation) with or without VHL overexpression (Cockman et al., 2000). However ubiquitin aldehyde was required to stabilise ubiquitinated HIF1α sufficiently to be visualised by autoradiography, and radiolabelling precludes further ubiquitin chain analysis by mass spectrometry.

It is possible that ubiquitinated HIF1α failed to bind to the GSH-resins or HIF1α antibody, as I always detected ubiquitinated HIF1α^{ODD} in the unbound resin fraction (flow through) (**Figure 6.3A**). In addition, only faint higher bands

were visualised in comparison with the intensity of the main HIF1α^{ODD} migrating species, suggesting that ubiquitination of the recombinant protein was inefficient despite the addition of exogenous E1, E2, ubiquitin and ATP. An alternative approach to isolate the relatively low abundant pool of ubiquitinated HIF1α would be to use the affinity of polyubiquitin for UBDs. For example, Tandem Ubiquitin Binding Entities (TUBEs) have been developed that bind to polyubiquitin chains (Hjerpe et al., 2009), and it would be of interest to use these TUBEs to isolate polyubiquitinated HIF1α and analyse these chains by mass spectrometry.

6.3.2 Alternative methods to identify the types of ubiquitin linkages involved in the regulation of HIF1α.

One of my aims in designing an *in vitro* assay of HIF1α ubiquitination was to determine whether K11-chains were formed on HIF1α and whether this mediated non-proteasomal degradation (Bremm et al., 2014) in a non-VHL dependent manner. Initially, I used a HIF1α peptide that incorporated both the prolines and lysine residues modified by PHDs and VHL. However, this assumes that other E3 ligases ubiquitinate HIF1α similarly to VHL. Immunoprecipitation of ubiquitinated endogenous HIF1α should enable determination of lysine residues modified and chain types formed in the presence or absence of VHL. However, despite stabilization of ubiquitinated HIF1α by proteasomal inhibition, ubiquitinated HIF1α peptides could not be identified by mass spectrometry. An alternative strategy would be to generate cells expressing an endogenously tagged HIF1α (using CRISPR/Cas9 knock-in), which may improve the efficiency of the HIF1α immunoprecipitation, allowing detection of the ubiquitinated species.

A further complementary approach to identify ubiquitin linkages would be the Ubi-CREST system (Hospenthal et al., 2015). This system relies on the ability of linkage specific DUBs, which cleave specific ubiquitin lysine linkages to identify which chain types are formed on protein substrates (Hospenthal et al., 2015). Lastly, it would be possible to express ubiquitin mutants in cells and determine linkage specificity in this way. However, there are limitations to the

use of overexpression as this may alter the activity of the ubiquitin molecule and result in ubiquitination of proteins not normally ubiquitinated in cells.

6.4 Summary

In this chapter, having developed a robust assay of HIFα prolyl hydroxylation, I examined if I could use this to ubiquitinate HIF1α and determine the linkages involved. However, ubiquitination of HIF1α proved difficult to identify, and while ubiquitinated HIF1α could be visualised in cells, the quantities generated were insufficient for mass spectrometry analysis. Therefore, the analysis of the ubiquitin-linked chains formed on HIF1α will require the development of alternative experimental approaches.

Chapter 7: Summary and Discussion

7.1 Summary

K11-linked chains are the third most abundant ubiquitin linkage in cells but whether they functioned as signals for proteasome-mediated degradation was unclear. Therefore, I sought to identify how K11-linked polyubiquitin chains are recognised by UBPs and if they bind directly to the proteasome. I found that the proteasome has a markedly different ability to recognise K11-chains compared to K48-linked polyubiquitin chains, with homotypic K11-chains binding weakly to the proteasome in comparison to K48-chains. However, heterotypic K11/K48-chains not only bound to the proteasome but stimulated the degradation of cyclin B1. Therefore, my studies uncovered a potentially novel mechanism for proteasome-mediated degradation, whereby the nature of the K11-ubiquitin linkages directly governed association with the 19S ubiquitin receptors (Grice et al., 2015). Using enzymatically synthesised K11-linked polyubiquitin conjugates I went on to examine how K11-chains may be recognised by ubiquitin receptors and whether K11-selective UBPs could be identified. Several UBPs that bound K11-linkages were identified, including the mitophagy ubiquitin receptors, TAX1BP1 and Myosin VI (Kruppa et al, 2018 *in press*). However, whether K11-specific UBPs are present in cells remains to be determined.

The functional outcomes of homotypic K11-chains remained elusive and to investigate this I focused on the HIF pathway, as K11-ubiquitination had been implicated in HIF non-proteasomal degradation. I first developed *in vitro* assays to determine how ubiquitination of HIFα may be initiated, through prolyl hydroxylation. By recombinantly expressing the oxygen-sensitive domain of HIF1α and HIF2α I established a robust assay of prolyl hydroxylation, which gave new insights into the metabolic regulation of HIFα stability. In particular, I demonstrated that TCA metabolites, succinate, 2-OG and L-2-HG inhibit the prolyl hydroxylation of both HIF1α and HIF2α, and showed that cells deficient in OGDH or LIAS have a decreased capacity to directly hydroxylate HIF1α or HIF2α.

In addition, I found that inhibition of the V-ATPase leads to a reversible reduction in prolyl hydroxylation of both HIF1α and HIF2α due to intracellular iron depletion. However, while these studies successfully established new methods for measuring HIFα prolyl hydroxylation, and lead to several publications (Burr et al., 2016; Miles et al., 2017), generating an assay to ubiquitinate HIF1α proved extremely challenging.

7.2 K11-polyubiquitin chains

7.2.1 What do my studies tell us about the biological roles of K11-linked polyubiquitin chains?

Prior to the start of my studies the major function of K11-linked polyubiquitination was attributed to cell cycle progression. However, it is now apparent that homotypic K11-ubiquitin conjugates do not signal proteasome-mediated degradation (Grice et al., 2015). Indeed, prior to my studies the Rape group demonstrated that heterotypic K11/K48-linked polyubiquitin chains were mainly formed by the APC/C on cell cycle substrates such as cyclin B1 (Jin et al., 2008). My experiments to some extent support these findings, but rather than K48/K11-heterotypic chains acting as a more efficient signal than homotypic K48-linkages, my results suggest that the presence of K11-linkages within the heterotypic chain decrease the rate of proteasome-mediated degradation.

It was therefore likely that K11-linked polyubiquitin chains were involved in proteasome-independent pathways, and I hypothesised that by identifying the K11-selective UBPs I could determine these uncharacterised functions of K11-chains. This approach was partially successful, as I did identify a number of UBPs that could bind K11-linked polyubiquitin conjugates, including the mitophagy related proteins, TAX1BP1 and Myosin VI. However, the exact role of K11-linkages in this context remain to be fully determined, as we and others observe that K63-linkages bind more strongly to Myosin VI than K11-linked ubiquitin chains (He et al., 2016).

7.2.2 How important are different ubiquitin linkages for stimulating protein degradation?

The finding that homotypic K11-linked polyubiquitin chains did not signal proteasome-mediated degradation was unexpected (Grice et al., 2015), particularly as it was previously shown that ubiquitin receptors on the 19S showed no specificity for K48- and K63-polyubiquitin lysine linkages (Kim et al., 2007; Nathan et al., 2013; Peth et al., 2010). Currently, there is little data to show whether K6, K27, K29 or K33-linked polyubiquitin chains are recognised by the proteasome, as atypical chains have been difficult to generate in sufficiently large amounts for *in vitro* experiments. Recently, however, the Matouschek group used chain-specific E2 enzymes and chain terminating ubiquitin mutations, to generate GFP-tagged substrates with K48, K63 and K11-linked tetra-ubiquitin chains, and measured their ability to bind the proteasome (Martinez-Fonts and Matouschek, 2016). Consistent with my findings, they observed minimal proteasome-mediated degradation of GFP-K11-Ub^4. While these studies focussed on the degradation of K48, K63 and K11-linked chains, enzymatic methods to generate K29 and K33-linked chains, using HECT E3 ligases and chain-specific DUBs (Kristariyanto et al., 2015; Michel et al., 2015), have now been developed and it will be of interest to explore their direct binding to the proteasome.

Other methods of generating atypical ubiquitin chains for proteasome-mediated degradation *in vitro* include chemical synthesis of polyubiquitin linkages (Hemantha et al., 2014) and other non-enzymatic techniques (relying on using a silver-mediated condensation reaction between the C-terminal thioester of one ubiquitin and the amine of a specific lysine on the other ubiquitin) (Castaneda et al., 2011; Faggiano et al., 2016). However, there are limitations to these methods, as it is not clear that the structures of chemically formed polyubiquitin chains are the same as those formed enzymatically. Moreover, these pure *in vitro* techniques of proteasome degradation should not be interpreted in isolation, as they may miss the requirement of chain-specific ubiquitin binding proteins that facilitate binding to the proteasome in cells. *In vivo*, ubiquitin chains may also form branched chains involving many different linkages. Until ubiquitin chains can be isolated from cells and chain structure

analysed in addition to chain linkage, it will be difficult to determine the subtleties of ubiquitin modifications in cells.

Lastly, post-translational modification of ubiquitin itself may be important in modulating the binding of polyubiquitin chains to the proteasome. Ubiquitin is phosphorylated on residue Serine 65 (Ser65) by the Ser/Thr kinase, PTEN-induced putative kinase 1 (PINK1) which leads to allosteric activation of the E3 ligase, Parkin and is required for the clearance of damaged mitochondria (Koyano et al., 2014). Interestingly, how these chains are disassembled or degraded is not clear, as polyubiquitin chains containing Ser65- phosphorylated ubiquitin are less readily disassembled by DUBs than non-phosphorylated ubiquitin (Swaney et al., 2015; Wauer et al., 2015). Although studies have shown that a Ser65- phosphorylated ubiquitin mimetic mutant binds to the proteasome shuttling factor, Rad23 (Swaney et al., 2015), whether they are recognised by the proteasome is not clear.

7.2.3 Are there K11-specific ubiquitin binding proteins?

A K11-specific UBP has yet to be identified. My mass spectrometry studies suggest that FAM115A may bind K11-linked polyubiquitin conjugates, but as this has proved difficult to recombinantly express, we do not yet know if this is direct. Moreover, the fact that no K11-specific UBPs have been identified raises the question of whether homotypic K11-chains form in cells or whether they exist more commonly as heterotypic linkages. Indeed, several studies identifying roles for K11-chains in cells have shown them to be of mixed linkage rather than homotypic, including K11/K63 heterotypic chains in MHC Class I internalisation (Boname et al., 2010) and K11/K48-chains in cell cycle control (Meyer and Rape, 2014). Furthermore, if the abundance of homotypic K11-chains is low in cells and they are transiently formed for specific roles, identification of K11-specific UBPs will be difficult.

Despite these limitations to identifying K11-specific UBPs, the existence of a K11-specific DUB, Cezanne, suggests that K11-chains are recognised distinctly from other chain types (Bremm et al., 2010). The recent crystal structure of Cezanne in complex with K11-dimers reveals that binding of ubiquitin enables

conformational changes in Cezanne, but only K11-dimers are able to bind across the active site resulting in catalysis (Mevissen et al., 2016). If ubiquitin chain conformation specificity occurs for DUBs, it is highly likely that similar mechanisms occur for UBPs.

How ubiquitin binding proteins selectively bind polyubiquitin chains of distinct lysine linkages is still unclear, although it is likely that this relates to the affinity and avidity of the UBDs. Different lysine linked ubiquitin chains may alter the conformation of UBDs to facilitate their binding, as observed for the binding of Cezanne to K11-dimers (Mevissen et al., 2016), or alternatively, the presence and orientation of tandem UBDs within a UBP can alter the affinity of the UBP to specific polyubiquitin chain linkages (**Discussed 1.1.3**) (Elsasser et al., 2004; Ren and Hurley, 2010). Furthermore, endogenous modifications of UBDs can alter their avidity for ubiquitin. Matsumoto et al have shown that the phosphorylation of p62 UBA domain at serine 403 results in an increased affinity to polyubiquitin linkages (Matsumoto et al., 2011). Therefore, it will be important to investigate the binding of homotypic and heterotypic K11-polyubiquitin chains not only *in vitro* but also in a cellular context, as endogenous modifications of UBPs may alter their binding affinities.

7.3 HIFα prolyl hydroxylation and ubiquitination

7.3.1 Metabolic regulation of PHDs and therapeutic implications

Prior assays of PHD activity have required the use of purified PHD and addition of exogenous cofactors. This has not allowed these assays to determine the effect of altered levels of cofactors and small molecule metabolites on PHDs. I developed a novel *in vitro* assay that quantified the prolyl hydroxylation of a recombinant HIFα peptide using cell lysates. Moreover, our studies highlight the role of oxygen-independent regulation of PHD activity, through changes in small molecule metabolites or iron availability. The presence of L-2-HG in cell lysate clearly overcomes 2-OG levels but the mechanism of PHD inhibition is unclear. If

L-2-HG inhibition of PHD2 is allosteric, identifying its binding site would be of interest, and may point to new avenues for developing PHD inhibitors as drugs.

PHD inhibitors are currently being developed for the treatment of anaemia in chronic kidney disease (Maxwell and Eckardt, 2016). This form of anaemia primarily results from low erythropoietin levels. As EPO is a HIF target gene, predominantly mediated by HIF2α (Gale et al., 2008; Scortegagna et al., 2005), inhibition of HIF degradation using PHD inhibitors provides a novel therapeutic strategy for the treatment of renal anaemia. However, HIF upregulates many genes other than EPO and this may result in side effects. For example, an obvious concern is an increased risk of developing clear cell renal cell carcinoma, seen in patients with mutations in the VHL gene and also associated with activation of HIF2α (Kondo et al., 2003; Raval et al., 2005). In addition, PHD inhibitors may affect other 2-OG-DDs, for example chromatin modifiers, resulting in off-target effects.

Phase II clinical trials of PHD inhibitors are underway (Maxwell and Eckardt, 2016) and Roxadustat (FG-4592) has shown correction of renal anaemia in trial patients and has entered phase III trails (Rabinowitz, 2013). Given the clear requirement for an effective PHD inhibitor, it would be of interest in future studies to identify the mechanism by which L-2-HG inhibits PHD2 activity (see **Future Directions**).

7.3.2 Non-canonical ubiquitination of HIF1α

While my assays to measure HIF1α proved challenging, it is still likely that E3 enzymes aside from VHL are involved in the HIF pathway, particularly as VHL loss stabilises HIF1α, but it still has a half-life of approximately 1 hr (Cockman et al., 2000). Several groups have identified potential E3s or chaperones for VHL independent degradation, but as yet, none of these have been substantially validated.

Firstly, it has been proposed that HIF1α is degraded by chaperone-mediated autophagy, based on the observations that V-ATPase inhibitors stabilise HIF1α (Hubbi et al., 2013). However, we have clearly shown that this is

not independent of the PHD axis, and in fact depends on intracellular iron depletion.

Ubiquitin-independent proteasome-mediated degradation has also been proposed. Montagner et al suggest that SHARP1, a prognostic marker in triple negative breast cancer, directly mediates the proteasomal degradation of HIF1α by acting as a shuttling factor to the proteasome, increasing degradation of HIF1α independent from VHL, ubiquitination or oxygen (Montagner et al., 2012). However, this finding has never been reproduced in the literature, and ubiquitin-independent degradation by the proteasome is highly contentious.

Recently, Parkin was identified as an E3 ligase capable of ubiquitination of HIF1α leading to its proteasomal degradation (Liu et al., 2017). HIF1α ubiquitination by Parkin was determined using an *in vitro* ubiquitination reaction with E1, E2 (UbcH7), ubiquitin, purified GST-Parkin, recombinant PINK1 and purified His-Trx-HIF1α. Interestingly, they observed that Parkin ubiquitinated HIF1α at K477, and not the three previously identified lysines associated with VHL-mediated ubiquitination. Consistent with this finding, Parkin-mediated ubiquitination occurs independently of VHL and oxygen. Furthermore, efficient ubiquitination may rely on phospho-ubiquitin as HIF1α ubiquitination was reduced with a ubiquitin S65A mutant (Liu et al., 2017). However, there are several limitations to this study, most notably that prolyl-hydroxylation of HIF1α was not measured. Given that Parkin has a clear role in the clearance of damaged mitochondria, it is possible that stabilisation of HIF1α, when Parkin levels are reduced, is mediated by alterations in mitochondrial metabolite levels, thereby preventing HIF1α prolyl-hydroxylation. Thus, while it is likely that other E3 ligases or degradative pathways are involved in HIF1α stability, the mechanisms involved remain unclear. Therefore, in my future studies, I propose to use an unbiased forward genetic approach to uncover the ubiquitin machinery aside from VHL in HIF1α degradation.

7.4 Future directions.

My future aims are to develop my *in vitro* assays for metabolic inhibition of PHDs, and in particular, determine the mechanism by which L-2-HG inhibits PHD2 activity. Rather than focus solely on K11-polyubiquitination, I plan to explore the VHL-independent degradation of HIF1α using a genetic approach.

1) ***How does L-2-HG inhibit PHDs?*** Having demonstrated that relatively low concentrations of L-2-HG inhibit PHDs in a cell extract, I plan to determine if L-2-HG inhibits PHDs through competing for 2-OG binding, or through allosteric inhibition. These studies will involve the purification of a PHD2 recombinant protein and *in vitro* competition assays with 2-OG. Furthermore, as there are three PHD enzymes I also plan to explore if L-2-HG inhibits their activity similarly. Initially, I will generate PHD1, PHD2 and PHD3 null HeLa cells using CRISPR/Cas9 for my established assay of HIFα prolyl-hydroxylation. Further studies will be dependent on whether L-2-HG is a competitive or allosteric inhibitor of PHDs.

2) ***CRISPR/Cas9 forward genetic screens to uncover ubiquitin enzymes involved in HIF1α stability.*** I have already begun to establish a forward genetic screening approach to identify ubiquitin enzymes that regulate activation of our HRE-HIF1αODD-GFP reporter (Burr et al., 2016). Using a focussed 'ubiquitome' specific pooled sgRNA library, I am exploring whether ubiquitin enzymes aside from VHL regulate HIF1α levels. These screens involve using a stable HeLa clone expressing the sensitive GFP-HIF1α reporter, and enriching for rare GFP high cells (GFP^{HIGH}) by sequential fluorescence-activated cell sorting (FACS). My preliminary studies have validated this approach, and I have several candidate E3 ligases that I would like to evaluate. If these enzymes validate, I plan to elucidate how they regulate HIFα, using my assays of prolyl-hydroxylation, in the context of VHL loss. Ultimately, I hope that this approach will help elucidate the VHL-independent mechanisms of HIFα regulation.

Appendix 1: Ligation Independent Cloning Primers

FAM115A

Primer Name	Sequence (5'-3')
FAM115A_85FW	CAGGGACCCGGTTGCTCTTCCCCTGGGGCTCCC
FAM115A_88FW	CAGGGACCCGGTCCTGGGGCTCCCATTGGTGTA
FAM115A_92FW	CAGGGACCCGGTATTGGTGTACACCCATCCCTG
FAM115A_95FW	CAGGGACCCGGTCACCCATCCCTGGCACCTTTG
FAM115A_99FW	CAGGGACCCGGTGCACCTTTGGCCAAAATCCTC
FAM115A_102FW	CAGGGACCCGGTGCCAAAATCCTCGAGGGCTCT
FAM115A_107FW	CAGGGACCCGGTGGCTCTGGAGTGGATGCAAAG
FAM115A_112FW	CAGGGACCCGGTGCAAAGGTTGAGCCAGAAGTG
FAM115A_259RV	GGCACCAGAGCGTTACGCTATAACACAGCCATGGTA
FAM115A_264RV	GGCACCAGAGCGTTAGCCATAGCGGGCAGCCGCTAT
FAM115A_268RV	GGCACCAGAGCGTTACACCCGGCCCCGGCCATAGCG
FAM115A_273RV	GGCACCAGAGCGTTAATGGCCAGTCACAACCACCCG
FAM115A_276RV	GGCACCAGAGCGTTATAATACCTTATGGCCAGTCAC
FAM115A_279RV	GGCACCAGAGCGTTAAACAGTGAATAATACCTTATG
FAM115A_282RV	GGCACCAGAGCGTTACAGTTTACCAACAGTGAATAA
FAM115A_289RV	GGCACCAGAGCGTTAAGCATTGAGCAGAAAGGGGCC
FAM115A_295RV	GGCACCAGAGCGTTACCCATCCAGCCAGCGGACAGC
FAM115A_299RV	GGCACCAGAGCGTTAGCCTCTGCGGCCCCCATCCAG
FAM115A_303RV	GGCACCAGAGCGTTACACCACAATCTTGCCTCTGCG

HIF1α^{ODD}

Primer Name	Sequence (5'-3')
HIF ODD380FW	CAGGGACCCGGTTCAGAAGATACAAGTAGCCTC
HIF ODD401FW	CAGGGACCCGGTGCCCCAGCCGCTGGAGACACA
HIF ODD403FW	CAGGGACCCGGTGCCGCTGGAGACACAATCATA
HIF ODD530FW	CAGGGACCCGGTGAATTCAAGTTGGAATTGGTA
HIF ODD603RV	GGCACCAGAGCGTTACTGGAATACTGTAACTGTGCT
HIF ODD652RV	GGCACCAGAGCGTTAAGTAGTTTCTTTATGTATGTG

HIF2α^{ODD}

Primer Name	Sequence (5'-3')
HIF2Fw_377	CAGGGACCCGGTCAAGAAGATTTACTTCGTCGA
HIF2Fw_381	CAGGGACCCGGTCTTCGTCGATTCCCAGATCTT
HIF2Fw_495	CAGGGACCCGGTACATTAATAAGTGCAGCCAGA
HIF2Rv_578	GGCACCAGAGCGTTAAACAATGGCATCCTGGGCTTC
HIF2Rv_655	GGCACCAGAGCGTTATACGTCATTAGGAATAAATGC
HIF2Rv_667	GGCACCAGAGCGTTAAATGATGTGGAACATCTGTTT

References

Alexandru, G., Graumann, J., Smith, G.T., Kolawa, N.J., Fang, R., and Deshaies, R.J. (2008). UBXD7 binds multiple ubiquitin ligases and implicates p97 in HIF1alpha turnover. Cell *134*, 804-816.

An, W.G., Kanekal, M., Simon, M.C., Maltepe, E., Blagosklonny, M.V., and Neckers, L.M. (1998). Stabilization of wild-type p53 by hypoxia-inducible factor 1alpha. Nature *392*, 405-408.

Appelhoff, R.J., Tian, Y.M., Raval, R.R., Turley, H., Harris, A.L., Pugh, C.W., Ratcliffe, P.J., and Gleadle, J.M. (2004). Differential function of the prolyl hydroxylases PHD1, PHD2, and PHD3 in the regulation of hypoxia-inducible factor. The Journal of biological chemistry *279*, 38458-38465.

Beck, M., and Baumeister, W. (2016). Cryo-Electron Tomography: Can it Reveal the Molecular Sociology of Cells in Atomic Detail? Trends in cell biology *26*, 825-837.

Bellot, G., Garcia-Medina, R., Gounon, P., Chiche, J., Roux, D., Pouyssegur, J., and Mazure, N.M. (2009). Hypoxia-induced autophagy is mediated through hypoxia-inducible factor induction of BNIP3 and BNIP3L via their BH3 domains. Molecular and cellular biology *29*, 2570-2581.

Benita, Y., Kikuchi, H., Smith, A.D., Zhang, M.Q., Chung, D.C., and Xavier, R.J. (2009). An integrative genomics approach identifies Hypoxia Inducible Factor-1 (HIF-1)-target genes that form the core response to hypoxia. Nucleic acids research *37*, 4587-4602.

Berra, E., Benizri, E., Ginouves, A., Volmat, V., Roux, D., and Pouyssegur, J. (2003). HIF prolyl-hydroxylase 2 is the key oxygen sensor setting low steady-state levels of HIF-1alpha in normoxia. The EMBO journal *22*, 4082-4090.

Berra, E., Roux, D., Richard, D.E., and Pouyssegur, J. (2001). Hypoxia-inducible factor-1 alpha (HIF-1 alpha) escapes O(2)-driven proteasomal degradation irrespective of its subcellular localization: nucleus or cytoplasm. EMBO reports *2*, 615-620.

Besche, H.C., Haas, W., Gygi, S.P., and Goldberg, A.L. (2009). Isolation of mammalian 26S proteasomes and p97/VCP complexes using the ubiquitin-like domain from HHR23B reveals novel proteasome-associated proteins. Biochemistry *48*, 2538-2549.

Boname, J.M., Thomas, M., Stagg, H.R., Xu, P., Peng, J., and Lehner, P.J. (2010). Efficient internalization of MHC I requires lysine-11 and lysine-63 mixed linkage polyubiquitin chains. Traffic *11*, 210-220.

Bremm, A., Freund, S.M., and Komander, D. (2010). Lys11-linked ubiquitin chains adopt compact conformations and are preferentially hydrolyzed by the deubiquitinase Cezanne. Nature structural & molecular biology *17*, 939-947.

Bremm, A., Moniz, S., Mader, J., Rocha, S., and Komander, D. (2014). Cezanne (OTUD7B) regulates HIF-1alpha homeostasis in a proteasome-independent manner. EMBO Rep *15*, 1268-1277.

Bruick, R.K., and McKnight, S.L. (2001). A conserved family of prolyl-4-hydroxylases that modify HIF. Science (New York, NY) *294*, 1337-1340.

Brzovic, P.S., and Klevit, R.E. (2006). Ubiquitin transfer from the E2 perspective: why is UbcH5 so promiscuous? Cell cycle (Georgetown, Tex) *5*, 2867-2873.

Burana, D., Yoshihara, H., Tanno, H., Yamamoto, A., Saeki, Y., Tanaka, K., and Komada, M. (2016). The Ankrd13 Family of Ubiquitin-interacting Motif-bearing Proteins Regulates Valosin-containing Protein/p97 Protein-mediated Lysosomal Trafficking of Caveolin 1. The Journal of biological chemistry *291*, 6218-6231.

Burr, S.P., Costa, A.S., Grice, G.L., Timms, R.T., Lobb, I.T., Freisinger, P., Dodd, R.B., Dougan, G., Lehner, P.J., Frezza, C., and Nathan, J.A. (2016). Mitochondrial Protein Lipoylation and the 2-Oxoglutarate Dehydrogenase Complex Controls HIF1alpha Stability in Aerobic Conditions. Cell metabolism *24*, 740-752.

Buss, F., Kendrick-Jones, J., Lionne, C., Knight, A.E., Cote, G.P., and Paul Luzio, J. (1998). The localization of myosin VI at the golgi complex and leading edge of fibroblasts and its phosphorylation and recruitment into membrane ruffles of A431 cells after growth factor stimulation. The Journal of cell biology *143*, 1535-1545.

Carmeliet, P., Dor, Y., Herbert, J.M., Fukumura, D., Brusselmans, K., Dewerchin, M., Neeman, M., Bono, F., Abramovitch, R., Maxwell, P., Koch, C.J., Ratcliffe, P., Moons, L., Jain, R.K., Collen, D., and Keshert, E. (1998). Role of HIF-1alpha in hypoxia-mediated apoptosis, cell proliferation and tumour angiogenesis. Nature *394*, 485-490.

Castaneda, C.A., Dixon, E.K., Walker, O., Chaturvedi, A., Nakasone, M.A., Curtis, J.E., Reed, M.R., Krueger, S., Cropp, T.A., and Fushman, D. (2016). Linkage via K27 Bestows Ubiquitin Chains with Unique Properties among Polyubiquitins. Structure (London, England : 1993) *24*, 423-436.

Castaneda, C.A., Kashyap, T.R., Nakasone, M.A., Krueger, S., and Fushman, D. (2013). Unique structural, dynamical, and functional properties of k11-linked polyubiquitin chains. Structure *21*, 1168-1181.

Castaneda, C.A., Liu, J., Kashyap, T.R., Singh, R.K., Fushman, D., and Cropp, T.A. (2011). Controlled enzymatic synthesis of natural-linkage, defined-length polyubiquitin chains using lysines with removable protecting groups. Chemical communications (Cambridge, England) *47*, 2026-2028.

Chang, S.C., Momburg, F., Bhutani, N., and Goldberg, A.L. (2005). The ER aminopeptidase, ERAP1, trims precursors to lengths of MHC class I peptides by a "molecular ruler" mechanism. Proceedings of the National Academy of Sciences of the United States of America *102*, 17107-17112.

Chowdhury, R., Yeoh, K.K., Tian, Y.M., Hillringhaus, L., Bagg, E.A., Rose, N.R., Leung, I.K., Li, X.S., Woon, E.C., Yang, M., McDonough, M.A., King, O.N., Clifton, I.J., Klose, R.J., Claridge, T.D., Ratcliffe, P.J., Schofield, C.J., and Kawamura, A. (2011). The oncometabolite 2-hydroxyglutarate inhibits histone lysine demethylases. EMBO reports *12*, 463-469.

Clifford, S.C., Cockman, M.E., Smallwood, A.C., Mole, D.R., Woodward, E.R., Maxwell, P.H., Ratcliffe, P.J., and Maher, E.R. (2001). Contrasting effects on HIF-1alpha regulation by disease-causing pVHL mutations correlate with patterns of tumourigenesis in von Hippel-Lindau disease. Human molecular genetics *10*, 1029-1038.

Cockman, M.E., Masson, N., Mole, D.R., Jaakkola, P., Chang, G.W., Clifford, S.C., Maher, E.R., Pugh, C.W., Ratcliffe, P.J., and Maxwell, P.H. (2000). Hypoxia inducible factor-alpha binding and ubiquitylation by the von Hippel-Lindau tumor suppressor protein. The Journal of biological chemistry *275*, 25733-25741.

Cowey, C.L., and Rathmell, W.K. (2009). VHL gene mutations in renal cell carcinoma: role as a biomarker of disease outcome and drug efficacy. Current oncology reports *11*, 94-101.

Crosas, B., Hanna, J., Kirkpatrick, D.S., Zhang, D.P., Tone, Y., Hathaway, N.A., Buecker, C., Leggett, D.S., Schmidt, M., King, R.W., Gygi, S.P., and Finley, D. (2006). Ubiquitin chains are remodeled at the proteasome by opposing ubiquitin ligase and deubiquitinating activities. Cell *127*, 1401-1413.

Cunningham, C.N., Baughman, J.M., Phu, L., Tea, J.S., Yu, C., Coons, M., Kirkpatrick, D.S., Bingol, B., and Corn, J.E. (2015). USP30 and parkin homeostatically regulate atypical ubiquitin chains on mitochondria. Nature cell biology *17*, 160-169.

Dang, L., White, D.W., Gross, S., Bennett, B.D., Bittinger, M.A., Driggers, E.M., Fantin, V.R., Jang, H.G., Jin, S., Keenan, M.C., Marks, K.M., Prins, R.M., Ward, P.S., Yen, K.E., Liau, L.M., Rabinowitz, J.D., Cantley, L.C., Thompson, C.B., Vander Heiden, M.G., and Su, S.M. (2009). Cancer-associated IDH1 mutations produce 2-hydroxyglutarate. Nature *462*, 739-744.

Dao, K.H., Rotelli, M.D., Petersen, C.L., Kaech, S., Nelson, W.D., Yates, J.E., Hanlon Newell, A.E., Olson, S.B., Druker, B.J., and Bagby, G.C. (2012). FANCL ubiquitinates beta-catenin and enhances its nuclear function. Blood *120*, 323-334.

Dautry-Varsat, A., Ciechanover, A., and Lodish, H.F. (1983). pH and the recycling of transferrin during receptor-mediated endocytosis. Proceedings of the National Academy of Sciences of the United States of America *80*, 2258-2262.

Deng, L., Wang, C., Spencer, E., Yang, L., Braun, A., You, J., Slaughter, C., Pickart, C., and Chen, Z.J. (2000). Activation of the IkappaB kinase complex by TRAF6 requires a dimeric ubiquitin-conjugating enzyme complex and a unique polyubiquitin chain. Cell *103*, 351-361.

Deveraux, Q., Ustrell, V., Pickart, C., and Rechsteiner, M. (1994). A 26 S protease subunit that binds ubiquitin conjugates. The Journal of biological chemistry *269*, 7059-7061.

Dimova, N.V., Hathaway, N.A., Lee, B.H., Kirkpatrick, D.S., Berkowitz, M.L., Gygi, S.P., Finley, D., and King, R.W. (2012). APC/C-mediated multiple monoubiquitylation provides an alternative degradation signal for cyclin B1. Nature cell biology *14*, 168-176.

Dynek, J.N., Goncharov, T., Dueber, E.C., Fedorova, A.V., Izrael-Tomasevic, A., Phu, L., Helgason, E., Fairbrother, W.J., Deshayes, K., Kirkpatrick, D.S., and Vucic, D. (2010). c-IAP1 and UbcH5 promote K11-linked polyubiquitination of RIP1 in TNF signalling. The EMBO journal *29*, 4198-4209.

Elsasser, S., Chandler-Militello, D., Muller, B., Hanna, J., and Finley, D. (2004). Rad23 and Rpn10 serve as alternative ubiquitin receptors for the proteasome. The Journal of biological chemistry *279*, 26817-26822.

Elsasser, S., Gali, R.R., Schwickart, M., Larsen, C.N., Leggett, D.S., Muller, B., Feng, M.T., Tubing, F., Dittmar, G.A., and Finley, D. (2002). Proteasome subunit Rpn1 binds ubiquitin-like protein domains. Nature cell biology *4*, 725-730.

Ema, M., Taya, S., Yokotani, N., Sogawa, K., Matsuda, Y., and Fujii-Kuriyama, Y. (1997). A novel bHLH-PAS factor with close sequence similarity to hypoxia-inducible factor 1alpha regulates the VEGF expression and is potentially involved in lung and vascular development. Proceedings of the National Academy of Sciences of the United States of America *94*, 4273-4278.

Eng, C., Kiuru, M., Fernandez, M.J., and Aaltonen, L.A. (2003). A role for mitochondrial enzymes in inherited neoplasia and beyond. Nature reviews Cancer *3*, 193-202.

Epstein, A.C., Gleadle, J.M., McNeill, L.A., Hewitson, K.S., O'Rourke, J., Mole, D.R., Mukherji, M., Metzen, E., Wilson, M.I., Dhanda, A., Tian, Y.M., Masson, N., Hamilton, D.L., Jaakkola, P., Barstead, R., Hodgkin, J., Maxwell, P.H., Pugh, C.W., Schofield, C.J., and Ratcliffe, P.J. (2001). C. elegans EGL-9 and mammalian homologs define a family of dioxygenases that regulate HIF by prolyl hydroxylation. Cell *107*, 43-54.

Faggiano, S., Alfano, C., and Pastore, A. (2016). The missing links to link ubiquitin: Methods for the enzymatic production of polyubiquitin chains. Analytical biochemistry *492*, 82-90.

Ferreira, J.V., Soares, A.R., Ramalho, J.S., Pereira, P., and Girao, H. (2015). K63 linked ubiquitin chain formation is a signal for HIF1A degradation by Chaperone-Mediated Autophagy. Scientific reports *5*, 10210.

Figueroa, M.E., Abdel-Wahab, O., Lu, C., Ward, P.S., Patel, J., Shih, A., Li, Y., Bhagwat, N., Vasanthakumar, A., Fernandez, H.F., Tallman, M.S., Sun, Z., Wolniak, K., Peeters, J.K., Liu, W., Choe, S.E., Fantin, V.R., Paietta, E., Lowenberg, B., Licht, J.D.*, et al.* (2010). Leukemic IDH1 and IDH2 mutations result in a hypermethylation phenotype, disrupt TET2 function, and impair hematopoietic differentiation. Cancer cell *18*, 553-567.

Finley, D. (2009). Recognition and processing of ubiquitin-protein conjugates by the proteasome. Annu Rev Biochem *78*, 477-513.

Fishbain, S., Prakash, S., Herrig, A., Elsasser, S., and Matouschek, A. (2011). Rad23 escapes degradation because it lacks a proteasome initiation region. Nature communications *2*, 192.

Flamme, I., Frohlich, T., von Reutern, M., Kappel, A., Damert, A., and Risau, W. (1997). HRF, a putative basic helix-loop-helix-PAS-domain transcription factor is closely related to hypoxia-inducible factor-1 alpha and developmentally expressed in blood vessels. Mechanisms of development *63*, 51-60.

Fukuba, H., Yamashita, H., Nagano, Y., Jin, H.G., Hiji, M., Ohtsuki, T., Takahashi, T., Kohriyama, T., and Matsumoto, M. (2007). Siah-1 facilitates ubiquitination and degradation of factor inhibiting HIF-1alpha (FIH). Biochemical and biophysical research communications *353*, 324-329.

Gale, D.P., Harten, S.K., Reid, C.D., Tuddenham, E.G., and Maxwell, P.H. (2008). Autosomal dominant erythrocytosis and pulmonary arterial hypertension associated with an activating HIF2 alpha mutation. Blood *112*, 919-921.

Garnett, M.J., Mansfeld, J., Godwin, C., Matsusaka, T., Wu, J., Russell, P., Pines, J., and Venkitaraman, A.R. (2009). UBE2S elongates ubiquitin chains on APC/C substrates to promote mitotic exit. Nature cell biology *11*, 1363-1369.

Gatti, M., Pinato, S., Maiolica, A., Rocchio, F., Prato, M.G., Aebersold, R., and Penengo, L. (2015). RNF168 promotes noncanonical K27 ubiquitination to signal DNA damage. Cell reports *10*, 226-238.

Gkika, D., Lemonnier, L., Shapovalov, G., Gordienko, D., Poux, C., Bernardini, M., Bokhobza, A., Bidaux, G., Degerny, C., Verreman, K., Guarmit, B., Benahmed, M., de Launoit, Y., Bindels, R.J., Fiorio Pla, A., and Prevarskaya, N. (2015). TRP channel-associated factors are a novel protein family that regulates TRPM8 trafficking and activity. The Journal of cell biology *208*, 89-107.

Grice, G.L., Lobb, I.T., Weekes, M.P., Gygi, S.P., Antrobus, R., and Nathan, J.A. (2015). The Proteasome Distinguishes between Heterotypic and Homotypic Lysine-11-Linked Polyubiquitin Chains. Cell reports *12*, 545-553.

Groll, M., Bajorek, M., Kohler, A., Moroder, L., Rubin, D.M., Huber, R., Glickman, M.H., and Finley, D. (2000). A gated channel into the proteasome core particle. Nature structural biology *7*, 1062-1067.

Guo, J., Chakraborty, A.A., Liu, P., Gan, W., Zheng, X., Inuzuka, H., Wang, B., Zhang, J., Zhang, L., Yuan, M., Novak, J., Cheng, J.Q., Toker, A., Signoretti, S., Zhang, Q., Asara, J.M., Kaelin, W.G., Jr., and Wei, W. (2016). pVHL suppresses kinase activity of Akt in a proline-hydroxylation-dependent manner. Science (New York, NY) *353*, 929-932.

Hager, M., Haufe, H., Kemmerling, R., Hitzl, W., Mikuz, G., Moser, P.L., and Kolbitsch, C. (2009). Increased activated Akt expression in renal cell carcinomas and prognosis. Journal of cellular and molecular medicine *13*, 2181-2188.

Haglund, K., Sigismund, S., Polo, S., Szymkiewicz, I., Di Fiore, P.P., and Dikic, I. (2003). Multiple monoubiquitination of RTKs is sufficient for their endocytosis and degradation. Nature cell biology *5*, 461-466.

Harper, S., Besong, T.M., Emsley, J., Scott, D.J., and Dreveny, I. (2011). Structure of the USP15 N-terminal domains: a beta-hairpin mediates close association between the DUSP and UBL domains. Biochemistry *50*, 7995-8004.

He, F., Wollscheid, H.P., Nowicka, U., Biancospino, M., Valentini, E., Ehlinger, A., Acconcia, F., Magistrati, E., Polo, S., and Walters, K.J. (2016). Myosin VI Contains a Compact Structural Motif that Binds to Ubiquitin Chains. Cell reports *14*, 2683-2694.

Heissmeyer, V., Krappmann, D., Hatada, E.N., and Scheidereit, C. (2001). Shared pathways of IkappaB kinase-induced SCF(betaTrCP)-mediated ubiquitination and degradation for the NF-kappaB precursor p105 and IkappaBalpha. Molecular and cellular biology *21*, 1024-1035.

Hemantha, H.P., Bavikar, S.N., Herman-Bachinsky, Y., Haj-Yahya, N., Bondalapati, S., Ciechanover, A., and Brik, A. (2014). Nonenzymatic polyubiquitination of expressed proteins. Journal of the American Chemical Society *136*, 2665-2673.

Hershko, A., and Ciechanover, A. (1998). The ubiquitin system. Annu Rev Biochem *67*, 425-479.

Hewitson, K.S., Lienard, B.M., McDonough, M.A., Clifton, I.J., Butler, D., Soares, A.S., Oldham, N.J., McNeill, L.A., and Schofield, C.J. (2007a). Structural and mechanistic studies on the inhibition of the hypoxia-inducible transcription factor hydroxylases by tricarboxylic acid cycle intermediates. The Journal of biological chemistry *282*, 3293-3301.

Hewitson, K.S., Schofield, C.J., and Ratcliffe, P.J. (2007b). Hypoxia-inducible factor prolyl-hydroxylase: purification and assays of PHD2. Methods in enzymology *435*, 25-42.

Hjerpe, R., Aillet, F., Lopitz-Otsoa, F., Lang, V., England, P., and Rodriguez, M.S. (2009). Efficient protection and isolation of ubiquitylated proteins using tandem ubiquitin-binding entities. EMBO Rep *10*, 1250-1258.

Hoffman, M.A., Ohh, M., Yang, H., Klco, J.M., Ivan, M., and Kaelin, W.G., Jr. (2001). von Hippel-Lindau protein mutants linked to type 2C VHL disease preserve the ability to downregulate HIF. Human molecular genetics *10*, 1019-1027.

Hofmann, R.M., and Pickart, C.M. (2001). In vitro assembly and recognition of Lys-63 polyubiquitin chains. The Journal of biological chemistry *276*, 27936-27943.

Hospenthal, M.K., Mevissen, T.E.T., and Komander, D. (2015). Deubiquitinase-based analysis of ubiquitin chain architecture using Ubiquitin Chain Restriction (UbiCRest). Nature protocols *10*, 349-361.

Huang, L.E., Gu, J., Schau, M., and Bunn, H.F. (1998). Regulation of hypoxia-inducible factor 1alpha is mediated by an O2-dependent degradation domain via the ubiquitin-proteasome pathway. Proceedings of the National Academy of Sciences of the United States of America *95*, 7987-7992.

Hubbi, M.E., Gilkes, D.M., Hu, H., Kshitiz, Ahmed, I., and Semenza, G.L. (2014). Cyclin-dependent kinases regulate lysosomal degradation of hypoxia-inducible factor 1alpha to promote cell-cycle progression. Proceedings of the National Academy of Sciences of the United States of America *111*, E3325-3334.

Hubbi, M.E., Hu, H., Kshitiz, Ahmed, I., Levchenko, A., and Semenza, G.L. (2013). Chaperone-mediated autophagy targets hypoxia-inducible factor-1alpha (HIF-1alpha) for lysosomal degradation. The Journal of biological chemistry *288*, 10703-10714.

Hurley, J.H., Lee, S., and Prag, G. (2006). Ubiquitin-binding domains. The Biochemical journal *399*, 361-372.

Husnjak, K., Elsasser, S., Zhang, N., Chen, X., Randles, L., Shi, Y., Hofmann, K., Walters, K.J., Finley, D., and Dikic, I. (2008). Proteasome subunit Rpn13 is a novel ubiquitin receptor. Nature *453*, 481-488.

Hutton, J.J., Jr., Kaplan, A., and Udenfriend, S. (1967). Conversion of the amino acid sequence gly-pro-pro in protein to gly-pro-hyp by collagen proline hydroxylase. Archives of biochemistry and biophysics *121*, 384-391.

Ikeda, F., and Dikic, I. (2008). Atypical ubiquitin chains: new molecular signals. 'Protein Modifications: Beyond the Usual Suspects' review series. EMBO Rep *9*, 536-542.

Iliopoulos, O., Kibel, A., Gray, S., and Kaelin, W.G., Jr. (1995). Tumour suppression by the human von Hippel-Lindau gene product. Nature medicine *1*, 822-826.

Intlekofer, A.M., Dematteo, R.G., Venneti, S., Finley, L.W., Lu, C., Judkins, A.R., Rustenburg, A.S., Grinaway, P.B., Chodera, J.D., Cross, J.R., and Thompson, C.B. (2015). Hypoxia Induces Production of L-2-Hydroxyglutarate. Cell metabolism *22*, 304-311.

Ivan, M., Kondo, K., Yang, H., Kim, W., Valiando, J., Ohh, M., Salic, A., Asara, J.M., Lane, W.S., and Kaelin, W.G., Jr. (2001). HIFalpha targeted for VHL-mediated destruction by proline hydroxylation: implications for O2 sensing. Science (New York, NY) *292*, 464-468.

Jaakkola, P., Mole, D.R., Tian, Y.M., Wilson, M.I., Gielbert, J., Gaskell, S.J., von Kriegsheim, A., Hebestreit, H.F., Mukherji, M., Schofield, C.J., Maxwell, P.H., Pugh, C.W., and Ratcliffe, P.J. (2001). Targeting of HIF-alpha to the von Hippel-Lindau ubiquitylation complex by O2-regulated prolyl hydroxylation. Science (New York, NY) *292*, 468-472.

Jacobson, A.D., Zhang, N.Y., Xu, P., Han, K.J., Noone, S., Peng, J., and Liu, C.W. (2009). The lysine 48 and lysine 63 ubiquitin conjugates are processed differently by the 26 s proteasome. The Journal of biological chemistry *284*, 35485-35494.

Jiang, B.H., Semenza, G.L., Bauer, C., and Marti, H.H. (1996). Hypoxia-inducible factor 1 levels vary exponentially over a physiologically relevant range of O2 tension. The American journal of physiology *271*, C1172-1180.

Jin, L., Williamson, A., Banerjee, S., Philipp, I., and Rape, M. (2008). Mechanism of ubiquitin-chain formation by the human anaphase-promoting complex. Cell *133*, 653-665.

Jin, S., Tian, S., Chen, Y., Zhang, C., Xie, W., Xia, X., Cui, J., and Wang, R.F. (2016). USP19 modulates autophagy and antiviral immune responses by deubiquitinating Beclin-1. The EMBO journal *35*, 866-880.

Jung, C.R., Hwang, K.S., Yoo, J., Cho, W.K., Kim, J.M., Kim, W.H., and Im, D.S. (2006). E2-EPF UCP targets pVHL for degradation and associates with tumor growth and metastasis. Nat Med *12*, 809-816.

Kaelin, W.G., Jr. (2008). The von Hippel-Lindau tumour suppressor protein: O2 sensing and cancer. Nature reviews Cancer *8*, 865-873.

Kaelin, W.G., Jr., and Ratcliffe, P.J. (2008). Oxygen sensing by metazoans: the central role of the HIF hydroxylase pathway. Molecular cell *30*, 393-402.

Kamura, T., Koepp, D.M., Conrad, M.N., Skowyra, D., Moreland, R.J., Iliopoulos, O., Lane, W.S., Kaelin, W.G., Jr., Elledge, S.J., Conaway, R.C., Harper, J.W., and Conaway, J.W. (1999). Rbx1, a component of the VHL tumor suppressor complex and SCF ubiquitin ligase. Science (New York, NY) *284*, 657-661.

Kamura, T., Sato, S., Iwai, K., Czyzyk-Krzeska, M., Conaway, R.C., and Conaway, J.W. (2000). Activation of HIF1alpha ubiquitination by a reconstituted von Hippel-Lindau (VHL) tumor suppressor complex. Proceedings of the National Academy of Sciences of the United States of America *97*, 10430-10435.

Kelley, L.A., Mezulis, S., Yates, C.M., Wass, M.N., and Sternberg, M.J. (2015). The Phyre2 web portal for protein modeling, prediction and analysis. *10*, 845-858.

Kelly, B.D., Hackett, S.F., Hirota, K., Oshima, Y., Cai, Z., Berg-Dixon, S., Rowan, A., Yan, Z., Campochiaro, P.A., and Semenza, G.L. (2003). Cell type-specific regulation of angiogenic growth factor gene expression and induction of angiogenesis in nonischemic tissue by a constitutively active form of hypoxia-inducible factor 1. Circulation research *93*, 1074-1081.

Kim, H.T., Kim, K.P., Lledias, F., Kisselev, A.F., Scaglione, K.M., Skowyra, D., Gygi, S.P., and Goldberg, A.L. (2007). Certain pairs of ubiquitin-conjugating enzymes (E2s) and ubiquitin-protein ligases (E3s) synthesize nondegradable forked ubiquitin chains containing all possible isopeptide linkages. The Journal of biological chemistry *282*, 17375-17386.

Kim, H.T., Kim, K.P., Uchiki, T., Gygi, S.P., and Goldberg, A.L. (2009). S5a promotes protein degradation by blocking synthesis of nondegradable forked ubiquitin chains. The EMBO journal *28*, 1867-1877.

Kirkpatrick, D.S., Hathaway, N.A., Hanna, J., Elsasser, S., Rush, J., Finley, D., King, R.W., and Gygi, S.P. (2006). Quantitative analysis of in vitro ubiquitinated cyclin B1 reveals complex chain topology. Nature cell biology *8*, 700-710.

Kisselev, A.F., Akopian, T.N., Woo, K.M., and Goldberg, A.L. (1999). The sizes of peptides generated from protein by mammalian 26 and 20 S proteasomes. Implications for understanding the degradative mechanism and antigen presentation. The Journal of biological chemistry *274*, 3363-3371.

Klose, R.J., Kallin, E.M., and Zhang, Y. (2006). JmjC-domain-containing proteins and histone demethylation. Nature reviews Genetics *7*, 715-727.

Ko, H.S., Uehara, T., Tsuruma, K., and Nomura, Y. (2004). Ubiquilin interacts with ubiquitylated proteins and proteasome through its ubiquitin-associated and ubiquitin-like domains. FEBS letters *566*, 110-114.

Koegl, M., Hoppe, T., Schlenker, S., Ulrich, H.D., Mayer, T.U., and Jentsch, S. (1999). A novel ubiquitination factor, E4, is involved in multiubiquitin chain assembly. Cell *96*, 635-644.

Kohli, R.M., and Zhang, Y. (2013). TET enzymes, TDG and the dynamics of DNA demethylation. Nature *502*, 472-479.

Koivunen, P., Lee, S., Duncan, C.G., Lopez, G., Lu, G., Ramkissoon, S., Losman, J.A., Joensuu, P., Bergmann, U., Gross, S., Travins, J., Weiss, S., Looper, R., Ligon, K.L., Verhaak, R.G., Yan, H., and Kaelin, W.G., Jr. (2012). Transformation by the (R)-enantiomer of 2-hydroxyglutarate linked to EGLN activation. Nature *483*, 484-488.

Komander, D., Clague, M.J., and Urbe, S. (2009). Breaking the chains: structure and function of the deubiquitinases. Nature reviews Molecular cell biology *10*, 550-563.

Kondo, K., Kim, W.Y., Lechpammer, M., and Kaelin, W.G., Jr. (2003). Inhibition of HIF2alpha is sufficient to suppress pVHL-defective tumor growth. PLoS biology *1*, E83.

Kondo, K., Klco, J., Nakamura, E., Lechpammer, M., and Kaelin, W.G., Jr. (2002). Inhibition of HIF is necessary for tumor suppression by the von Hippel-Lindau protein. Cancer cell *1*, 237-246.

Koyano, F., Okatsu, K., Kosako, H., Tamura, Y., Go, E., Kimura, M., Kimura, Y., Tsuchiya, H., Yoshihara, H., Hirokawa, T., Endo, T., Fon, E.A., Trempe, J.F., Saeki, Y., Tanaka, K., and Matsuda, N. (2014). Ubiquitin is phosphorylated by PINK1 to activate parkin. Nature *510*, 162-166.

Kozik, P., Hodson, N.A., Sahlender, D.A., Simecek, N., Soromani, C., Wu, J., Collinson, L.M., and Robinson, M.S. (2013). A human genome-wide screen for regulators of clathrin-coated vesicle formation reveals an unexpected role for the V-ATPase. Nature cell biology *15*, 50-60.

Kranendijk, M., Struys, E.A., Salomons, G.S., Van der Knaap, M.S., and Jakobs, C. (2012). Progress in understanding 2-hydroxyglutaric acidurias. Journal of inherited metabolic disease *35*, 571-587.

Kravtsova-Ivantsiv, Y., Cohen, S., and Ciechanover, A. (2009). Modification by single ubiquitin moieties rather than polyubiquitination is sufficient for proteasomal processing of the p105 NF-kappaB precursor. Molecular cell *33*, 496-504.

Kristariyanto, Y.A., Choi, S.Y., Rehman, S.A., Ritorto, M.S., Campbell, D.G., Morrice, N.A., Toth, R., and Kulathu, Y. (2015). Assembly and structure of Lys33-linked polyubiquitin reveals distinct conformations. The Biochemical journal *467*, 345-352.

Lam, Y.A., Lawson, T.G., Velayutham, M., Zweier, J.L., and Pickart, C.M. (2002). A proteasomal ATPase subunit recognizes the polyubiquitin degradation signal. Nature *416*, 763-767.

Lando, D., Peet, D.J., Gorman, J.J., Whelan, D.A., Whitelaw, M.L., and Bruick, R.K. (2002). FIH-1 is an asparaginyl hydroxylase enzyme that regulates the transcriptional activity of hypoxia-inducible factor. Genes & development *16*, 1466-1471.

Lang, V., Janzen, J., Fischer, G.Z., Soneji, Y., Beinke, S., Salmeron, A., Allen, H., Hay, R.T., Ben-Neriah, Y., and Ley, S.C. (2003). betaTrCP-mediated proteolysis of NF-kappaB1 p105 requires phosphorylation of p105 serines 927 and 932. Molecular and cellular biology *23*, 402-413.

Lazarou, M., Sliter, D.A., Kane, L.A., Sarraf, S.A., Wang, C., Burman, J.L., Sideris, D.P., Fogel, A.I., and Youle, R.J. (2015). The ubiquitin kinase PINK1 recruits autophagy receptors to induce mitophagy. Nature *524*, 309-314.

Lee, B.H., Lu, Y., Prado, M.A., Shi, Y., Tian, G., Sun, S., Elsasser, S., Gygi, S.P., King, R.W., and Finley, D. (2016). USP14 deubiquitinates proteasome-bound substrates that are ubiquitinated at multiple sites. Nature *532*, 398-401.

Lee, D.C., Sohn, H.A., Park, Z.Y., Oh, S., Kang, Y.K., Lee, K.M., Kang, M., Jang, Y.J., Yang, S.J., Hong, Y.K., Noh, H., Kim, J.A., Kim, D.J., Bae, K.H., Kim, D.M., Chung, S.J., Yoo, H.S., Yu, D.Y., Park, K.C., and Yeom, Y.I. (2015). A lactate-induced response to hypoxia. Cell *161*, 595-609.

Lee, M.J., Lee, B.H., Hanna, J., King, R.W., and Finley, D. (2011). Trimming of ubiquitin chains by proteasome-associated deubiquitinating enzymes. Molecular & cellular proteomics : MCP *10*, R110.003871.

Leggett, D.S., Hanna, J., Borodovsky, A., Crosas, B., Schmidt, M., Baker, R.T., Walz, T., Ploegh, H., and Finley, D. (2002). Multiple associated proteins regulate proteasome structure and function. Molecular cell *10*, 495-507.

Licchesi, J.D., Mieszczanek, J., Mevissen, T.E., Rutherford, T.J., Akutsu, M., Virdee, S., El Oualid, F., Chin, J.W., Ovaa, H., Bienz, M., and Komander, D. (2011). An ankyrin-repeat ubiquitin-binding domain determines TRABID's specificity for atypical ubiquitin chains. Nature structural & molecular biology *19*, 62-71.

Lieb, M.E., Menzies, K., Moschella, M.C., Ni, R., and Taubman, M.B. (2002). Mammalian EGLN genes have distinct patterns of mRNA expression and regulation. Biochemistry and cell biology = Biochimie et biologie cellulaire *80*, 421-426.

Lim, J.H., Park, J.W., Kim, M.S., Park, S.K., Johnson, R.S., and Chun, Y.S. (2006). Bafilomycin induces the p21-mediated growth inhibition of cancer cells under hypoxic conditions by expressing hypoxia-inducible factor-1alpha. Molecular pharmacology *70*, 1856-1865.

Lim, J.H., Park, J.W., Kim, S.J., Kim, M.S., Park, S.K., Johnson, R.S., and Chun, Y.S. (2007). ATP6V0C competes with von Hippel-Lindau protein in hypoxia-inducible factor 1alpha (HIF-1alpha) binding and mediates HIF-1alpha expression by bafilomycin A1. Molecular pharmacology *71*, 942-948.

Liu, J., Zhang, C., Zhao, Y., Yue, X., Wu, H., Huang, S., Chen, J., Tomsky, K., Xie, H., Khella, C.A., Gatza, M.L., Xia, D., Gao, J., White, E., Haffty, B.G., Hu, W., and Feng, Z. (2017). Parkin targets HIF-1alpha for ubiquitination and degradation to inhibit breast tumor progression. Nature communications *8*, 1823.

Loenarz, C., and Schofield, C.J. (2008). Expanding chemical biology of 2-oxoglutarate oxygenases. Nature chemical biology *4*, 152-156.

Losman, J.A., Looper, R.E., Koivunen, P., Lee, S., Schneider, R.K., McMahon, C., Cowley, G.S., Root, D.E., Ebert, B.L., and Kaelin, W.G., Jr. (2013). (R)-2-hydroxyglutarate is sufficient to promote leukemogenesis and its effects are reversible. Science (New York, NY) *339*, 1621-1625.

Lu, Y., Lee, B.H., King, R.W., Finley, D., and Kirschner, M.W. (2015). Substrate degradation by the proteasome: a single-molecule kinetic analysis. Science (New York, NY) *348*, 1250834.

Maltepe, E., Krampitz, G.W., Okazaki, K.M., Red-Horse, K., Mak, W., Simon, M.C., and Fisher, S.J. (2005). Hypoxia-inducible factor-dependent histone deacetylase activity determines stem cell fate in the placenta. Development (Cambridge, England) *132*, 3393-3403.

Manalo, D.J., Rowan, A., Lavoie, T., Natarajan, L., Kelly, B.D., Ye, S.Q., Garcia, J.G., and Semenza, G.L. (2005). Transcriptional regulation of vascular endothelial cell responses to hypoxia by HIF-1. Blood *105*, 659-669.

Mancias, J.D., Wang, X., Gygi, S.P., Harper, J.W., and Kimmelman, A.C. (2014). Quantitative proteomics identifies NCOA4 as the cargo receptor mediating ferritinophagy. Nature *509*, 105-109.

Mansour, W., Nakasone, M.A., von Delbrueck, M., Yu, Z., Krutauz, D., Reis, N., Kleifeld, O., Sommer, T., Fushman, D., and Glickman, M.H. (2014). Disassembly of Lys11- and mixed-linkage polyubiquitin conjugates provide insights into function of proteasomal deubiquitinases Rpn11 and Ubp6. The Journal of biological chemistry.

Marin, I., Lucas, J.I., Gradilla, A.C., and Ferrus, A. (2004). Parkin and relatives: the RBR family of ubiquitin ligases. Physiological genomics *17*, 253-263.

Martinez-Fonts, K., and Matouschek, A. (2016). A Rapid and Versatile Method for Generating Proteins with Defined Ubiquitin Chains. Biochemistry *55*, 1898-1908.

Masson, N., Willam, C., Maxwell, P.H., Pugh, C.W., and Ratcliffe, P.J. (2001). Independent function of two destruction domains in hypoxia-inducible factor-alpha chains activated by prolyl hydroxylation. The EMBO journal *20*, 5197-5206.

Matsumoto, G., Wada, K., Okuno, M., Kurosawa, M., and Nukina, N. (2011). Serine 403 phosphorylation of p62/SQSTM1 regulates selective autophagic clearance of ubiquitinated proteins. Molecular cell *44*, 279-289.

Matsumoto, M.L., Wickliffe, K.E., Dong, K.C., Yu, C., Bosanac, I., Bustos, D., Phu, L., Kirkpatrick, D.S., Hymowitz, S.G., Rape, M., Kelley, R.F., and Dixit, V.M. (2010). K11-linked polyubiquitination in cell cycle control revealed by a K11 linkage-specific antibody. Molecular cell *39*, 477-484.

Maxwell, P.H., and Eckardt, K.U. (2016). HIF prolyl hydroxylase inhibitors for the treatment of renal anaemia and beyond. Nature reviews Nephrology *12*, 157-168.

Maxwell, P.H., and Ratcliffe, P.J. (2002). Oxygen sensors and angiogenesis. Seminars in cell & developmental biology *13*, 29-37.

Maxwell, P.H., Wiesener, M.S., Chang, G.W., Clifford, S.C., Vaux, E.C., Cockman, M.E., Wykoff, C.C., Pugh, C.W., Maher, E.R., and Ratcliffe, P.J. (1999). The tumour suppressor protein VHL targets hypoxia-inducible factors for oxygen-dependent proteolysis. Nature *399*, 271-275.

McCullough, J., Clague, M.J., and Urbe, S. (2004). AMSH is an endosome-associated ubiquitin isopeptidase. The Journal of cell biology *166*, 487-492.

McDonough, M.A., Li, V., Flashman, E., Chowdhury, R., Mohr, C., Lienard, B.M., Zondlo, J., Oldham, N.J., Clifton, I.J., Lewis, J., McNeill, L.A., Kurzeja, R.J., Hewitson, K.S., Yang, E., Jordan, S., Syed, R.S., and Schofield, C.J. (2006). Cellular oxygen sensing: Crystal structure of hypoxia-inducible factor prolyl hydroxylase (PHD2). Proceedings of the National Academy of Sciences of the United States of America *103*, 9814-9819.

McNeill, L.A., Flashman, E., Buck, M.R., Hewitson, K.S., Clifton, I.J., Jeschke, G., Claridge, T.D., Ehrismann, D., Oldham, N.J., and Schofield, C.J. (2005). Hypoxia-inducible factor prolyl hydroxylase 2 has a high affinity for ferrous iron and 2-oxoglutarate. Molecular bioSystems *1*, 321-324.

Mevissen, T.E.T., Kulathu, Y., Mulder, M.P.C., Geurink, P.P., Maslen, S.L., Gersch, M., Elliott, P.R., Burke, J.E., van Tol, B.D.M., Akutsu, M., Oualid, F.E., Kawasaki, M., Freund, S.M.V., Ovaa, H., and Komander, D. (2016). Molecular basis of Lys11-polyubiquitin specificity in the deubiquitinase Cezanne. Nature *538*, 402-405.

Meyer, H.J., and Rape, M. (2014). Enhanced protein degradation by branched ubiquitin chains. Cell *157*, 910-921.

Michel, M.A., Elliott, P.R., Swatek, K.N., Simicek, M., Pruneda, J.N., Wagstaff, J.L., Freund, S.M., and Komander, D. (2015). Assembly and specific recognition of k29- and k33-linked polyubiquitin. Molecular cell *58*, 95-109.

Michel, M.A., Swatek, K.N., Hospenthal, M.K., and Komander, D. (2017). Ubiquitin Linkage-Specific Affimers Reveal Insights into K6-Linked Ubiquitin Signaling. Molecular cell *68*, 233-246.e235.

Miles, A.L., Burr, S.P., Grice, G.L., and Nathan, J.A. (2017). The vacuolar-ATPase complex and assembly factors, TMEM199 and CCDC115, control HIF1alpha prolyl hydroxylation by regulating cellular iron levels. *6*.

Min, M., and Lindon, C. (2012). Substrate targeting by the ubiquitin-proteasome system in mitosis. Seminars in cell & developmental biology *23*, 482-491.

Moller, A., House, C.M., Wong, C.S., Scanlon, D.B., Liu, M.C., Ronai, Z., and Bowtell, D.D. (2009). Inhibition of Siah ubiquitin ligase function. Oncogene *28*, 289-296.

Montagner, M., Enzo, E., Forcato, M., Zanconato, F., Parenti, A., Rampazzo, E., Basso, G., Leo, G., Rosato, A., Bicciato, S., Cordenonsi, M., and Piccolo, S. (2012). SHARP1 suppresses breast cancer metastasis by promoting degradation of hypoxia-inducible factors. Nature *487*, 380-384.

Morris, J.R., and Solomon, E. (2004). BRCA1 : BARD1 induces the formation of conjugated ubiquitin structures, dependent on K6 of ubiquitin, in cells during DNA replication and repair. Human molecular genetics *13*, 807-817.

Morriswood, B., Ryzhakov, G., Puri, C., Arden, S.D., Roberts, R., Dendrou, C., Kendrick-Jones, J., and Buss, F. (2007). T6BP and NDP52 are myosin VI binding partners with potential roles in cytokine signalling and cell adhesion. Journal of cell science *120*, 2574-2585.

Mutoh, T., Sanosaka, T., Ito, K., and Nakashima, K. (2012). Oxygen levels epigenetically regulate fate switching of neural precursor cells via hypoxia-inducible factor 1alpha-notch signal interaction in the developing brain. Stem cells (Dayton, Ohio) *30*, 561-569.

Myllyharju, J., and Kivirikko, K.I. (2004). Collagens, modifying enzymes and their mutations in humans, flies and worms. Trends in genetics : TIG *20*, 33-43.

Nakayama, K., and Ronai, Z. (2004). Siah: new players in the cellular response to hypoxia. Cell cycle (Georgetown, Tex) *3*, 1345-1347.

Nakjang, S., Ndeh, D.A., Wipat, A., Bolam, D.N., and Hirt, R.P. (2012). A novel extracellular metallopeptidase domain shared by animal host-associated mutualistic and pathogenic microbes. PloS one *7*, e30287.

Nathan, J.A., Kim, H.T., Ting, L., Gygi, S.P., and Goldberg, A.L. (2013). Why do cellular proteins linked to K63-polyubiquitin chains not associate with proteasomes? The EMBO journal *32*, 552-565.

Neumann, H.P., Pawlu, C., Peczkowska, M., Bausch, B., McWhinney, S.R., Muresan, M., Buchta, M., Franke, G., Klisch, J., Bley, T.A., Hoegerle, S., Boedeker, C.C., Opocher, G., Schipper, J., Januszewicz, A., and Eng, C. (2004). Distinct clinical features of paraganglioma syndromes associated with SDHB and SDHD gene mutations. Jama *292*, 943-951.

Oldham, W.M., Clish, C.B., Yang, Y., and Loscalzo, J. (2015). Hypoxia-Mediated Increases in L-2-hydroxyglutarate Coordinate the Metabolic Response to Reductive Stress. Cell metabolism *22*, 291-303.

Ordureau, A., Heo, J.M., Duda, D.M., Paulo, J.A., Olszewski, J.L., Yanishevski, D., Rinehart, J., Schulman, B.A., and Harper, J.W. (2015). Defining roles of PARKIN and ubiquitin phosphorylation by PINK1 in mitochondrial quality control using a ubiquitin replacement strategy. Proceedings of the National Academy of Sciences of the United States of America *112*, 6637-6642.

Ordureau, A., Sarraf, S.A., Duda, D.M., Heo, J.M., Jedrychowski, M.P., Sviderskiy, V.O., Olszewski, J.L., Koerber, J.T., Xie, T., Beausoleil, S.A., Wells, J.A., Gygi, S.P., Schulman, B.A., and Harper, J.W. (2014). Quantitative proteomics reveal a feedforward mechanism for mitochondrial PARKIN translocation and ubiquitin chain synthesis. Molecular cell *56*, 360-375.

Palazon, A., Goldrath, A.W., Nizet, V., and Johnson, R.S. (2014). HIF transcription factors, inflammation, and immunity. Immunity *41*, 518-528.

Paltoglou, S., and Roberts, B.J. (2007). HIF-1alpha and EPAS ubiquitination mediated by the VHL tumour suppressor involves flexibility in the ubiquitination mechanism, similar to other RING E3 ligases. Oncogene *26*, 604-609.

Paraskevopoulos, K., Kriegenburg, F., Tatham, M.H., Rosner, H.I., Medina, B., Larsen, I.B., Brandstrup, R., Hardwick, K.G., Hay, R.T., Kragelund, B.B., Hartmann-Petersen, R., and Gordon, C. (2014). Dss1 is a 26S proteasome ubiquitin receptor. Molecular cell *56*, 453-461.

Pathare, G.R., Nagy, I., Sledz, P., Anderson, D.J., Zhou, H.J., Pardon, E., Steyaert, J., Forster, F., Bracher, A., and Baumeister, W. (2014). Crystal structure of the proteasomal deubiquitylation module Rpn8-Rpn11. Proceedings of the National Academy of Sciences of the United States of America *111*, 2984-2989.

Pause, A., Lee, S., Worrell, R.A., Chen, D.Y., Burgess, W.H., Linehan, W.M., and Klausner, R.D. (1997). The von Hippel-Lindau tumor-suppressor gene product forms a stable complex with human CUL-2, a member of the Cdc53 family of proteins. Proceedings of the National Academy of Sciences of the United States of America *94*, 2156-2161.

Percy, M.J., McMullin, M.F., Jowitt, S.N., Potter, M., Treacy, M., Watson, W.H., and Lappin, T.R. (2003). Chuvash-type congenital polycythemia in 4 families of Asian and Western European ancestry. Blood *102*, 1097-1099.

Percy, M.J., Zhao, Q., Flores, A., Harrison, C., Lappin, T.R., Maxwell, P.H., McMullin, M.F., and Lee, F.S. (2006). A family with erythrocytosis establishes a role for prolyl hydroxylase domain protein 2 in oxygen homeostasis. Proceedings of the National Academy of Sciences of the United States of America *103*, 654-659.

Peters, J.P., Her, Y.F., and Maher, L.J., 3rd (2015). Modeling dioxygenase enzyme kinetics in familial paraganglioma. Biology open *4*, 1281-1289.

Peth, A., Besche, H.C., and Goldberg, A.L. (2009). Ubiquitinated proteins activate the proteasome by binding to Usp14/Ubp6, which causes 20S gate opening. Molecular cell *36*, 794-804.

Peth, A., Uchiki, T., and Goldberg, A.L. (2010). ATP-dependent steps in the binding of ubiquitin conjugates to the 26S proteasome that commit to degradation. Molecular cell *40*, 671-681.

Pickart, C.M. (2001). Mechanisms underlying ubiquitination. Annu Rev Biochem *70*, 503-533.

Pines, J. (2011). Cubism and the cell cycle: the many faces of the APC/C. Nature reviews Molecular cell biology *12*, 427-438.

Pollard, P.J., Briere, J.J., Alam, N.A., Barwell, J., Barclay, E., Wortham, N.C., Hunt, T., Mitchell, M., Olpin, S., Moat, S.J., Hargreaves, I.P., Heales, S.J., Chung, Y.L., Griffiths,

J.R., Dalgleish, A., McGrath, J.A., Gleeson, M.J., Hodgson, S.V., Poulsom, R., Rustin, P.*, et al.* (2005). Accumulation of Krebs cycle intermediates and over-expression of HIF1alpha in tumours which result from germline FH and SDH mutations. Human molecular genetics *14*, 2231-2239.

Prakash, S., Tian, L., Ratliff, K.S., Lehotzky, R.E., and Matouschek, A. (2004). An unstructured initiation site is required for efficient proteasome-mediated degradation. Nature structural & molecular biology *11*, 830-837.

Pugh, C.W., and Ratcliffe, P.J. (2003). Regulation of angiogenesis by hypoxia: role of the HIF system. Nature medicine *9*, 677-684.

Qin, Y., Zhou, M.T., Hu, M.M., Hu, Y.H., Zhang, J., Guo, L., Zhong, B., and Shu, H.B. (2014). RNF26 temporally regulates virus-triggered type I interferon induction by two distinct mechanisms. PLoS pathogens *10*, e1004358.

Rabinowitz, M.H. (2013). Inhibition of hypoxia-inducible factor prolyl hydroxylase domain oxygen sensors: tricking the body into mounting orchestrated survival and repair responses. Journal of medicinal chemistry *56*, 9369-9402.

Radmer, R.J., and Klein, T.E. (2006). Triple helical structure and stabilization of collagen-like molecules with 4(R)-hydroxyproline in the Xaa position. Biophysical journal *90*, 578-588.

Raval, R.R., Lau, K.W., Tran, M.G., Sowter, H.M., Mandriota, S.J., Li, J.L., Pugh, C.W., Maxwell, P.H., Harris, A.L., and Ratcliffe, P.J. (2005). Contrasting properties of hypoxia-inducible factor 1 (HIF-1) and HIF-2 in von Hippel-Lindau-associated renal cell carcinoma. Molecular and cellular biology *25*, 5675-5686.

Ren, X., and Hurley, J.H. (2010). VHS domains of ESCRT-0 cooperate in high-avidity binding to polyubiquitinated cargo. The EMBO journal *29*, 1045-1054.

Reyes-Turcu, F.E., and Wilkinson, K.D. (2009). Polyubiquitin binding and disassembly by deubiquitinating enzymes. Chemical reviews *109*, 1495-1508.

Richly, H., Rape, M., Braun, S., Rumpf, S., Hoege, C., and Jentsch, S. (2005). A series of ubiquitin binding factors connects CDC48/p97 to substrate multiubiquitylation and proteasomal targeting. Cell *120*, 73-84.

Rock, K.L., Gramm, C., Rothstein, L., Clark, K., Stein, R., Dick, L., Hwang, D., and Goldberg, A.L. (1994). Inhibitors of the proteasome block the degradation of most cell proteins and the generation of peptides presented on MHC class I molecules. Cell *78*, 761-771.

Rock, K.L., York, I.A., Saric, T., and Goldberg, A.L. (2002). Protein degradation and the generation of MHC class I-presented peptides. Advances in immunology *80*, 1-70.

Saeki, Y., Kudo, T., Sone, T., Kikuchi, Y., Yokosawa, H., Toh-e, A., and Tanaka, K. (2009). Lysine 63-linked polyubiquitin chain may serve as a targeting signal for the 26S proteasome. The EMBO journal *28*, 359-371.

Sahlender, D.A., Roberts, R.C., Arden, S.D., Spudich, G., Taylor, M.J., Luzio, J.P., Kendrick-Jones, J., and Buss, F. (2005). Optineurin links myosin VI to the Golgi complex and is involved in Golgi organization and exocytosis. The Journal of cell biology *169*, 285-295.

Salceda, S., and Caro, J. (1997). Hypoxia-inducible factor 1alpha (HIF-1alpha) protein is rapidly degraded by the ubiquitin-proteasome system under normoxic conditions. Its stabilization by hypoxia depends on redox-induced changes. The Journal of biological chemistry *272*, 22642-22647.

Salmeron, A., Janzen, J., Soneji, Y., Bump, N., Kamens, J., Allen, H., and Ley, S.C. (2001). Direct phosphorylation of NF-kappaB1 p105 by the IkappaB kinase complex on serine 927 is essential for signal-induced p105 proteolysis. The Journal of biological chemistry *276*, 22215-22222.

Sato, Y., Yoshikawa, A., Yamagata, A., Mimura, H., Yamashita, M., Ookata, K., Nureki, O., Iwai, K., Komada, M., and Fukai, S. (2008). Structural basis for specific cleavage of Lys 63-linked polyubiquitin chains. Nature *455*, 358-362.

Schreiner, P., Chen, X., Husnjak, K., Randles, L., Zhang, N., Elsasser, S., Finley, D., Dikic, I., Walters, K.J., and Groll, M. (2008). Ubiquitin docking at the proteasome through a novel pleckstrin-homology domain interaction. Nature *453*, 548-552.

Sciacovelli, M., Goncalves, E., Johnson, T.I., Zecchini, V.R., da Costa, A.S., Gaude, E., Drubbel, A.V., Theobald, S.J., Abbo, S.R., Tran, M.G., Rajeeve, V., Cardaci, S., Foster, S., Yun, H., Cutillas, P., Warren, A., Gnanapragasam, V., Gottlieb, E., Franze, K., Huntly, B.*, et al.* (2016). Fumarate is an epigenetic modifier that elicits epithelial-to-mesenchymal transition. Nature *537*, 544-547.

Scortegagna, M., Ding, K., Zhang, Q., Oktay, Y., Bennett, M.J., Bennett, M., Shelton, J.M., Richardson, J.A., Moe, O., and Garcia, J.A. (2005). HIF-2alpha regulates murine hematopoietic development in an erythropoietin-dependent manner. Blood *105*, 3133-3140.

Selak, M.A., Armour, S.M., MacKenzie, E.D., Boulahbel, H., Watson, D.G., Mansfield, K.D., Pan, Y., Simon, M.C., Thompson, C.B., and Gottlieb, E. (2005). Succinate links TCA cycle dysfunction to oncogenesis by inhibiting HIF-alpha prolyl hydroxylase. Cancer cell *7*, 77-85.

Selfridge, A.C., Cavadas, M.A., Scholz, C.C., Campbell, E.L., Welch, L.C., Lecuona, E., Colgan, S.P., Barrett, K.E., Sporn, P.H., Sznajder, J.I., Cummins, E.P., and Taylor, C.T. (2016). Hypercapnia Suppresses the HIF-dependent Adaptive Response to Hypoxia. The Journal of biological chemistry *291*, 11800-11808.

Semenza, G.L. (1994). Regulation of erythropoietin production. New insights into molecular mechanisms of oxygen homeostasis. Hematology/oncology clinics of North America *8*, 863-884.

Semenza, G.L. (2012). Hypoxia-inducible factors in physiology and medicine. Cell *148*, 399-408.

Semenza, G.L. (2013). HIF-1 mediates metabolic responses to intratumoral hypoxia and oncogenic mutations. The Journal of clinical investigation *123*, 3664-3671.

Shabek, N., Herman-Bachinsky, Y., Buchsbaum, S., Lewinson, O., Haj-Yahya, M., Hejjaoui, M., Lashuel, H.A., Sommer, T., Brik, A., and Ciechanover, A. (2012). The size of the proteasomal substrate determines whether its degradation will be mediated by mono- or polyubiquitylation. Molecular cell *48*, 87-97.

Shi, Y., Chen, X., Elsasser, S., Stocks, B.B., Tian, G., Lee, B.H., Shi, Y., Zhang, N., de Poot, S.A., Tuebing, F., Sun, S., Vannoy, J., Tarasov, S.G., Engen, J.R., Finley, D., and Walters, K.J. (2016). Rpn1 provides adjacent receptor sites for substrate binding and deubiquitination by the proteasome. Science (New York, NY) *351*.

Shimizu, Y., Taraborrelli, L., and Walczak, H. (2015). Linear ubiquitination in immunity. Immunological reviews *266*, 190-207.

Smith, D.M., Chang, S.C., Park, S., Finley, D., Cheng, Y., and Goldberg, A.L. (2007). Docking of the proteasomal ATPases' carboxyl termini in the 20S proteasome's alpha ring opens the gate for substrate entry. Molecular cell *27*, 731-744.

Smith, D.M., Fraga, H., Reis, C., Kafri, G., and Goldberg, A.L. (2011). ATP binds to proteasomal ATPases in pairs with distinct functional effects, implying an ordered reaction cycle. Cell *144*, 526-538.

Smith, D.M., Kafri, G., Cheng, Y., Ng, D., Walz, T., and Goldberg, A.L. (2005). ATP binding to PAN or the 26S ATPases causes association with the 20S proteasome, gate opening, and translocation of unfolded proteins. Molecular cell *20*, 687-698.

Spratt, D.E., Walden, H., and Shaw, G.S. (2014). RBR E3 ubiquitin ligases: new structures, new insights, new questions. The Biochemical journal *458*, 421-437.

Spudich, G., Chibalina, M.V., Au, J.S., Arden, S.D., Buss, F., and Kendrick-Jones, J. (2007). Myosin VI targeting to clathrin-coated structures and dimerization is mediated by binding to Disabled-2 and PtdIns(4,5)P2. Nature cell biology *9*, 176-183.

Straud, S., Zubovych, I., De Brabander, J.K., and Roth, M.G. (2010). Inhibition of iron uptake is responsible for differential sensitivity to V-ATPase inhibitors in several cancer cell lines. PloS one *5*, e11629.

Swaney, D.L., Rodriguez-Mias, R.A., and Villen, J. (2015). Phosphorylation of ubiquitin at Ser65 affects its polymerization, targets, and proteome-wide turnover. EMBO reports *16*, 1131-1144.

Takeda, K., Ho, V.C., Takeda, H., Duan, L.J., Nagy, A., and Fong, G.H. (2006). Placental but not heart defects are associated with elevated hypoxia-inducible

factor alpha levels in mice lacking prolyl hydroxylase domain protein 2. Molecular and cellular biology *26*, 8336-8346.

Takeuchi, J., Chen, H., and Coffino, P. (2007). Proteasome substrate degradation requires association plus extended peptide. The EMBO journal *26*, 123-131.

Tanimoto, K., Makino, Y., Pereira, T., and Poellinger, L. (2000). Mechanism of regulation of the hypoxia-inducible factor-1 alpha by the von Hippel-Lindau tumor suppressor protein. The EMBO journal *19*, 4298-4309.

Tanno, H., Yamaguchi, T., Goto, E., Ishido, S., and Komada, M. (2012). The Ankrd 13 family of UIM-bearing proteins regulates EGF receptor endocytosis from the plasma membrane. Molecular biology of the cell *23*, 1343-1353.

Tarhonskaya, H., Rydzik, A.M., Leung, I.K., Loik, N.D., Chan, M.C., Kawamura, A., McCullagh, J.S., Claridge, T.D., Flashman, E., and Schofield, C.J. (2014). Non-enzymatic chemistry enables 2-hydroxyglutarate-mediated activation of 2-oxoglutarate oxygenases. Nature communications *5*, 3423.

Thienpont, B., Steinbacher, J., Zhao, H., D'Anna, F., Kuchnio, A., Ploumakis, A., Ghesquiere, B., Van Dyck, L., Boeckx, B., Schoonjans, L., Hermans, E., Amant, F., Kristensen, V.N., Peng Koh, K., Mazzone, M., Coleman, M., Carell, T., Carmeliet, P., and Lambrechts, D. (2016). Tumour hypoxia causes DNA hypermethylation by reducing TET activity. Nature *537*, 63-68.

Thrower, J.S., Hoffman, L., Rechsteiner, M., and Pickart, C.M. (2000). Recognition of the polyubiquitin proteolytic signal. The EMBO journal *19*, 94-102.

Tian, H., McKnight, S.L., and Russell, D.W. (1997). Endothelial PAS domain protein 1 (EPAS1), a transcription factor selectively expressed in endothelial cells. Genes & development *11*, 72-82.

Tran, H., Hamada, F., Schwarz-Romond, T., and Bienz, M. (2008). Trabid, a new positive regulator of Wnt-induced transcription with preference for binding and cleaving K63-linked ubiquitin chains. Genes & development *22*, 528-542.

Tuckerman, J.R., Zhao, Y., Hewitson, K.S., Tian, Y.M., Pugh, C.W., Ratcliffe, P.J., and Mole, D.R. (2004). Determination and comparison of specific activity of the HIF-prolyl hydroxylases. FEBS letters *576*, 145-150.

Tumbarello, D.A., Manna, P.T., Allen, M., Bycroft, M., Arden, S.D., Kendrick-Jones, J., and Buss, F. (2015). The Autophagy Receptor TAX1BP1 and the Molecular Motor Myosin VI Are Required for Clearance of Salmonella Typhimurium by Autophagy. PLoS pathogens *11*, e1005174.

van Nocker, S., Sadis, S., Rubin, D.M., Glickman, M., Fu, H., Coux, O., Wefes, I., Finley, D., and Vierstra, R.D. (1996). The multiubiquitin-chain-binding protein Mcb1 is a component of the 26S proteasome in Saccharomyces cerevisiae and plays a nonessential, substrate-specific role in protein turnover. Molecular and cellular biology *16*, 6020-6028.

Verma, R., Aravind, L., Oania, R., McDonald, W.H., Yates, J.R., 3rd, Koonin, E.V., and Deshaies, R.J. (2002). Role of Rpn11 metalloprotease in deubiquitination and degradation by the 26S proteasome. Science (New York, NY) *298*, 611-615.

Virdee, S., Ye, Y., Nguyen, D.P., Komander, D., and Chin, J.W. (2010). Engineered diubiquitin synthesis reveals Lys29-isopeptide specificity of an OTU deubiquitinase. Nature chemical biology *6*, 750-757.

Wang, G.L., and Semenza, G.L. (1995). Purification and characterization of hypoxia-inducible factor 1. The Journal of biological chemistry *270*, 1230-1237.

Wauer, T., Swatek, K.N., Wagstaff, J.L., Gladkova, C., Pruneda, J.N., Michel, M.A., Gersch, M., Johnson, C.M., Freund, S.M., and Komander, D. (2015). Ubiquitin Ser65 phosphorylation affects ubiquitin structure, chain assembly and hydrolysis. The EMBO journal *34*, 307-325.

Wickliffe, K.E., Lorenz, S., Wemmer, D.E., Kuriyan, J., and Rape, M. (2011). The mechanism of linkage-specific ubiquitin chain elongation by a single-subunit E2. Cell *144*, 769-781.

Wiesener, M.S., Jurgensen, J.S., Rosenberger, C., Scholze, C.K., Horstrup, J.H., Warnecke, C., Mandriota, S., Bechmann, I., Frei, U.A., Pugh, C.W., Ratcliffe, P.J., Bachmann, S., Maxwell, P.H., and Eckardt, K.U. (2003). Widespread hypoxia-inducible expression of HIF-2alpha in distinct cell populations of different organs. FASEB journal : official publication of the Federation of American Societies for Experimental Biology *17*, 271-273.

Wilkins, S.E., and Abboud, M.I. (2016). Targeting Protein-Protein Interactions in the HIF System. *11*, 773-786.

Williamson, A., Jin, L., and Rape, M. (2009a). Preparation of synchronized human cell extracts to study ubiquitination and degradation. Methods in molecular biology *545*, 301-312.

Williamson, A., Wickliffe, K.E., Mellone, B.G., Song, L., Karpen, G.H., and Rape, M. (2009b). Identification of a physiological E2 module for the human anaphase-promoting complex. Proceedings of the National Academy of Sciences of the United States of America *106*, 18213-18218.

Worden, E.J., Padovani, C., and Martin, A. (2014). Structure of the Rpn11-Rpn8 dimer reveals mechanisms of substrate deubiquitination during proteasomal degradation. Nature structural & molecular biology *21*, 220-227.

Wu, T., Merbl, Y., Huo, Y., Gallop, J.L., Tzur, A., and Kirschner, M.W. (2010). UBE2S drives elongation of K11-linked ubiquitin chains by the anaphase-promoting complex. Proceedings of the National Academy of Sciences of the United States of America *107*, 1355-1360.

Xu, P., Duong, D.M., Seyfried, N.T., Cheng, D., Xie, Y., Robert, J., Rush, J., Hochstrasser, M., Finley, D., and Peng, J. (2009). Quantitative proteomics reveals

the function of unconventional ubiquitin chains in proteasomal degradation. Cell *137*, 133-145.

Xu, W., Yang, H., Liu, Y., Yang, Y., Wang, P., Kim, S.H., Ito, S., Yang, C., Wang, P., Xiao, M.T., Liu, L.X., Jiang, W.Q., Liu, J., Zhang, J.Y., Wang, B., Frye, S., Zhang, Y., Xu, Y.H., Lei, Q.Y., Guan, K.L.*, et al.* (2011). Oncometabolite 2-hydroxyglutarate is a competitive inhibitor of alpha-ketoglutarate-dependent dioxygenases. Cancer cell *19*, 17-30.

Yao, T., and Cohen, R.E. (2002). A cryptic protease couples deubiquitination and degradation by the proteasome. Nature *419*, 403-407.

Yau, R., and Rape, M. (2016). The increasing complexity of the ubiquitin code. Nature cell biology *18*, 579-586.

Yu, H., Kago, G., Yellman, C.M., and Matouschek, A. (2016). Ubiquitin-like domains can target to the proteasome but proteolysis requires a disordered region. *35*, 1522-1536.

Zhang, H., Bosch-Marce, M., Shimoda, L.A., Tan, Y.S., Baek, J.H., Wesley, J.B., Gonzalez, F.J., and Semenza, G.L. (2008). Mitochondrial autophagy is an HIF-1-dependent adaptive metabolic response to hypoxia. The Journal of biological chemistry *283*, 10892-10903.

Zhang, J., Hu, M.M., Wang, Y.Y., and Shu, H.B. (2012). TRIM32 protein modulates type I interferon induction and cellular antiviral response by targeting MITA/STING protein for K63-linked ubiquitination. The Journal of biological chemistry *287*, 28646-28655.

Zhang, Z., Yang, J., Kong, E.H., Chao, W.C., Morris, E.P., da Fonseca, P.C., and Barford, D. (2013). Recombinant expression, reconstitution and structure of human anaphase-promoting complex (APC/C). The Biochemical journal *449*, 365-371.

Zhao, S., Lin, Y., Xu, W., Jiang, W., Zha, Z., Wang, P., Yu, W., Li, Z., Gong, L., Peng, Y., Ding, J., Lei, Q., Guan, K.L., and Xiong, Y. (2009). Glioma-derived mutations in IDH1 dominantly inhibit IDH1 catalytic activity and induce HIF-1alpha. Science (New York, NY) *324*, 261-265.

Zhdanov, A.V., Dmitriev, R.I., and Papkovsky, D.B. (2012). Bafilomycin A1 activates HIF-dependent signalling in human colon cancer cells via mitochondrial uncoupling. Bioscience reports *32*, 587-595.

Zhong, B., Zhang, L., Lei, C., Li, Y., Mao, A.P., Yang, Y., Wang, Y.Y., Zhang, X.L., and Shu, H.B. (2009). The ubiquitin ligase RNF5 regulates antiviral responses by mediating degradation of the adaptor protein MITA. Immunity *30*, 397-407.